



Activation of the unfolded protein response sensor Ire1 by lipid bilayer stress

Dissertation
zur Erlangung des Doktorgrades
der Naturwissenschaften

vorgelegt beim Fachbereich Biochemie, Chemie und Pharmazie
der Johann Wolfgang Goethe-Universität
in Frankfurt am Main

von
Kristina Halbleib

aus Offenbach am Main

Frankfurt, 2017

(D30)

Vom Fachbereich Biochemie, Chemie und Pharmazie der
Johann Wolfgang Goethe-Universität als Dissertation angenommen.

Dekan: Prof. Dr. Michael Karas

Gutachter: 1. Prof. Dr. Robert Ernst
2. Prof. Dr. Martin Grininger

Datum der Disputation:

Teile der vorliegenden Arbeit wurden in folgenden Publikationen zusammengefasst:

Stordeur, C.*, **Puth, K.***, Saenz, J.P., Ernst, R. Crosstalk of lipid and protein homeostasis to maintain membrane function. *Biol. Chem.* (2014), Vol. 395 (3), 313-326.

Puth, K.*, Hofbauer, H.F.*, Saenz, J.P., Ernst, R. Homeostatic control of biological membranes by dedicated lipid and membrane packing sensors. *Biol. Chem.* (2015), Vol. 396 (9-10), 1043-1058.

Covino, R.*, Ballweg, S.*, Stordeur, C.*, Michaelis, J.B., **Puth, K.**, Wernig, F., Bahrami, A., Ernst, A.M., Hummer, G., Ernst, R. A eukaryotic sensor for membrane lipid saturation. *Mol. Cell* (2016), Vol. 63, 49-59.

Halbleib, K., Pesek, K., Covino, R., Hofbauer, H.F., Wunnicke, D., Hänel, I., Hummer, G., Ernst, R. Activation of the unfolded protein response by lipid bilayer stress. *Mol. Cell* (2017), Vol. 67, 673-684.

Für meine Familie

Index

Index	I
List of Figures	V
List of Tables	VIII
List of Abbreviations.....	IX
Zusammenfassung	XII
Abstract.....	XVII
1. Introduction.....	1
1.1. The complexity of biological membranes	1
1.1.1. Diversity of the cellular lipidome.....	3
1.1.2. Lipid composition correlates with organelle function.....	6
1.2. The ER and its cellular function	8
1.2.1. Architecture of the ER.....	8
1.2.2. Cellular function of the ER	10
1.2.3. Yeast as a model system to study ER homeostasis.....	11
1.3. Integral and membrane-associated membrane property sensors.....	11
1.4. Correlating ER-stress and lipid metabolism	16
1.4.1. The Unfolded protein response (UPR)	16
1.4.2. More than just UPR: Activation of the UPR by lipid bilayer stress	21
1.4.3. Insights into the molecular organization of Ire1	25
2. Aim	29
3. Materials	30
3.1. Chemicals and reagents	30
3.2. Commercially available systems	32
3.3. Enzymes.....	33
3.4. Antibodies.....	33
3.5. Supplies and Equipment.....	34
3.6. Peptides	36
3.7. Plasmids.....	36
3.7.1. Construction of <i>IRE1</i> knock-in constructs.....	37
3.7.2. Construction of MBP-fusion constructs	38
3.8. Oligonucleotides	38
3.9. Organisms	44
3.10. Media.....	46

3.10.1.	Media and plates for cultivation of <i>E. coli</i>	46
3.10.2.	Media and plates for cultivation of <i>S. cerevisiae</i>	47
4.	Methods.....	49
4.1.	Microbiological methods.....	49
4.1.1.	Generation of chemically competent <i>E. coli</i>	49
4.1.2.	Transformation of competent <i>E. coli</i>	49
4.1.3.	Cultivation and storage of <i>E. coli</i>	49
4.1.4.	Generation of competent <i>S. cerevisiae</i>	50
4.1.5.	Transformation of competent <i>S. cerevisiae</i>	50
4.1.6.	Cultivation and storage of <i>S. cerevisiae</i>	50
4.2.	Molecular biological methods.....	51
4.2.1.	Polymerase chain reaction (PCR).....	51
4.2.2.	Agarose gel electrophoresis.....	51
4.2.3.	Restriction digest.....	52
4.2.4.	Ligation.....	52
4.2.5.	Site-directed mutagenesis (SDM).....	53
4.2.6.	Engineering <i>IRE1</i> utilizing the Q5 Site-Directed Mutagenesis Kit.....	53
4.2.7.	Genomic tagging in <i>S. cerevisiae</i>	54
4.2.8.	Colony PCR of <i>S. cerevisiae</i>	54
4.2.9.	Plasmid preparation from <i>E. coli</i>	55
4.2.10.	RNA preparation from <i>S. cerevisiae</i>	55
4.2.11.	Reverse transcription (RT).....	55
4.2.12.	DNA sequencing.....	55
4.3.	Biochemical methods.....	56
4.3.1.	<i>In vivo</i> methods.....	56
4.3.1.1.	Preparation of cell extracts for immunoblotting.....	56
4.3.1.2.	Membrane fractionation & extraction.....	56
4.3.1.3.	Reverse transcription-quantitative PCR (RT-qPCR).....	57
4.3.1.4.	Immunoprecipitation.....	57
4.3.2.	<i>In vitro</i> methods.....	57
4.3.2.1.	Heterologous expression and purification of MBP-Ire1 ^{AH+TMH}	57
4.3.2.2.	Spinlabeling of MBP-Ire1 ^{AH+TMH}	58
4.3.2.3.	Size exclusion chromatography (SEC).....	59
4.3.2.4.	SDS-Polyacrylamide gel electrophoresis (SDS-PAGE).....	59
4.3.2.5.	Coomassie blue staining.....	60
4.3.2.6.	Immunoblotting.....	60

4.3.2.7. Liposome preparation.....	60
4.3.2.8. Reconstitution of MBP-Ire1 ^{AH+TMH} fusion proteins in liposomes	61
4.3.2.9. Sucrose step gradient centrifugation	62
4.3.2.10. Carbonate extraction as quality control of proteoliposomes.....	63
4.3.2.11. Proteinase K digest	63
4.3.2.12. Hoechst 33342 measurements.....	63
4.3.2.13. C-Laurdan fluorescence measurements of liposomes	64
4.3.2.14. Oxygen mediated cysteine crosslinking of MBP-Ire1 ^{AH+TMH} fusion proteins in proteoliposomes	64
4.3.2.15. Circular dichroism (CD) spectroscopy	65
4.4. Biophysical methods.....	65
4.4.1. Continuous wave (cw) EPR spectroscopy measurements	65
4.4.2. Analysis of cwEPR spectra.....	65
4.5. Cell biology	66
4.5.1. Yeast growth assay.....	66
4.5.2. Live cell confocal microscopy.....	66
5. Results.....	68
5.1. Establishing a knock-in strategy to express <i>IRE1</i> at its endogenous locus and expression levels	68
5.2. The functional role of Ire1's TMH in ER stress	72
5.3. Bioinformatic identification and <i>in vivo</i> validation of an amphipathic helix in Ire1....	75
5.3.1. Mutations in the hydrophobic face of the AH interfere with Ire1 functionality ..	76
5.3.2. A conserved acidic residue at position 540 is important for Ire1 function.....	80
5.4. Functionally impaired AH mutant variants are capable to interact with known interaction partners.....	84
5.5. Crosstalk of Ire1's AH with two known luminal interfaces.....	86
5.6. The AH of Ire1 is not required for activation by protein induced ER stress.....	88
5.7. Establishing a minimal sensor domain for <i>in vitro</i> studies	90
5.8. Membrane-sensitive oligomerization of the minimal sensor	95
5.9. Exploring the structural dynamics of Ire1's AH during activation by lipid bilayer stress	101
5.10. AH mutations partially unfold the helix	105
5.11. The AH of Ire1 induces a local compression in the lipid bilayer.....	106
5.12. The structural and functional role of Ire1's TMH in ER stress.....	107
5.12.1. Structural analysis of the TMH by cysteine cross-linking	107
6. Discussion	111

6.1. Endogenous expression of a fully functional <i>IRE1</i> construct.....	111
6.2. An array of functional <i>in vivo</i> assays in combination with <i>in vitro</i> studies is required to analyze Ire1 mutants	112
6.3. A membrane-based mechanism for Ire1 activation by lipid bilayer stress	114
6.3.1. Ire1 is not the only protein activated by a membrane-based mechanism	116
6.4. Conservation of the membrane-based activation mechanism of Ire1 by lipid bilayer stress	119
6.5. Crosstalk of protein folding and lipid bilayer stress.....	121
References	123
Supplementary Information	140
Conservation of the AH in <i>IRE1</i> among species	140
PELDOR Experiments of the reconstituted minimal sensor domain of Ire1	141
Danksagung.....	142
<i>Curriculum vitae</i>	144
Eidesstattliche Erklärung.....	147

List of Figures

Figure 1 The Fluid-Mosaic-Model of cell membranes.	1
Figure 2 Lipid species differ in shape and chemistry.	4
Figure 3 Lipid synthesis and composition of different organelles in eukaryotic cells.	7
Figure 4 Structure of the ER network in eukaryotic cells.....	9
Figure 5 ER morphology of <i>S. cerevisiae</i>	10
Figure 6 Transcriptional regulation of dedicated TM sensor proteins.....	13
Figure 7 Soluble membrane sensors bearing amphipathic helix (AH) motifs to sense membrane properties.	15
Figure 8 Activation of the UPR in <i>S. cerevisiae</i> upon protein folding stress.....	18
Figure 9 Time-dependent activation of the mammalian UPR sensors.	20
Figure 10 Negative genetic interactions of <i>IRE1</i> with genes involved in ERAD, PC synthesis and fatty acid saturation.	22
Figure 11 Metabolic pathways of PC synthesis in <i>S. cerevisiae</i>	23
Figure 12 Activation of Ire1 by protein folding and lipid bilayer stress.....	24
Figure 13 Schematic representation, and structural organization of Ire1's ER-luminal sensor domain.	26
Figure 14 Schematic representation, and structural organization of Ire1.	27
Figure 15 Schematic illustration of a homologous recombination event in yeast and its verification by colony PCR.	54
Figure 16 Lipid compositions used for reconstitution.	61
Figure 17 Knock-in strategy of <i>IRE1</i> for the integration at the endogenous locus.....	69
Figure 18 The <i>IRE1</i> knock-in construct used in this study	70
Figure 19 Analysis of Ire1 integration by membrane fractionation and extraction experiments.	70
Figure 20 Ire1 _{3xHA-GFP} protein production from <i>CEN</i> -based plasmids and from the endogenous locus.....	72
Figure 21 Mutation of the F-cluster (F544,548,551A) does not impair Ire1 functionality. ...	73
Figure 22 Exchange of the TMH of Ire1 by poly leucine helices.	74
Figure 23 Ire1 contains an amphipathic helix (AH) adjacent to the transmembrane helix (TMH) on the ER-luminal side of Ire1.....	75
Figure 24 Mutations in the hydrophobic phase of the AH impair Ire1 functionality.	77
Figure 25 Fractionation and integration of AH mutants.....	78

Figure 26 Mutations in the AH affect the formation of Ire1 clusters in ER-stress.	79
Figure 27 <i>HAC1</i> splicing and upregulation of <i>PDI1</i> mRNA levels are reduced in the V535R mutant.....	80
Figure 28 The negative charge of E540 in Ire1 is conserved among species.	81
Figure 29 Substitution of the negative charge at position 540 leads to a functional defect in Ire1.	82
Figure 30 The E540A mutation affects the formation of Ire1 clusters in ER-stress conditions.....	83
Figure 31 <i>HAC1</i> splicing and upregulation of <i>PDI1</i> mRNA levels is reduced in the E540A mutant.....	84
Figure 32 Ire1 AH mutants retain their ability to interact with known interaction partners...	85
Figure 33 A growth assay reveals negative epistasis between mutations in the AH and ER-luminal interfaces.	87
Figure 34 qRT-PCR reveals negative crosstalk between the V535R or E540A mutations and ER-luminal interfaces.	88
Figure 35 Activation of the Ire1 by supplementation of different ER stress inducers.	89
Figure 36 Purification of spin-labeled MBP-Ire1 ^{AH+TMH} and analysis of concentration dependent oligomerization.	91
Figure 37 A ER-stress assay reveals the C552S mutant is fully functional.	92
Figure 38 Reconstitution of spin-labeled MBP-Ire1 ^{AH+TMH} in different lipid environments. ..	93
Figure 39 Quality control of MBP-Ire1 ^{AH+TMH} containing proteoliposomes.	94
Figure 40 In vitro strategy to explore lipid modulated oligomerization of MBP-Ire1 ^{AH+TMH} ...	95
Figure 41 cwEPR spectroscopy of MBP-Ire1 ^{AH+TMH} in different lipid environments.	97
Figure 42 cwEPR spectra of MBP-Ire1 ^{AH+TMH} variants and their spin-diluted controls.	99
Figure 43 Concentration dependent spectral broadening of cwEPR spectra from MBP-Ire1 ^{AH+TMH} variants.....	100
Figure 44 Alternative C552 residue for cwEPR spectroscopy.....	101
Figure 45 cwEPR spectra of MBP-Ire1 ^{AH+TMH} labeled at the indicated residues and reconstituted in distinct membrane environments.....	103
Figure 46 Representative structures of the initial and final configuration of the Ire1 minimal sensor in MD simulations.	104
Figure 47 The AH of Ire1 unfolds when a positive charge is introduced at positions F531 or V535.	105
Figure 48 The minimal sensor peptide induces a lipid bilayer compression and lipid acyl chain disorder.	106

Figure 49 Reconstitution and quality control of MBP-Ire1 ^{AH+TMH} containing proteoliposomes.	108
Figure 50 <i>In vitro</i> crosslinking studies of the reconstituted minimal sensor.	109
Figure 51 MD simulations reveal the formation of a X-shaped dimer.	110
Figure 52 Schematic model of the membrane-based mechanism of Ire1 activation by lipid bilayer stress.	115
Figure 53 MD simulations of the minimal sensor domain.	116
Figure 54 Channel formation and regulation is associated with local bilayer deformation.	118
Figure 55 Bioinformatics analyses suggests the existence of putative AH motifs in mammalian UPR sensors.	120
Figure 56 Functionality of Ire1 and its mutants in the presence of different ER-stress inducers.	122
Figure S1 / A juxta-membrane AH is conserved in Ire1.	140
Figure S2 / PELDOR measurements of the minimal sensor domain of Ire1 in different lipid environments.	141

List of Tables

Table 1 List of buffer components, salts and additives.	30
Table 2 List of lipid species.	31
Table 3 List of chemicals for cultivation and selection.	31
Table 4 List of solvents.....	31
Table 5 List of kits and standards.....	32
Table 6 List of enzymes.	33
Table 7 List of primary and secondary antibodies used in this study, including their dilution for immunoblotting.	33
Table 8 List of consumables.....	34
Table 9 List of laboratory equipment.	35
Table 10 List of peptides.	36
Table 11 Plasmids used in this study.	36
Table 12 Oligonucleotides for homologous recombination.	39
Table 13 Oligonucleotides for molecular cloning.	39
Table 14 Oligonucleotides for insertion, deletion or exchange of domains in <i>IRE1</i>	40
Table 15 Oligonucleotides for site-directed mutagenesis of <i>IRE1</i>	40
Table 16 Oligonucleotides for sequencing.....	43
Table 17 Oligonucleotides for colony PCR	43
Table 18 Oligonucleotides for RT-qPCR.	44
Table 19 <i>E. coli</i> strains used in this study.....	44
Table 20 yeast strains used in this study.....	45
Table 21 Media and plates for cultivation of <i>E. coli</i> used in this study.....	47
Table 22 Media and plates for cultivation of <i>S. cerevisiae</i> used in this study.	48
Table 23 Standard reaction mixture and conditions for PCR.	51
Table 24 Standard reaction mixture for restriction digestion.	52
Table 25 Standard reaction mixture and conditions for SDM.....	53
Table 26 Protein and lipid amounts and their molar ratios used for reconstitution.	61
Table 27 Microscope settings for fluorescence live cell imaging used for quantitative analysis and respective quantification parameters.	66

List of Abbreviations

AA	Amino acid
Acyl-CoA	Acyl coenzyme A
AD	Alzheimers disease
AH	Amphipathic helix
ALPS	Amphipathic lipid packing sensor
Atf1	Acyltransferase 1
Atf2	Acyltransferase 2
ATF4	Cyclic AMP-dependent transcription factor ATF-4
ATF6	Cyclic AMP-dependent transcription factor ATF-6
<i>B. subtilis</i>	<i>Bacillus subtilis</i>
BCR	B-cell receptor
bp	Base pair
CaCl ₂	Calcium chloride
CCT α	CTP:phosphocholine cytidyltransferase
CD	Circular dichroism
CDP-DAG	Cytidine Diphosphate Diacylglycerol
<i>C. elegans</i>	<i>Caenorhabditis elegans</i>
cLD	Core lumenal domain
Co-IP	Co-immunoprecipitation
CSM	Complete synthetic mixture
CV	Column volume
cwEPR	Continuous wave electron paramagnetic resonance
DAG	Diacylglycerol
DIC	Differential interference contrast
<i>D. melanogaster</i>	<i>Drosophila melanogaster</i>
DMPE	N,N-dimethyl phosphatidylethanolamine
DMSO	Dimethylsulfoxid
dNTP	Deoxynucleotide triphosphate
DOPC	1,2-Dioleoyl-sn-glycero-3-phosphocholine
DOPE	1,2-dioleoyl-sn-glycero-3-phosphoethanolamine
Dpm1	Dolichyl-phosphatase mannosyltransferase
DPPC	1,2-dipalmitoyl-sn-glycero-3-phosphocholine
DTT	Dithiothreitol
E-MAP	Epistatic miniarray profiles
EDTA	Ethylendiaminetetraacetic acid
EGFR	Epidermal growth factor receptor
eIF2 α	Elongation initiation factor 2-alpha
EPL	<i>E. coli</i> polar lipids
ER	Endoplasmic reticulum
ERAD	ER-associated degradation
<i>Escherichia coli</i>	<i>E. coli</i>
FRET	Förster resonance energy transfer
fwd	Forward

List of Abbreviations

GOI	Gene of interest
GP	Generalized polarization
GpA	Glycophorin A
GPCR	G-protein coupled receptor
GPI	Glycosylphosphatidylinositol
GPL	Glycerophospholipid
HCl	Hydrochloric acid
HEPES	4-(2-hydroxyethyl)-1-piperazineethanesulfonic acid
<i>Homo sapiens</i>	<i>H. sapiens</i>
HPLC	Hi-throughput liquid chromatography
IF _C	Cytosolic IF
IF _L	Luminal IF
IPTG	Isopropyl-β-D-thiogalactopyranosid
Ire1	Inositol-requiring enzyme 1
IRE1 _α	Inositol-requiring enzyme 1-alpha
KAc	Potassium acetate
Kar2	78 kDa glucose-regulated protein homolog Kar2
KCl	Potassium chloride
kDA	Kilo dalton
LAT	Linker of activated T-cells
LiAc	Lithium acetate
MBP	Maltose binding protein
MD	Molecular dynamics
MgCl ₂	Magnesium chloride
MHC-I	major-histocompatibility complex I
MMPE	N-monomethyl phosphatidyletanolamine
MnCl ₂	Mangan(II)-chloride (1-Oxyl-2,2,5,5-tetramethylpyrroline-3-methyl)
MTSSL	Methanethiosulfonate
(NH ₄)SO ₄	Ammonium sulfate
Na ₂ HPO ₄	<i>di</i> -Sodium hydrogen phosphate
NaCl	Sodium Chloride
NADH	Nicotinamide adenine dinucleotide
NaH ₂ PO ₄	Sodium di-hydrogen phosphate
NaN ₃	Sodium azide
NaOH	Sodium hydroide
OD	Optical density
ODu	Optical density unit
PA	Phosphatidic acid
PBS	Phosphate buffered saline
PC	Phosphatidylcholine
PCR	Polymerase chain reaction
PD	Parkinsons disease
PDI1	Protein disulfide isomerase
PE	Phosphatidyletanolamine
PEG	Polyethylene glycol
PELDOR	Pulsed electron-electron double resonance.

PERK	Protein kinase (PRK)-like ER kinase
Pgk1	Phosphoglycerate kinase 1
PI	Phosphatidylinositol
PIPES	Piperazine-N,N'-bis(2-ethanesulfonic acid)
PL	Phospholipid
P:L	Protein:lipid
PM	Plasma membrane
POPC	1-palmitoyl-2-oleoyl-sn-glycero-3-phosphocholine
POPE	1-palmitoyl-2-oleoyl-sn-glycero-3-phosphoethanolamine
PS	Phosphatidylserine
qPCR	Quantitative polymerase chain reaction
RER	Rough ER
rev	Reversed
RNase	Ribonuclease
RT	Reverse transcription
RTK	Receptor tyrosine kinase
<i>S. cerevisiae</i>	<i>Saccharomyces cerevisiae</i>
SCD	Synthetic complete glucose
SDM	Site-directed mutagenesis
SDS	Sodium dodecyl sulfate
SDS-PAGE	SDS-Polyacrylamide gel electrophoresis
SEC	Size-exclusion chromatography
Sec61	Protein transport protein Sec61
Sec63	Protein transport protein Sec63
SER	Smooth ER
SL	Sphingolipid
SNARE	soluble N-ethylmaleimide-sensitive-factor attachment receptor
Soy-PI	L- α -phosphatidylinositol
TAG	Triacylglycerol
TCEP	Tris(2-carboxyethyl)phosphine
TCR	T-cell receptor
TM	Transmembrane
Tm	Tunicamycin
TMD	Transmembrane domain
TMH	Transmembrane helix
TMR	Transmembrane region
Tris	Tris(hydroxymethyl)-aminomethan
UPR	Unfolded protein response
UPRE	Unfolded protein response element
v/v	Volume per volume
w/v	Weight per volume
YNB	Yeast nitrogen base
β -OG	Octyl β -D-glucopyranoside

Zusammenfassung

Die Zusammensetzung zellulärer Membranen ist äußerst komplex und die Mechanismen der Membranhomöostase sind nur unzureichend verstanden. Die Lipidzusammensetzungen unterschiedlicher Membransysteme trägt entscheidend zur Identität, Form und Funktion der Organellen bei. Physikalische Membraneigenschaften wie Membrandicke, Lipidpackungsdichte und Ladung der Membranoberfläche, werden durch die Lipidzusammensetzung gesteuert und verändern sich graduell entlang des sekretorischen Weges.

Das endoplasmatische Retikulum (ER) bildet eines der größten Organellen in eukaryotischen Zellen und ist ein zentraler Ort der Lipidsynthese. Das ER bildet ein kontinuierliches Membransystem, das sowohl in seiner Morphologie als auch in seiner Funktion spezialisierte Subdomänen bilden kann. Da es den Ursprung des sekretorischen Weges darstellt, müssen alle sekretorischen Proteine und Transmembranproteine am ER synthetisiert werden. Sekretorische Proteine können ko-translational und post-translational in das Lumen des ER gelangen, während Membranproteine in die ER-Membran inseriert werden. Im oxidativen Milieu des ER können die Proteine, unterstützt durch ein Netzwerk von Faltungshelfern, sogenannte chaperone, in ihre native Form falten. Werden die Faltungskapazitäten des ER überschritten, kommt es zu einer Akkumulation von fehlgefalteten und ungefalteten Proteinen im Lumen des ER, welche zentrale Funktionen des ER blockieren können.

Die *unfolded protein response* (UPR) ist ein in Eukaryonten hochkonserviertes Programm, das durch ungefaltete und misgefaltete Proteine im Lumen des ER aktiviert wird. Die UPR löst eine breitgefächerte Antwort aus, um die Homöostase der Proteinproduktion und Proteinfaltung, die Proteostase, wiederherzustellen. Der Mechanismus dieser Aktivierung wird bereits seit mehr als 20 Jahren intensiv untersucht, was dazu führte, dass viele seiner molekularen Details bereits gut charakterisiert sind. 7 – 8% aller Gene in der Hefe *Saccharomyces cerevisiae* (*S. cerevisiae*) werden durch diesen Signalweg reguliert. Neuere Erkenntnisse legen nahe, dass nicht nur die Akkumulation ungefalteter und misgefalteter Proteine im Lumen des ER, sondern auch gestörte Lipidzusammensetzungen der ER-Membran die UPR aktivieren können. Gestörte Lipidzusammensetzungen, welche zu einer Aktivierung der UPR führen, werden als Lipid-*bilayer* Stress bezeichnet. Der molekulare Mechanismus dieser Membran-aktivierten UPR blieb bis zuletzt ungeklärt.

Diese Studie untersucht die UPR von *S. cerevisiae* anhand von Studien am *inositol requiring enzyme 1* (Ire1). Ire1 stellt den einzigen UPR Sensor der Hefe *S. cerevisiae* dar. Dieses Typ 1

α -helikale Membranprotein hat ein Molekulargewicht von 127 kDa und besitzt eine Sensordomäne für ungefaltete Proteine im Lumen des ER (lumenale Sensordomäne), die über eine Transmembranhelix (TMH) mit einer Kinase-, sowie einer Ribonuklease- (RNase) Domäne im zytosolischen Teil verbunden ist. In der Abwesenheit von ER-Stress liegt Ire1 in der ER-Membran als Monomer vor und wird möglicherweise zusätzlich durch das Chaperon Kar2 in diesem Zustand stabilisiert. Wenn ungefaltete Proteine im Lumen des ER akkumulieren und an die lumenale Sensordomäne von Ire1 binden, so führt dies simultan zur Dissoziation des Chaperons Kar2 und zur Oligomerisierung von Ire1, was in Folge zur Aktivierung des UPR Sensors führt. Hierzu lagern sich zunächst zwei Ire1 Monomere in einer *front-to-front* Konfiguration aneinander an und bilden Ire1 Homodimere. Diese Homodimere lagern sich wiederum in einer *back-to-back* Konfiguration zusammen und bilden höhere Homo-Oligomere. Hierfür werden Oligomerisierungsflächen in der lumenalen Sensordomäne genutzt, die für die Bildung von stabilen Ire1 Oligomeren essentiell sind. Durch die Ausbildung von Homo-Oligomeren im Lumen des ER, werden auch die zytosolischen Bereiche von Ire1 in räumliche Nähe gebracht, wodurch es zu einer Aktivierung der Kinase- und RNase Domänen von Ire1, und zum Spleißen von *HAC1* mRNA kommt. Hierbei entfernt die aktive RNase Domäne von Ire1 ein Intron aus der Prä-mRNA von *HAC1* und nach der Ligation der verbleibenden Exons durch die tRNA Ligase Rlg1 kann der funktionale Transkriptionsfaktor Hac1 produziert werden. Der Transkriptionsfaktor Hac1 wandert in den Nukleus, wo dieser die Expression von UPR Zielgenen aktiviert. Auf diese Weise überwacht Ire1 den Zustand im ER, um über den Transkriptionsfaktor Hac1 die Proteostase aufrecht zu erhalten.

S. cerevisiae besitzt einzig Ire1 als UPR Stress Sensor. Säuger sind mit drei UPR Sensoren ausgestattet. Während die Funktion des Ire1 Orthologs, IRE1 α , konserviert ist, besitzen diese Organismen weiterhin die Protein Kinase (PRK)-ähnliche ER Kinase (PERK), und den aktivierenden Transkriptionsfaktor 6 (ATF6), die ebenfalls als UPR Sensoren fungieren.

Es gibt eine Vielzahl von auffälligen Überschneidungen zwischen Prozessen der Protein-Qualitätskontrolle und der Regulation des Lipidmetabolismus. Auf UPR Aktivität basierende genetische Screens identifizierten, dass die UPR neben der Regulation von u.a. Chaperonen, ER-assoziierten Degradation (ERAD) Komponenten und intrazellulären *trafficking* Komponenten, zudem kritische Aspekte im Lipidmetabolismus reguliert. Auch konnte beobachtet werden, dass diverse Deletionsmutanten, die zentrale Schritte des Lipidmetabolismus und dessen Regulation in *S. cerevisiae* stören, zur Aktivierung von Ire1 führen. Interessanterweise umfassten diese Schritte die Regulation der Cholesterolhomöostase, die Synthese von Sphingolipiden und die Herstellung von

Phosphatidylcholine (PC) aus Phosphatidylethanolamin (PE), sowie die Regulation der Fettsäure Desaturierung. Auch ein akuter Mangel an Inositol, einem Vorläufermolekül für die Synthese von Phosphatidylinositol, führt zur Aktivierung von Ire1. Diese und weitere Beobachtungen verschiedener Labore legten nahe, dass die UPR nicht nur durch die Akkumulation von ungefalteten und misgefalteten Proteinen im Lumen des ER, sondern auch durch eine Störung der Lipidhomöostase, i.e. Lipid-*bilayer* Stress, hervorgerufen werden kann.

Diese Studie untersucht die UPR von *S. cerevisiae* anhand ihres einzigen Sensors für die UPR, Ire1. Hierbei wird eine Kombination von *in vivo* und *in vitro* Experimenten genutzt, welche durch *Molecular Dynamics* (MD) Simulationen komplementiert wird, um die Aktivierung von Ire1 durch Lipid-*bilayer* Stress auf molekularer Ebene zu verstehen. Im Rahmen dieser Studie wurde insbesondere der Juxta- und / oder Transmembranbereich von Ire1 analysiert. Im Zuge bioinformatischer Analysen wurde eine ER-lumenale amphipathische Helix (AH) direkt N-Terminal von, und teilweise überlappend mit Ire1's Transmembranhelix (TMH) identifiziert. Die AH inseriert mit ihrer hydrophoben Seite in die ER-Membran, was eine ungewöhnliche, geneigte Orientierung der TMH in der ER-Membran bewirkt. Die daraus resultierende ungewöhnliche Architektur von AH und TMH stellt das grundlegende Element für die Aktivierung von Ire1 in Anwesenheit von Lipid-*bilayer* Stress dar. Weiterhin ist eine Aminosäure mit negativer Ladung zwischen AH und TMH konserviert von der Hefe bis hin zum Menschen. Dies legt eine besondere Bedeutung von elektrostatischen Interaktionen zwischen dem konservierten Rest, bei dem es sich in *S. cerevisiae* um ein Glutamat an Position 540 (E540) handelt, und den Kopfgruppen der Membranlipide nahe.

Um die Funktion der AH in Ire1 im physiologischen Kontext zu analysieren, wurden verschiedene Varianten von Ire1 für *in vivo* Studien in *S. cerevisiae* an den endogenen Genlokus inseriert und exprimiert. Durch das Einfügen von geladenen Aminosäureresten in der hydrophoben Seite der AH wurden Mutanten (F531R, V535R) erzeugt, bei denen der amphipathische Charakter der AH zerstört wurde. Zudem wurde eine Reihe von Mutanten hergestellt, bei denen das Glutamat durch ungeladene oder positiv geladene Aminosäuren ersetzt wurde.

Zellen, die eine Wildtypvariante oder Mutanten von Ire1 exprimieren, wurden in Anwesenheit von unterschiedlich hohen Konzentrationen des Reduktionsreagenz Dithiothreitol (DTT) kultiviert, um deren DTT-Resistenz zu prüfen. Fluoreszenzmikroskopische Experimente wurden durchgeführt, um die Oligomerisierung von Ire1 zu analysieren. Die Fähigkeit von Ire1,

HAC1 mRNA zu spleißen, sowie die Menge von mRNA Transkripten des UPR Zielgens *PDI1* wurden nach reverser Transkription mittels quantitativer PCR (RT-qPCR) analysiert. Weiterhin wurden *steady-state* Proteinmengen von Ire1 und dessen Mutanten mittels Immunoblot Analyse untersucht, die Integration des Proteins in die ER-Membran, sowie die Interaktion unterschiedlicher Ire1 Varianten mit den bekannten Interaktionspartnern Kar2 und Sec63 analysiert.

Es konnte gezeigt werden, dass die Einführung einer positiven Ladung in der hydrophoben Seite der AH (F531R, V535R), sowie die Mutation des Glutamats (E540A), die Funktionalität von Ire1 bei ER-Stress auf allen Ebenen der Signalkaskade signifikant verringert. Die Integration dieser Mutanten in die ER-Membran, *steady-state* Proteinmengen, sowie die Interaktion dieser Mutanten mit bekannten Interaktionspartnern waren jedoch nicht betroffen, was eine kritische Rolle der AH bei der Aktivierung von Ire1 bei ER-Stress nahelegt.

Eine Kombination der in dieser Arbeit erzeugten Juxta-Membran Mutationen (V535R, E540A) mit Mutanten, die Interaktionsschnittstellen in der lumenalen Sensordomäne zerstören, führte zu einem vollständigen Aktivitätsverlust von Ire1 und somit zu einer Unempfindlichkeit dieser Mutanten gegenüber ER-Stress. Dies legt eine gemeinschaftliche Beteiligung der Interaktionsflächen der lumenalen Sensordomäne und dem Juxta-Membranbereich für die Oligomerisierung und Aktivierung von Ire1 nahe.

Die Etablierung eines *in vitro* Systems zur Analyse der Membran-vermittelten Oligomerisierung von Ire1 ermöglichte die isolierte Betrachtung der Funktion von AH und TMH im Aktivierungsprozess durch Lipid-*bilayer* Stress in dieser Studie. Ein Fusionskonstrukt, bestehend aus der Sequenz des Maltose Binde Proteins (MBP) aus *Escherichia coli* (*E. coli*) und der AH und TMH von Ire1, dem sogenannten Minimalsensor, wurde hergestellt. Die heterologe Produktion des Fusionsproteins in *E. coli*, dessen Markierung mit dem Spin-*label* Methanethiosulfonate (MTSSL), sowie die Reinigung und Rekonstitution dieses Minimalsensors in Liposomen verschiedener Zusammensetzung wurde im Rahmen dieser Arbeit etabliert. Der Einfluss der Lipidumgebung auf den oligomeren Zustand des Minimalsensors wurde mittels *continuous wave* Elektronenspinresonanz (cwESR) untersucht.

Anhand der durchgeführten cwESR Studien am Spin-markierten Minimalsensor in verschiedenen Lipidbedingungen konnte gezeigt werden, dass die molekulare Packungsdichte der Lipide einen signifikanten Einfluss auf die Oligomerisierung des Spin-markierten Minimalsensors hat: erhöhte Packungsdichten führen zur Oligomerisierung des Minimalsensors. Die F531R Variante des Minimalsensors, bei welcher der amphipathische

Charakter der AH durch eine Mutation zerstört ist, zeigte unter identischen Bedingungen keine Membran-abhängige Oligomerisierung.

Die Wildtyp Version der AH von Ire1 (Ire1⁵²²⁻⁵⁴³), sowie die F531R und V535R Mutanten wurden synthetisch hergestellt und für CD-spektroskopische Messungen verwendet. Während das vom Wildtyp abgeleitete Peptid eine α -helikale Sekundärstruktur in Detergenzlösung aufwies, waren die beiden Mutanten hingegen unstrukturiert. MD Simulationen des Minimalsensors konnten sowohl die Einbettung der gefalteten AH in verschiedenen Lipidumgebungen, sowie die Entfaltung derer durch Einführung von positiven Ladungen bestätigen.

Obwohl in vorherigen Studien gezeigt werden konnte, dass ein Membrananker für die Aktivierung von Ire1 wichtig ist, konnte erst im Rahmen dieser Studie der molekulare Mechanismus der Aktivierung von Ire1 durch Lipid-*bilayer* Stress beschrieben werden. Basierend auf den gewonnenen Daten dieser Arbeit wurde ein Model für die Membran-vermittelte Aktivierung der UPR entwickelt: Die Insertion der hydrophoben Seite der AH von Ire1 führt lokal zu einer Kompression der Membran. Da Membrandicke und Acylkettenordnung miteinander verbunden sind, führt diese Kompression gleichzeitig zu einer lokal erhöhten Unordnung der Acylketten im hydrophoben Kern der Membran. *Molecular Dynamics* (MD) Simulationen von Roberto Covino und Gerhard Hummer (MPI für Biophysik, Frankfurt) belegen, dass die Kompression der Membran in einer Lipidumgebung mit hoher Packungsdichte stärker und großflächiger ist, als in einer Lipidumgebung mit niedriger Packungsdichte. Die energetischen Kosten für die lokale Membrankompression bei hoher Lipidpackungsdichte sind folglich erhöht, werden allerdings durch die Oligomerisierung von Ire1 minimiert. Dabei überlappen die ungeordneten und komprimierten Membranbereiche miteinander. Dementsprechend bildet die Minimierung der energetischen Kosten für die Membrandeformation von Ire1 die Basis für die Aktivierung von Ire1 durch Lipid-*bilayer* Stress.

Somit beruht die Aktivierung von Ire1 durch Lipid-bilayer Stress auf der Änderung von kollektiven, physiko-chemischen Membraneigenschaften, welche durch veränderte Lipidzusammensetzungen hervorgerufen werden. Die Konservierung einer putativen AH in zwei der drei UPR Sensoren von Säugern: dem Ire1 Ortholog IRE1 α und dem UPR Sensor PERK, legt nahe, dass dieser Mechanismus in ähnlicher Form in Eukaryonten konserviert sein könnte.

Abstract

The composition of cellular membranes is extremely complex and the mechanisms underlying their homeostasis are poorly understood. Organelles within a eukaryotic cell require a non-random distribution of membrane lipids and a tight regulation of the membrane lipid composition is a prerequisite for the maintenance of specific organellar functions. Physical membrane properties such as bilayer thickness, lipid packing density and surface charge are governed by the lipid composition and change gradually from the early to the late secretory pathway. As the endoplasmic reticulum (ER) is situated at the beginning of the cells secretory pathway, it has to accept and accommodate a great variety and quantity of secretory and transmembrane proteins, which enter the ER on their way to their final cellular destination. Secretory proteins can be translocated into the lumen of the ER co- or posttranslationally and membrane proteins are being inserted and released into the ER membrane. In the oxidative milieu of the ER-lumen, supported by a variety of chaperones, proteins can fold into their native form.

If the folding capacity of the ER-lumen is exceeded, an accumulation of mis- or unfolded proteins in the lumen of the ER occurs, consequently triggering the unfolded protein response (UPR). This highly conserved program activates a wide-spread transcriptional response to restore protein folding homeostasis. In fact, 7 – 8% of all genes in the yeast *Saccharomyces cerevisiae* (*S. cerevisiae*) are regulated by the UPR. The mechanism underlying the activation of the UPR by protein folding stress has been investigated thoroughly in the last decades and many of its mechanistic details have been elucidated. Recently, it became evident that aberrant lipid compositions of the ER membrane, collectively referred to as lipid bilayer stress, are equally potent in activating the UPR. The underlying molecular mechanism of this membrane-activated UPR, however, remained unclear.

This study focuses on the UPR in *S. cerevisiae* and characterizes the inositol requiring enzyme 1 (Ire1) as the sole UPR sensor in *S. cerevisiae*. Active Ire1 forms oligomers and, collaboratively with the tRNA ligase Rlg1, splices immature mRNA of the transcription factor *HAC1*, which results in the synthesis of mature *HAC1* mRNA and the production of the active Hac1 protein, which binds to UPR-elements in the nucleus and activates the expression of UPR target genes. Here, the combination of *in vivo* and *in vitro* experiments is being used, which is supplemented by molecular dynamics (MD) simulations performed by Roberto Covino and Gerhard Hummer (MPI for Biophysics, Frankfurt), aiming to identify the molecular mechanism of Ire1 activation by lipid bilayer stress. This study focuses on the analysis of the juxta- and transmembrane region of Ire1. Bioinformatic analyses revealed a putative ER-

luminal amphipathic helix (AH) N-terminally of and partially overlapping with the transmembrane helix (TMH). This predicted AH contains a large hydrophobic face, which inserts into the ER membrane, forcing the TMH into a tilted orientation within the membrane. The resulting unusual architecture of Ire1's AH and TMH constitutes a unique structural element required for the activation of Ire1 by lipid bilayer stress.

To investigate the function of the AH in the physiological context, different variants of Ire1 were produced under the control of their endogenous promoter and from their endogenous locus. The functional role of the AH was tested, by disrupting its amphipathic character by the introduction of charged residues into the hydrophobic face of the AH. The role of a conserved negative residue between the TMH and the AH (E540 in *S. cerevisiae*) was tested by substituting it by a unipolar, polar, or positively charged residue. These variants were intensively characterized using a series of assays:

This thesis provides evidence that the AH is crucial for the function of Ire1: Mutant variants with a disrupted (F531R, V535R) or otherwise modified AH (E540A) exhibited a lower degree of oligomerization and failed to catalyze the splicing of the *HAC1* mRNA as the Wildtype control. Likewise, the induction of *PDI1*, a target gene of the UPR, was greatly reduced in mutants with a disrupted or defective AH. These data revealed an important functional role of the AH for normal Ire1 function.

An *in vitro* system was established to analyze the membrane-mediated oligomerization of Ire1. This system enabled the isolated functional analysis of the AH and TMH during Ire1 activation by lipid bilayer stress. A fusion construct, coding for the maltose binding protein (MBP) from *Escherichia coli* (*E. coli*), N-terminally to the AH and TMH of Ire1 was produced. The heterologous production in *E. coli*, the purification and reconstitution of this minimal sensor of Ire1 in liposomes was established as part of this study. To analyze the oligomeric status of the minimal sensor in different lipid environments, *continuous wave* electron paramagnetic resonance (cwEPR) spectroscopic experiments were performed. These experiments revealed that the molecular packing density of the lipids had a significant influence of the oligomerization of the spin-labeled membrane sensor: increasing packing densities resulted in sensor oligomerization. The AH-disruptive F531R mutant, in which the amphipathic character of the AH was destroyed, showed no membrane-sensitive changes in its oligomerization status.

Thus, the activation of Ire1 by lipid bilayer stress is achieved by a membrane-based mechanism. According to the current model, the AH induces a local membrane compression by inserting its large hydrophobic face into the membrane. As membrane thickness and acyl

chain order are interconnected, this compression simultaneously results in an increased local disordering of lipid acyl chains. Supporting MD simulations performed by Roberto Covino and Gerhard Hummer revealed that the bilayer compression is significantly more pronounced in a densely packed lipid environment, than in a lipid environment of lower lipid packing density. Hence, the energetic cost of the local compression increases with the packing density of the membrane, but is compensated for by the oligomerization of Ire1. This minimization of energetic cost induced by the membrane deformation of Ire1 forms the basis for the activation of Ire1 by lipid bilayer stress.

1. Introduction

1.1. The complexity of biological membranes

Biological membranes act as selective barriers in cells and separate the intracellular milieu from the extracellular environment (van Meer et al., 2008; Pietzsch, 2004). The organelles of eukaryotes exhibit membranes with characteristic lipid compositions, which play an active role in shaping the organelle properties and function thereby defining their identity (1.1.2) (Bigay and Antony, 2012; Hammond et al., 2012; van Meer et al., 2008). Biological membranes are semi-permeable, allowing for selective exchange from one compartment to another, active participation in cellular communication and play an important role in signal transduction (Simons and Toomre, 2000). The ability to fulfill these tasks is achieved by the complex membrane lipid and protein compositions (van Meer et al., 2008). The maintenance of a specific protein and lipid composition despite the tremendous complexity of biological membrane systems is thus pivotal for cellular life.

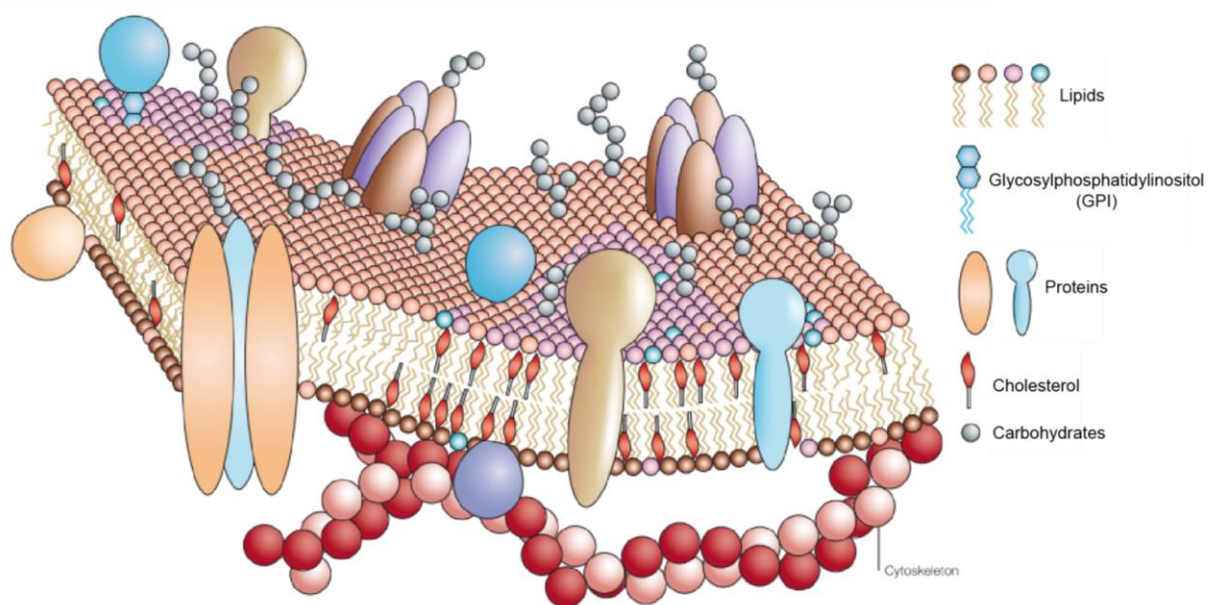


Figure 1 | The Fluid-Mosaic-Model of cell membranes.

Functional membranes are complex mosaic-like structures composed of phospholipids, cholesterol and proteins. Within the two-dimensional bilayer, lateral transfusion occurs, while transverse movement is impeded. Figure adapted from Pietzsch *et al.*, (Pietzsch, 2004.).

The Fluidic-Mosaic Model (Fig.1) was proposed in 1972, to describe the structural and dynamic properties of biological membranes and their constituents (Singer and Nicolson,

1972). A lipid bilayer is formed by the self-assembly of phospholipids to result in functional membranes as fluid and dynamic mosaic-like structures (Singer and Nicolson, 1972). The natural repulsion between lipids and water drives the self-assembly of the lipid bilayer as hydrophobic effect (Singer and Nicolson, 1972). Membrane proteins are embedded into the lipid bilayer where they can interact with the membrane lipids by electrostatic interactions and hydrogen bonding to participate in the macromolecular structure of these two-dimensional fluidic structures (Singer and Nicolson, 1972). More than 30% of all protein coding genes translate into membrane proteins, highlighting the importance of these proteins for cellular function (Krogh et al., 2001; Pietzsch, 2004). While some membrane proteins span the lipid bilayer (transmembrane (TM) proteins, tail-anchored proteins), others are thought to be embedded in only one membrane leaflet (hairpin proteins). Other classes of membrane proteins are peripherally attached to lipids or membrane-spanning proteins or covalently linked to lipid anchors (e.g. Glycosylphosphatidylinositol (GPI)-anchored proteins) (Lingwood and Simons, 2010; Pietzsch, 2004; Singer and Nicolson, 1972). Membrane proteins play an important role in many cellular processes such as the selective transport of substrates across membranes and intracellular signaling. They act as receptors for cell growth and development, are involved in the immune response, hormone action and neuronal signaling, among many other functions (Coskun et al., 2011; Drbal et al., 2007; Pietzsch, 2004; Simons and Toomre, 2000; Sohn et al., 2008).

It has become evident that membrane lipids are co-players in many physiological processes and modulate protein function. The self-organization of lipids and proteins has been shown to laterally subcompartmentalize biological membranes (Lingwood and Simons, 2010; Simons and Vaz, 2004). Biological membranes can form short-lived, nanoscale assemblies, such as lipid rafts, enriched for sphingolipids (SL), cholesterol, which can selectively enrich for membrane proteins with an higher partition coefficient for nanodomains of increased lipid order (Bagnat and Simons, 2002; Bagnat et al., 2000; Levental et al., 2010; Lingwood and Simons, 2010; Simons and Toomre, 2000). The increased local protein concentration that is facilitated by lipid connectivity is crucial in cellular signaling and vesicular trafficking (Hancock, 2006; Lingwood and Simons, 2010; Simons and Vaz, 2004). The size and stability of lipid rafts varies with temperature and is dependent on the lipid and protein composition of the bilayer. Upon clustering, e.g. due to ligand binding, receptor molecules can coalesce their lipid nanodomains into signaling-active platforms, which can attract additional proteins solely based on their preference for certain membrane properties.

The propensity to form lipid rafts in the plasma membrane is strong, as it contains high levels of cholesterol (van Meer et al., 2008; Mesmin and Maxfield, 2009). The TM protein linker of activated T-cells (LAT), for example, is located in the plasma membrane of T-cells and an obligate component of lipid rafts during the formation of the immunological synapse (Zech et al., 2009). Lipid rafts contribute significantly to the sorting of GPI-anchored proteins and are crucial for the clathrin-independent endocytosis (Mayor and Pagano, 2007). Moreover, lipid rafts have been implicated in the signaling of the human epidermal growth factor receptor (EGFR) (Coskun et al., 2011), the T-cell receptor (TCR) (Drbal et al., 2007) and the B-cell receptor (BCR) (Sohn et al., 2008).

1.1.1. Diversity of the cellular lipidome

Eukaryotic cells use approximately 5 % of their genes to synthesize a diverse repertoire of lipids. Lipids can serve as membrane building blocks or storage lipids such as triacylglycerol (TAG) and sterol esters. Some membrane lipids have important signaling functions as second messengers and to mark certain cellular territories for the molecular membrane recognition (van Meer et al., 2008). The GPL phosphatidylinositol (PI), for example, is substrate for a variety of lipid kinases and phosphatases and modified to form many kinds of phosphoinositides (PIP's). These PIP's, in turn, are substrates of phospholipases, which release second messengers. The phospholipase C, for instance, hydrolyses phosphatidylinositol(4,5)-biphosphate to generate diacylglycerol (DAG) and phosphatidylinositol(1,4,5)-triphosphate in response to external stimuli (Strahl and Thorner, 2007). In yeast, PI derived molecules have been firmly implicated in vesicular membrane trafficking and MAP kinase signaling (Strahl and Thorner, 2007). This work will mainly focus on the role of cellular lipids as building blocks and their impact on cellular signaling via collective membrane properties.

Eukaryotic membrane lipids are categorized in GPL's, sphingolipids (SL's) and sterols (Fig. 2). GPLs and SLs share the same general structure with a polar headgroup, defining the lipid class, and two hydrophobic hydrocarbon chain moieties (Holthuis and Levine, 2005; Klose et al., 2013; van Meer et al., 2008). While the hydrocarbon chains vary in length and their degree of saturation and/or hydroxylation, lipid headgroups differ in their charge, shape, and chemistry (Holthuis and Levine, 2005; Klose et al., 2013; van Meer et al., 2008).

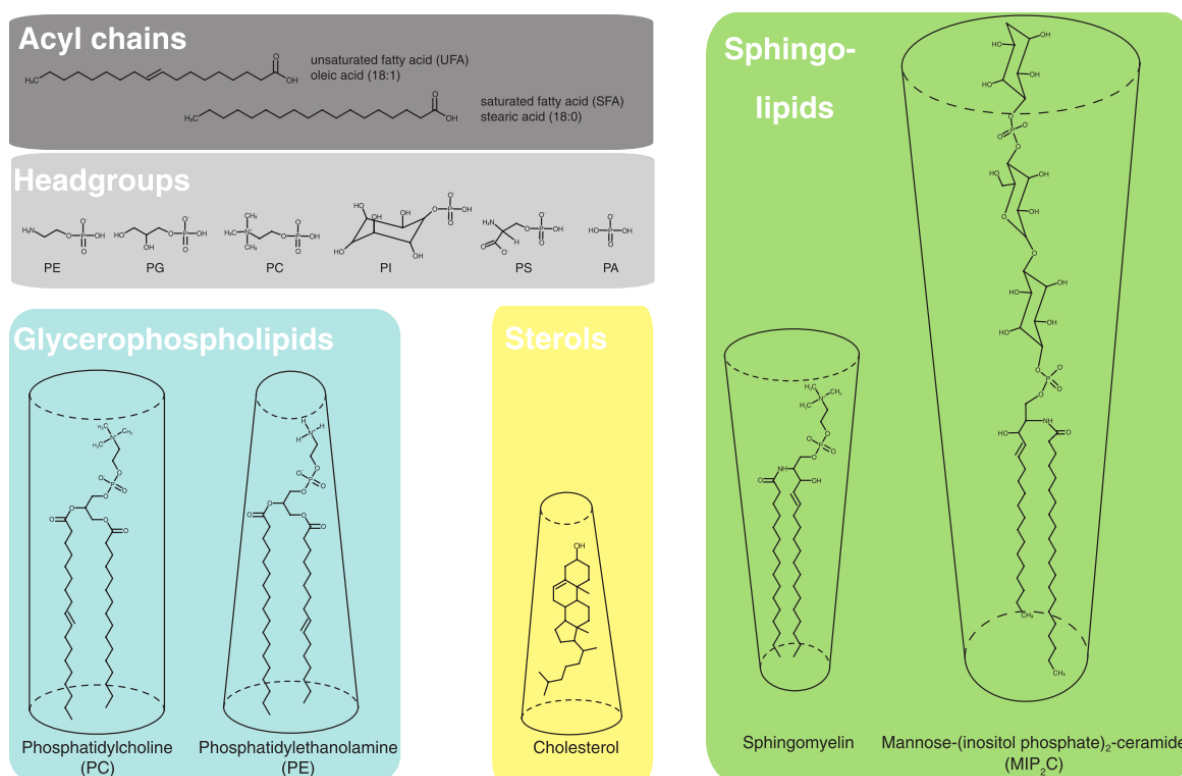


Figure 2 | Lipid species differ in shape and chemistry.

Three abundant classes of lipids are the major building blocks of biological membranes: Glycerophospholipids (GPL; blue), sterols (yellow) and sphingolipids (SL; green). GPL's vary in their headgroup (light grey) and acyl chain (dark gray) composition. Depicted is the relative size and shape of Phosphatidylcholine (PC; with 18:1, 16:0 fatty acids), Phosphatidylethanolamine (PE; with 18:0, 16:1 fatty acids), cholesterol, sphingomyeline and MIP₂C. Lipid diversity derives from the combination of depicted headgroups and diacylglycerol (forming GPL's) or a ceramide backbone (forming SL's) with a variety of different acyl chain compositions. Illustration taken from Stordeur *et al.* (Stordeur *et al.*, 2014).

The different classes of GPLs: phosphatidic acid (PA), phosphatidylcholine (PC), phosphatidylethanolamine (PE), phosphatidylserine (PS) or phosphatidylinositol (PI), are the major lipid components of eukaryotic membranes. In most cases, the two fatty acids are esterified to the glycerol backbone at the *sn*-1 and *sn*-2 positions. As the length and the degree of saturation of these aliphatic chains varies and by their combination the repertoire of GPLs is rather complex (Sud *et al.*, 2007). In the baker's yeast the complexity of the lipid acyl chains is limited, because *S. cerevisiae* encodes only a single fatty acid desaturase (Ole1), a Δ^9 -desaturase, which converts palmitic acid (16:0) and stearic acid (18:0) into monounsaturated palmitoleic (16:1) and stearic (18:1) fatty acid species (Stukey *et al.*, 1990). Mammals can ingest saturated membrane phospholipids and generate UFAs, as they possess a much larger variety of fatty acid desaturases: the Stearoyl-CoA desaturase-1 (SCD-1), a Δ^9 -desaturase, which acts similar to Ole1, as well as Δ^5 and Δ^6 -desaturases, which can synthesize mono-, di- or poly-unsaturated fatty acids (UFAs), resulting in a variety of thousands of different species

(Nakamura and Nara, 2003, 2004). The degree of acyl chain saturation, as well as physicochemical properties of the polar headgroups have a major impact on the molecular lipid packing of the lipids and the resulting membrane thickness. Longer and more saturated acyl chains form thicker and more rigid membranes, compared to shorter, unsaturated ones. The steric and electrostatic characteristics of the polar headgroups influence the molecular lipid packing and the lateral pressure profile (Coskun and Simons, 2011; Holthuis and Levine, 2005; van Meer and Vaz, 2005). In the yeast *Saccharomyces cerevisiae* (*S. cerevisiae*; also termed yeast throughout this work) PC, PI and PE are the most abundant classes of GPLs (Zinser et al., 1991).

SL's are a lipid category that increases in concentration along the secretory pathway. They fulfill a structurally important role as they have the potential to form hydrogen bonds with cholesterol. SL's are composed of a long chain sphingoid base (generally C₁₈) that is linked to a saturated C₁₆ to C₂₆ fatty acid, resulting in a ceramide (Dickson, 1998). The types of ceramides differ in different organisms. In yeast, sphingolipids mostly contain a PI head group (forming inositol sphingolipids) and are generally mannosylated. In mammals, the head group of sphingolipids is PC (forming sphingomyelin), PE (ethanolaminephosphoryl ceramide) or a monosaccharide chain that is linked to the ceramide moiety (forming a glycosphingolipid). Other types of glukosphingolipids are gangliosides, which are characterized by their complex glycan structures composed of up to seven monosaccharides (Ernst et al., 2016; van Meer et al., 2008). Gangliosides play an important role in the determination of blood groups (Yamakawa and Iida, 1953). In addition to the role of sphingolipids as structural lipids, the sphingolipid precursor ceramides play an important role as second messengers in cell signaling, resulting in cell cycle arrest, apoptosis, or senescence (Dickson, 1998).

The third category of lipids, sterols, is unique in structure and function. The concentration of sterols in the membrane is tightly controlled and increases along the secretory pathway. While ergosterol is the most abundant sterol in the membranes in *S. cerevisiae*, cholesterol is a component of mammalian cell membranes. Although sterols are synthesized in the endoplasmic reticulum (ER) both in mammals and yeast, the molar concentration of sterols is rather low in this organelle. However, the sterol concentration increases along the secretory pathway and makes up 30-40 mol% of all plasma membrane lipids (Goldstein et al., 2006; Holthuis and Menon, 2014; van Meer et al., 2008; Radhakrishnan et al., 2008). A striking functional feature of sterols is that they have the potential to fluidize gel phases, while it increases the acyl chain order of GPLs and SL in the membrane (Holthuis and Menon, 2014; van Meer et al., 2008; Radhakrishnan et al., 2008). The potential of sterols to form hydrogen

bonds with SLs to promote lipid raft formation has already been discussed (Lingwood and Simons, 2010; Simons and Vaz, 2004).

1.1.2. Lipid composition correlates with organelle function

Collective physicochemical membrane properties such as the bilayer thickness, the molecular lipid packing density and the surface charge change along the secretory pathway and are crucial to specific different membrane territories of the cell (Holthuis and Menon, 2014). The membranes of organelles in the early secretory pathway (ER to cis-Golgi) exhibit a rather low negative surface charge density on their cytosolic leaflet and are characterized by a rather high density of lipid packing defects (Bigay and Antonny, 2012). Membranes of the late secretory pathway, such as the trans-Golgi network, secretory vesicles, endosomes, and the cytosolic leaflet of the PM, are characterized by a much tighter molecular lipid packing and an increased content of anionic lipids in the cytosolic membrane face (Bigay and Antonny, 2012; Fairn et al., 2011).

The ER is a major site of lipid biosynthesis (Bell et al., 1981) and its membrane is composed of all major classes of GPLs and sterols (cholesterol in mammals, ergosterol in yeast) (Fig. 3) (van Meer et al., 2008; Zinser et al., 1991). Moreover, the ER plays a fundamental role for the folding and post-translational modification of secretory and membrane proteins. In fact, the ER marks the entry point of the secretory pathway. The sorting of transmembrane proteins along the secretory pathway was hypothesized to rely, at least in part, on the hydrophobic thickness of the protein and the surrounding membranes: The average length of transmembrane helices (TMHs) increases along the secretory pathway from the ER to the plasma membrane just as the molecular lipid packing density (Bretscher and Munro, 1993; Kaiser et al., 2011a; van Meer et al., 2008; Mitra et al., 2004; Sharpe et al., 2010). The ER must accommodate TM proteins of all different lengths and the lipids of the ER membrane must adapt to the resulting hydrophobic mismatch by 'stretching' their hydrophobic tails, which also results in a local lipid ordering. Crucial to this elasticity of membrane thickness is a low membrane compression modulus, due to a low sterol content and a high molar fraction of lipids with two unsaturated fatty acyl chains (Kaiser et al., 2011a). In fact, the cholesterol level in the ER membrane of mammalian cells is tightly regulated and maintained at ~5 mol% of the total lipids (Goldstein et al., 2006; Holthuis and Menon, 2014; van Meer et al., 2008; Radhakrishnan et al., 2008). At higher concentrations of sterols the energetic burden of hydrophobic mismatches increases significantly (Kaiser et al., 2011a), a phenomenon is exploited for protein sorting (Kaiser et al., 2011a; Quiroga et al., 2013).

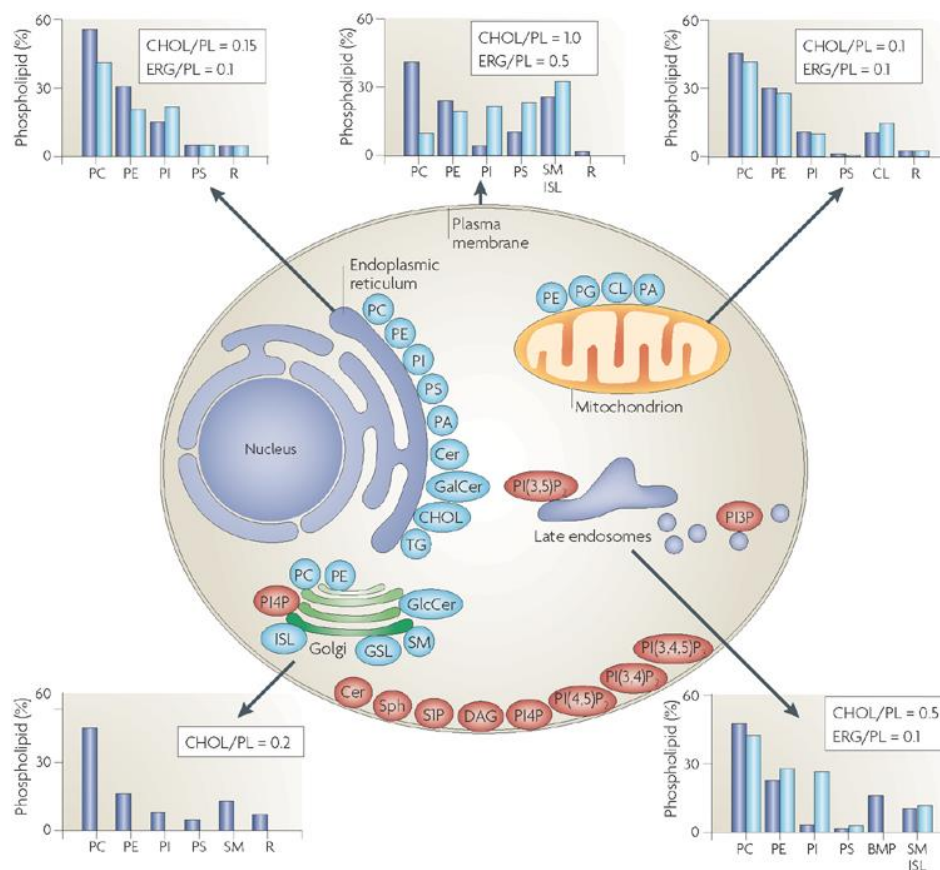


Figure 3 | Lipid synthesis and composition of different organelles in eukaryotic cells.

The distribution of lipids varies from one organelle to another. The lipid compositions of indicated organelles are shown in graphs as a percentage of total GPLs (PLs) for mammals (dark blue) and yeast (light blue). The sterol content is depicted as a molar ratio of cholesterol (CHOL) or ergosterol (ERG) to GPLs. The sites of lipid synthesis are indicated by a blue background color, while lipids involved in signaling pathways are depicted in red. The ER is the major site of lipid synthesis and assembles all prominent GPL classes, among other lipids. The molar fraction of sterols increases along the secretory pathway. The plasma membrane contains the highest proportion of sphingolipids and sterols. Mitochondrial membranes resemble the lipid composition of bacteria. This illustration is adapted from van Meer *et al.* (van Meer *et al.*, 2008).

Lipid synthesis (e.g. of PLs and SLs) (Fig. 3) and sorting also take place further downstream of the secretory pathway, at the Golgi complex. Here, membrane material is packaged into vesicular carriers of different lipid content to form lipid raft-like platforms (Coskun and Simons, 2011; Klemm *et al.*, 2009; Simons and Gerl, 2010; Surma *et al.*, 2011). The plasma membrane (PM) of unicellular organisms, such as yeast, often faces prompt and vigorous environmental changes (van Meer *et al.*, 2008). Therefore, the most crucial function of the plasma membrane is to protect the cell and maintain the cytosolic milieu (Ejising *et al.*, 2009; Schneiter *et al.*, 1999). A prerequisite of a low permeability of the plasma membrane is a particularly dense lipid packing, which is achieved by SLs, sterols and saturated GPLs (Holthuis and Levine, 2005; Klemm *et al.*, 2009; van Meer *et al.*, 2008).

The ER, Golgi, plasma and endosomal membranes of eukaryotic cells are all asymmetric. In mammals, the outer leaflet of the plasma membrane is enriched for PC and SM, while aminophospholipids such as PS and PE are preferentially located in the inner membrane leaflet (Holthuis and Levine 2005). The plasma membrane of yeast is also asymmetric and contains enriched levels of inositol sphingolipids and ergosterol in the outer leaflet, while PS and PE are enriched in the inner leaflet (Devaux, 1991). This asymmetry is generated by the interplay of aminophospholipid flippases for the inward transport of lipids and lipid broadly specific lipid floppases for transport in the opposite direction (Graham, 2004).

In the ER, most lipids distribute symmetrically across both leaflets due to the activity of unspecific ER flippases allowing for bi-directional transverse lipid transport (Vishwakarma et al., 2005). Recent studies with genetically encoded PS probes, however revealed that PS is distributed asymmetrically: PS is enriched in the inner leaflet of the ER membrane, revealing an asymmetric distribution opposite to that of PS in the plasma membrane (Fairn et al., 2011). It has been speculated, that this PS distribution is based on accessibility to phospholipases and it remains unclear to date, what the specific function of this PS asymmetry of the ER membrane is (Fairn et al., 2011).

1.2. The ER and its cellular function

1.2.1. Architecture of the ER

The ER is a continuous membrane system with a continuous interluminal space spanning the entire cell periphery. It exhibits morphologically and functionally distinct regions that comprise the outer nuclear membranes, ER-sheets, ER-tubules and a dense network of tubular matrices, which altogether make up ~50 % of all membranes content in eukaryotic cells (Goyal and Blackstone, 2013; Nixon-Abell et al., 2016; Pietzsch, 2004; Voeltz et al., 2002). These distinct structures are highly dynamic and can be remodeled in response to cellular needs (Nixon-Abell et al., 2016; Puhka et al., 2012). The ER network in higher eukaryotes is formed by juxta-nuclear sheets and tubular structures in the cell periphery (Fig. 4) (Goyal and Blackstone, 2013; Puhka et al., 2007). Visualization of the ER by electron microscopy revealed structurally distinct domains: Rough ER (RER) and smooth ER (SER). The RER is formed by ER-sheets decorated with translating ribosomes, a major site of co-translational protein translocation, protein quality control and modification of secreted and transmembrane proteins (Goyal and Blackstone, 2013; Park and Rapoport, 2012; Ron and Walter, 2007). The tubular, smooth ER (SER) forms an interconnected network throughout the entire cell periphery and

is functionally associated with lipid synthesis, metabolism of carbohydrates and the formation of membrane contact site with other organelles (Elbaz and Schuldiner, 2011; Henry et al., 2012; Park and Blackstone, 2010; Schuldiner and Weissman, 2013; Shibata et al., 2006). Although the SER was originally believed to exclusively comprise peripheral sheets, recent studies at increased spatiotemporal resolution revealed that these structures are also partly made of highly dynamic dense tubular matrices (Nixon-Abell et al., 2016).

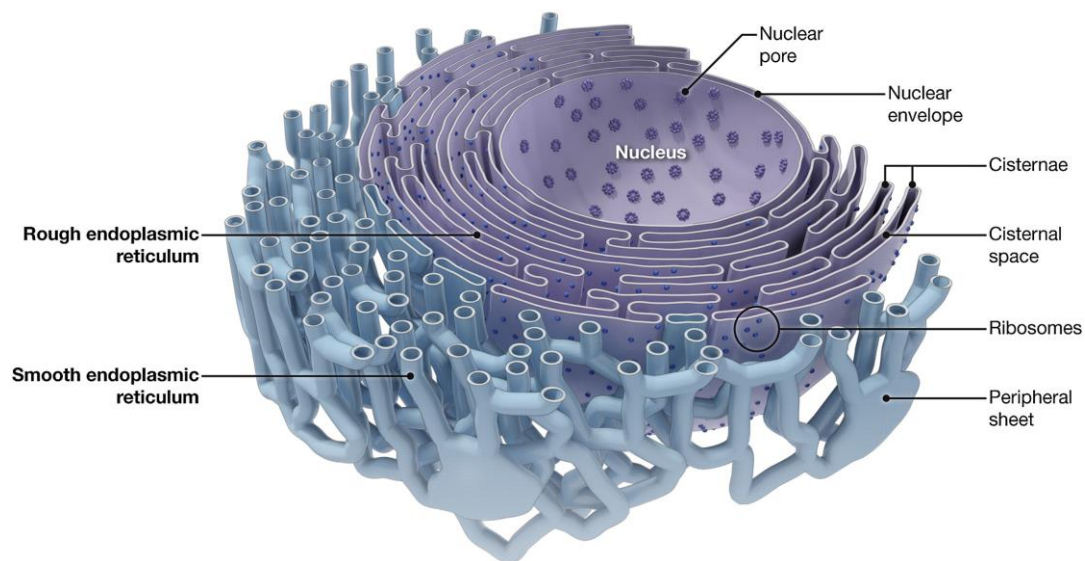


Figure 4 | Structure of the ER network in eukaryotic cells.

Illustrated are the different structural features of the continuous ER membrane system. Encapsulating the nucleus, the ribosome decorated rough ER (RER) is extending throughout the cell forming ER sheet structures (violet). The smooth ER (SER) tubules spread into the cell periphery (blue). This illustration is adapted from Goyal and Blackstone (Goyal and Blackstone, 2013).

In *S. cerevisiae*, a large portion of the ER is found closely juxtaposed to the plasma membrane and connected with the nuclear envelope only by a few tubules (Koning et al., 1993; Prinz et al., 2000). Hence, these two regions of the ER are referred to as the nuclear and the cortical ER (Fig. 5) (Voeltz et al., 2002).

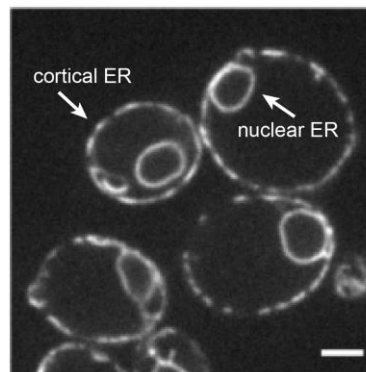


Figure 5 | ER morphology of *S. cerevisiae*.

A confocal fluorescence micrograph of live yeast cells producing Sec63-GFP highlights different domains of the ER membrane: The nuclear ER and the cortical ER. This illustration was adapted from Schuck *et al.* (Schuck *et al.*, 2009).

1.2.2. Cellular function of the ER

A major function of the ER is the folding of membrane and secretory proteins and their quality control. To achieve protein insertion into the ER, co- and post-translational modes of protein translocation take place. Proteins targeted to the ER or other compartments of the secretory pathway enter the ER co-translationally as nascent polypeptide chains through the translocon, a proteinaceous channel in the ER membrane (Zimmermann *et al.*, 2011). In contrast to the cytosol, the lumen of the ER has an oxidative milieu. It also contains many chaperones to promote protein folding, and enzymes enabling co- and post translational modifications, such as disulfide-bond formation, signal sequence cleavage and N-glycosylation and GPI-anchor addition, to promote correct protein folding (Anelli and Sitia, 2008; Ellgaard and Helenius, 2003; Hebert and Molinari, 2007).

Folding of the translocated proteins occurs co- and post-translationally in the ER-lumen, a process that requires a variety of chaperones (Ellgaard and Helenius, 2003; Hebert and Molinari, 2007). These ER-luminal chaperones assist the folding of proteins and their assembly into oligomeric structures by interacting with folding intermediates and the nascent polypeptide chain to prevent misfolding and irreversible aggregation. When protein folding fails, the ER associated degradation (ERAD) machinery retro-translocates the misfolded proteins into the cytosol for ubiquitin dependent proteasomal degradation (Ellgaard and Helenius, 2003; Hebert and Molinari, 2007; Hegde and Ploegh, 2010; Printsev *et al.*, 2016).

The ER is the major site of lipid synthesis within the cell. The lipid metabolic network of the ER is highly complex and the biosynthetic pathways are interconnected. Many enzymes are

required for synthesis of GPLs at the ER membrane (Henry et al., 2012; van Meer et al., 2008; Zinser et al., 1991) and as it turns out, it is impossible to interfere with specific steps of lipid metabolism by mutagenesis or pharmacological means without inducing ripple effects throughout the entire lipidome (Ernst et al., 2016; Stordeur et al., 2014).

How exactly the ER senses imbalances sterol content and phospholipid composition is not fully understood and subject to this work. It has been suggested, however that an imbalance in ER membrane lipid composition, e.g. an increase in GPL saturation induces lipid bilayer stress and activates the unfolded protein response (Deguil et al., 2011; Pineau et al., 2009; Promlek et al., 2011; Surma et al., 2013; Thibault et al., 2012; Volmer et al., 2013).

1.2.3. Yeast as a model system to study ER homeostasis

Already in the 1980's, Botstein and Fink established the yeast *S. cerevisiae* as a model organism to study functional genomics (Botstein and Fink, 1985). Several decades later, the yeast *S. cerevisiae* has evolved to a general model organism for eukaryotic cell biology, which has helped tremendously to understand diverse aspects of cell biology and paved the way towards a eukaryotic systems biology (Botstein and Fink, 2011). Genetic manipulation of *S. cerevisiae* by homologous recombination is feasible, and the rapid growth and simple cultivation of yeast in strictly defined medium conditions has led to the use of yeast as a model system to generate libraries of genetically manipulated deletion libraries to perform systematic screenings. As pathways in lipid synthesis and subcellular organization are highly conserved among eukaryotes (Daum et al., 1998; Lykidis, 2007), *S. cerevisiae* is an appropriate model system to study ER homeostasis.

Despite the reduced complexity of the system, studies in yeast made it possible to identify and characterize previously non-described genes and to identify their orthologs in higher eukaryotes (Botstein and Fink, 2011) and a great variety of pathogenic conditions in humans can be recapitulated in yeast.

1.3. Integral and membrane-associated membrane property sensors

Dedicated integral and membrane-associated membrane property sensors have evolved as a strategy to measure bulk membrane properties and are particularly sensitive to alterations in levels of these specific membrane components (Fig. 6 and 7). Membrane property sensors are either embedded in the lipid bilayer as integral, α -helical membrane proteins or are soluble

proteins, which require membrane recruitment prior to performing their task of membrane property sensing. Sensor proteins that span the membrane use α -helical TMHs. A typical TMH comprises 18–23 hydrophobic amino acid residues, with only few polar residues. TMH and juxta-membrane regions of integral membrane are ideally positioned to sense the lipid bilayer properties and represent major sites for lipid interaction. In contrast, soluble proteins are recruited to their target membranes by amphipathic helix (AH) motifs. These AHs of conditionally membrane-associated proteins are unstructured in aqueous solution and fold into an α -helix only upon membrane binding (Segrest et al., 1990). Despite the differences of integral and soluble membrane property sensors, the α -helix emerges as key structural motif for lipid and membrane sensing (Puth et al., 2015).

In the following, several examples for integral membrane property sensors from different organisms will be discussed more extensively (Fig. 6).

The mechanism of activation of the prokaryotic sensor for membrane lipid saturation, DesK, which controls fatty acid desaturation in *Bacillus subtilis* (*B. subtilis*), has been studied extensively (Aguilar et al., 2001; Altabe et al., 2003; Cybulski et al., 2004, 2010; Inda et al., 2014). The polytopic TM protein DesK employs a signaling machinery, which switches between a kinase-active and a phosphatase-active state in response to changes in membrane thickness to control the expression of the sole Δ^5 acyl-lipid desaturase (Altabe et al., 2003). Fatty acid desaturation is crucial to maintain lipid packing and membrane functions, so it comes as no surprise that eukaryotes also employ mechanisms to regulate the membrane lipid saturation.

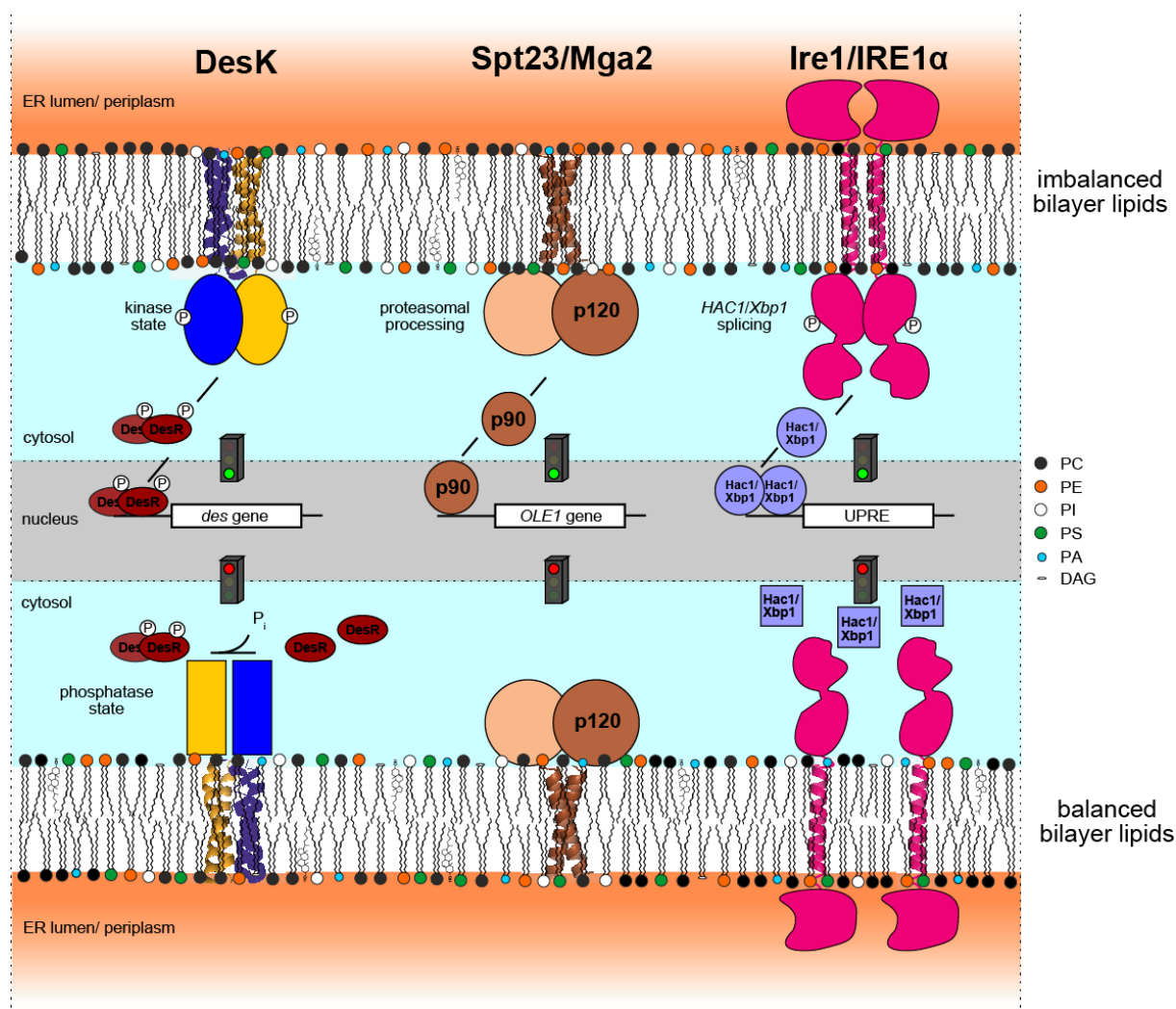


Figure 6 | Transcriptional regulation of dedicated TM sensor proteins.

Aberrances in lipid homeostasis are sensed by dedicated integral membrane sensors. The bacterial sensor for membrane lipid saturation in *B. subtilis*, DesK, switches from a phosphatase to a kinase state when the ambient temperature or lipid saturation thickens the membrane. Phosphorylation of DesR by the kinase mediates the induction of *des*, the gene encoding for the sole Δ^5 acyl-lipid desaturase in *B. subtilis*. Mga2 and Spt23 are transcriptional activators of the sole Δ^9 fatty acid desaturase in *S. cerevisiae*, Ole1. When lipid saturation in the ER membrane is increased, Mga2 and Spt23 are activated by proteasomal cleavage, which is mediated by components of the ERAD machinery to release the soluble and active form, p90. The p90 form of Mga2 and Spt23 travels to the nucleus where it activates the expression of *OLE1*. The UPR sensor Ire1 is conserved from yeast to man. When activated, Ire1 oligomerizes, leading to an activation of the cytosolic RNase domains. In an unconventional splicing reaction, Ire1 splices the mRNA of the transcription factor *HAC1/Xbp1* mRNA, which is in turn translated, travels to the nucleus and activates the expression of UPR target genes. This illustration is adapted from Puth *et al.* (Puth *et al.*, 2015).

The fungal transcription factors Spt23 and Mga2 sense the requirement for lipid desaturation in the ER membrane (Covino *et al.*, 2016; Degreif *et al.*, 2017). In their inactive form, these single-pass membrane proteins reside in the ER membrane as membrane bound precursors of 120 kDa (p120). During activation, ubiquitylation of several lysine residues in Mga2 and Spt23 is performed by the E3 ubiquitin-protein ligase Rsp5, and proteolytic processing of the precursors is mediated by the proteasome and facilitated by Cdc48 and Ubx2, components of

the ERAD machinery. Active transcription factors (p90) are released, which promote the transcription of *OLE1* and ultimately the production of the Δ^9 -fatty acid desaturase Ole1 (Hoppe et al., 2000; Rape et al., 2001).

Recently, it became evident that Mga2 acts as a lipid-packing sensor to control the production of unsaturated fatty acids (Covino et al., 2016). The TMH of Mga2 p120 homo-dimers has a pivotal role in this intra-membrane sensing mechanism. The TMHs of Mga2 rotate against each other and different degrees of lipid saturation stabilize alternative rotational orientations. A tryptophan residue (W1042) is positioned deep within the membrane, ideal to sense membrane voids in a loosely packed lipid bilayer. It has been proposed, that the bulky side chain of the tryptophan may be easier to accommodate in a more disordered, hence loosely packed lipid bilayer, as compared to a more saturated and more ordered lipid bilayer (Covino et al., 2016). Therefore, increased saturation of the lipid bilayer would favor an inward rotation of the tryptophan, hence an alternative orientation is stabilized in which the tryptophan resides at the helix-helix-interface of the Mga2 dimer (Covino et al., 2016). It has been hypothesized, that these rotational repositions make several lysine residues at the N-terminal juxta-membrane region of Mga2 accessible for ubiquitylation, as a signal for subsequent processing of Mga2 and, release of the active transcription factor p90 to restore homeostasis of the ER membrane (Covino et al., 2016).

Soluble proteins that act as membrane property sensors use AHs for membrane recruitment and sensing (Fig.7). AHs bearing a polar and a non-polar face. The polar face remains exposed to the aqueous environment and can interact with the lipid headgroups of the lipid bilayer. The non-polar, hydrophobic is formed by mostly apolar and aromatic amino acids that penetrate into the lipid bilayer to sense acyl chain composition at the hydrophobic core of the membrane (Antonny, 2011). Correlating with the physicochemical properties of the target membranes, the structural properties of sensory AHs may vary to warrant selective membrane recognition. AHs binding to membranes of the early secretory pathway such as amphipathic lipid packing sensors (ALPS), bear serine (S; the single letter code for amino acids will be used throughout this work), glycine (G) and threonine (T) residues in their polar face and bulky hydrophobic, especially aromatic, residues in the non-polar face, which enables them to intercalate into lipid packing defects. As lipid packing defects increase with increasing membrane curvature, the ALPS motif is also a common feature in membrane curvature sensors of the early secretory pathway (Antonny, 2011; Bigay et al., 2005; Drin et al., 2007).

There is a variety of cytosolic proteins that control membrane lipid homeostasis in membranes of the early secretory pathway by probing cellular membrane composition utilizing AHs (Fig. 7).

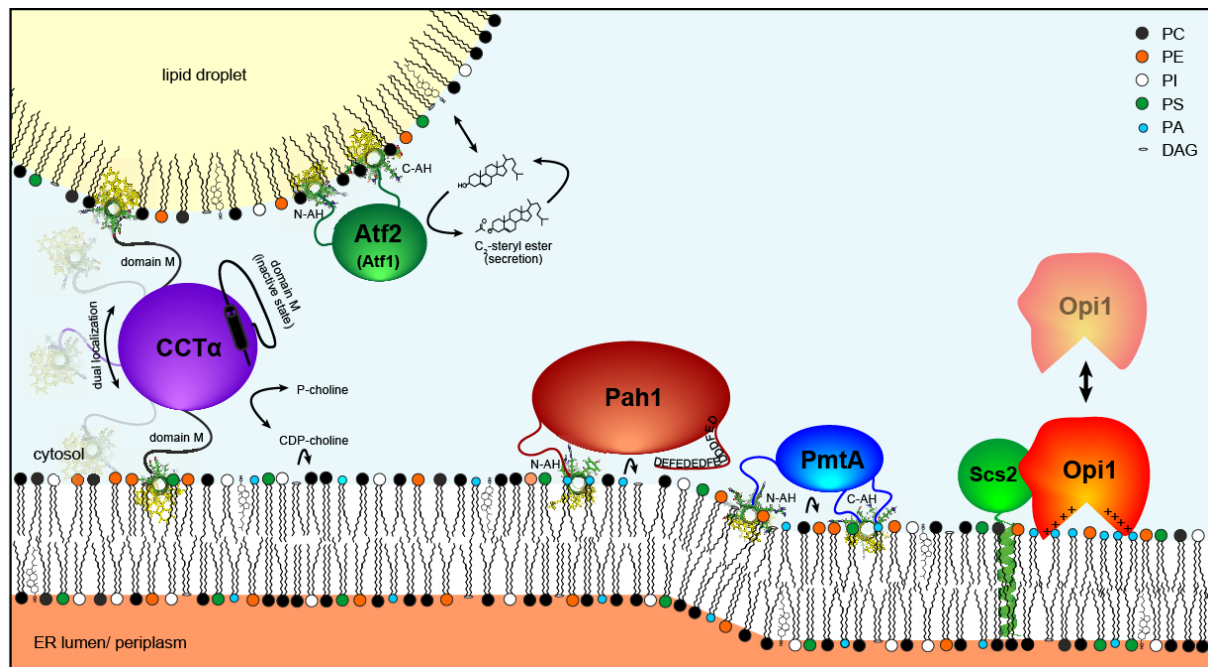


Figure 7 | Soluble membrane sensors bearing amphipathic helix (AH) motifs to sense membrane properties.

Cytosolic proteins control membrane lipid homeostasis by probing cellular membrane composition. The acyltransferases Atf1 and Atf2 employ two AHs (N- and C-terminal) required for localization to lipid droplets and the regulation of sterol content in yeast. The mammalian CTP:phosphocholine cytidyltransferase CCT α regulates PC synthesis via the Kennedy pathway by sensing lipid packing defects at lipid droplets and the ER membrane. The phosphatidate phosphatase Pah1 and Opi1 are sensors for PA in the ER membrane of *S. cerevisiae*. While Pah1 is recruited to PA-rich membranes via its N-terminal AH and catalyzes the dephosphorylation of PA to DAG, the transcriptional repressor Opi1 regulates the expression of PL biosynthetic genes. The bacterial phospholipid methyltransferase PmtA recognizes anionic lipids via its N-terminal AH and induces the formation of PC via the CDP-DAG pathway. This illustration is adapted from Puth *et al.* (Puth *et al.*, 2015).

Atf1 and Atf2, for example, are acyltransferases employing two AHs (N- and C-terminal) required for localization to lipid droplets and regulate the content of sterols in the ER-membrane of yeast (Tiwari *et al.*, 2007). The mammalian CTP:phosphocholine cytidyltransferase (CCT α) also resides at lipid droplets and the ER membrane, where it senses lipid packing defects and regulates PC synthesis via the Kennedy pathway (Danne *et al.*, 2015; Krahmer *et al.*, 2011). The phosphatidate phosphatase Pah1 and Opi1 are sensors for PA in the ER membrane of *S. cerevisiae*. While Pah1 is recruited to PA-rich membranes via its N-terminal AH and catalyzes the dephosphorylation of PA to DAG, Opi1 is a transcriptional repressor, which regulates the expression of PL biosynthetic genes (Henry *et al.*, 2012; Hofbauer *et al.*, 2014).

The binding of AHs in the late secretory pathway is not driven by their insertion into lipid packing defects, but mediated by hydrophobic and electrostatic interactions. Consequently, the design of these AHs differs strongly from the previously described ALPS motifs (Bigay and Antonny, 2012). A well described example of an AH in the late secretory pathway is the synaptic vesicle protein α -synuclein, which lacks bulky hydrophobic residues on the non-polar side and contains positively charged lysine residues in the polar face of the AH (Chandra et al., 2003; Pranke et al., 2011). The enrichment for charged residues in α -synuclein's polar face and lack of large residues on the non-polar side explains its selectivity for membranes of the late secretory pathway where membrane lipid packing is relatively high and AH binding is not governed by lipid packing defects (Bigay and Antonny, 2012; Drin and Antonny, 2010). This finding highlights that ionic protein-lipid interactions govern the recruitment of AHs in the late secretory pathway independent of membrane curvature (Antonny, 2011).

1.4. Correlating ER-stress and lipid metabolism

The ER is the major compartment for membrane biogenesis, which raises the question how the diverse cellular functions of this organelle (lipid synthesis, membrane protein insertion, folding and quality control) are coordinated. The ER employs a cellular surveillance system, the UPR, which monitors the load of mis- and unfolded proteins in the ER lumen. Moreover, the UPR regulates critical aspects in lipid metabolism and ER expansion, which serve as a mechanism to counterbalance ER luminal protein folding stress.

The great research effort in this field within the last decades elucidating how the ER is capable of orchestrating all these tasks strongly suggest that the homeostasis of lipids and proteins are interdependent. Along these lines, it comes as no surprise that a homeostatic program dealing with protein induced ER-stress also counteracts lipid induced ER-stress. Indeed, activation of the UPR by various perturbations in lipid metabolism has been reported. This connection is highlighted by increasing evidence suggesting that neurodegenerative disorders of the proteostasis network including Alzheimer's (AD) and Parkinson's disease (PD) are not limited to the realm of proteins and can be linked to an imbalanced lipid homeostasis (Ruipérez et al., 2010; Yadav and Tiwari, 2014).

1.4.1. The Unfolded protein response (UPR)

When the secretory load exceeds the folding capacity of the ER, misfolded proteins accumulate in the lumen of the ER and induce ER-stress. The UPR represents a large-scale transcriptional program to alleviate ER-stress. The targets of the UPR include genes involved

in protein folding, secretion, and degradation, as well as lipid biosynthesis (Cox et al., 1993; Jonikas et al., 2009; Travers et al., 2000; Walter and Ron, 2011). The UPR is not just a cytoprotective response, but can also trigger cell death: When cells fail to restore ER homeostasis, UPR activation in mammals ultimately induces apoptosis (Korennykh and Walter, 2012; Walter and Ron, 2011). Thus, the UPR is a key component of the ER quality control system and makes decisions of life and death (Tabas and Ron, 2011). Intriguingly, a chronic activation of the UPR has been implicated in the pathogenesis of many diseases, including viral infections, type II diabetes mellitus, neurodegenerative diseases and cancer (Fonseca et al., 2011; Lin et al., 2008).

Higher eukaryotes rely on three mechanistically distinct UPR transducers, initiating three pathways that collectively regulate the expression of numerous genes and attenuate protein translation. The integrated of the three UPR branches can adjust the secretory capacity of a cell to the current demands. Ire1 (IRE1 α/β in mammals) is the evolutionary most conserved UPR sensor, and the sole transducer for ER-stress in yeast (Fig. 8) (Kimata and Kohno, 2011; Mori, 2009; Mori et al., 1993; Tirasophon et al., 1998). In mammals, there are two isoforms of IRE1: IRE1 α , which is expressed in all cells, and IRE1 β , which is restricted to the gastrointestinal and respiratory tracts (Kimata and Kohno, 2011). The other two mammalian branches of the UPR are named after the protein kinase (PRK)-like ER kinase (PERK) (Harding et al., 1999), and the activating transcription factor 6 (ATF6) (Yoshida et al., 1998). Each of these stress transducers senses the load of misfolded proteins in the ER-lumen and employ distinct downstream signaling factors to control specific responses (Walter and Ron, 2011).

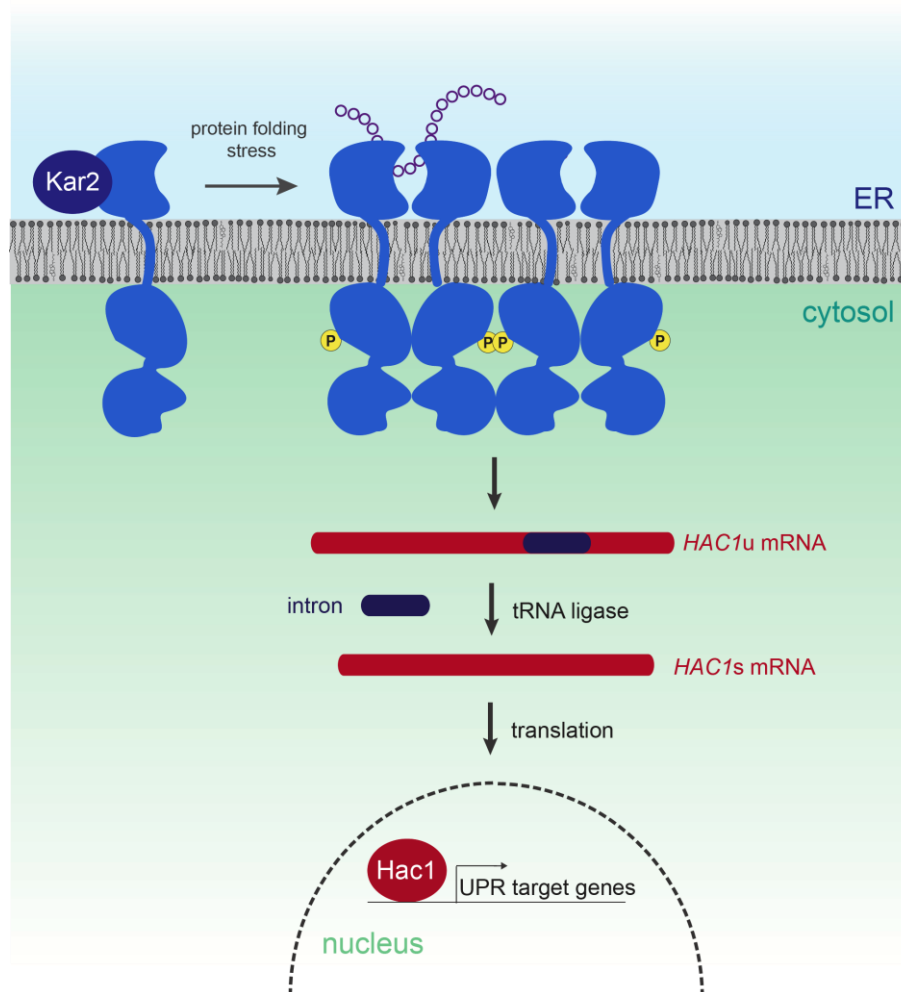


Figure 8 | Activation of the UPR in *S. cerevisiae* upon protein folding stress.

The UPR sensor Ire1 (blue) is an ER-resident transmembrane protein. In the absence of ER-stress, Ire1 is kept monomeric by an interaction with the major ER chaperone, Kar2. In response to protein folding stress, Ire1 binds misfolded proteins via its ER-luminal sensor domain and oligomerizes, which leads to activation of the cytosolic effector domains. The RNase domain of Ire1 initiates splicing of premature *HAC1* mRNA and, jointly with the tRNA ligase Rlg1, initiates the production of the transcriptional activator Hac1. Hac1 migrates to the nucleus and binds to UPRES, regulating the expression of UPR target genes. This illustration is adapted from Halbleib *et al.* (Halbleib *et al.*, 2017).

Ire1/IRE1 α is embedded in the ER membrane and senses unfolded proteins via its N-terminal ER-luminal sensor domain. In the cytosol, Ire1/IRE1 α contains a kinase and a ribonuclease (RNase) effector domain (Cox *et al.*, 1993; Mori *et al.*, 1993; Sidrauski and Walter, 1997). Binding of misfolded proteins and the concomitant dissociation of the ER chaperone Kar2 (BiP in mammals) triggers the oligomerization of Ire1 (Gardner and Walter, 2011; Kimata *et al.*, 2004, 2007). Although the kinase domain is not essential for yeast Ire1 function, it is bifunctional: It acts not only as an allosterically regulated scaffold that enables oligomerization of the RNase domain (Korenykh *et al.*, 2009), moreover, trans-autophosphorylation of Ire1 kinase domains results in stronger self-association within the oligomeric structure and

promotes a rapid shutdown of Ire1 activity upon ER adaptation (Chawla et al., 2011; Korennykh et al., 2009; Rubio et al., 2011). The RNase domain of Ire1/IRE1 α cleaves premature *HAC1* (*Xbp1* in mammals) mRNA at two unconventional splice sites, thereby releasing an intron (Cox and Walter, 1996). This nonconventional splicing process, performed jointly with the tRNA ligase Rlg1 (RtcB in mammals), serves as a prerequisite for the production of the transcriptional activator Hac1 (XBP1 in mammals) (Mori et al., 1996; Sidrauski and Walter, 1997; Sidrauski et al., 1996). Hac1 (XBP1 in mammals) migrates to the nucleus where it binds to unfolded protein response elements (UPREs) and drives a major transcriptional program that regulates the expression of UPR target genes (Fig. 8) (Cox et al., 1993; Mori et al., 1996). This set of UPR targets activated by Ire1 includes genes involved in protein translocation, lipid and inositol metabolism, protein folding, glycosylation (ER and Golgi), protein degradation, ER-Golgi-transport, and many other processes and make up 7 – 8% of all genes in yeast (Travers et al., 2000).

Despite the many similarities of the Ire1 branches in yeast and mammals, detailed studies on the transcription factors Hac1 and XBP1 revealed some differences. While the 252 nucleotide intron of unspliced *HAC1* blocks translation of the unspliced transcription factor in yeast (Chapman et al., 1997; Kawahara et al., 1997), the *Xbp1* intron only contains 26 nucleotides in mammals, which is not sufficient to block translation. Thus, unspliced XBP1 is translated as XBP1(U) (U stands for unspliced) (Calfon et al., 2002; Yoshida et al., 2001). The splicing reaction is, however as critical in mammals as it is in yeast, because the excision of the intron joins the C-terminal transcriptional activation domain and the N-terminal DNA binding domain to form the highly active transcription factor XBP1 (Yoshida et al., 2001). Moreover, the unspliced XBP1(U) in mammals contains a nuclear exclusion signal, leading to a shuffling of the pre-mature transcription factor between the nucleus and the cytosol, and a degradation domain at the C-terminal end (Yoshida et al., 2006, 2009). The shuffling allows XBP1(U) to interact and form complexes with XBP1(S) (S stands for spliced) in the nucleus, which are sequestered from the nucleus and degraded because of the presence of the degradation domain in the cytosol by the proteasome. This finding suggests that XBP1(U) serves as a negative regulator of XBP1(S) (Yoshida et al., 2009), in contrast to the yeast system.

PERK exhibits a mechanism similar to that of the Ire1 branch: PERK contains a N-terminal ER-luminal sensor domain, which interacts with the ER-resident chaperone BiP in its inactive state and oligomerizes upon binding of misfolded proteins. When the cytosolic kinase domains of PERK oligomerize, they are activated and phosphorylate the translation initiation factor eIF2 α . This, in turn, leads to a block of translation initiation and thus lower the burden of the

ER. Under these conditions, the transcription factor ATF4 is selectively and preferentially produced. It binds to UPRs and drives the expression of UPR target genes (Bertolotti et al., 2000; Cui et al., 2011; Koumenis, 2006; Lin et al., 2009; Walter and Ron, 2011).

ATF6 is a type II transmembrane protein, which is activated by proteolysis (Haze et al., 1999, 2001). The mechanism, how ATF6 senses misfolded proteins remains elusive, while the downstream events of ATF6 signaling are much better understood. In its inactive state, ATF6 interacts with BiP. Upon activation BiP dissociates, ATF6 is packaged into transport vesicles and delivered to the Golgi apparatus. Here, proteolysis occurs via the action of Site-1 and Site-2 proteases. Subsequently, the cytosolic transcription factor is liberated from its membrane tether, migrates to the nucleus and activates UPR target gene expression (Haze et al., 1999; Kohno, 2010; Okada et al., 2003; Ye et al., 2000; Yoshida et al., 2001). In mammals, these three branches of the UPR do not just coexist, but are interconnected to form a UPR signaling network, which acts in concert to alleviate ER-stress (Walter and Ron, 2011).

The number of UPR sensors increased during evolution from one (Ire1) in yeast, to two in metazoans (ire-1 and pek-1 in *Caenorhabditis elegans*; IRE1 and PEK/PERK in *Drosophila melanogaster*) and three (IRE1 α/β , PERK, ATF6) in mammals. It was hypothesized that mammalian cells can cope with ER stress in a much more sophisticated manner (Mori, 2009).

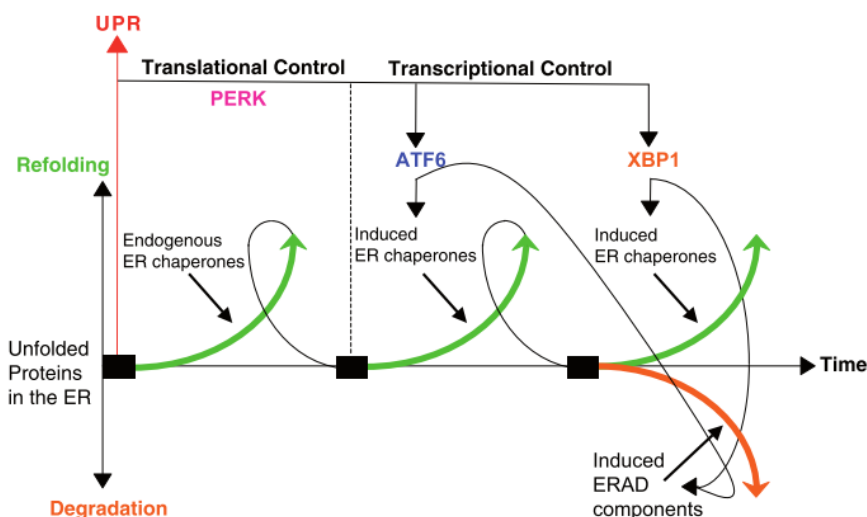


Figure 9 | Time-dependent activation of the mammalian UPR sensors.

Accumulation of unfolded proteins in the ER lead to an activation of the UPR. The activation of the different UPR branches occurs individually in time-dependent phase shifts. The PERK branch (translational control) is activated first in response to accumulating proteins. If this branch of the UPR fails to restore protein homeostasis, the UPR shifts to the transcriptional control phase, starting with activation of the ATF6 and, if this branch is not able to sufficiently cope with the load of unfolded proteins, the IRE1/XBP1 branch. This illustration has been taken from Mori *et al.* (Mori, 2009).

A major advantage of having three UPR sensors in mammals apart from the ability to counteract ER stress on different levels comes with the capability to activate these branches individually in time-dependent phase shifts to cope with ER stress more effectively (Fig.9) (Mori, 2009). Upon accumulation of unfolded proteins in the ER-lumen, the so called translational control phase of the UPR is activated. This phase employs the PERK branch of the UPR. PERK mediates the attenuation of general protein translation in mammalian cells and reduces the amount of unfolded proteins using endogenously expressed ER chaperones (Mori, 2009; Ron and Walter, 2007). If ER homeostasis cannot be restored by the PERK branch of the UPR, and unfolded proteins continue to accumulate, the UPR shifts to a transcriptional control phase dependent on ATF6 to induce of the production of ER chaperones. If the activation of the ATF6 branch fails to restore ER homeostasis, more XBP1 is produced, which heterodimerizes with ATF6 and induces the production of ERAD components (Mori, 2009; Yamamoto et al., 2007).

1.4.2. More than just UPR: Activation of the UPR by lipid bilayer stress

Aberrant ER lipid compositions have been reported to activate the UPR: Deregulated SL (Han et al., 2006) or sterol homeostasis (Pineau et al., 2009), inositol depletion (Lajoie et al., 2012; Promlek et al., 2011), impaired PC biosynthesis (Thibault et al., 2012), and increased proportions of saturated membrane lipids (Pineau et al., 2009; Surma et al., 2013; Volmer et al., 2013). All perturbations of lipid metabolism that activate the UPR are collectively referred to as lipid bilayer stress throughout this thesis. A variety of genetic screens identified a crosstalk of the protein and lipid homeostatic programs (Jonikas et al., 2009; Schuldiner et al., 2005; Surma et al., 2013). A quantitative genetic screen that scored the activation of the UPR in a set of single gene knockout mutants in yeast, for example, identified a central role of genes involved in lipid metabolism as potent UPR modulators (Jonikas et al., 2009).

Surma *et al.* identified that a failure to regulate the fatty acid desaturation via *MGA2* in yeast activates the UPR (Surma et al., 2013). Moreover, they generated a large set of double knockout mutants in yeast to identify genetic interactions genes. The resulting epistatic miniarray profile (E-MAP) revealed that genes involved in PC synthesis (*OPI3*, *CHO2*) and fatty acid desaturation (*MGA2*, *OLE1*) have negative genetic interactions with the UPR genes *IRE1* and *HAC1* (synthetic sickness and lethality), thereby genetically linking the UPR to key steps in lipid metabolism (Fig. 10) (Surma et al., 2013).

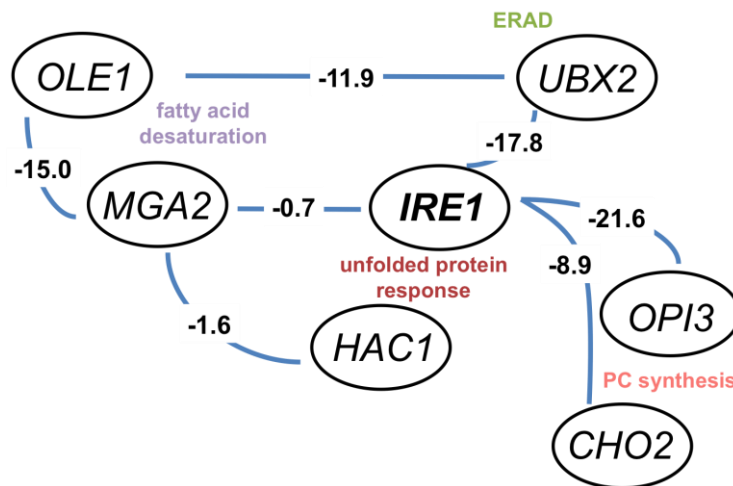


Figure 10 | Negative genetic interactions of *IRE1* with genes involved in ERAD, PC synthesis and fatty acid saturation. Genetic interactions of *IRE1* highlight the crosstalk of the UPR (*IRE1*, *HAC1*) the ERAD machinery (*UBX2*), fatty acid desaturation (*OLE1*, *MGA2*) and PC synthesis (*OPI3*, *CHO2*). This illustration is adapted from Surma *et al.* (Surma *et al.*, 2013).

The transcriptional regulation of *OLE1* mediated by the transcription factors Spt23 and Mga2 (Martin *et al.*, 2007; Stukey *et al.*, 1990), which activate *OLE1* expression (Hoppe *et al.*, 2000; Rape *et al.*, 2001). The *Mga2Δire1Δ* strain showed a negative genetic interaction of the respective genes in the E-MAP performed by Surma *et al.* (Surma *et al.*, 2013). The authors could also show that deletion of *MGA2* significantly shifted the saturation profile of the cellular lipidome towards more saturated lipid species. The population of diunsaturated GPLs was significantly reduced to a similar extent as the population of saturated GPLs was increased. These findings, and the identification of *MGA2* deletion as an activator of the UPR highlights the intricate connection of lipid and protein homeostasis and suggests, that increased GPL saturation induces lipid bilayer stress, hence activates the UPR (Surma *et al.*, 2013).

Cells lacking *Cho2* were previously reported to be severely sick, yet viable when grown in synthetic media without choline (Carman and Henry, 1999; McGraw and Henry, 1989; Thibault *et al.*, 2012; Zinser *et al.*, 1991). *Opi3* and *Cho2* are phosphatidyletanolamine N-methyltransferases in the CDP-DAG pathway of GPL biosynthesis and are required for the production of PC from PE in *S. cerevisiae* (Fig. 11) (van Meer *et al.*, 2008).

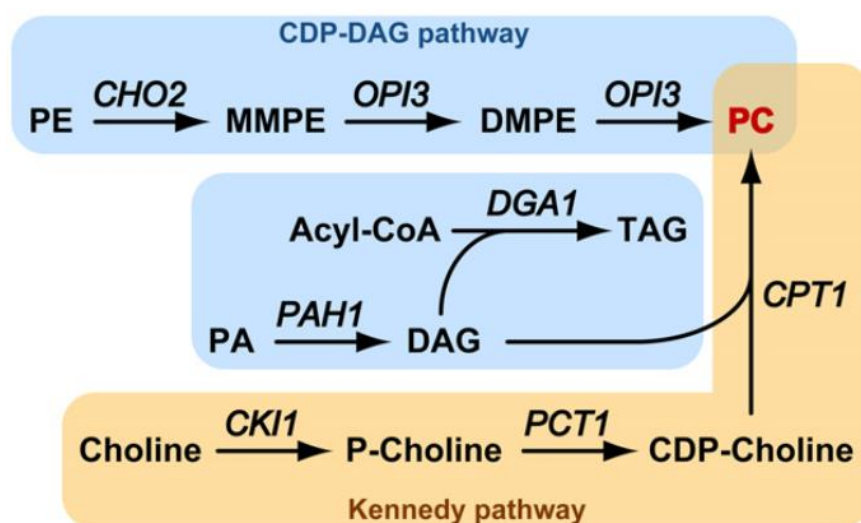


Figure 11 | Metabolic pathways of PC synthesis in *S. cerevisiae*.

The CDP-DAG (blue) and Kennedy pathway (yellow) are depicted. PE is methylated to MMPE by Cho2, which is further methylated by Opi3 in two sequential steps to form PC. The Kennedy pathway serves as an alternative route of PC synthesis when choline is supplemented to the growth medium of *S. cerevisiae*. This illustration is adapted from Thibault *et al.* (Thibault *et al.*, 2012).

Cho2 methylates PE to generate N-monomethyl PE (MMPE) and Opi3 sequentially methylates MMPE to form N,N-dimethyl PE (DMPE) and DMPE to form PC (Kodaki and Yamashita, 1987, 1989). Lipidomic analyses revealed that the deletion of either *OPI3* or *CHO2* significantly decreases the PC:PE ratio in *S. cerevisiae* (McGraw and Henry, 1989; Zinser *et al.*, 1991). Because *cho2Δ* cells cannot produce MMPE from PE, the absolute PE content increases in these cells, and a reduction in PC levels takes place. The lipidome of *opi3Δ* cells, however, revealed an accumulation of MMPE along with a reduction of total PE and PC levels, although the molar ratio of PC:PE was significantly reduced in these cells (Boumann *et al.*, 2006; Thibault *et al.*, 2012). In good agreement with the finding that *cho2Δ* and *opi3Δ* show negative genetic interactions with *HAC1* and *IRE1*, the authors could show that these mutants in PC synthesis activate the UPR in the absence of choline, the substrate required for PC synthesis via the alternative Kennedy pathway. Strikingly, supplementation of choline to the growth medium rescued this phenotype by restoring the PC:PE balance by the activation of the Kennedy pathway. These data provide genetic evidence that a decreased PC:PE ratio might activate Ire1, directly or indirectly, to compensate for an otherwise lethal condition of lipid induced ER-stress (Thibault *et al.*, 2012).

Depletion of inositol from the growth medium of *S. cerevisiae* has also been described to induce the UPR (Henry *et al.*, 2014; Lajoie *et al.*, 2012; Merksamer *et al.*, 2008). Apart from its function as a key component of sphingolipids in yeast, which play an essential role in

signaling and membrane function, inositol serves as a precursor for the synthesis of PI, one of the major lipid classes in eukaryotic membranes (Carman and Han, 2009; Henry et al., 2012). Cells grown in the absence of inositol contain PI levels that are 4-5 times reduced in comparison to cells grown in the presence of inositol (Henry et al., 2014). This has consequences on the production of other lipids as well as of lipid metabolites directly derived from PI, such as PIPs, SL or GPI anchors (Alvarez-Vasquez et al., 2005; Carman and Han, 2009; Jesch et al., 2010). Intriguingly, Ire1 is activated when inositol is depleted from the growth medium and a *ire1* Δ strain is an inositol auxotroph (Nikawa and Yamashita, 1992). Mechanistic details on how inositol deprivation activates Ire1 remained elusive (Chang et al., 2002; Cox et al., 1997; Jesch et al., 2006; Pincus et al., 2010).

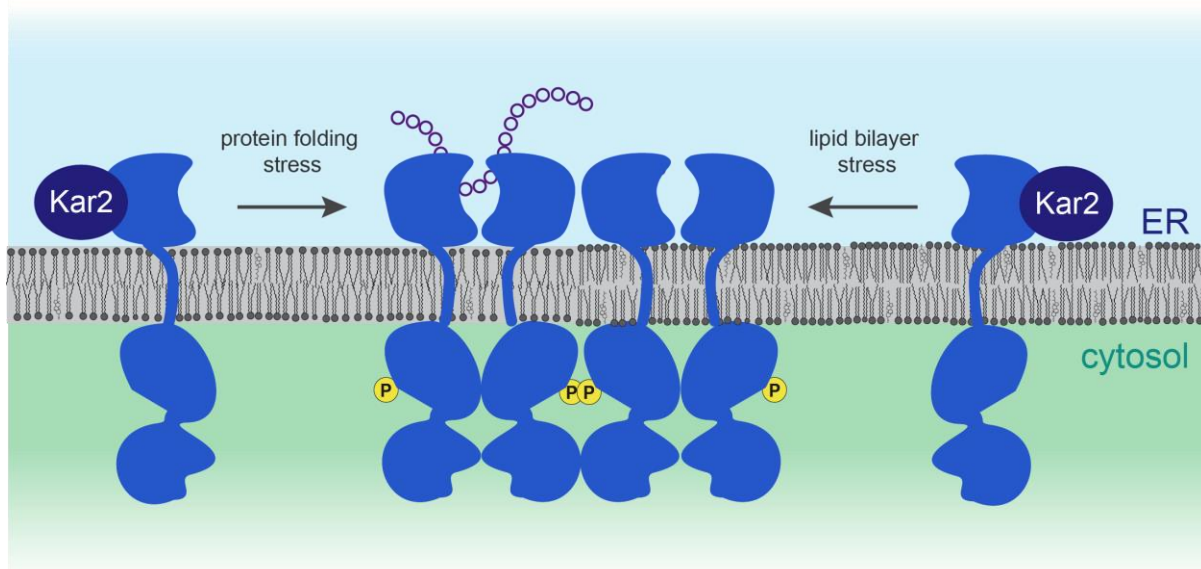


Figure 12 | Activation of Ire1 by protein folding and lipid bilayer stress.

Ire1 is directly activated by lipid bilayer stress. The mechanism how Ire1 is activated by aberrant membrane lipid composition still remains elusive. This illustration is adapted from Halbleib *et al.* (Halbleib et al., 2017)

These observations brought up the question, as to whether membrane aberrancies can activate the UPR. Do aberrant membrane lipid compositions activate Ire1 directly or do they induce protein misfolding, which in turn activates the UPR? In fact, the folding and topology of membrane proteins is lipid-dependent (Bogdanov et al., 2002; Dowhan and Bogdanov, 2009; Wang et al., 2002; White and von Heijne, 2005; Zhang et al., 2003). However, yeast grown in the absence of inositol exhibit a robust activation of the UPR without affecting the mobility of the ER chaperone Kar2, indicating a UPR activation in the absence of accumulating misfolded proteins in the ER-lumen (Fig. 12) (Lajoie et al., 2012). Even more strikingly, a deletion mutant of yeast Ire1 lacking the ER-luminal binding domain for misfolded proteins (Δ III; AA 253–272)

that cannot bind misfolded proteins, can react to inositol depletion (Kimata et al., 2004, 2007; Promlek et al., 2011). Strikingly, observations implying direct activation of the UPR by membrane aberrancies are not limited to Ire1 in yeast, but have also been made for mammalian UPR sensors. Recent reconstitution experiments with liposomes of defined lipid compositions and a minimal UPR-transducer, encompassing only the kinase domain of the mammalian PERK and its endogenous transmembrane domain (TMD), showed that the degree of acyl chain saturation correlated with increasing kinase activities. Exchanging the TMD of PERK with the TMD of an unrelated protein did not affect the outcome, which suggested that membrane tethering, irrespective of TMD sequence, might be sufficient for lipid-dependent UPR signaling (Volmer et al., 2013). Despite all concern regarding the choice of the lipid matrix in these experiments, the data suggested that a direct activation of the UPR by membrane aberrancies may be evolutionally conserved from yeast to man. Hence, it is of great interest to reveal how structurally and functionally distinct lipids contribute to Ire1 activation to identify the mechanism underlying this activation.

1.4.3. Insights into the molecular organization of Ire1

The crystal structure of Ire1's ER-luminal domain from *S. cerevisiae* has been solved in an oligomeric state (Credle et al., 2005). The structure provided valuable structural information promoting the characterization of Ire1's activation mechanism. It revealed interfaces for oligomerization and the presence of a putative binding site for unfolded proteins (Credle et al., 2005). Systematic deletion studies have helped to divide the luminal domain of Ire1 into five functionally distinct subregions (Fig.13, A and B). Subregion I (AA 25-104) has a regulatory function that serves to inhibit Ire1's self-association in the absence of ER-stress (Oikawa et al., 2007). Subregion V contains a binding site for the ER chaperone Kar2 (BiP), which is known to bind Ire1 in the absence of ER-stress, and is thought to keep it in a monomeric inactive state (Kimata et al., 2004). Simultaneous deletion of these two regulatory subregions results in self-association of Ire1 molecules and renders Ire1 constitutively active (Oikawa et al., 2007; Promlek et al., 2011). The subregions II (AA 105-235), III (AA 236-265) and IV (AA 266-447) form the core luminal domain (cLD), the protein folding stress-sensing region of Ire1. These subregions mostly form β -sheets, and subregions II and III form the peptide binding groove within the cLD of Ire1. The cLD is conserved among species and contains a peptide binding groove for unfolded proteins and tends to oligomerize (Fig. 13 D). The peptide binding groove shows striking similarities to the geometry of the central peptide binding groove in major-histocompatibility complex I (MHC-I) molecules (Bjorkman et al., 1987). The cLD consists of β -sheets forming a flat bottom surface and two parallel α -helices, which lay on top

of the flat structure formed by the β -sheets. Thus, the two alpha helices form the outside border of a peptide binding groove (Fig. 13 D). When Ire1 dimerizes, the peptide binding groove fully assembles and its hydrophobic nature allows for a direct interaction of Ire1 with unfolded proteins, which has been proposed to drive the oligomerization of Ire1 upon binding unfolded proteins (Credle et al., 2005; Gardner and Walter, 2011; Oikawa et al., 2007).

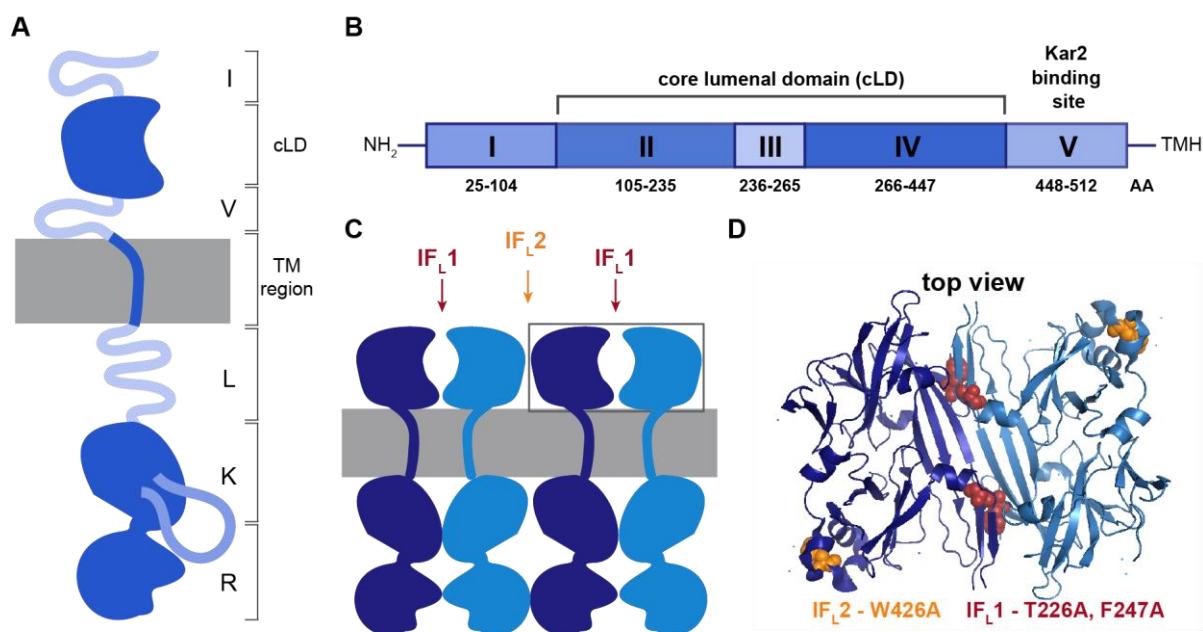


Figure 13 | Schematic representation, and structural organization of Ire1's ER-luminal sensor domain.

(A) Schematic representation of full-length Ire1. The ER-luminal domain consists of subregions I and V (I; V) and the core luminal domain (cLD). The luminal domain is connected to the cytosolic kinase (K) and RNase (R) domain by a TMH, followed by a large loop region. (B) Organization of the ER-luminal domain. Subregions I to V and their respective amino acid regions are depicted. The cLD and localization of the Kar2 binding domain are labeled. (C) Schematic representation of IF_{L1} and IF_{L2} localization in Ire1 oligomers and (D) x-ray structure of the dimeric luminal domain of Ire1 (pdb: 2BE1; (Credle et al., 2005). Mutations destroying the IF_{L1} (T226A, F247A; red) and IF_{L2} (W426A; yellow) are depicted. Individual figures are adapted from Halbleib *et al.* (Halbleib et al., 2017).

Oligomerization of Ire1's luminal domain is crucial for the activation of Ire1. During this process, two interaction interfaces are established. The luminal interface 1 (IF_{L1}) is located at the interface of two Ire1 monomers (Fig. 13, C and D). The mutation of two residues in the cLD domain (T226, F247) destroys the formation of this interface, resulting in a diminished formation of Ire1 dimers and consequently, impaired Ire1 functionality. The luminal interface 2 (IF_{L2}) is located at the interface of two Ire1 dimers (Fig. 13, C and D). Mutation of the W426 residue in the cLD destroys this interface, hence inhibits the formation of high-order Ire1 oligomers, which reduces the functionality of Ire1 to the same extent (Credle et al., 2005).

Dimerization of Ire1's luminal domain leads to a simultaneous dimerization of the cytosolic

part of the protein in a back-to-back fashion (Lee et al., 2008). The dimerization is followed by the formation of higher order oligomers by the cytosolic portion of Ire1. This oligomerization renders Ire1's kinase and RNase domains active by providing an interaction of cytosolic domains of neighboring Ire1 molecules. The interaction is a prerequisite for trans-autophosphorylation of the kinase domains at specific serine and threonine residues (S840, S841 and T844), and for stabilizing the active sites of the RNase domains of neighboring Ire1 molecules, which collectively form an RNA-substrate binding cavity (Korennykh et al., 2009; Walter and Ron, 2011).

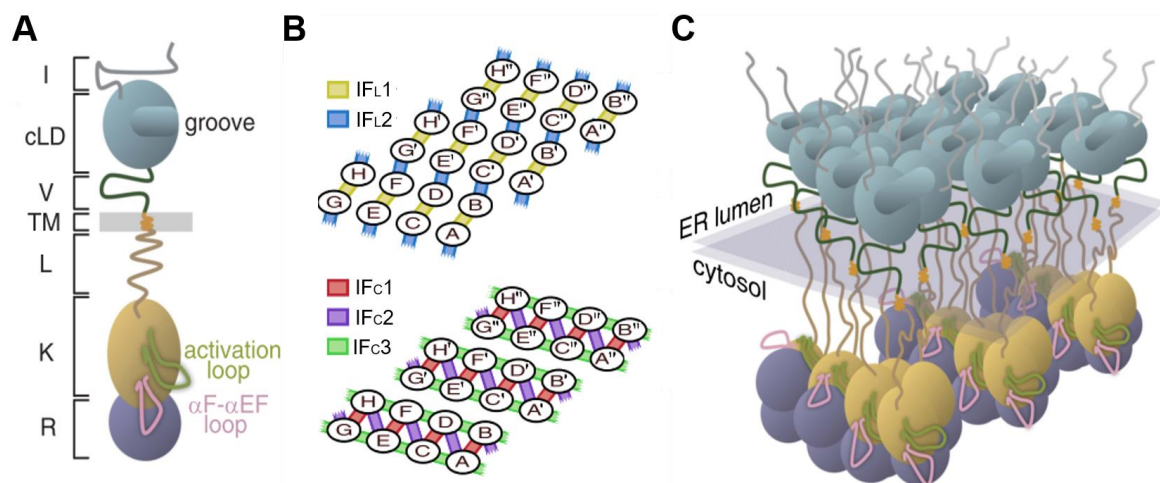


Figure 14 | Schematic representation, and structural organization of Ire1.

(A) Schematic representation of full-length Ire1. The ER-luminal domain consists of subregions I and V (I; V) and the core luminal domain (cLD). The luminal domain is connected to the cytosolic kinase (K) and RNase (R) domain by a TMH, followed by a large loop region. The activation loop in the kinase domain is illustrated in green. (B) Organization of Ire1 monomers within high-order oligomers of Ire1. This illustration is based on the x-ray structure (pdb: 2RIO) by Korennykh et al. (Korennykh et al., 2009). The interaction interfaces are highlighted by the illustrated color code. (C) 3-dimensional model of the organization of Ire1 monomers within high-order oligomers as described in (B). Figures were adapted from Van Anken *et al.* (van Anken et al., 2014)

As previously described for the luminal domain of Ire1, the cytosolic domain also establishes interaction interfaces, which are pivotal for Ire1 function. Three cytosolic interfaces have been identified, and Ire1's functionality is impaired, when residues forming these interfaces are mutated (Fig. 14) (van Anken et al., 2014; Korennykh et al., 2009): i) IF_c1 establishes RNase-RNase contacts of two neighboring Ire1 molecules in the back-to-back dimer. ii) IF_c2 establishes interactions of RNase and kinase domains of inter-dimeric Ire1 molecules within higher oligomers. iii) IF_c3 establishes a kinase-kinase interaction of inter-dimeric Ire1 molecules within higher oligomers (Korennykh et al., 2009).

While active RNase domains of Ire1 are required for processing of *HAC1* mRNA and therefore essential for Ire1 function, it has been reported that kinase activity of Ire1 is not required for

Ire1 activation. It rather serves as a regulator in the process of Ire1 deactivation by changing the position of an activation loop, located in the kinase domain of Ire1 (Fig.14 B and C) (Korennykh et al., 2009; Rubio et al., 2011). These and other observations emphasize that the intermolecular interactions of Ire1 molecules are extremely complex, which in turn highlights the importance of the formation of inter- and intradimer interfaces to stabilize the formation of high-order Ire1 oligomers to reach full Ire1 signaling activity.

The transmembrane helix and juxta-membrane regions of Ire1 (collectively referred to as transmembrane region; TMR) connects the ER-luminal domain of Ire1 with the cytosolic effector domains. The underlying hypothesis of this thesis is that the TMH and/ or juxta-membrane region of Ire1 is involved in the sensing and activation mechanism of Ire1 by lipid bilayer stress.

2. Aim

The UPR was originally identified as a conserved homeostatic program activated by the accumulation of unfolded proteins in the lumen of the ER. In the past decade, it became evident that aberrant lipid compositions are equally potent to activate the UPR. Although a direct activation mechanism of Ire1 by lipid bilayer stress was postulated, the underlying molecular mechanism of this activation remains elusive (Promlek et al., 2011; Volmer et al., 2013).

This study focuses on the identification of the molecular mechanisms that activate the UPR sensor Ire1 from *S. cerevisiae* upon lipid bilayer stress. Special emphasis is laid on the role of Ire1's transmembrane and juxta-membrane region in transducing ER-stress. As the TMR of Ire1 interacts most intimately with the membrane, it is a prime candidate to sense membrane aberrances.

In the course of this study, a variety of assays will be developed and implemented to achieve functional analyses of different Ire1 variants expressed from the endogenous *IRE1* locus and mutants of the TMR and other functionally required domains of the protein will be analyzed for their functionality *in vivo*.

To investigate the hypothesis, that the TMR of Ire1 acts as a sensor for the membrane environment, this study establishes a minimal sensor, consisting solely of the TMR and the maltose binding protein (MBP) as a solubility and detection tag that is reconstituted in defined lipid environments. Oligomerization of Ire1 will be studied in various strictly defined lipid compositions to investigate the modulation of oligomerization by the membrane lipid environment by continuous wave electron paramagnetic resonance (cwEPR) spectroscopy.

Moreover, this study aims for the structural characterization of Ire1's transmembrane helix (TMH) in lipid bilayer stress to map the dimerization interface of Ire1's TMHs. To this end, liposomes with a very high degree of molecular packing will be used, mimicking a membrane composition inducing lipid bilayer stress.

3. Materials

3.1. Chemicals and reagents

All chemicals, organic solvents, components of media or buffers, and lipids are listed in Tables 1-4.

Table 1 | List of buffer components, salts and additives.

Name	Source
Acetic acid	VWR Prolabo
AlexaFluor 647 C2-maleimide	Life Technologies
Agarose	Sigma-Aldrich
Ammonium sulfate ((NH ₄)SO ₄)	Carl Roth
Antipain	Carl Roth
Bromphenol blue	Carl Roth
Calcium chloride (CaCl ₂)	Carl Roth
Chymostatin	Sigma-Aldrich
Digitonin	Carl Roth
Dithiothreitol (DTT)	Sigma-Aldrich
Deoxynucleotide (dNTP) mix	NEB
Ethidium bromide	Amresco
Ethylendiaminetetraacetic acid (EDTA)	Carl Roth
Glycerole 99.5%	VWR Prolabo
Glycine	Carl Roth
4-(2-hydroxyethyl)-1-piperazineethanesulfonic acid (HEPES)	Carl Roth
Hydrochloric acid (HCl)	Sigma-Aldrich
Isopropyl-β-D-thiogalactopyranosid (IPTG)	Carl Roth
Lithium acetate (LiAc)	Carl Roth
Magnesium chloride (MgCl ₂)	Carl Roth
Mangan(II)-chloride (MnCl ₂)	Carl Roth
2-Mercaptoethanol	Sigma-Aldrich
(1-Oxyl-2,2,5,5-tetramethylpyrroline-3-methyl) methanethiosulfonate (MTSSL)	Enzo Life Sciences
Octyl β-D-glucopyranoside (β-OG)	Calbiochem
Pepstatin	Sigma-Aldrich
Piperazine-N,N'-bis(2-ethanesulfonic acid) (PIPES)	Carl Roth
Phosphate buffered saline (PBS)	Sigma-Aldrich
Polyethylene glycol (PEG) 4000	Sigma-Aldrich
Potassium acetate (KAc)	Sigma-Aldrich
Potassium chloride (KCl)	Carl Roth
RNase Away Reagent	Ambion
Saccharose D (Sucrose)	Carl Roth
Salmon sperm DNA	Invitrogen
Skim milk powder	Carl Roth
Sodium azide (NaN ₃)	Carl Roth
Sodium carbonate (Na ₂ CO ₃)	Merck
Sodium chloride (NaCl)	Carl Roth
Sodium dodecyl sulfate (SDS)	Carl Roth
Sodium di-hydrogen phosphate (NaH ₂ PO ₄)	Carl Roth

Materials

Name	Source
<i>d</i> -Sodium hydrogen phosphate (Na ₂ HPO ₄)	Merck
Sodium hydroxide (NaOH)	Carl Roth
Tris(2-carboxyethyl)phosphine (TCEP)	Carl Roth
Tris(hydroxymethyl)-aminomethan (Tris)	Sigma-Aldrich
Triton X-100	Carl Roth
Tunicamycin	Carl Roth
Tween 20	Sigma-Aldrich
Urea	Carl Roth

Table 2 | List of lipid species.

Lipid	Source
1,2-Dioleoyl-sn-glycero-3-phosphocholine (DOPC)	Avanti Polar Lipids
1-palmitoyl-2-oleoyl-sn-glycero-3-phosphocholine (POPC)	Avanti Polar Lipids
1,2-dipalmitoyl-sn-glycero-3-phosphocholine (DPPC)	Avanti Polar Lipids
1,2-dioleoyl-sn-glycero-3-phosphoethanolamine (DOPE)	Avanti Polar Lipids
1-palmitoyl-2-oleoyl-sn-glycero-3-phosphoethanolamine (POPE)	Avanti Polar Lipids
L- α -phosphatidylinositol (Soy) (Soy-PI)	Avanti Polar Lipids
Cholesterol	Avanti Polar Lipids

Table 3 | List of chemicals for cultivation and selection.

Name	Source
Agar-Agar (Agar)	ForMedium
Ampicilin sodium salt	Carl Roth
Chloramphenicol	Carl Roth
Complete Supplement Mixture (CSM)	
w/o histidine	MP
w/o uracile	MP
G418 disulfate salt	Sigma-Aldrich
Glucose	Carl Roth
Tryptone/Peptone	Carl Roth
Yeast Extract	Carl Roth
Yeast Nitrogen Base (YNB)	BD Bioscience
YNB w/o inositol	ForMedium

Table 4 | List of solvents.

Name	Source
Chloroform \geq 99%	Carl Roth
Dimethylsulfoxid (DMSO)	Carl Roth
Ethanol 96% + 1% MEK	Carl Roth
Ethanol 96%	NeoLab
Isopropanol	AppliChem
Methanol	Carl Roth
RNAse free water	Qiagen
Ultrapure water	Millipore

3.2. Commercially available systems

Kits and standards used in this study are listed in Table 5. All kits were used according to the manufacturer's protocol if not stated otherwise.

Table 5 | List of kits and standards.

Name	Source
Absolute qPCR SYBR Green Mix	Thermo Scientific
Anti-HA high affinity matrix slurry	Roche
Clarity Western ECL Substrate	BioRad
DNA loading dye	NEB
GeneRuler 1kb DNA Ladder	NEB
GeneRuler 100 bp DNA Ladder	NEB
HighQu qPCR SYBR Green Mix	HiQu
InstantBlue	Expedeon
4-15% Mini-PORTEAN-TGX gels	BioRad
Oligo (dT) 12-18 Primer	Life Technologies
PageRuler Prestained Protein Ladder	Thermo Scientific
Red Anti-FLAG M2 Beads	Sigma-Aldrich
RiboLock Rnase Inhibitor	Thermo Scientific
RNeasy Plus Mini Kit	Qiagen
Q5 Site-directed Mutagenesis Kit	NEB
QIAprep Spin Miniprep Kit	Qiagen
QIAquick Gel Extraction Kit	Qiagen
QIAquick PCR Purification Kit	Qiagen
Quick Ligation Kit	NEB
SuperScript II Reverse Transcriptase	Invitrogen
SuperSignal West Femto ECL developing solution	Thermo Scientific

3.3. Enzymes

A list of all commercially available enzymes used for molecular cloning and other biochemical purposes is shown in Table 6. If not stated otherwise, these enzymes were used following the manufacturer's recommendations.

Table 6 | List of enzymes.

Name	Source
Antarctic Phosphatase	NEB
Benzonase	Sigma-Aldrich
<i>DpnI</i>	NEB
<i>BamHI</i>	NEB
<i>EcoRI</i>	NEB
<i>HindIII</i>	NEB
<i>XhoI</i>	NEB
PHUSION DNA Polymerase	NEB
Proteinase K	Invitrogen

3.4. Antibodies

All antibodies used for immunoblotting are listed in Table 7. All dilutions of the primary and secondary antibodies were prepared in 3-5% skim milk powder in TBS-T (20 mM Tris-HCl pH 8.0, 150 mM NaCl, 0.1% (v/v) Tween 20), if not stated otherwise.

Table 7 | List of primary and secondary antibodies used in this study, including their dilution for immunoblotting.

Primary antibodies	Dilution	Source
Anti-Dpm1 monoclonal (5C5A7) (mouse)	1:2000	Life Technologies
Anti-FLAG monoclonal (M2) (mouse)	1:5000	Santa Cruz
Anti-HA monoclonal (3F10) (rat)	1:2000	Roche
Anti-Kar2 polyclonal (y-115) (rabbit)	1:1000	Santa Cruz
Anti-MBP monoclonal (mouse)	1:20000	NEB
Anti-Pgk1 monoclonal (22C5) (mouse) (A6457)	1:20000	Invitrogen
Secondary antibodies	Dilution	Source
Anti-mouse-HRP (goat)	1:40000	Dianova
Anti-rabbit-HRP (goat)	1:20000	BioRad
Anti-rat-HRP (goat)	1:20000	Dianova

3.5. Supplies and Equipment

Consumables and laboratory equipment used in this study are listed in Table 8 and Table 9.

Table 8 | List of consumables.

Name	Source
96-well plates, sterile and unsterile	Brand
96-deep-well plates Genetix	Genetix
BD Microlance 3 hypodermic needle (0.5 x 25 mm)	BD
Clear optical sealing film for Piko-PCR	Thermo Scientific
Cover slips (24 x 50 mm)	Menzel-Gläser
Cryogenic tubes NUNC with external thread (1.8 ml)	VWR
Culture flasks (100 ml, 250 ml, 500 ml, 2 l, 5 l)	VWR
Culture tubes with cap, sterile (14 ml)	VWR
Cuvettes, disposable (semi-micro)	VWR
Eppendorff Gel Loader 0.5-20 µl Tips	Eppendorff
Falcon tubes (15 ml, 50 ml)	Greiner
Filter paper	BioRad
Incultation Loops	VWR
Microcentrifuge tubes (0.5 ml, 1.5 ml, 2 ml)	Carl Roth
Microscopy slides (76 x 26 mm)	Carl Roth
Petri dishes, sterile (ø 90 mm)	VWR
Piko PCR Plate, 96-well, white	Thermo Scientific
Pipette tips, refill, next generation (10 µl, 200 µl)	VWR
Pipette tips (1000 µl)	Carl Roth
PVDF-membrane 0.45 µm	PALL
Ringcaps 50 µl	Hirschmann
Surphob SafeSeal filter pipette tips (10 µl, 20 µl, 200 µl, 1000 µl)	Biozym
Scalpel	Braun
Serological pipettes (5 ml, 10 ml, 25 ml)	VWR
Silicon stoppers SILICOSEN© C-type	VWR
Sterican hypodermic needle (0.9 x 40 mm)	Braun
Syringe filters (0.2 µm)	VWR
Syringes, luer-lock (1 ml, 5 ml)	Braun
Vacuum filtration systems (150 ml, 0.2 µm)	VWR
Zirkonia Beads (ø 0.5 mm)	Carl Roth

Table 9 | List of laboratory equipment.

Name	Source
96-well plate reader (BMG Fluostar Galaxy)	MTX Lab Systems
Äkta Pure	GE Healthcare
Balance	Satorius
Block Heater, Dual control	Stuart
Cell density meter, Ultrospec™ 10 Classic	GE Healthcare
Microcentrifuges (5415R, 5417R, 5424, 5804R)	Eppendorf
Table top Ultracentrifuge (XLS)	Beckmann
Ultracentrifuge	Beckmann
ChemiDoc™ MP System	BioRad
Disrupter Genie, analog	USA Scientific
Electrophoresis chamber	BioRad
Flow-cytometer Attune	Life Technologies
FluoroMax 4 spectrometer	Horiba Scientific
Gyro-rocker SSL3	Stuart
Incubator Innova 42	Eppendorf
LSM 780	ZEISS
LSM 880	ZEISS
Magnetic stirrer with heating plate	Heidolph
Mini-PROTEAN Tetra Cell	BioRad
Multichannel pipette, motorized (100 µl, 300 µl)	Eppendorf
NanoDrop (ND-1000)	PeqLab
NanoSight LM10	NanoSight
Nutating mixer	VWR
PCR thermal cycler	Analytik Jena AG
PikoReal™ Real-Time PCR system	Thermo Scientific
Pipettes (10 µl, 20 µl, 200 µl, 1000 µl)	Gilson
Pipette (5000 µl)	Eppendorf
Power supply (PowerPac™ HC)	BioRad
Thermal shaker	Eppendorf
TransBlot Turbo™ transfer system	BioRad
Sonifier cell disrupter	Branson Ultrasonics
Vortex Genie 2	USA Scientific

3.6. Peptides

Synthetic biotinylated peptides were purchased from the Center of Innovation Competence for Molecular Engineering (ZIK B CUBE) at TU Dresden and purified to >90% purity. The supplier verified the quality of the peptide by mass spectrometry. Peptides used in this study are listed in Table 10.

Table 10 | List of peptides.

Name	Sequence	Source
Ire1 ⁵²²⁻²⁴³	Biotin -K N Q N S L L L K F G S L V Y R I I E T G V-CONH ₂	ZIK B CUBE
Ire1 ⁵²²⁻²⁴³ F531R	Biotin -K N Q N S L L L K R G S L V Y R I I E T G V-CONH ₂	ZIK B CUBE
Ire1 ⁵²²⁻²⁴³ V535R	Biotin -K N Q N S L L L K F G S L R Y R I I E T G V-CONH ₂	ZIK B CUBE

3.7. Plasmids

All plasmids used for *in vivo* and *in vitro* experiments in this study are listed in Table 11.

Table 11 | Plasmids used in this study.

Plasmid	Description	Reference
<i>in vivo</i>		
pEvA200	pRS315- <i>IRE1</i> -GFP WT	(van Anken et al., 2014)
pRE488	pRS315- <i>IRE1</i> -3xHA-GFP WT	this study
pRE419	pcDNA3.1(+)- <i>IRE1</i> -GFP WT	this study
pRE450	pcDNA3.1(+)- <i>IRE1</i> -GFP C552S	this study
pRE451	pcDNA3.1(+)- <i>IRE1</i> -3xHA-GFP WT	this study
pRE453	pcDNA3.1(+)- <i>IRE1</i> -3xHA-GFP R537A	this study
pRE454	pcDNA3.1(+)- <i>IRE1</i> -3xHA-GFP R537E	this study
pRE455	pcDNA3.1(+)- <i>IRE1</i> -3xHA-GFP IF2 (W426A)	this study
pRE456	pcDNA3.1(+)- <i>IRE1</i> -3xHA-GFP E540N	this study
pRE457	pcDNA3.1(+)- <i>IRE1</i> -3xHA-GFP E540D	this study
pRE458	pcDNA3.1(+)- <i>IRE1</i> -3xHA-GFP Δ III (Δ 253-272)	this study
pRE460	pcDNA3.1(+)- <i>IRE1</i> -3xHA-GFP L16 TMH	this study
pRE461	pcDNA3.1(+)- <i>IRE1</i> -3xHA-GFP E540A	this study
pRE462	pcDNA3.1(+)- <i>IRE1</i> -3xHA-GFP E540Q	this study
pRE463	pcDNA3.1(+)- <i>IRE1</i> -3xHA-GFP F544,548,551A	this study
pRE465	pcDNA3.1(+)- <i>IRE1</i> -3xHA-GFP IF1 (T226A F247A)	this study
pRE468	pcDNA3.1(+)- <i>IRE1</i> -3xHA-GFP E540A IF1 (T226A F247A)	this study
pRE469	pcDNA3.1(+)- <i>IRE1</i> -3xHA-GFP E540A IF2 (W426A)	this study
pRE471	pcDNA3.1(+)- <i>IRE1</i> -3xHA-GFP E540K	this study
pRE551	pcDNA3.1(+)- <i>IRE1</i> -3xHA-GFP V535R	Laura Henke (Bachelor Thesis)
pRE553	pcDNA3.1(+)- <i>IRE1</i> -3xHA-GFP V535R, IF1	Laura Henke (Bachelor Thesis)
pRE555	pcDNA3.1(+)- <i>IRE1</i> -3xHA-GFP V535R, IF2	Laura Henke (Bachelor Thesis)
pRE556	pcDNA3.1(+)- <i>IRE1</i> -3xHA-GFP F531R	Laura Henke (Bachelor Thesis)
pRE557	pcDNA3.1(+)- <i>IRE1</i> -3xHA-GFP F531R, IF1	this study
pRE558	pcDNA3.1(+)- <i>IRE1</i> -3xHA-GFP F531R, IF2	this study
pRE170	pFA6a-6xGLY-3xFLAG-kanMX6	Funakoshi 2009
pRE650	pcDNA3.1- <i>IRE1</i> -3xHA-GFP L13 TMH	This study

Plasmid <i>in vitro</i>	Description	Reference
pRE420	MBP- <i>IRE1</i> -AH+TMH wild type +Cys	this study
pRE421	MBP- <i>MGA2</i> -TMH wild type +Cys	this study
pRE422	MBP- <i>SPT23</i> -TMH wild type +Cys	this study
pRE424	MBP- <i>IRE1</i> -AH+TMH wild type	Jonas Michaelis (Diploma Thesis)
pRE431	MBP- <i>IRE1</i> -AH+TMH C552S	Julian Wagner (Diploma Thesis)
pRE432	MBP- <i>IRE1</i> -AH+TMH C552S R537C	Julian Wagner (Diploma Thesis)
pRE433	MBP- <i>IRE1</i> -AH+TMH C552S I538C	Julian Wagner (Diploma Thesis)
pRE434	MBP- <i>IRE1</i> -AH+TMH C552S I539C	Julian Wagner (Diploma Thesis)
pRE435	MBP- <i>IRE1</i> -AH+TMH C552S E540C	Julian Wagner (Diploma Thesis)
pRE436	MBP- <i>IRE1</i> -AH+TMH C552S T541C	Julian Wagner (Diploma Thesis)
pRE437	MBP- <i>IRE1</i> -AH+TMH C552S V543C	Julian Wagner (Diploma Thesis)
pRE438	MBP- <i>IRE1</i> -AH+TMH C552S L545C	this study
pRE439	MBP- <i>IRE1</i> -AH+TMH C552S L546C	Julian Wagner (Diploma Thesis)
pRE440	MBP- <i>IRE1</i> -AH+TMH C552S L547C	Julian Wagner (Diploma Thesis)
pRE441	MBP- <i>IRE1</i> -AH+TMH C552S F548C	Julian Wagner (Diploma Thesis)
pRE442	MBP- <i>IRE1</i> -AH+TMH C552S L549C	Julian Wagner (Diploma Thesis)
pRE443	MBP- <i>IRE1</i> -AH+TMH C552S I550C	this study
pRE446	MBP- <i>IRE1</i> -AH+TMH C552S G542C	Julian Wagner (Diploma Thesis)
pRE447	MBP- <i>IRE1</i> -AH+TMH C552S F544C	Julian Wagner (Diploma Thesis)
pRE448	MBP- <i>IRE1</i> -AH+TMH C552S F551C	Julian Wagner (Diploma Thesis)
pRE566	MBP- <i>IRE1</i> -AH+TMH C552S L534C	this study
pRE567	MBP- <i>IRE1</i> -AH+TMH C552S V535C	this study
pRE568	MBP- <i>IRE1</i> -AH+TMH C552S Y536C	this study
pRE630	MBP- <i>IRE1</i> -AH+TMH C552S R537C F531R	this study
pRE629	MBP- <i>IRE1</i> -AH+TMH F531R	this study

3.7.1. Construction of *IRE1* knock-in constructs

A His3MX6 marker cassette flanked by the endogenous 3' sequence of the *IRE1* locus (for genomic insertion of *IRE1* at the endogenous locus) was synthesized and amplified by PCR including *HindIII/BamHI* restriction sites and cloned into the pcDNA3.1 (+) vector. Subsequently, the sequence of *IRE1-GFP* including the endogenous Promoter of *IRE1* (-1 to -551 bp) and the endogenous 5' terminator sequence were amplified from pEvA200 (van Anken et al., 2014) by PCR and equipped with *BamHI/XhoI* restriction sites for cloning into pcDNA3.1 (+). A pre-existing C-terminal 1xHA-tag encoding sequence in *IRE1* was removed from the resulting plasmid, and a 3xHA-tag encoding sequence was introduced using the Q5 site-directed mutagenesis kit (NEB) at the position H875 to yield pcDNA3.1-*IRE1*^{3xHA-GFP}. Site-directed mutagenesis of this plasmid was performed using a PCR-based strategy based on the QuickChange® method (Stratagene) using PHUSION polymerase (NEB). Deletion, exchange or introduction of DNA sequences >6bp was performed using the Q5 site-directed

mutagenesis kit (NEB). For subsequent transformation of *S. cerevisiae* YRE127, the knock-in plasmid was linearized using *Hind*III and *Xho*I restriction enzymes.

In analogy to the knock-in construct, a *CEN*-based construct was cloned based on the pEvA200 plasmid (van Anken et al., 2014) by deletion of the C-terminal 1xHA-tag encoding sequence and subsequent introduction of a 3xHA-tag encoding sequence utilizing the Q5 site-directed mutagenesis kit (NEB).

3.7.2. Construction of MBP-fusion constructs

The region encoding for the minimal sensor of *IRE1* (S526-L561) was cloned into the pMAL-C2x-TEV *E. coli* expression vector. Two synthetic, complementary oligonucleotides (Table 13) with the desired *IRE1* sequence including a stop codon and *Eco*RI/ *Hind*III restriction sites were purchased from Sigma-Aldrich and annealed, prior to ligation into the pMAX-C2x-TEV vector. Mutagenesis was performed using a polymerase chain reaction (PCR)-based strategy based on the QuickChange® method (Stratagene) using oligonucleotides listed in Table 15 and PHUSION polymerase (NEB) utilizing whole plasmid PCR.

3.8. Oligonucleotides

Oligonucleotides used in this study were purified by high-throughput liquid chromatography (HPLC) and purchased from Sigma-Aldrich. Oligonucleotides utilized for homologous recombination in yeast are listed in Table 12. Oligonucleotides used for molecular cloning are listed in Table 13. Oligonucleotides used for the introduction of specific insertions, exchanges or deletions in the *IRE1* constructs are shown in Table 14, and Oligonucleotides for the site-directed mutagenesis are specified in Table 15.

Materials

Table 12 | Oligonucleotides for homologous recombination.

Name	Sequence (5'→ 3')	Description
TP027	GCTTTTAGGGACAGTTCTATTCTTCCAACGTGCGAAGCGTTCCAAC	bp -551 (fwd)
	AGCTGAAGCTTCGTACGC	delete <i>IRE1</i> promoter + <i>IRE1</i>
TP028	TTAATGCAATAATCAACCAAGAAGAAGCAGAGGGGCATGAACATGG	bp 3345 (rev)
	CATAGGCCACTAGTGGATCTG	delete <i>IRE1</i> promoter + <i>IRE1</i>
TP354	CGATACGGATACAGAAGCTGAAGATGATGAATCACCAGAAGGGGG	<i>SEC63</i> tagging (fwd)
	AGGCGGGGGTGGGA	pFA6a-6xGly-3xFlag-kanMX6
TP355	CGTCTAAGAGCTAAAATGAAAACTATACTAATCACTTATATCTAGAA	<i>SEC63</i> tagging (rev)
	TTCGAGCTCGTTTAAAC	pFA6a-6xGly-3xFlag-kanMX6
TP356	GGGTTTACTAAGAACCTCGTCCAGGATTTTCTGATTTGATGGGGG	<i>SEC61</i> tagging (fwd)
	GAGGCGGGGGTGGGA	pFA6a-6xGly-3xFlag-kanMX6
TP357	GCGATTTTTTTTTCTTTGGATATTATTTTCATTTTATATTCAGAATTC	<i>SEC61</i> tagging (rev)
	GAGCTCGTTTAAAC	pFA6a-6xGly-3xFlag-kanMX6

Table 13 | Oligonucleotides for molecular cloning.

Name	Sequence (5'→ 3')	Description
TP025	CGCGGATCCGAAACTCTGCTGCGCGCTGAA	CGC- <i>BamHI</i> - <i>IRE1</i> -551 bp (fwd)
TP124	CGCCTCGAGGCAATAATCAACCAAGAAGAAGCAGAGGGGCATGAA	CGC- <i>XhoI</i> - <i>IRE1</i> 3345 bp (rev)
	CATGTTATGAATACAAAAATTCACGTAATAATTTGATCG	
TP122	CGCAAGCTTGCTTTTAGGGACAGTTCTATTCTTCC	CGC- <i>HindIII</i> -5'homology <i>IRE1</i> (fwd)
TP123	CGCGGATCCAGTATAGCGACCAGC	CGC- <i>BamHI</i> -3'homology <i>IRE1</i> (rev)
TP166	GCAGAGGGGCATGAACATGTTATGAATACAAAAATTCACG	Delete C-terminal 1xHA tag from <i>IRE1</i> (rev)
TP167	CGTGAATTTTTGTATTCATAACATGTTTCATGCCCTCTGC	Delete C-terminal 1xHA tag from <i>IRE1</i> (fwd)
TP116	AATTCCTTTGCTACTGAAGTTTGAAGTCTAGTATATCGAATTATA	<i>EcoRI</i> - <i>IRE1</i> _AH+TMH-Cys-TAA- <i>HindIII</i> (fwd)
	GAGACTGGAGTATTTCTGTTGTTATTTCTCATTTTTGTGCAATACT	
TP117	ACAAAGATTCAAAATTTGTGTTAAA	<i>HindIII</i> -TTA-Cys- <i>IRE1</i> _AH+TMH- <i>EcoRI</i>
	AGCTTTTAAACA AAAATTTTGAATCTTTGTAGTATTGCACAAAAAT	
TP118	GAGAAATAACAACAGAAATACTCCAGTCTCTATAATTCGATATACTA	<i>EcoRI</i> -MGA2_TMh-Cys-TAA- <i>HindIII</i> (fwd)
	GACTTCCAACTTCAGTAGCAAAGAG	
TP119	AATTCGAAATGATAAAATGTTAATATTTTTCTGGATACCCCTTAACA	<i>HindIII</i> -TTA-Cys-MGA2_TMh- <i>EcoRI</i>
	CTACTACTTTTGACATGGTTCATCATGTACAAAATTTGGCAACCAAGA	
TP120	TTGTTAAA	<i>EcoRI</i> -SPT23_TMh-Cys-TAA- <i>HindIII</i> (fwd)
	AGCTTTTAAACAATCTTGGTTGCCAAATTTGTACATGATGAACCATGT	
TP121	CAAAAGTAGTAGTGTAAAGGGTATCCAGAAAAATATTAACATTTTAT	<i>HindIII</i> -TTA-Cys-SPT23_TMh- <i>EcoRI</i>
	CATTTCCGG	
TP120	AATTCAGAAATGATAAGATGCTCCTATTCTTTTGGATCCCTTAACT	<i>EcoRI</i> -SPT23_TMh-Cys-TAA- <i>HindIII</i> (fwd)
	TTAGTACTCTTATTATGTTTCACATTATCGAATTTGGGAAAGATTG	
TP121	TTAAA	<i>HindIII</i> -TTA-Cys-SPT23_TMh- <i>EcoRI</i>
	AGCTTTTAAACAATCTTCCCAAATTCGATAATGTGAAACATAATAA	
TP121	GAGTACTAAAGTTAAGGGGATCCAAAAGAATAGGAGCATCTTATCA	<i>HindIII</i> -TTA-Cys-SPT23_TMh- <i>EcoRI</i>
	TTCTGG	

Table 14 | Oligonucleotides for insertion, deletion or exchange of domains in *IRE1*.

Name	Sequence (5'→ 3')	Description
TP264	CCGGACTATGCAGGATCCTATCCATATGACGTTCCAGATTACGCTTCTAA AGGTGAAGAATTATTCAC	Introduce 3xHA after H815 (fwd)
TP265	GACGTCATACGGATAGCCCGCATAGTCAGGAACATCGTATGGGTAGTGTT CCGTTTCGACTTG	Introduce 3xHA after H815 (red)
TP266	GAATGTGAAAATATGATTGTAATAGG	Delete <i>IRE1</i> Δ III 253-272 (fwd)
TP267	TTTTGAACCAGGTCCGAAC	Delete <i>IRE1</i> Δ III 253-272 (rev)
TP274	CTTTTATTGCTGCTATTACTTCTTCAAAGATTCAAATTTTGCCG	Exchange TMH to L16 (fwd)
TP275	CAACAGCAATAACAGCAACAACAGTATAATTCGATATACTAGACTTCC	Exchange TMH to L16 (rev)
TP396	ATTGCTGCTATTACTTCTTCAAAGATTCAAATTTTGCCG	Exchange TMH to L13 (fwd)
TP397	AAAAGCAACAGCAATAACAGTCCAGTCTCTATAATTCG	Exchange TMH to L13 (rev)

Table 15 | Oligonucleotides for site-directed mutagenesis of *IRE1*.

Name	Sequence (5'→ 3')	Description
TP059	GTTTGAAGTCTAGTATATGCAATTATAGAGACTGGAGTATTTTC	R537A (fwd) ¹
TP060	GAAACTCCAGTCTCTATAATTGCATATACTAGACTTCCAAAC	R537A (rev) ¹
TP061	GTTTGAAGTCTAGTATATGAAATTATAGAGACTGGAGTATTTTC	R537E (fwd) ¹
TP062	GAAACTCCAGTCTCTATAATTTTCATATACTAGACTTCCAAAC	R537E (rev) ¹
TP063	GTCTAGTATATCGAATTATAGCGACTGGAGTATTTCTGTTG	E540A (fwd) ¹
TP064	CAACAGAAATACTCCAGTCGCTATAATTCGATATACTAGAC	E540A (rev) ¹
TP065	GTCTAGTATATCGAATTATAAAGACTGGAGTATTTCTGTTG	E540K (fwd) ¹
TP066	CAACAGAAATACTCCAGTCTTTATAATTCGATATACTAGAC	E540K (rev) ¹
TP150	GAAGATGAAAAGGTCTACGCGGGATCGATGAGAAC	T226A (fwd) ¹
TP151	GTTCTCATCGATCCCGCTAGACCTTTTCATCTTC	T226A (rev) ¹
TP152	GGTGAATTATATCAGCGGCCGACCTGGTTCAAAAAACG	F247A (fwd) ¹
TP153	CGTTTTTTGAACCAGGTCCGCGCGCTGATATAATTTACC	F247A (rev) ¹
TP154	CGCTCCAGTGACCGTGCAGGGTGTCTCAATTTTGG	W426A (fwd) ¹
TP155	CAAAAATTGAAGACACCCTCGCACGGTCACTGGAAGCG	W426A (rev) ¹
TP175	GTATTTCTGTTGTTAGCTCTCATTGCTTGCAATACTACAAAG	F548,551A (fwd) ¹
TP176	CTTTGTAGTATTGCACAAGCAATGAGAGCTAACAACAGAAATAC	F548,551A (rev) ¹

¹ oligonucleotides used for SDM of *in vivo* *IRE1* constructs

Materials

TP177	CTGGAGTAGCTCTGTTGTTATTTCTCATTTTTTG	F544A (fwd) ¹
TP178	CAAAAAATGAGAAATAACAACAGAGCTACTCCAG	F544A (rev) ¹
TP179	GAGACTGGAGTAGCTCTGTTGTTAGCTCTCATTGCTTGTGCAACTACTACAAAG	F544,548,551A (fwd) ¹
TP180	CTTTGTAGTATTGCACAAGCAATGAGAGCTAACAACAGAGCTACTCCAGTCTC	F544,548,551A (rev) ¹
TP208	GCTACTGAAGTTTGGAAAGTCTAGTATATTGTATTATAGAGACTGGAGTATTTCTGTTG	R537C (fwd) ²
TP209	CAACAGAAATACTCCAGTCTCTATAATACAATATACTAGACTTCCAAACTTCAGTAGCA AAG	R537C (rev) ²
TP210	GCTACTGAAGTTTGGAAAGTCTAGTATATCGATGTATAGAGACTGGAGTATTTCTGTTG	I538C (fwd) ²
TP211	CAACAGAAATACTCCAGTCTCTATACATCGATATACTAGACTTCCAAACTTCAGTAGC	I538C (rev) ²
TP212	CTGAAGTTTGGAAAGTCTAGTATATCGAATTTGTGAGACTGGAGTATTTCTGTTGTTATT TC	I539C (fwd) ²
TP213	GAAATAACAACAGAAATACTCCAGTCTCACAAATTCGATATACTAGACTTCCAAACTTC AG	I539C (rev) ²
TP214	GAAGTTTGGAAAGTCTAGTATATCGAATTATATGACTGGAGTATTTCTGTTG	E540C (fwd) ²
TP215	GAAATAACAACAGAAATACTCCAGTACATATAATTCGATATACTAGACTTCCAAACTTC AG	E540C (rev) ²
TP216	AGTTTGGAAAGTCTAGTATATCGAATTATAGAGTGTGGAGTATTTCTGTTG	T541C (fwd) ²
TP217	TGAGAAATAACAACAGAAATACTCCACACTCTATAATTCGATATACTAGACTTCCAAAC	T541C (rev) ²
TP218	GAAGTTTGGAAAGTCTAGTATATCGAATTATAGAGACTTGTGTATTTCTGTTGTTATTTCT CA	G542C (fwd) ²
TP219	TGAGAAATAACAACAGAAATACACAAGTCTCTATAATTCGATATACTAGACTTCCAAAC	G542C (rev) ²
TP220	GTCTAGTATATCGAATTATAGAGACTGGATGTTTTCTGTTGTTATTTCTCAT	V543C (fwd) ²
TP221	ATGAGAAATAACAACAGAAAACATCCAGTCTCTATAATTCGATATACTAGAC	V543C (rev) ²
TP222	AGTATATCGAATTATAGAGACTGGAGTATGTCTGTTGTTATTTCTCATTTTTTCTGC	F544C (fwd) ²
TP223	TGCAGAAAAAATGAGAAATAACAACAGACATACTCCAGTCTCTATAATTCGATATACT	F544C (rev) ²
TP224	CGAATTATAGAGACTGGAGTATTTTGTGTTATTTCTCATTTTTTCTGCAACTACTAC	L545C (fwd) ²
TP225	GTAGTATTGCAGAAAAAATGAGAAATAACAACAAAATACTCCAGTCTCTATAATTCG	L545C (rev) ²
TP226	CGAATTATAGAGACTGGAGTATTTCTGTGTTATTTCTCATTTTTTCTGCAACTACTACAA AG	L546C (fwd) ²
TP227	CTTTGTAGTATTGCAGAAAAAATGAGAAATAACAACAGAAATACTCCAGTCTCTATAAT TCG	L546C (rev) ²
TP228	CGAATTATAGAGACTGGAGTATTTCTGTTGTGTTTTCTCATTTTTTCTGCAACTACTACAA AG	L547C (fwd) ²
TP229	CTTTGTAGTATTGCAGAAAAAATGAGAAAACACAACAGAAATACTCCAGTCTCTATAAT TCG	L547C (rev) ²
TP230	AGAGACTGGAGTATTTCTGTTGTTATGTCTCATTTTTTCTGCAACTACTACAAAGA	F548C (fwd) ²

² oligonucleotides used for SDM of *in vitro* IRE1 constructs

TP231	TCTTTGTAGTATTGCAGAAAAAATGAGACATAACAACAGAAATACTCCAGTCTCT	F548C (rev) ²
TP232	AGACTGGAGTATTTCTGTTGTTATTTTGTATTTTTCTGCAATACTACAAAGATTCAAAA TTTTG	L549C (fwd) ²
TP233	CAAAATTTTGAATCTTTGTAGTATTGCAGAAAAAATACAAAATAACAACAGAAATACTCC AGTC	L549C (rev) ²
TP234	AGACTGGAGTATTTCTGTTGTTATTTCTCTGTTTTCTGCAATACTACAAAGA	I550C (fwd) ²
TP235	TGAATCTTTGTAGTATTGCAGAAAAACAGAGAAATAACAACAGAAATACTCCAGTCT	I550C (rev) ²
TP236	GACTGGAGTATTTCTGTTGTTATTTCTCATTGTTCTGCAATACTACAAAGATTC	F551C (fwd) ²
TP237	GAATCTTTGTAGTATTGCAGAACAAATGAGAAATAACAACAGAAATACTCCAGTC	F551C (rev) ²
TP238	ACTGGAGTATTTCTGTTGTTATTTCTCATTGTTTCTGTATACTACAAAGATTCAAAATTT TGT	A553C (fwd) ²
TP239	ACAAAATTTTGAATCTTTGTAGTATAACAAGAAAAATGAGAAATAACAACAGAAATACT CCAG	A553C (rev) ²
TP240	ACTGGAGTATTTCTGTTGTTATTTCTCATTGTTTCTGCATGCTACAAAGATTCAAAATTT TTGT	I554C (fwd) ²
TP241	ACAAAATTTTGAATCTTTGTAGACATGCAGAAAAAATGAGAAATAACAACAGAAATACT CCAGT	I554C (rev) ²
TP242	CTGTTGTTATTTCTCATTGTTTCTGCAATATGTCAAAGATTCAAAATTTTGTAAAAGCTT GGC	L555C (fwd) ²
TP243	GCCAAGCTTTTACAAAATTTTGAATCTTTGACATATTGCAGAAAAAATGAGAAATAACA ACAG	L555C (rev) ²
TP244	GTATTTCTGTTGTTATTTCTCATTGTTTCTGCAATACTACAAAGATTCAAAATTTTG	C552S (fwd) ²
TP245	CAAAATTTTGAATCTTTGTAGTATTGCAGAAAAAATGAGAAATAACAACAGAAATACTC C	C552S (rev) ²
TP260	GTATATCGAATTATACAGACTGGAGTATTTCTGTTG	E540Q (fwd) ¹
TP261	GAAATACTCCAGTCTGTATAATTCGATATACTAGAC	E540Q (rev) ¹
TP268	GTATATCGAATTATAAACACTGGAGTATTTCTGTTG	E540N (fwd) ¹
TP269	GAAATACTCCAGTGTTTATAATTCGATATACTAGAC	E540N (rev) ¹
TP270	GTATATCGAATTATAGACACTGGAGTATTTCTGTTG	E540D (fwd) ¹
TP271	GAAATACTCCAGTGTCTATAATTCGATATACTAGAC	E540D (rev) ¹
TP344	GCTACTGAAGTTTGAAGTCTACGATATCGAATTATAGAGAC	V535R (fwd) ^{1,2}
TP345	CTCCAGTCTCTATAATTCGATATCGTAGACTTCCAACTTCAG	V535R (rev) ^{1,2}
TP348	CCAAAATTTCTTTGCTACTGAAGCGTGAAGTCTAGTATATCG	F531R (fwd) ¹
TP349	CTATAATTCGATATACTAGACTTCCACGCTTCAGTAGCAAAG	F531R (rev) ¹
TP364	CTGAAGTTTGAAGTTGCGTATATCGAATTATAGAG	L534C (fwd) ²
TP365	CTATAATTCGATATACGCAACTTCCAACTTCAGTGAC	L534C (rev) ²
TP366	GAAGTTTGAAGTCTATGCTATCGAATTATAGAGACTGG	V535C (fwd) ²
TP367	CTCTATAATTCGATAGCATAGACTTCCAACTTCAGTAGC	V535C (rev) ²

Materials

TP368	GTTTGAAGTCTAGTATGCCGAATTATAGAGACTGG	Y536C (fwd) ²
TP369	GTCTCTATAATTCGGCATACTAGACTTCCAACTTCAG	Y536C (rev) ²
TP370	TCTTTGCTACTGAAGCGTGGAAGTCTAGTATATCG	F531R (fwd) ²
TP371	CGATATACTAGACTTCCACGCTTCAGTAGCAAAG	F531R (rev) ²

Oligonucleotides used for sequencing are listed in Table 16, and colony PCR primers in Table 17, respectively.

Table 16 | Oligonucleotides for sequencing.

Name	Sequence (5'→3')	Description
TP005	CGCAGCCGACGTTGAGGGTGGACTTC	bp 371 (fwd) Check <i>IRE1</i> sequence
TP006	CAAGTTGTCGTATGGATAAAGGCAG	bp 599 (rev) Check <i>IRE1</i> sequence
TP007	GGACGGCATGTGCATAGCGCCTTTCCG	bp 962 (fwd) Check <i>IRE1</i> sequence
TP008	GCTACTGAAGTTTGGAACTCTAG	bp 1580 (fwd) Check <i>IRE1</i> sequence
TP009	GAGGAAAAGAGGTTTCGAGAGGAG	bp 1931 (fwd) Check <i>IRE1</i> sequence
TP010	CTAGACTCTGGTCAGTCTTCATT	bp 2502 (fwd) Check <i>IRE1</i> sequence
TP011	GCAGAAGCTACAGATCTGATCTC	bp 2850 (fwd) Check <i>IRE1</i> sequence
TP025	CGCGGATCCTGAACTCTGCTGCGCGTGAA	bp -551 (fwd) Check <i>IRE1</i> sequence
TP031	ATGATTATACATGGGGATGT	Check sequence His3MX6 cassette (fwd)
TP034	CCCTCCTTGACAGTCTTGAC	Heukan fwd
TP099	GGCTGGAGCTTACGACTTTACTC	Check sequence His3MX6 cassette (rev)
RE133	GTCAAGACTGTCAAGGAGGG	Heukan rev

Table 17 | Oligonucleotides for colony PCR

Name	Sequence (5'→3')	Description
TP11	GCAGAAGCTACAGATCTGATCTC	check integration of <i>IRE1</i> -3xHA-GFP 5' fwd
TP202	CGGGTAGTTTATGTAGGGATGAG	check integration of <i>IRE1</i> -3xHA-GFP 5' rev
RE133	GTCAAGACTGTCAAGGAGGG	check integration of <i>IRE1</i> -3xHA-GFP 3' fwd
TP201	GCAAGTATGAACTATTTGGAAACAC	check integration of <i>IRE1</i> -3xHA-GFP 3' rev

Oligonucleotides used for reverse transcription quantitative PCR (RT-qPCR) are specified in Table 18.

Table 18 | Oligonucleotides for RT-qPCR.

Name	Sequence (5' → 3')	Description
TP286	GCGTAATCCAGAAGCGCAGT	Spliced <i>HAC1</i> (fwd)
TP128	GTGATGAAGAAATCATTCAATTCAAATG	Spliced <i>HAC1</i> (rev)
TP324	GATCGATTACGAGGGACCTAGA	<i>PDI1</i> (fwd)
TP325	GCGGAGGGCAAGTAAATAGAA	<i>PDI1</i> (rev)
TP169	TGTCACCAACTGGGACGATA	<i>ACT1</i> (fwd)
TP170	AACCAGCGTAAATTGGAACG	<i>ACT1</i> (rev)

3.9. Organisms

Escherichia coli (*E. coli*) was used for protein production and/or the amplification of various cloning and expression vectors produced by standard molecular biological techniques or by site-directed mutagenesis. All *E. coli* strains utilized in this study are listed in Table 19.

Table 19 | *E. coli* strains used in this study.

Name	Genotype	Source
BL21 Star (DE3) pRARE	F-ompT gal dcm lon hsdSB(rB-mB-) λ(DE3) pLysS(cmR) F-Φ80lacZΔM15Δ(lacZYA-argF) U169 recA1 endA1	Tampé Lab
DH5α (K12 strain)	hsdR17 (rK-, mK+) phoA supE44λ-thi-1 gyrA96 relA1	Invitrogen

E. coli BL21 Star (DE3) pRARE cells were transformed with all plasmids for expression in *E. coli* and are listed in Table 11.

All *S. cerevisiae* strains are listed in Table 20, respectively. These strains are isogenic to the standard laboratory strain BY4741. Yeast strains were received from the European *Saccharomyces cerevisiae* Archive For Functional Analysis (EUROSCARF) gene deletion library if not stated otherwise.

A $\Delta IRE1$ strain (YRE127) was generated using the pUG72-URA deletion cassette. The *IRE1* promoter (-1 to -551 bp) and the *IRE1* gene were removed from the genome and substituted by a URA selection marker. For transformation of *S. cerevisiae*, the knock-in plasmid was linearized as described in (3.7.1). Subsequently, the knock-in construct was introduced into the YRE127 strain. *SEC63* was C-terminally equipped with a 3xFLAG-tag by targeting a PCR product from the pFA6a-6xGly-3xFLAG-kanMX6 plasmid (Longtine et al., 1998) containing the tag-coding sequence to the 3'-end of *SEC63* using oligonucleotides listed in Table 12.

After transformation with linearized DNA and subsequent selection via the kanMX6 marker, the strains expressed a chromosomally tagged variant of *SEC63* from the endogenous promoter.

Table 20 | yeast strains used in this study.

Strain Number	Description	Genotype	Source	Plasmid
YRE001	BY4741	MATa; his3 Δ 1; leu2 Δ 0; met15 Δ 0; ura3 Δ 0	EUROSCARF	
YRE127	Δ IRE1	MATa; his3 Δ 1; leu2 Δ 0; met15 Δ 0; ura3 Δ 0; ire1 Δ ::URA	this study	(Gueldener et al., 2002)
YRE046	Δ IRE1	MATa; his3 Δ 1; leu2 Δ 0; met15 Δ 0; ura3 Δ 0; ire1 Δ ::kanMX3	EUROSCARF	
YRE420	IRE1-GFP WT	MATa; his3 Δ 1; leu2 Δ 0; met15 Δ 0; ura3 Δ 0; ire1 Δ ::URA IRE1-3xHA-GFP::HIS	this study	pRE419
YRE424	IRE1-GFP C552S	MATa; his3 Δ 1; leu2 Δ 0; met15 Δ 0; ura3 Δ 0; ire1 Δ ::URA IRE1-3xHA-GFP::HIS	this study	pRE450
YRE425	IRE1-3xHA-GFP WT	MATa; his3 Δ 1; leu2 Δ 0; met15 Δ 0; ura3 Δ 0; ire1 Δ ::URA IRE1-3xHA-GFP::HIS	this study	pRE451
YRE710	pRS315-Ire1-3xHA-GFP WT	MATa; his3 Δ 1; leu2 Δ 0; met15 Δ 0; ura3 Δ 0; ire1 Δ ::URA IRE1-3xHA-GFP::HIS	this study	pRE488
YRE426	IRE1-3xHA-GFP R537A	MATa; his3 Δ 1; leu2 Δ 0; met15 Δ 0; ura3 Δ 0; ire1 Δ ::URA IRE1-3xHA-GFP::HIS	this study	pRE453
YRE427	IRE1-3xHA-GFP R537E	MATa; his3 Δ 1; leu2 Δ 0; met15 Δ 0; ura3 Δ 0; ire1 Δ ::URA IRE1-3xHA-GFP::HIS	this study	pRE454
YRE428	IRE1-3xHA-GFP IF2 (W426A)	MATa; his3 Δ 1; leu2 Δ 0; met15 Δ 0; ura3 Δ 0; ire1 Δ ::URA IRE1-3xHA-GFP::HIS	this study	pRE455
YRE429	IRE1-3xHA-GFP E540N	MATa; his3 Δ 1; leu2 Δ 0; met15 Δ 0; ura3 Δ 0; ire1 Δ ::URA IRE1-3xHA-GFP::HIS	this study	pRE456
YRE430	IRE1-3xHA-GFP E540D	MATa; his3 Δ 1; leu2 Δ 0; met15 Δ 0; ura3 Δ 0; ire1 Δ ::URA IRE1-3xHA-GFP::HIS	this study	pRE457
YRE431	IRE1-3xHA-GFP Δ III (Δ 253-272)	MATa; his3 Δ 1; leu2 Δ 0; met15 Δ 0; ura3 Δ 0; ire1 Δ ::URA IRE1-3xHA-GFP::HIS	this study	pRE458
YRE708	IRE1-3xHA-GFP V535R Δ III (Δ 253-272)	MATa; his3 Δ 1; leu2 Δ 0; met15 Δ 0; ura3 Δ 0; ire1 Δ ::URA IRE1-3xHA-GFP::HIS	this study	pRE655
YRE433	IRE1-3xHA-GFP L16 TMH	MATa; his3 Δ 1; leu2 Δ 0; met15 Δ 0; ura3 Δ 0; ire1 Δ ::URA IRE1-3xHA-GFP::HIS	this study	pRE460
YRE703	IRE1-3xHA-GFP L13 TMH	MATa; his3 Δ 1; leu2 Δ 0; met15 Δ 0; ura3 Δ 0; ire1 Δ ::URA IRE1-3xHA-GFP::HIS	this study	pRE650
YRE434	IRE1-3xHA-GFP E540A	MATa; his3 Δ 1; leu2 Δ 0; met15 Δ 0; ura3 Δ 0; ire1 Δ ::URA IRE1-3xHA-GFP::HIS	this study	pRE461
YRE435	IRE1-3xHA-GFP E540Q	MATa; his3 Δ 1; leu2 Δ 0; met15 Δ 0; ura3 Δ 0; ire1 Δ ::URA IRE1-3xHA-GFP::HIS	this study	pRE462
YRE436	IRE1-3xHA-GFP F544,548,551A	MATa; his3 Δ 1; leu2 Δ 0; met15 Δ 0; ura3 Δ 0; ire1 Δ ::URA IRE1-3xHA-GFP::HIS	this study	pRE463
YRE438	IRE1-3xHA-GFP IF1 (T226A F247A)	MATa; his3 Δ 1; leu2 Δ 0; met15 Δ 0; ura3 Δ 0; ire1 Δ ::URA IRE1-3xHA-GFP::HIS	this study	pRE465

YRE444	<i>IRE1</i> -3xHA-GFP E540A IF1 (T226A F247A)	MATa; his3Δ1; leu2Δ0; met15Δ0; ura3Δ0; ire1Δ::URA <i>IRE1</i> -3xHA-GFP::HIS	this study	pRE468
YRE445	<i>IRE1</i> -3xHA-GFP E540A IF2 (W426A)	MATa; his3Δ1; leu2Δ0; met15Δ0; ura3Δ0; ire1Δ::URA <i>IRE1</i> -3xHA-GFP::HIS	this study	pRE469
YRE463	<i>IRE1</i> -3xHA-GFP E540K	MATa; his3Δ1; leu2Δ0; met15Δ0; ura3Δ0; ire1Δ::URA <i>IRE1</i> -3xHA-GFP::HIS	this study	pRE471
YRE498	<i>IRE1</i> -3xHA-GFP V535R	MATa; his3Δ1; leu2Δ0; met15Δ0; ura3Δ0; ire1Δ::URA <i>IRE1</i> -3xHA-GFP::HIS	Laura Henke (Bachelor Thesis)	pRE551
YRE500	<i>IRE1</i> -3xHA-GFP V535R, IF1 (T226A F247A)	MATa; his3Δ1; leu2Δ0; met15Δ0; ura3Δ0; ire1Δ::URA <i>IRE1</i> -3xHA-GFP::HIS	Laura Henke (Bachelor Thesis)	pRE553
YRE502	<i>IRE1</i> -3xHA-GFP V535R, IF2 (T426A)	MATa; his3Δ1; leu2Δ0; met15Δ0; ura3Δ0; ire1Δ::URA <i>IRE1</i> -3xHA-GFP::HIS	Laura Henke (Bachelor Thesis)	pRE555
YRE503	<i>IRE1</i> -3xHA-GFP F531R	MATa; his3Δ1; leu2Δ0; met15Δ0; ura3Δ0; ire1Δ::URA <i>IRE1</i> -3xHA-GFP::HIS	Laura Henke (Bachelor Thesis)	pRE556
YRE504	<i>IRE1</i> -3xHA-GFP F531R, IF1 (T226A F247A)	MATa; his3Δ1; leu2Δ0; met15Δ0; ura3Δ0; ire1Δ::URA <i>IRE1</i> -3xHA-GFP::HIS	this study	pRE557
YRE505	<i>IRE1</i> -3xHA-GFP F531R, IF2 (T426A)	MATa; his3Δ1; leu2Δ0; met15Δ0; ura3Δ0; ire1Δ::URA <i>IRE1</i> -3xHA-GFP::HIS	this study	pRE558
YRE510	<i>IRE1</i> -3xHA-GFP WT <i>SEC61</i> -3xFLAG	MATa; his3Δ1; leu2Δ0; met15Δ0; ura3Δ0; ire1Δ::URA; <i>IRE1</i> -3xHA-GFP::HIS3MX6; <i>SEC61</i> -FLAG::kanMX4	This study	(Funakoshi and Hochstrasser, 2009)
YRE511	<i>IRE1</i> -3xHA-GFP WT <i>SEC63</i> -3xFLAG	MATa; his3Δ1; leu2Δ0; met15Δ0; ura3Δ0; ire1Δ::URA; <i>IRE1</i> -3xHA-GFP::HIS3MX6; <i>SEC63</i> -FLAG::kanMX4	This study	(Funakoshi and Hochstrasser, 2009)
YRE512	<i>IRE1</i> -3xHA-GFP E540A <i>SEC61</i> -3xFLAG	MATa; his3Δ1; leu2Δ0; met15Δ0; ura3Δ0; ire1Δ::URA; <i>IRE1</i> -3xHA-GFP::HIS3MX6; <i>SEC61</i> -FLAG::kanMX4	This study	(Funakoshi and Hochstrasser, 2009)
YRE513	<i>IRE1</i> -3xHA-GFP E540A <i>SEC63</i> -3xFLAG	MATa; his3Δ1; leu2Δ0; met15Δ0; ura3Δ0; ire1Δ::URA; <i>IRE1</i> -3xHA-GFP::HIS3MX6; <i>SEC63</i> -FLAG::kanMX4	This study	(Funakoshi and Hochstrasser, 2009)
YRE516	<i>IRE1</i> -3xHA-GFP F531R <i>SEC61</i> -3xFLAG	MATa; his3Δ1; leu2Δ0; met15Δ0; ura3Δ0; ire1Δ::URA; <i>IRE1</i> -3xHA-GFP::HIS3MX6; <i>SEC61</i> -FLAG::kanMX4	This study	(Funakoshi and Hochstrasser, 2009)
YRE517	<i>IRE1</i> -3xHA-GFP F531R <i>SEC63</i> -3xFLAG	MATa; his3Δ1; leu2Δ0; met15Δ0; ura3Δ0; ire1Δ::URA; <i>IRE1</i> -3xHA-GFP::HIS3MX6; <i>SEC63</i> -FLAG::kanMX4	This study	(Funakoshi and Hochstrasser, 2009)
YRE518	BY4741 <i>SEC61</i> -3xFLAG	MATa; his3Δ1; leu2Δ0; met15Δ0; ura3Δ0; ire1Δ::URA; <i>SEC63</i> -FLAG::kanMX4	This study	(Funakoshi and Hochstrasser, 2009)
YRE519	BY4741 <i>SEC63</i> -3xFLAG	MATa; his3Δ1; leu2Δ0; met15Δ0; ura3Δ0; ire1Δ::URA; <i>SEC63</i> -FLAG::kanMX4	This study	(Funakoshi and Hochstrasser, 2009)
YRE520	<i>IRE1</i> -3xHA-GFP V535R <i>SEC61</i> -3xFLAG	MATa; his3Δ1; leu2Δ0; met15Δ0; ura3Δ0; ire1Δ::URA; <i>IRE1</i> -3xHA-GFP::HIS3MX6; <i>SEC61</i> -FLAG::kanMX4	This study	(Funakoshi and Hochstrasser, 2009)
YRE521	<i>IRE1</i> -3xHA-GFP V535R <i>SEC63</i> -3xFLAG	MATa; his3Δ1; leu2Δ0; met15Δ0; ura3Δ0; ire1Δ::URA; <i>IRE1</i> -3xHA-GFP::HIS3MX6; <i>SEC63</i> -FLAG::kanMX4	This study	(Funakoshi and Hochstrasser, 2009)

3.10. Media

3.10.1. Media and plates for cultivation of *E. coli*

Table 21 shows the composition of media and plates for the cultivation of *E. coli*. All media

were prepared utilizing ultrapure water and were sterilized by autoclaving. For the selection with antibiotics, 100 µg/ml ampicillin and/ or 34 µg/ml chloramphenicol were added to LB media, LB-rich media and LB-plates.

Table 21 | Media and plates for cultivation of *E. coli* used in this study.

Media	Composition
LB medium	1% (w/v) NaCl 1% (w/v) Peptone/Tryptone 0.5% (w/v) Yeast Extract
LB-rich medium	1% (w/v) NaCl 1% (w/v) Peptone/Tryptone 0.5% (w/v) Yeast Extract 0.5% Glucose
LB plates	1.5 - 2% Agar in 1% (w/v) NaCl 1% (w/v) Peptone/Tryptone 0.5% (w/v) Yeast Extract
SOB medium	2% (w/v) Peptone/Tryptone 0.5% (w/v) Yeast Extract 10 mM NaCl 2.5 mM KCl 10 mM MgCl ₂ 10 mM MgSO ₄

3.10.2. Media and plates for cultivation of *S. cerevisiae*

Media and plates for cultivation of *S. cerevisiae* and their composition can be found in Table 22. All media were prepared with ultrapure water and sterilized by autoclaving. The complete supplement mixture (CSM) was dissolved in autoclaved ultrapure water and heated to 80°C until the powder was dissolved completely. For sterilization, a 0.2 µm syringe filter was used to filtrate the CSM. For additional antibiotic selection, 200 µg/ml G418 was added to media and plates when indicated.

Table 22 | Media and plates for cultivation of *S. cerevisiae* used in this study.

Media	Composition
YPD	2% (w/v) Glucose 2% (w/v) Peptone/Tryptone 1% (w/v) Yeast Extract
SCD complete	0.5% (w/v) Ammonium sulfate 0.077% CSM complete 2% Glucose 0.17% (w/v) Yeast Nitrogen Base
SCD complete w/o inositol	0.5% (w/v) Ammonium sulfate 0.077% CSM complete 2% Glucose 0.17% (w/v) Yeast Nitrogen Base w/o inositol
SCD – URA	0.5% (w/v) Ammonium sulfate 0.077% CSM w/o URA 2% Glucose 0.17% (w/v) Yeast Nitrogen Base
SCD – HIS	0.5% (w/v) Ammonium sulfate 0.077% CSM w/o HIS 2% Glucose 0.17% (w/v) Yeast Nitrogen Base
YPD plates	1.5 - 2% Agar in 2% (w/v) Glucose 2% (w/v) Peptone/Tryptone 1% (w/v) Yeast Extract
SC plates	1.5 - 2% Agar in 0.5% (w/v) Ammonium sulfate 0.077% CSM 2% Glucose 0.17% (w/v) Yeast Nitrogen Base

4. Methods

4.1. Microbiological methods

4.1.1. Generation of chemically competent *E. coli*

DH5 α and BL21+pRARE competent *E. coli* cells were generated utilizing the Inoue method (Inoue et al., 1990). DH5 α cells were used for DNA preparation, while BL21+pRARE cells were used for expression of indicated MBP-fusion constructs. In all cases, an aliquot of frozen competent *E. coli* cells was thawed on ice, used to inoculate 4 mL of SOB media and grown at 37°C under shaking conditions over night. 200 μ L of this overnight culture were inoculated in 100 mL SOB media and grown until they reached an OD₆₀₀ of 0.4 – 0.5. Cells were harvested by centrifugation (4,000x g, 10 min, 4°C) and the resulting cell pellet resuspended in 16 mL pre-cooled TB buffer (10 mM PIPES, 55 mM MnCl₂, 15 mM CaCl₂, 250 mM KCl; pH 6.7). The cells were collected (4,000x g, 10 min, 4°C) and the pellets resuspended in 10 mL pre-cooled TB buffer supplemented with 700 μ l DMSO and mixed by pipetting. The cells (aliquots of 100 μ L each) were frozen in liquid nitrogen and stored at -80°C.

4.1.2. Transformation of competent *E. coli*

Competent cells (4.1.1) were thawed on ice, supplemented with 50 – 200 ng DNA and incubated at 4°C for 30 min. A heat shock at 42°C was performed for 60 s. The cells were cooled down and recovered at 4°C for 5 min prior to the addition of 500 μ L LB media. The mixture was incubated for 30 – 45 min at 37°C, rocking. The cell suspension was centrifuged (3,000x g, 5 min, room temperature) and resuspended in 100 μ L of fresh LB media before the transformed cells were plated onto selective LB-agar plates, containing ampicillin (DH5 α) or ampicillin and chloramphenicol (BL21+pRARE) and incubated at 37°C until colonies had formed.

4.1.3. Cultivation and storage of *E. coli*

E. coli cultures were grown at 37 °C in LB liquid media under shaking conditions (180 rpm) or on LB-agar plates overnight. For antibiotic selections, 100 μ g/ml ampicillin and/or 34 μ g/ml Chloramphenicol were added to the growth medium. For long-term storage of plasmid containing *E. coli* cells, stationary overnight cultures were adjusted to 22.2% (v/v) glycerol utilizing a 50% (v/v) glycerol solution in a total volume of 900 μ l, and stored at -80 °C.

4.1.4. Generation of competent *S. cerevisiae*

The lithium acetate-based method was used for preparation of competent yeast (Ito et al., 1983). To this end, a 3 ml pre-culture in YPD was inoculated with a single yeast colony and grown at 30°C overnight, shaking at 220 rpm. The pre-culture was used to inoculate a 50 ml YPD culture to an OD₆₀₀ of 0.2. Cells were grown at 30°C until an OD₆₀₀ of 0.8 – 1.0 was reached and harvested by centrifugation (3,000x g, RT, 5 min). Cells were washed once with 1 ml LATE buffer (10 mM Tris-HCl, 0.1 M LiAc, 1 mM EDTA; pH 8.0) and finally resuspended in 250 µl LATE buffer. Competent yeast were stored at 4°C for one week.

4.1.5. Transformation of competent *S. cerevisiae*

50 µl of competent yeast (4.1.4) were supplemented with 5 µl Sperm ssDNA, which was denatured at 95°C for 10 min and cooled on ice prior to use. 0.5 - 1 µg DNA were added and the reaction incubated for 20 min at RT. Subsequently, 10 µl DMSO and 150 µl PLATE buffer (10 mM Tris-HCl, 0.1 M LiAc, 1 mM EDTA, 40% PEG-4000; pH 8.0) were added and the mixture was incubated for 30 min at 30°C. A heat shock at 42°C for 15 min was performed to facilitate the uptake of DNA by competent cells. The cells were pelleted by centrifugation (6,000x g, RT, 5 min), washed with 1 ml sterile water and resuspended in 80 µl sterile water, prior to plating on appropriate selective agar plates. Plates were incubated at 30°C for 2 to 3 days, to allow formation of yeast single colonies. Single colonies were selected twice on dropout agar plates, followed by cultivation on YPD plates for 3 – 4 days prior to a third selection on selective plates, respectively, before they were used for long-term storage (4.1.6). Positively selected cells were tested by colony-PCR (4.2.8) and used for long-term storage (4.1.6). Respective selection markers of individual constructs and the resulting genotype of all yeast strains created and utilized in this study can be extracted from Table 20.

4.1.6. Cultivation and storage of *S. cerevisiae*

If not stated otherwise, liquid cultures of *S. cerevisiae* cells were grown at 30°C and 220 rpm. A single colony was used to inoculate overnight pre-cultures of 3 ml in indicated liquid medium. Overnight pre-cultures were used to inoculate main cultures to an OD₆₀₀ = 0.2. For long-term storage of yeast strains, cells were grown to stationary phase. 3 ml pre-cultures in respective liquid media were inoculated with a single colony and grown overnight. 500 µl of the cell suspension were adjusted to 22.2% (v/v) glycerol utilizing a 50% (v/v) glycerol solution and stored as glycerol stocks at -80°C. For each experiment, yeast strains from glycerol stocks were plated on respective agar plates and incubated 2 – 3 days at 30°C until single colonies

had formed. Plates were stored at 4°C and used to inoculate cultures for a maximum of one week.

4.2. Molecular biological methods

4.2.1. Polymerase chain reaction (PCR)

Polymerase chain reaction (PCR) was performed to amplify specific DNA sequences, site-directed mutagenesis, for C-terminal tagging of endogenous genes in yeast, and to test the correct insertion of DNA fragments by homologous recombination into the yeast genome. Oligonucleotides used for PCR are listed in Tables 13 and 17. Standard reaction conditions of PCR reactions performed in this study can be extracted from Table 23.

Table 23 | Standard reaction mixture and conditions for PCR.

Standard PCR reaction mixture		Standard reaction conditions			
Template (50 ng)	x	Initial denaturation	1x	98°C	30 s
Forward Primer (10 pmol/μl)	2.5 μl	Denaturation	32x	98°C	10 s
Reverse Primer (10 pmol/μl)	2.5 μl	Annealing	32x	x	10 s
5x HF Buffer	10 μl	Elongation	32x	72°C	x
dNTP's (10 mM)	1 μl	Final elongation	1x	72°C	5 min
DMSO (optional)	2.5 μl				
PHUSION DNA Polymerase	0.5 μl				
ddH ₂ O (autoclaved)	x				
Total volume	50 μl				

The elongation time and annealing temperature utilized in this study were adjusted according to the predicted melting temperature of the primers and the size of the PCR product, respectively. Generally, the elongation time was adjusted to 30 s per kbp of the amplified product. Agarose gel electrophoresis was used to control the amplification of the PCR product (4.2.2). PCR products used for molecular cloning were purified using the QIAquick Gel Extraction Kit according to the manufacturer's protocol, eluted in 30 μl ddH₂O (autoclaved) and stored for further use at -20°C. Absorption measurements at 260 nm using a spectrophotometer (NanoDrop) were utilized to determine DNA concentrations of the purified products.

4.2.2. Agarose gel electrophoresis

For analysis and separation of DNA fragments by their size, agarose gel electrophoresis was used. DNA samples were supplemented with 6x DNA loading dye (NEB) and added onto agarose gels containing 0.7 – 1.5% (w/v) agarose in TAE buffer (40 mM Tris-Acetate, 1 mM EDTA, pH 8.0). A DNA standard was included and the DNA was separated by electrophoresis

at 140 V. The gels were stained utilizing ethidium bromide (0.5 µg/ml) to visualize DNA fragments by UV-light illumination. Specific DNA fragments could be extracted and purified using the QIAquick Gel Extraction Kit according to the manufacturer's instructions including all optional washing steps. DNA elution was performed in 30 µl ddH₂O (autoclaved) and stored for further use at -20°C. Absorption measurements at 260 nm using a spectrophotometer (NanoDrop) were utilized to determine DNA concentrations of the purified products.

4.2.3. Restriction digest

In this study, cloning of an *IRE1* knock-in construct (3.7.1) and MBP fusion constructs (3.7.2) was achieved by classical molecular cloning utilizing restriction enzymes.

Table 24 | Standard reaction mixture for restriction digestion.

Standard reaction mixture	
Plasmid (2-5 µg)	x
10x Cut Smart Buffer	5 µl
Restriction Enzyme I	1 µl
Restriction Enzyme II	1 µl
ddH ₂ O (autoclaved)	x
Total volume	50 µl

Restriction reactions were incubated overnight at RT. Heat inactivation of the restriction enzymes was performed by incubation of the reaction mixtures at 80°C for 10 min. Utilizing Antarctic Phosphatase, the digested vector was dephosphorylated to reduce the number of false positive clones. To this end, 1 µl Antarctic Phosphatase and 6 µl reaction buffer were added to the reaction mixture and the total volume was adjusted to 60 µl with ddH₂O. The reaction mixture was incubated for 1.5 h at 37°C and inactivated at 70°C for 5 min. The resulting DNA fragments were analyzed and purified by agarose gel electrophoresis (4.2.2).

4.2.4. Ligation

The NEB Quick Ligation Kit was used according to the manufacturer's protocol to ligate the digested vector backbones with the digested insert. Briefly, 50 - 100 ng of the vector backbone were incubated with a threefold molar excess of the insert for ligation. Transformation of competent *E. coli* DH5α cells with 2 µl of ligation mix was performed as described in (4.1.2) prior to plating on ampicillin containing LB-agar plates. Incubation of respective plates was performed at 37°C until single colonies had formed. Plasmids were isolated from single colonies (4.2.9) and successful cloning verified by DNA sequencing (4.2.12).

4.2.5. Site-directed mutagenesis (SDM)

Mutations were introduced into the *IRE1* gene of the knock-in construct and the MBP-Ire1^{AH+TMH} fusion construct utilizing a PCR-based strategy derived from the QuikChange® method (Stratagene). To this end, two complementary oligonucleotide primers were designed that differed in up to six nucleotides from the original template for mutagenesis. To achieve binding to the template, the mutagenesis primers were flanked by a 15-20bp homology. Tables 14 and 15 list all forward (fwd) and reverse (rev) primers utilized for SDM in this study. Standard reaction conditions of SDM reactions performed in this study can be extracted from Table 25. Generally, the elongation time was adjusted to 45 s per kbp of the amplified product.

Table 25 | Standard reaction mixture and conditions for SDM.

Standard SDM reaction mixture		Standard SDM reaction conditions			
Template (20 – 50 ng)	x	Initial denaturation	1x	98°C	30 s
Forward Primer (10 pmol/μl)	0.5 μl	Denaturation	25x	98°C	30 s
Reverse Primer (10 pmol/μl)	0.5 μl	Annealing	25x	x	10 s
5x HF Buffer	10 μl	Elongation	25x	72°C	x
dNTP's (10 mM)	1.25 μl	Final elongation	1x	72°C	15 min
DMSO (optional)	2.5 μl				
PHUSION DNA Polymerase	0.5 μl				
ddH ₂ O (autoclaved)	x				
Total volume	50 μl				

When multiple mutations were introduced at a time, a megaprimer PCR was utilized for mutagenesis. In this two-step mutagenesis reaction, two mutagenic oligonucleotide primers were used in a first PCR reaction to produce a megaprimer, which was used for a second PCR reaction to amplify the entire plasmid. Non-mutated, methylated template DNA was removed from the reaction mix by incubation with 10 units of *DpnI* at 37 °C for 3 hours. Transformation of competent *E. coli* DH5α cells with 1 μl of SDM reaction mixture was performed as described in (4.1.2) prior to plating on ampicillin containing LB-agar plates. Incubation of respective plates was performed at 37°C until single colonies had formed. Plasmids were isolated from single colonies (4.2.9) and successful mutagenesis verified by DNA sequencing (4.2.12).

4.2.6. Engineering *IRE1* utilizing the Q5 Site-Directed Mutagenesis Kit

The Q5 Mutagenesis kit is a commercially available system designed to delete, substitute or insert sequences of up to 100 nucleotides into a template plasmid DNA using the robust Q5 Hot Start High-Fidelity Polymerase. Primers are listed in Table 14 and the design was performed utilizing the NEBase changer online tool (New England Biosciences). Mutagenesis

was performed according to the manufacturer's protocol, followed by a kinase, ligase & DpnI (KLD) treatment. To decrease the number of false positive clones, incubation of the KLD reaction was increased to 15 min. Transformation of competent *E. coli* DH5 α cells with 2 μ l of the KLD reaction was performed as described in (4.1.2).

4.2.7. Genomic tagging in *S. cerevisiae*

The pFA6a plasmids were designed to facilitate C-terminal tagging of any gene of interest (GOI) in *S. cerevisiae* (Longtine et al., 1998). The desired tag and a marker cassette, which is required for selection, can be amplified using the standardized F2 and R1 primers (Longtine et al., 1998). In this study, the pFA6a-6xGly-3xFLAG-kanMX6 plasmid (Funakoshi and Hochstrasser, 2009) was used to obtain C-terminally 3xFLAG-tagged variants of *SEC61* and *SEC63* under the control of their own promoter and at their endogenous locus, using primers listed in Table 12.

4.2.8. Colony PCR of *S. cerevisiae*

Colony PCR was utilized to verify genomic insertions of a DNA fragment by homologous recombination (Fig. 15). Two PCR reactions were performed to verify the correct insertion of the DNA fragment into the genome at the 5' end (colony PCR primer A+B) and at the 3' end (colony PCR primer C+D). A third colony PCR was performed for the *IRE1* knock-in construct (colony PCR primers A+D) to result in a full-length product for subsequent DNA sequencing.

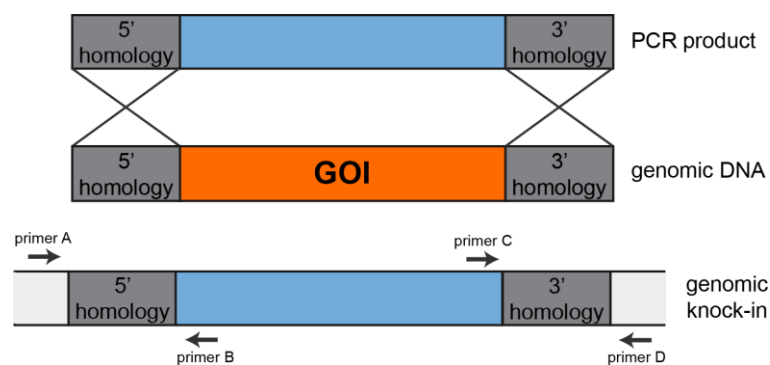


Figure 15 | Schematic illustration of a homologous recombination event in yeast and its verification by colony PCR.

Briefly, single colony from a selective agar plate was lysed by resuspension in 50 μ l 20 mM NaOH and heated to 95°C for 20 min. For removal of cell debris, the suspension was centrifuged (16,000x g, RT, 1 min). 5 μ l of the remaining supernatant was used as a template for the PCR reaction. The standard reaction mixture and conditions were used for colony PCR (4.2.1), all used oligonucleotides are depicted in Table 17.

4.2.9. Plasmid preparation from *E. coli*

For plasmid DNA preparation, competent DH5 α *E. coli* cells were previously transformed with the desired plasmid and grown on LB-agar plates until single colonies had formed. A single colony was picked and used to inoculate 5 ml of LB media supplemented with respective antibiotics and incubated over night at 37°C under shaking conditions. The plasmid preparation was carried out following the manufacturer's protocol utilizing the QIAprep Spin Miniprep Kit and the total amount of purified DNA determined by absorption measurements at 260 nm using the NanoDrop[®] photospectrometer.

4.2.10. RNA preparation from *S. cerevisiae*

For RNA preparation, an overnight culture (30 ml) was inoculated from one single colony of the required yeast strains and cultured at 30°C in YPD or SCD complete media until they reached the mid-exponential phase and used to inoculate a fresh culture of 30 ml in respective media to an OD₆₀₀ = 0.2. In order to induce lipid bilayer stress by inositol depletion, the cells were thoroughly washed with inositol-depleted medium before cultivation in inositol-depleted medium for an additional 3 h. In order to induce massive ER-stress, the cells were first grown in YPD for 3 h and then stressed by adjusting the medium to 4 mM DTT for further cultivation for 1 h. After cultivation, 5 OD₆₀₀ equivalents of cells were harvested by centrifugation, washed with PBS (137 mM NaCl, 2,7 mM KCl, 8 mM Na₂HPO₄, 1.5 mM KH₂PO₄) and snap frozen utilizing liquid N₂ and stored at -80°C. Total RNA was extracted using the RNeasy Plus RNA Isolation Kit according to the manufacturer's protocol. RNA samples were quantified by absorption measurements using a NanoDrop spectrophotometer.

4.2.11. Reverse transcription (RT)

cDNA was synthesized from 500 ng total RNA using oligo(dt)12-18 primers (0.5 μ g), PCR grade dNTP mix (0.5 μ M) First Strand Buffer (1x), DTT (10mM) and Superscript[™] II Reverse Transcriptase (Invitrogen) according to the manufacturer's protocol.

4.2.12. DNA sequencing

DNA sequencing was performed by the SeqLab Sequence Laboratories. 200 ng of plasmid DNA were premixed with 2 μ M sequencing primer and adjusted to a total volume of 10 μ l with ddH₂O. All oligonucleotide primers used for sequencing are listed in Table 16.

4.3. Biochemical methods

4.3.1. *In vivo* methods

4.3.1.1. *Preparation of cell extracts for immunoblotting*

For immunoblotting, 20 OD₆₀₀ equivalents of cells grown to the mid-exponential phase (OD₆₀₀ = 1.0) were harvested by centrifugation, washed with PBS (137 mM NaCl, 2,7 mM KCl, 8 mM Na₂HPO₄, 1.5 mM KH₂PO₄) and frozen at -20°C. Cell pellets were lysed in 1 ml lysis buffer (PBS, 10 µg/ml chymostatin, 10 µg/ml antipain, 10 µg/ml pepstatin) by bead beating (disruptor genie, Scientific Industries) with zirconia beads (Roth) for 5 min at 4°C. For SDS-PAGE (4.3.2.4) followed by immunoblotting (4.3.2.6), the cell lysate was mixed with 5x reducing sample buffer (8 M urea, 0.1 M Tris-HCl pH 6.8, 5 mM EDTA, 3.2% (w/v) SDS, 0.15% (w/v) bromphenol blue, 4% (v/v) glycerol, 4% (v/v) β-mercaptoethanol) at a ratio of 5:1 and heated to 95°C for 10 min for denaturation.

4.3.1.2. *Membrane fractionation & extraction*

For membrane fractionation, 80 OD₆₀₀ equivalents of cells grown to the mid-exponential phase (OD₆₀₀ = 1.0) were harvested by centrifugation, washed with PBS (137 mM NaCl, 2,7 mM KCl, 8 mM Na₂HPO₄, 1.5 mM KH₂PO₄) and frozen. All subsequent steps were performed at 4°C. The cell pellets were resuspended in 1 ml lysis buffer (50 mM HEPES, pH 7.4, 150 mM NaCl, 1 mM EDTA, 10 µg/ml chymostatin, 10 µg/ml antipain, 10 µg/ml pepstatin) and disrupted by bead beating (disruptor genie, Scientific Industries) with zirconia beads (Roth) for 5 x 1 min. Cell debris was removed by centrifugation (5 min, 800x g) and the cleared lysate was further centrifuged (10 min, 5,000x g) for sedimentation of mitochondria. Subsequently, the samples were centrifuged (45 min, 100,000x g) to pellet the microsomal membrane fraction. For membrane extraction experiments, the remaining supernatant was divided into equal parts and mixed with an equal volume of lysis buffer supplemented with 0.2 M Na₂CO₃ (pH 11.0), 2% Triton X-100, 5 M urea or without further additives and incubated for 1 h on an overhead rotator. Subsequently, the samples were centrifuged (45 min, 100,000x g) to pellet the microsomal membrane fraction, the pellet resuspended and supplemented with 5x reducing sample buffer (8 M urea, 0.1 M Tris-HCl pH 6.8, 5 mM EDTA, 3.2% (w/v) SDS, 0.15% (w/v) bromphenol blue, 4% (v/v) glycerol, 4% (v/v) β-mercaptoethanol) at a ratio of 5:1 and heated to 95°C for 10 min for denaturation, followed by further analysis using SDS-PAGE (4.3.2.4) and immunoblotting (4.3.2.6).

4.3.1.3. Reverse transcription-quantitative PCR (RT-qPCR)

Quantitative Real Time PCR was conducted on a PikoReal Real-time PCR system (Thermo Scientific) utilizing Absolute qPCR SYBR Green Mix (Thermo Scientific) or HiQu SYBR Green reaction Mix (HiQu). *ACT1*, *PDI1* and spliced *HAC1* were amplified using primers listed in Table 18. All reactions were performed in technical duplicate. Non-template control (RNA) and non-reaction control (H₂O) were routinely performed. The qPCR program included Step 1: 95°C, 15 min; Step 2: 95°C, 20s; Step 3: 58°C, 20s; Step 4: 72°C, 30s, Step 5: 72°C, 5 min; 40 cycles of steps 2-4 were carried out. Relative quantification was performed after normalization to *ACT1* levels based on the comparative $\Delta\Delta CT$ method (StepOnePlus™ user Manual, Applied Biosystems)

4.3.1.4. Immunoprecipitation

For (co-) immunoprecipitation (co-IP), 50 OD₆₀₀ equivalents of cells grown to the mid-exponential phase (OD₆₀₀) were harvested by centrifugation, washed with PBS and frozen. All subsequent steps were performed at 4°C. The cell pellets were resuspended in 1 ml lysis buffer (50 mM HEPES, pH 7.4, 150 mM NaCl, 1 mM EDTA, 10 µg/ml chymostatin, 10 µg/ml antipain, 10 µg/ml pepstatin) and disrupted by bead beating (disruptor genie, Scientific Industries) with zirconia beads (Roth) for 5 x 1 min. Cell debris was pelleted by centrifugation (5 min, 800x g) and the cleared lysate was adjusted to 1% digitonin (Sec63 co-IP) or 1% Triton X-100 (Kar2 co-IP) for solubilization for 1h on an overhead rotator. Non-solubilized components were removed by centrifugation (10 min, 21,000x g). HA-tagged and FLAG-tagged proteins were retrieved using 20 µl anti-HA high affinity matrix slurry (Roche) and 20 µl EZview™ Red ANTI-FLAG® M2 affinity Gel beads, respectively. Beads were washed thoroughly with IP buffer (50 mM HEPES, pH 7.4, 150 mM NaCl, 1 mM EDTA, 0.1% of respective detergent) prior to protein elution in 2.5x reducing sample buffer (4 M urea, 0.05 M Tris-HCl pH 6.8, 2.5 mM EDTA, 1.6% (w/v) SDS, 0.075% (w/v) bromphenol blue, 2% (v/v) glycerol, 2% (v/v) β-mercaptoethanol) and heated to 95°C for 10 min for denaturation, followed by further analysis using SDS-PAGE (4.3.2.4) and immunoblotting (4.3.2.6).

4.3.2. In vitro methods

4.3.2.1. Heterologous expression and purification of MBP-Ire1^{AH+TMH}

In this study, the expression and purification of MBP-Ire1^{AH+TMH} and other MBP-TMH fusion proteins used in the lab (MBP-Mga2^{TMH}, MBP-Spt23^{TMH}) were established. The strategy was modified from a publication by the group of Britta Brügger (Contreras et al., 2012) and has been published for MBP-Mga2^{TMH} (Covino et al., 2016). Heterologous expression of all MBP-

Ire1^{AH+TMH} variants was performed in *E. coli* BL21 Star (DE3) pRARE cells. 2 l culture in LB-rich medium supplemented with 100 µg/ml ampicillin and 34 µg/ml chloramphenicol was inoculated 1:50 from an overnight culture and grown at 37°C until an OD₆₀₀ = 0.6 was reached. Protein production was induced by the addition of 0.3 mM IPTG for 3 h at 37°C and the cells were harvested by centrifugation (4,000x g, 20 min). The cell pellet was stored at -20°C until further use. All further procedures were carried out at 4°C. For cell lysis, the cell pellet was resuspended in 10 ml lysis buffer (50 mM HEPES, pH 7.4, 150 mM NaCl, 1 mM EDTA, 10 µg/ml chymostatin, 10 µg/ml antipain, 10 µg/ml pepstatin, 2 mM DTT, 5 U/ml benzonase) per liter culture and disrupted by sonication (3x60s, amplitude 30%, 70% duty cycle). For MBP-Ire1^{AH+TMH} solubilization, the lysate was adjusted to a concentration of 50 mM β-OG and incubated for 10 min while gently shaking. Cell debris and non-solubilized material was removed by centrifugation (30 min, 100,000x g) prior to application to 1.5 ml amylose resin (NEB) per liter culture. The column was washed with 25 CV (column volumes) of wash buffer (50 mM HEPES, pH 7.4, 150 mM NaCl, 1 mM EDTA, 50 ml β-OG). The protein was eluted in 2.5 CV elution buffer (50 mM HEPES, pH 7.4, 150 mM NaCl, 1 mM EDTA, 50 ml β-OG, 10 mM maltose, 5 mM TCEP). Protein concentration was determined using the absorbance at 280 nm and the extinction coefficient after the Lambert-Beer-Equation (Source). The extinction coefficient and molecular weight of for MBP-Ire1^{AH+TMH} and its mutants was estimated utilizing the PROTPARAM tool (Gasteiger et al., 2005). Samples for SDS-PAGE were prepared by supplementation of 5x reducing sample buffer (8 M urea, 0.1 M Tris-HCl pH 6.8, 5 mM EDTA, 3.2% (w/v) SDS, 0.15% (w/v) bromphenol blue, 4% (v/v) glycerol, 4% (v/v) β-mercaptoethanol) at a ratio of 5:1 and heated to 95°C for 10 min for denaturation, followed by further analysis using SDS-PAGE (4.3.2.4) and immunoblotting (4.3.2.6).

4.3.2.2. Spinlabeling of MBP-Ire1^{AH+TMH}

Single cysteine mutants of MBP-Ire1^{AH+TMH} were expressed as described in (4.3.2.1). Purification of the fusion protein was performed with minor modifications. After the solubilized lysate was added to the amylose resin, the column was washed with 20 CV (column volumes) of wash buffer 1 (50 mM HEPES, pH 7.4, 150 mM NaCl, 1 mM EDTA, 50 ml β-OG, 1 mM TCEP), followed by 20 CV of wash buffer 2 (50 mM HEPES, pH 7.4, 150 mM NaCl, 1 mM EDTA, 50 ml β-OG) to remove residual reducing agents. Site-directed spin-labeling with 1 mM MTSSL (Enzo Life Sciences) was performed for 4 h while gently shaking. Excessive spin label was removed by extensive washing with 20 CV of wash buffer 2 prior to protein elution in 2.5 CV elution buffer (50 mM HEPES, pH 7.4, 150 mM NaCl, 1 mM EDTA, 50 ml β-OG, 10 mM maltose). Samples for SDS-PAGE were prepared by supplementation of 5x reducing sample buffer (8 M urea, 0.1 M Tris-Hcl pH 6.8, 5 mM EDTA, 3.2% (w/v) SDS, 0.15% (w/v) bromphenol

blue, 4% (v/v) glycerol, 4% (v/v) β -mercaptoethanol) at a ratio of 5:1 and heated to 95°C for 10 min for denaturation. The quality of the purified fusion protein was controlled by SDS-PAGE (4.3.2.4) followed by coomassie staining (Instant Blue™; Expedeon) (4.3.2.5) and immunoblotting (4.3.2.6). Spin-labeling efficiencies were determined for all constructs by double-integration of the EPR resonances. A 100 μ M standard of free MTS-SL in identical buffer conditions was compared to each construct and the estimated spin-label concentration correlated with the protein concentration of each sample. Protein concentrations were determined by absorption measurements at OD₂₈₀. Labeling efficiencies ranged from 75 – 95%.

4.3.2.3. Size exclusion chromatography (SEC)

Analytical size exclusion chromatography (SEC) was performed to investigate the oligomeric state of the protein using a Superdex 200 10/300 increase column (24 ml bed volume, GE Healthcare) in filtered, degassed SEC buffer (50 mM HEPES, pH 7.4, 150 mM NaCl, 1 mM EDTA, 50 ml β -OG) utilizing a Äkta Pure (GE Healthcare) FPLC system. Concentration dependent oligomerization of the fusion construct was analyzed by injection of different protein concentrations (0.1 – 2.0 mg/ml). Before application, the protein sample was cleared for larger particles by centrifugation (20.000x g, 10 min, 4°C). A 100 μ l sample loop was used and the SEC-run performed at a flow rate of 0.5 ml/min and fractions of 0.5 ml were collected for further analysis. Samples for SDS-PAGE were prepared by supplementation of 5x reducing sample buffer (8 M urea, 0.1 M Tris-Hcl pH 6.8, 5 mM EDTA, 3.2% (w/v) SDS, 0.15% (w/v) bromphenol blue, 4% (v/v) glycerol, 4% (v/v) β -mercaptoethanol) at a ratio of 5:1 and heated to 95°C for 10 min for denaturation. The quality of the purified fusion protein was controlled by SDS-PAGE (4.3.2.4) followed by coomassie staining (Instant Blue™; Expedeon) (4.3.2.5) and/ or immunoblotting (4.3.2.6).

4.3.2.4. SDS-Polyacrylamide gel electrophoresis (SDS-PAGE)

Discontinuous SDS-PAGE was performed to separate proteins based on their molecular weight using 4-15% Mini-PROTEAN-TGX gels (Biorad). To avoid cysteine oxidation or reduce existing disulfide bridges, protein samples were mixed with 5x reducing sample buffer (8 M urea, 0.1 M Tris-Hcl pH 6.8, 5 mM EDTA, 3.2% (w/v) SDS, 0.15% (w/v) bromphenol blue, 4% (v/v) glycerol, 4% (v/v) β -mercaptoethanol) at a 5:1 ratio and were denatured by heating for 10 min at 95 °C. For crosslinking experiments, non-reducing sample buffer was added to the protein samples, respectively. Denatured samples were loaded on respective gels and the electrophoresis performed at a constant voltage of 180 V in Running Buffer (25 mM Tris-HCl

pH 8.3, 192 mM glycine, 1% SDS) for 35 - 45 min. Separated proteins were visualized by immunodetection (4.3.2.6) or coomassie blue staining (Instant Blue™; Expedeon) (4.3.2.5).

4.3.2.5. Coomassie blue staining

After SDS-PAGE, the gels were stained utilizing the Instant Blue™ staining solution (Expedeon). Coomassie stain nonspecifically collocates with proteins in the gel by binding to basic and hydrophobic amino acid side chains, leading to the detection of all proteins residing in the gel. Gels were incubated at RT under constant agitation in Instant Blue™ (Expedeon) for 30 to 60 min and were incubated in dH₂O for 1 h, resulting in a blue signal for labeled proteins.

4.3.2.6. Immunoblotting

After SDS-PAGE, separated proteins were transferred from the polyacrylamide gel onto a methanol-activated PDVF membrane for immunodetection by semi-dry Western-Blotting (25 V, 1.0 A, 30 min) in Blotting Buffer (25 mM Tris-HCl pH 8.3, 192 mM glycine, 20% methanol) using a TransBlot® Turbo™ Transfer System (Bio-Rad). Prior to detection of the proteins, the membrane containing immobilized proteins was incubated in Blocking Buffer (3 – 5% (w/v) milk powder in TBS-T) for 15 min to block residual protein binding sites on the membrane. Primary antibodies specific to the protein of interest were added at an appropriate dilution in Blocking Buffer (Table 7) and membranes were incubated (1 h and RT or overnight at 4 °C). Membranes were washed (5x5 min in TBS-T) and incubated with a horseradish peroxidase coupled secondary antibody (see Table 9) specific to the primary antibody in Blocking Buffer for 1 h. Prior to detection, the membranes were washed extensively as previously described. Bound antibody was detected utilizing chemoluminescence of the horseradish peroxidase using the Clarity Western ECL Substrate (BioRad), or for proteins of low abundance, the SuperSignal West Femto ECL developing solution (Fisher Scientific). Resulting chemoluminescence was detected in a luminescence-imaging system (Biorad). If quantification was desired, the software Fiji was utilized.

4.3.2.7. Liposome preparation

All lipids used for liposome preparation were dissolved in chloroform as 20 mg/ml stock solutions and are listed in Table 2. The lipid mixtures shown in Fig. 16 were produced from *E. coli* polar lipids (EPL), 1,2-dioleoyl-*sn*-glycero-3-phosphocholine (DOPC), 1-palmitoyl-2-oleoyl-*sn*-glycero-3-phosphocholine (POPC), 1,2-dioleoyl-*sn*-glycero-3-phosphoethanolamine (DOPE), 1-palmitoyl-2-oleoyl-*sn*-glycero-3-phosphoethanolamine

(POPE), 1,2-dipalmitoyl-*sn*-glycero-3-phosphocholine (DPPC), L- α -phosphatidylinositol (Soy-PI) and cholesterol:

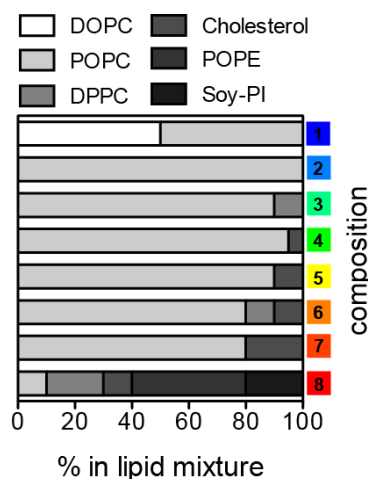


Figure 16 | Lipid compositions used for reconstitution.

These lipid mixtures comprise increasing fractions of saturated lipids, a change in PC:PE ratio, and increasing amounts of cholesterol and were utilized to mimic different degrees of molecular membrane packing. The lipids were mixed and the organic solvent evaporated utilizing a constant nitrogen stream at 60°C, while gently shaking. The lipid cake was dried using a desiccator under vacuum conditions for 1 h and hydrated using reconstitution buffer (20 mM HEPES, pH 7.4, 150 mM NaCl, 5% glycerol (w/v)) under strong agitation at 60°C for 20 min, yielding a lipid concentration of 10 mM. Subsequently, the dehydrated lipids were heated in a sonication water bath at 50°C for 30 min prior to snap freezing in liquid N₂ and storage at -80°C.

4.3.2.8. Reconstitution of MBP-Ire1^{AH+TMH} fusion proteins in liposomes

Purified fusion protein was reconstituted into liposomes with described lipid compositions at a molar protein:lipid (P:L) ratio of \approx 1:400 – 1:1000 for EPR studies. For cysteine-crosslinking experiments, reconstitution was performed at a molar ratio of \approx 1:6000. Table 26 shows the amount of protein and lipid added to the reconstitution mixture to achieve the above-mentioned molar ratios, respectively.

Table 26 | Protein and lipid amounts and their molar ratios used for reconstitution.

Molar P:L ratio	protein (μ g)	lipid (mM)
1:400	200	1.6
1:1000	100	2.0
1:6000	15	0.8

Multi-laminar liposomes were mixed with β -OG for complete solubilization and mixed with the respective amount of protein in reconstitution buffer to a final concentration of 37 mM β -OG and a total volume of 1 ml. The mixture was incubated for 20 min at room temperature. For detergent removal, 50 mg (reconstitution into *E. coli* polar lipid containing liposomes) or 100 mg (all other lipid compositions) of Bio-Beads™ SM-2 Adsorbent Media (BioRad) were added and the mixture was incubated for 90 min at room temperature in an overhead rotator. The solution was transferred to a fresh tube containing 350 mg (reconstitution into *E. coli* polar lipid containing liposomes) or 400 mg (all other lipid compositions) of Bio-Beads™ SM-2 Adsorbent Media (BioRad) and again incubated for 90 min, prior to harvesting of the proteoliposomes by centrifugation (1.5 h, 4°C, 450,000x g). The proteoliposomes were resuspended in reconstitution buffer and snap frozen in liquid N₂ for storage. Samples for SDS-PAGE were prepared by supplementation of 5x reducing sample buffer (8 M urea, 0.1 M Tris-Hcl pH 6.8, 5 mM EDTA, 3.2% (w/v) SDS, 0.15% (w/v) bromphenol blue, 4% (v/v) glycerol, 4% (v/v) β -mercaptoethanol) at a ratio of 5:1 and heated to 95°C for 10 min for denaturation. SDS-PAGE (4.3.2.4) and subsequent InstantBlue staining (4.3.2.5) were performed as previously described to estimate protein recovery of the reconstitution from the supernatant and the pelleted fractions.

4.3.2.9. Sucrose step gradient centrifugation

A sucrose step gradient centrifugation was performed to validate the incorporation of the MBP-Ire1^{AH+TMH} protein into proteoliposomes. Sucrose was dissolved in reconstitution buffer at final concentrations of 60% (w/v), 40% (w/v), 20% (w/v), 10% (w/v). A proteoliposome-containing sample was adjusted to a final concentration of 50% (w/v) sucrose at a volume of 500 μ l and filled into a UZ tube to form the bottom layer of the gradient and overlaid with 3 ml of each of the following sucrose solutions in reconstitution buffer: 40% (w/v), 20% (w/v), 10% (w/v), 0% (w/v). The resulting step-gradient was centrifuged (100,000x g, 16 h, no break) using a SW28.1 swing out rotor and subsequently fractionated in 1 ml fractions. Samples for SDS-PAGE were prepared by supplementation of 5x reducing sample buffer (8 M urea, 0.1 M Tris-Hcl pH 6.8, 5 mM EDTA, 3.2% (w/v) SDS, 0.15% (w/v) bromphenol blue, 4% (v/v) glycerol, 4% (v/v) β -mercaptoethanol) at a ratio of 5:1 and heated to 95°C for 10 min for denaturation. SDS-PAGE (4.3.2.4), subsequent immunoblotting (4.3.2.6) and Hoechst33342 fluorescence spectroscopy (4.3.2.11) were performed to analyze the protein and lipid content of each fraction.

4.3.2.10. Carbonate extraction as quality control of proteoliposomes

Carbonate extraction experiments were performed to investigate the incorporation and association of the MBP-Ire1^{AH+TMH} protein with liposomal membranes. The protein was reconstituted as described (4.3.2.8) and resuspended in 1 ml of reconstitution buffer. The proteoliposomes divided into equal parts and mixed with an equal volume of reconstitution buffer supplemented with **i)** 0.2 M Na₂CO₃ (pH 11.0), **ii)** 2% SDS or **iii)** without further additives and incubated on an overhead rotator (30 min, RT). Prior to centrifugation (90 min, 25°C, 450,000x g), the NaCO₃ treated sample was neutralized by addition of two volumes of neutralization buffer (200 mM HEPES pH 7.0, 150 mM NaCl), while the volume of all other samples was adjusted by the addition of equivalent amounts of reconstitution buffer. The samples were mixed with 5x reducing sample buffer (8 M urea, 0.1 M Tris-Hcl pH 6.8, 5 mM EDTA, 3.2% (w/v) SDS, 0.15% (w/v) bromphenol blue, 4% (v/v) glycerol, 4% (v/v) β-mercaptoethanol) at a ratio of 2:1 and heated to 95°C for 10 min, for SDS-PAGE (4.3.2.4) and subsequent InstantBlue staining (4.3.2.5) or immunoblotting (4.3.2.6).

4.3.2.11. Proteinase K digest

Proteinase K digestion experiments were performed to investigate the topology of MBP-Ire1^{AH+TMH} insertion into proteoliposomes. Proteoliposome containing samples (~0,25 µg/µl protein) were incubated with 5 µl reconstitution buffer and 1 µl Proteinase K for 1h at RT. As a control, proteoliposomes were treated with 6 µl of reconstitution buffer (negative control), or 5 µl 10% SDS and 1 µl Proteinase K (positive control). To inactivate the Proteinase K, all samples were boiled at 95°C for 15 min prior to mixing of the samples with 5x reducing sample buffer (8 M urea, 0.1 M Tris-Hcl pH 6.8, 5 mM EDTA, 3.2% (w/v) SDS, 0.15% (w/v) bromphenol blue, 4% (v/v) glycerol, 4% (v/v) β-mercaptoethanol) at a ratio of 2:1. Samples were heated to 95°C for 10 min for SDS-PAGE (4.3.2.4) and subsequent InstantBlue staining (4.3.2.5) or immunoblotting (4.3.2.6).

4.3.2.12. Hoechst 33342 measurements

The fluorescence intensity of the environment-sensitive Hoechst 33342 dye increases significantly in a hydrophobic environment (e.g. liposomes). Thus, Hoechst 33342 was used to estimate the relative lipid content of proteoliposome-containing samples (Jumpertz et al., 2011). To this end, samples were adjusted to a final concentration of 7 µM Hoechst33342 and the suspension was excited at 355 nm (slit width = 3 nm) and emission was recorded at 459 nm (slit width = 3 nm) using the Fluoromax-4 spectrometer (Horiba). The lipid content of each sample was estimated by using the background-corrected fluorescence intensity at 459 nm.

4.3.2.13. C-Laurdan fluorescence measurements of liposomes

C-Laurdan is a hydrophobic fluorescent dye, which intercalates into the lipid bilayer. This dye measures the degree of water penetration into the membrane, which directly reports on lipid packing (Kaiser et al., 2009). C-Laurdan has two characteristic emission maxima. In loosely packed lipid bilayers the emission maximum lies at 485 nm, while it shifts to 440 nm in a densely packed lipid environment (Kaiser et al., 2009). When excited at 375 nm, a generalized polarization (GP) value can be calculated by the integration of the fluorescence intensities from 400 – 460 nm (I_{ch1}) and 470 – 530 nm (I_{ch2}), thus reporting on the water penetration into the bilayer (Parasassi et al., 1990). While in theory, these GP values can range from +1 (very ordered) to -1 (very disordered), the experimental range of GP values is much lower, ranging from 0.51 for a 50% sphingomyelin and 50% cholesterol containing membrane at 23°C (Kaiser et al., 2009), to -0.35 for pure DOPC membranes at 24.7°C (Kim et al., 2007).

In this study, liposome suspensions at a final concentration of 0.33 mM were mixed with C-Laurdan (2p probes) to a final concentration of 0.4 μ M, resulting in a 1:832 ratio of C-Laurdan to lipid. The suspension was excited at 375 nm (slit width = 3 nm) and an emission spectrum was recorded at 30°C from 400 nm to 600 nm (slit width = 3 nm) using the Fluoromax-4 spectrometer (Horiba). The generalized polarization (GP) value was determined as described previously (Covino et al., 2016).

4.3.2.14. Oxygen mediated cysteine crosslinking of MBP-Ire1^{AH+TMH} fusion proteins in proteoliposomes

For cysteine crosslinking of reconstituted MBP-Ire1^{AH+TMH} variants, single-cysteine mutants of MBP-Ire1^{AH+TMH} were purified in the presence of 4 mM TCEP to keep the protein in its monomeric form as described previously (4.3.2.1). Reconstitution was performed at a molar protein to lipid ratio of 1:6000 as described in (4.3.2.8) and the resulting pellet was resuspended in 200 μ l reconstitution buffer. The crosslinking reaction was performed without the addition of catalysts of oxidative crosslinking.

Briefly, 25 μ l of proteoliposomes were incubated for 6.5 days at 37°C in an oxygen-containing atmosphere. To analyze the formation of protein oligomers, 10 μ l of each protein sample were mixed with 5x non-reducing sample buffer (8 M urea, 0.1 M Tris-HCl pH 6.8, 5 mM EDTA, 3.2% (w/v) SDS, 0.15% (w/v) bromphenol blue, 4% (v/v) glycerol, 4% (v/v)) at a ratio of 2:1 and heated to 95°C for 10 min, for SDS-PAGE (4.3.2.4) and subsequent immunoblotting (4.3.2.6).

4.3.2.15. Circular dichroism (CD) spectroscopy

CD spectroscopy was performed on a J-715 spectropolarimeter (Jasco). Peptides were measured at a concentration of 20 μM in the presence and absence of 1% DDM (w/v) in 20 mM sodium phosphate buffer, pH 7.0. Experiments were performed at room temperature in a HELLMA quartz cell with an optical path length of 0.01 cm. Each spectrum was obtained by averaging several scans recorded from 190 to 260nm with a bandwidth of 2 nm, a step of 1 nm and a scan speed of 20 nm/min. All spectra were blanked to their respective buffers.

4.4. Biophysical methods

4.4.1. Continuous wave (cw) EPR spectroscopy measurements

For continuous wave (cw) EPR spectroscopy, spin-labeled protein was reconstituted as described in (4.3.2.8) and resuspended in 15 μl reconstitution buffer. The spin-labeled samples were analyzed in glass capillaries with 1 mm inner diameter (Hirschmann). X-Band cwEPR spectra were recorded using the MiniScope MS 400 spectrometer (Magnetech) with 10 mW microwave power and 0.15 mT field modulation amplitude. EPR spectra were collected at 30°C and -115°C.

4.4.2. Analysis of cwEPR spectra

Analysis of cwEPR spectra recorded at low temperature ($T = -115^\circ\text{C}$) provide information on the polarity of the spin probe nano-environment based on the hyperfine splitting (A_{zz}) and inter-spin distances in a distance range below 1.8 nm. cwEPR spectra were recorded as the first derivative of the absorption signal. After baseline correction, all spectra were intensity normalized using the intensity of the middle field peak. 30°C spectra were recorded to investigate the relative mobility of the spin probe, which was determined by the line width of the middle field peak (ΔH^0) of respective EPR spectrum. To derive information on the polarity of the nano-environment of the spin probe, EPR spectra were recorded at -115°C and the difference in field strengths ($2A_{zz}$) between the low and high field peaks was determined. EPR spectra recorded at -115°C report on inter-spin distances below ≈ 1.8 nm when spectral broadening occurs due to dipolar coupling (Bordignon and Steinhoff, 2007). In a semi-quantitative manner, the ratio of intensities of the low (I_f) and middle field peaks (I_m determined as peak to peak distance divided by two) was used to derive the degree of spectral broadening, representing a measure for inter-spin distances.

4.5. Cell biology

4.5.1. Yeast growth assay

An overnight culture of the desired yeast strain in SCD complete or YPD media was grown until cells reached stationary phase and was used to inoculate a fresh culture in respective media to an $OD_{600} = 0.2$. Cells were grown at 30°C for 5-6 h and adjusted to an $OD_{600} = 0.05$. 50 μ l of cells were used to inoculate 180 μ l of respective media supplemented with 20 μ l DTT (end-concentration ranging from 0 – 2 mM in SCD complete or 0 – 8 mM in YPD media, 4:5 dilution series). Cells were grown for 18 h at 30°C in a 96-well plate and the OD_{620} determined using a 96-well plate compatible photospectrometer (BMG Fluostar Galaxy)

4.5.2. Live cell confocal microscopy

If not stated otherwise, cells were grown to mid-exponential growth phase as previously described. Cells were depleted for inositol by cultivation in inositol-depleted medium for 3 h. Massive ER-stress was induced by cultivating the cells in SCD complete medium containing 10 mM DTT for 1.5 h. Prior to imaging, the cells were immobilized on microscopic slides coated with the respective media containing 2% agar. Microscopy was performed using the Zeiss LSM 780 and Zeiss LSM 880 confocal laser scanning microscopes (Carl Zeiss AG), with spectral detection and a Plan-Apochromat 63 x 1.40 NA oil immersion objective. GFP fluorescence was excited at 488 nm. Fluorescence emission was detected between 500 – 600 nm. Transmission images were simultaneously recorded using differential interference contrast (DIC) optics. Data acquisition was performed in collaboration with Harald Hofbauer. Kristina Halbleib grew and manipulated the cells and performed the data analysis.

Table 27 | Microscope settings for fluorescence live cell imaging used for quantitative analysis and respective quantification parameters.

Experiment	ER stress condition	Microscope	Analysis	Threshold
WT s. WT <i>CEN</i>	10 mM DTT	LSM780	z-stacks	160/255
WT vs. F531R	10 mM DTT	LSM780	z-stacks	160/255
WT vs. V535R	10 mM DTT	LSM780	z-stacks	160/255
WT vs. E540A	10 mM DTT	LSM780	z-stacks	160/255
WT vs. F531R	inositol depletion	LSM880	single confocal plane	52/255
WT vs. V535R	inositol depletion	LSM880	single confocal plane	52/255
WT vs. E540A	inositol depletion	LSM780	single confocal plane	42/255

Cells expressing Ire1^{3xHA-GFP} and its mutants were analyzed and Ire1-positive clusters per cell were counted using an automated script established in Fiji (Schindelin et al., 2012).

Microscope settings for cells expressing respective mutants and their isogenic wild type versions are depicted in Table 16. For cells treated with 10 mM DTT, z-stacks (240 nm step-size) were recorded using 2% laser power to avoid rapid bleaching events and merged to z-projections (high intensity clusters). The image threshold was set to 160/255 to result in a b/w picture identifying fluorescent clusters of Ire1^{3xHA-GFP}. Selected clusters were analyzed utilizing the analyze particles function in Fiji counting all particles meeting set criteria (size: 4-infinity px; circularity: 0-1; including holes). For cells grown under inositol depletion conditions, microscopic images were recorded using 10% laser power and one confocal plane was monitored through the center of the cells (low intensity clusters). For Ire1 cluster analysis, the image threshold was set to 52/255. All subsequent steps were carried out as previously described. The number of analyzed cells was determined manually and dead cells were omitted from the analysis.

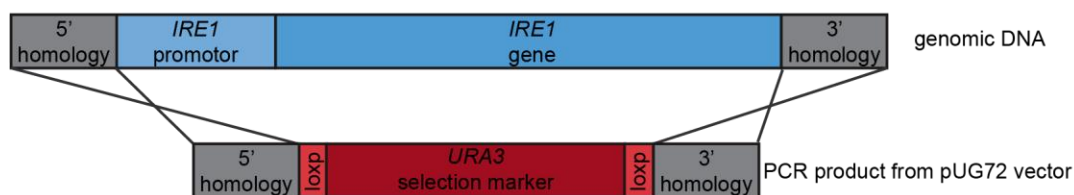
5. Results

5.1. Establishing a knock-in strategy to express *IRE1* at its endogenous locus and expression levels

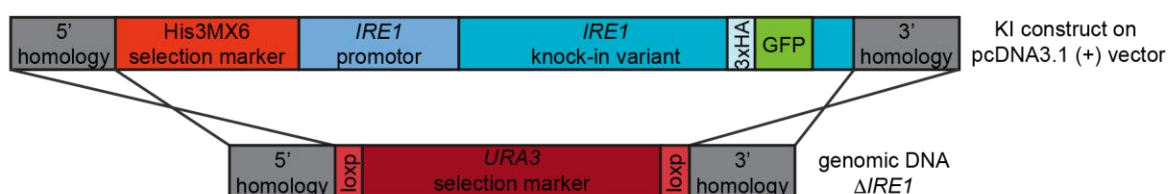
In order to study structure-function relationships of Ire1 in its native environment, a knock-in strain expressing a tagged variant of *IRE1* was generated. More specifically, an Δ *IRE1* strain was generated using an *URA3* selection marker (Fig. 17 A). The knock-in constructs of *IRE1* and its mutants were re-introduced at the native *IRE1* locus by homologous recombination to yield knock-in strains (Fig. 17 B). The correct integration of the knock-in cassette was verified by colony PCR (Fig. 17 C).

Previously, most genetic studies of Ire1 in the cellular context relied on expression systems such as 2 μ plasmids or *CEN*-based plasmids bearing *IRE1*'s native promoter (van Anken et al., 2014; Aragón et al., 2009; Kimata et al., 2004, 2007; Oikawa et al., 2007; Promlek et al., 2011; Sikorski and Hieter, 1989). Major disadvantages of these systems are the overproduction of *IRE1* and a relatively high cell-to-cell variation of the expression levels. Especially for Ire1, which oligomerizes upon activation, any difference from the endogenous protein level should be avoided as this would directly affect the signaling outcome. With only 60 (Kulak et al., 2014) to 259 copies per cell (Ghaemmaghami et al., 2003), Ire1 is an extremely low abundant protein and any overproduction should be avoided.

A knock-out strategy



B knock-in strategy



C knock-in verification



Figure 17 | Knock-in strategy of *IRE1* for the integration at the endogenous locus.

(A) A $\Delta IRE1$ strain was constructed using the pUG72-URA deletion cassette (Guedener et al., 2002). The promoter and coding region of *IRE1* was substituted by the *URA3* selection cassette in BY4741 cell to generate an *IRE1* knock-out. (B) The *IRE1* knock-in cassette, consisting of 551 bp of the *IRE1* promoter, a modified version of the *IRE1* gene encoding for affinity and GFP tags, and an His3MX6 marker cassette was generated as described in (3.7.1). A linear fragment of this cassette was targeted to the *IRE1* locus of the knockout strain. (C) The correct insertion of knock-in construct was verified utilizing colony-PCR using the primer pairs indicated in Table 17.

The knock-in cassette encoded for a tagged variant of Ire1: Based on a tagging strategy established by van Anken *et al.*, Ire1 was tagged internally at a flexible loop at position H875 (van Anken et al., 2014). This tag was comprised of a codon-optimized version of monomeric GFP as a fluorescent tag and an 3xHA epitope tag. The tagging strategy facilitated live cell microscopy experiments and the detection of Ire1 by immunoblotting using monoclonal antibodies directed against the HA-epitope (Fig. 18 A) (Halbleib et al., 2017). The functionality of the tagged variant was tested using a sensitive growth assay (Fig.18 B). Cells lacking *IRE1* were substantially more sensitive to the UPR-inducing agent dithiothreitol (DTT), while cells producing the internally tagged variant of Ire1 grew indistinguishable from isogenic wild-type cells. Consistent with previous observations by others (van Anken et al., 2014), this suggested that the tagged variant of Ire1 expressed from its endogenous locus and promoter is functional.

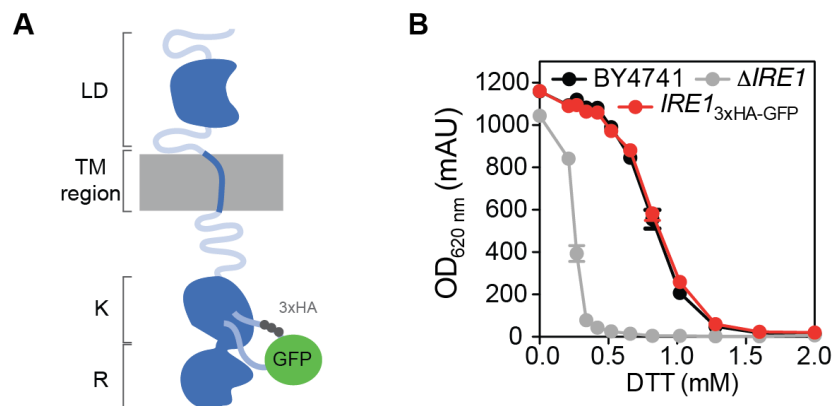


Figure 18 | The *IRE1* knock-in construct used in this study

(A) Schematic representation of the tagged variant of Ire1 used in this study. The luminal domain (LD), the transmembrane region (TM region), the kinase (K) and RNase domains (R) are shown in dark blue. Regions of high flexibility are indicated in light blue. A 3xHA epitope tag (grey) and a codon-optimized version of monomeric GFP (green) were introduced at a flexible loop at position H875. (B) Growth assay of the *IRE1* knock-in construct (*IRE1*_{3xHA-GFP}), its isogenic wild type strain (BY4741) and a $\Delta IRE1$ strain. Equal cell densities were used for the inoculation of minimal medium (SCD) supplemented with DTT at $OD_{600} = 0.01$ and 30°C for 18 h. The final density of the culture was determined using the OD_{620} . The error bars represent the mean \pm SEM of $n = 3$ biological replicates.

The proper insertion of Ire1 into the ER-membrane was validated by subcellular fractionation experiments and extraction assays, using Pgk1 (phosphoglycerate kinase 1; cytosolic protein) as a soluble, cytosolic reference protein and Dpm1 (dolichyl-phosphate mannosyltransferase 1; ER membrane protein) as a reference for a microsomal membrane protein. As expected, centrifugation at $100.000\times g$ allowed for a separation of soluble and ER membrane associated proteins (Fig. 19).

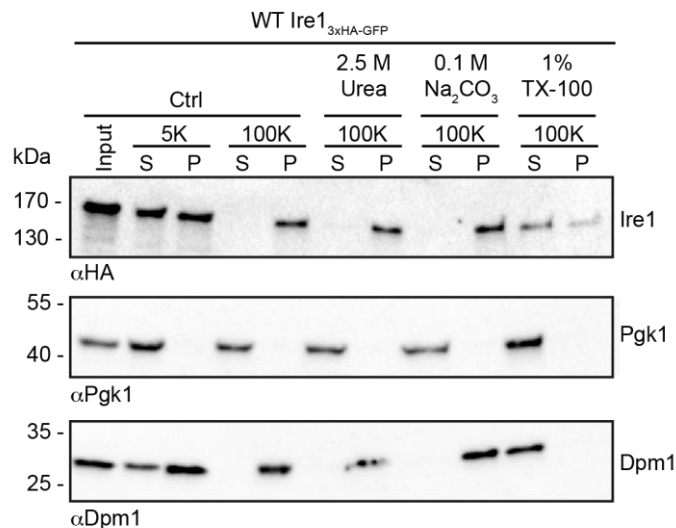


Figure 19 | Analysis of Ire1 integration by membrane fractionation and extraction experiments.

80 OD equivalents of exponentially growing cells producing *Ire1*_{3xHA-GFP} were harvested and lysed. Membrane fractionation revealed *Ire1*_{3xHA-GFP} localized into microsomal membranes (P100) pelleted by a centrifugation at $100.000\times g$. Carbonate and urea extraction experiments as described (4.3.1.2) were used to test the integration of *Ire1*_{3xHA-GFP} in the membrane, while Triton X-100 extraction experiments served to solubilize microsomal membranes. Samples were subjected to SDS-PAGE and immunoblotting using an anti-HA antibody for detection of *Ire1*_{3xHA-GFP}, Pgk1 (soluble protein) and Dpm1 (ER membrane protein) antibodies.

The microsomal pellet was resuspended in different buffers with excess of Na_2CO_3 or urea and did not extract Ire1 from the membrane, indicating a proper insertion into the ER-membrane. As expected, treatment of the microsomal membranes with the detergent Triton X-100 partially solubilized Ire1. These observations are consistent with previous observations by others (Kimata et al., 2007). In summary, these data suggest that the tagged variant of Ire1 is successfully integrated into the ER membrane and functional.

As a control, *IRE1*_{3xHA-GFP} was also cloned into a *CEN*-based expression vector under the control of its own promoter and introduced into a Δ *IRE1* strain (purchased from EUROSCARF). A comparative immunoblot analysis of cells producing Ire1 from *CEN*-based plasmids or its endogenous locus, respectively, revealed that the *CEN*-based expression resulted in an approximately 2.5-fold higher steady-state level of Ire1 (Fig. 20 A) and live cell microscopy revealed a striking cell-to-cell variation of expression (Fig. 20 B). While these data do not allow a statement on whether the knock-in construct of Ire1 is produced at the endogenous level found in isogenic wildtype strains, they suggest that the knock-in strategy is more suitable to study structure-function relationships than previously used strategies based on *CEN*- and 2 μ plasmids.

The activation of the UPR relies on the formation of signaling-active clusters of Ire1 (van Anken et al., 2014; Aragón et al., 2009; Cohen et al., 2017). In order to validate these findings with the knock-in construct that warrants a lower steady-state expression level, acutely stressed cells were imaged by confocal fluorescence microscopy. Clusters of Ire1 were clearly distinguishable from the background signal caused by auto-fluorescence. In the absence of ER stress, these clusters were absent (Fig. 20) (Halbleib et al., 2017).

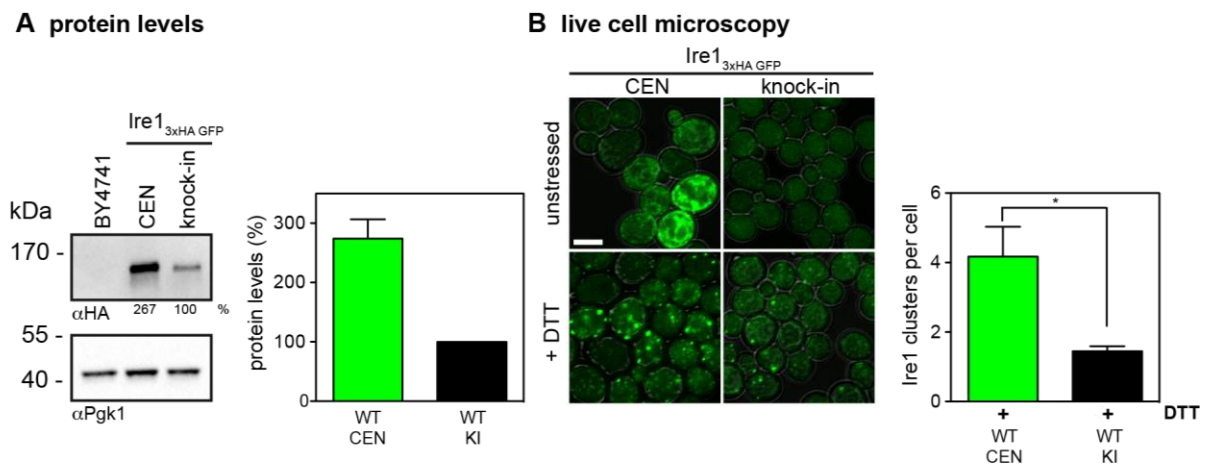


Figure 20 | Ire1_{3xHA-GFP} protein production from CEN-based plasmids and from the endogenous locus.

(A) Exponentially growing cells lacking an epitope-tagged variant of Ire1 (BY4741) or producing Ire1_{3xHA-GFP} from the endogenous promoter on a CEN-based plasmid (CEN) or from its endogenous genomic locus (knock-in) were harvested and lysed. The lysate was subjected to SDS-PAGE and immunoblotting using anti-HA antibodies. The isogenic wild type strain (BY4741) served as specificity control of the detection. Equal loading was validated using anti-Pgk1 antibodies. The error bars represent the mean \pm SEM of 5 independent experiments. (B) Confocal fluorescence microscopy with stressed (1.5h, 2 mM DTT, SCD medium) and unstressed (SCD medium) cells from the indicated strains. Quantification of high and low intensity clusters of Ire1 per cell based on a semi-automated script. A minimum of 40 cells was analyzed for each individual replicate. The error bars represent the mean \pm SEM of 5 independent experiments. Statistical significance was tested by an unpaired, two-tailed student's t-test. * $p < 0.05$.

5.2. The functional role of Ire1's TMH in ER stress

Ire1 is activated by lipid bilayer stress (Han et al., 2010; Pineau et al., 2009; Promlek et al., 2011; Volmer et al., 2013). In order to identify structural features that could mediate membrane-sensitivity, TMH region of Ire1 was subjected to a closer inspection. A helical-wheel presentation of the predicted TMH (Ire1⁵³⁸⁻⁵⁵⁵) revealed a cluster of three phenylalanines (F), namely F544, F548 and F551 on one side on the TMH (Fig. 21 A). Interestingly, aromatic amino acid (AA) residues can promote the dimerization of TMHs by pi-pi-stacking or hydrophobic interactions (Sal-Man et al., 2007). Thus, the inspection of Ire1's TMH led to the hypothesis that this cluster of phenylalanines (or F-cluster) might serve as a dimerization interface. To investigate this hypothesis, in triple mutant was generated in which all three F residues were mutated to alanine (A).

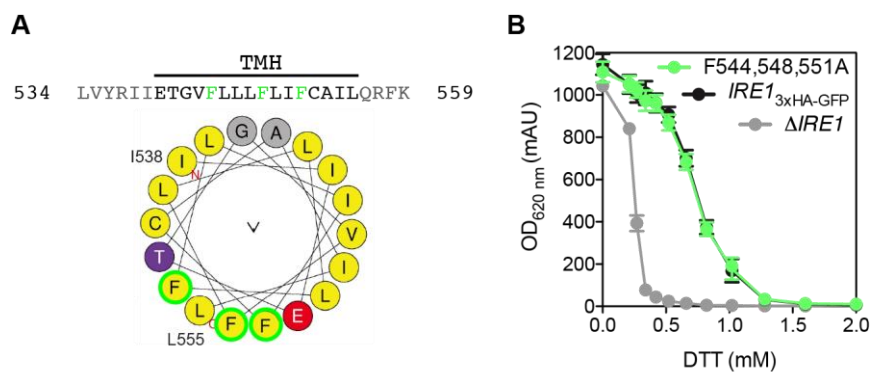


Figure 21 | Mutation of the F-cluster (F544,548,551A) does not impair Ire1 functionality.

(A) AA sequence and helical wheel representation of the TMH of Ire1 predicted by the HeliQuest bioinformatics tool. (B) Growth assay of the *IRE1* knock-in construct (*IRE1*_{3xHA-GFP}), the F-cluster mutant (F544,548,551A) strain and an Δ *IRE1* strain. Cells were cultivated in minimal medium (SCD) supplemented with DTT at 30°C for 18 h and the density of the culture was determined using the OD₆₂₀. The errorbars represent the mean \pm SEM of n = 3 biological replicates.

To test if the mutation of the F-cluster has an impact on the functionality of Ire1, cells expressing the F-cluster mutant were analyzed using a sensitive growth assay (or ER-stress resistance test) under conditions of increasing ER stress induced by DTT in the cultivation medium. In this ER-stress resistance assay, cells lacking *IRE1* were substantially more sensitive to DTT, while cells expressing the F-cluster triple mutant were indistinguishable from wild type cells (Fig. 21 B). Thus, the hypothesis of a functionally relevant F-cluster was rejected.

To test if the TMH of Ire1 harbors specific sequence features that would be functionally relevant, parts of the TMH region were exchanged by a poly leucine (L) L16⁵⁴⁰⁻⁵⁵⁵ or L13⁵⁴³⁻⁵⁵⁵ stretch without affecting the overall length of the construct (Fig. 22 A). The sensitive ER-stress resistance test was performed with these mutant variants (Fig. 22 B, C). Cells expressing the L13⁵⁴³⁻⁵⁵⁵ variant of Ire1 were indistinguishable from cells expressing wild type Ire1 (Fig. 22 C). This finding shows, that Ire1 can tolerate the exchange of 13 AA residues of its TMH to leucines. However, cells expressing the L16⁵⁴⁰⁻⁵⁵⁵ TMH showed an increased sensitivity ER-stress (Fig. 22 B).

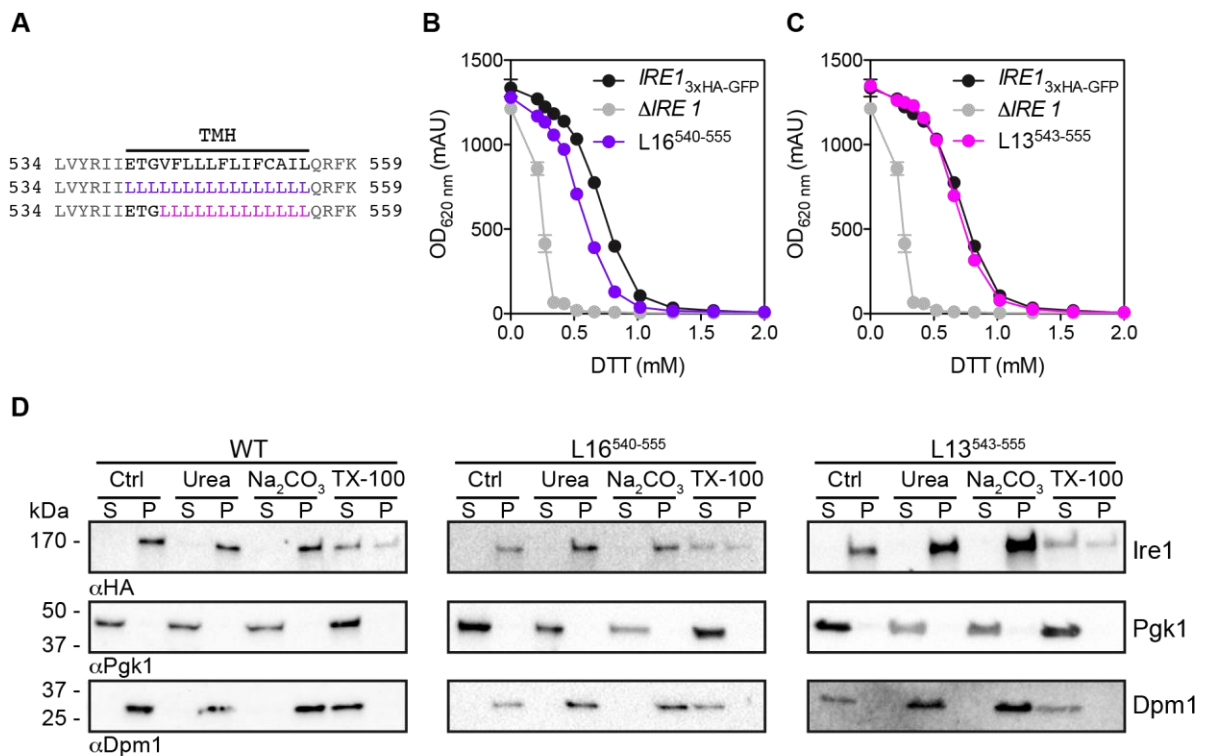


Figure 22 | Exchange of the TMH of Ire1 by poly leucine helices.

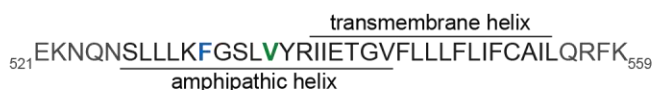
(A) AA sequence of the TMH of Ire1 and the engineered poly L versions. (B, C) Growth assay of the *IRE1* knock-in construct (*IRE1*_{3xHA-GFP}), L16⁵⁴⁰⁻⁵⁵⁵ and L13⁵⁴³⁻⁵⁵⁵ mutant strains and an Δ *IRE1* strain. Cells were cultivated in minimal medium (SCD) supplemented with DTT at 30°C for 18 h and the density of the culture was determined using the OD₆₂₀. (B) Growth of an *IRE1* L16⁵⁴⁰⁻⁵⁵⁵ expressing strain. (C) Growth of an *IRE1* L13⁵⁴³⁻⁵⁵⁵ expressing strain. The errorbars represent the mean \pm SEM of n = 3 biological replicates. (D) 80 ODU of exponentially growing cells producing Ire1_{3xHA-GFP} wild type and its mutants were harvested and lysed. Membrane fractionation revealed that all variants localized into microsomal membranes (P100) which are pelleted at a centrifugation speed of 100.000x g. Carbonate and urea extraction validates proper membrane integration of all investigated *IRE1*_{3xHA-GFP} variants, while treatment with Triton X-100 served as a positive control, solubilizing microsomal membranes. Samples were subjected to SDS-PAGE and immunoblotting using anti-HA antibodies for detection of Ire1_{3xHA-GFP}, Pgc1 (cytosolic protein) and Dpm1 (ER membrane protein) antibodies were used to investigate the localization of marker proteins in this assay.

These findings suggested that the three N-terminal residues of the TMH (Ire1⁵⁴⁰⁻⁵⁴²) might be of particular functional importance for Ire1. It should be noted that poly L stretches tend to oligomerize within the membrane. In fact, the substitution of a TMH by poly L stretches is commonly used to induce a dimerization of TMHs for example in receptor tyrosine kinases (Brooks et al., 2014). In light of this, the observation of a functional defect for the L16⁵⁴⁰⁻⁵⁵⁵ variant was not anticipated and further emphasize the possibility that the residues Ire1⁵⁴⁰⁻⁵⁴² may have a particular role for function. Importantly, fractionation and membrane extraction experiments verified that both mutant X versions were correctly inserted into microsomal membranes as the wild type variant (Fig. 22 D). Having establish a functional role of the N-terminal region of the TMH, this region was subjected to a more thorough bioinformatic analysis.

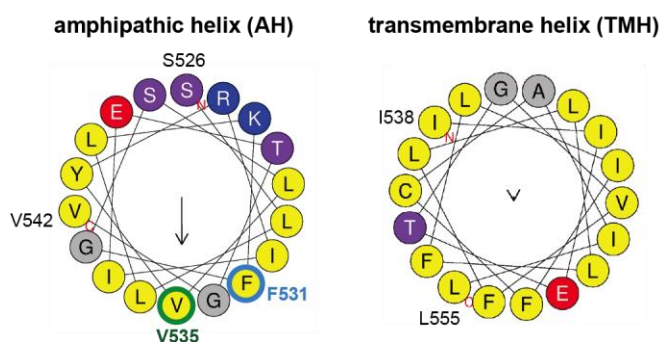
5.3. Bioinformatic identification and *in vivo* validation of an amphipathic helix in Ire1

Analysis of the TMH region of Ire1 using HeliQuest (Gautier et al., 2008) revealed a putative, juxta-membrane AH directly N-terminal to the TMH. Given the topology of the protein, this putative AH would be located in the lumen of the ER (Fig. 23 A and B). The analysis suggested that the putative AH would contain a large hydrophobic/non-polar face (yellow) with two glycine residues (grey), and a hydrophilic/polar phase (purple) with three charged residues (red, blue). The putative AH is predicted to have rather established hydrophobic moment $\langle\mu_H\rangle$ of 0.434, and a hydrophobicity $\langle H\rangle$ of 0.729 which is expectedly lower than the hydrophobicity of the transmembrane helix ($\langle H\rangle = 1.320$).

A Sequence of Ire1's AH + TMH



B HeliQuest analyses



C CD spectroscopy of Ire1⁵²²⁻⁵⁴³

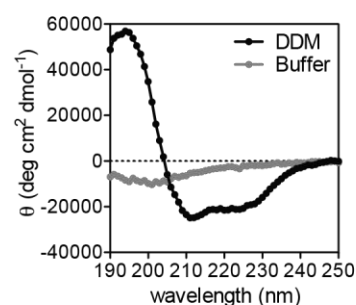


Figure 23 | Ire1 contains an amphipathic helix (AH) adjacent to the transmembrane helix (TMH) on the ER-luminal side of Ire1.

(A) The predicted TMH of Ire1 overlaps with a putative AH on the ER-luminal side. Residues mutated in the course of this study are highlighted in blue (F531) and green (V535). (B) HeliQuest analyses of the AH (Ire1⁵²⁶⁻⁵⁴⁷) and the TMH (Ire1⁵³⁸⁻⁵⁵⁵) of Ire1. Residues mutated in the course of this study are labeled in blue (F531) and green (V535), the residue number of the N- and C-terminal residue is given for both projections. (C) CD-spectroscopic analysis of a synthetic AH peptide derived from Ire1 (Ire1⁵²²⁻⁵⁴³) in sodium carbonate buffer (pH 7.0) and in the presence (black) and absence (grey) of 1% n-dodecyl β -D-maltoside (DDM).

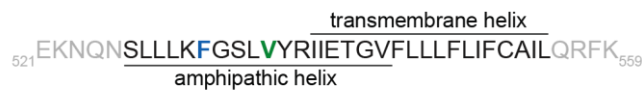
Ire1 is conserved among eukaryotes. Strikingly, HeliQuest analyses confirmed the conservation of an amphipathic character in this region of Ire1 for orthologs of diverse eukaryotes including plants and pathogenic yeast strains, although no sequence homology became obvious (Fig. S1).

To investigate if the region of the putative AH has the potential to fold into an alpha helix, a synthetic peptide corresponding to Ire1⁵²²⁻⁵⁴³ was synthesized and analyzed by CD-spectroscopy. These experiments revealed that the predicted AH folded into an α -helix in the presence of the non-ionic detergent (DDM, 1%), while it was unstructured in aqueous buffer (Fig. 23 C). Thus, the potential of the predicted AH region to fold into an α -helix was confirmed.

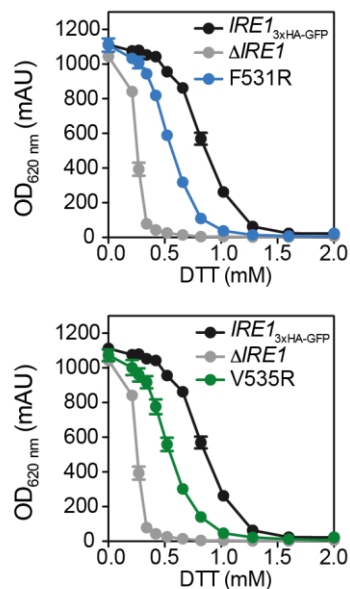
5.3.1. Mutations in the hydrophobic face of the AH interfere with Ire1 functionality

The functional relevance of the putative AH was tested by disrupting the amphipathic character. To this end, the residues F531 and V535 in the hydrophobic face of the AH were mutated individually to arginine. Subsequently, ER-stress assays were performed to investigate whether the mutating affected the sensitivity of cells expressing the F531R and V535R mutants to ER-stress induced by DTT. Cells producing *IRE1* with a disrupted AH showed an increased sensitivity to ER-stress compared to wild type cells (Fig. 24 B). Strikingly, this was not due to changes in the steady-state protein levels (Fig. 24 C). These data indicate that both mutants exhibit a functional defect and emphasize that both mutations are equally disruptive for Ire1 functionality (Halbleib et al., 2017).

A AH+TMH sequence



B cell viability of AH mutants



C protein levels of AH mutants

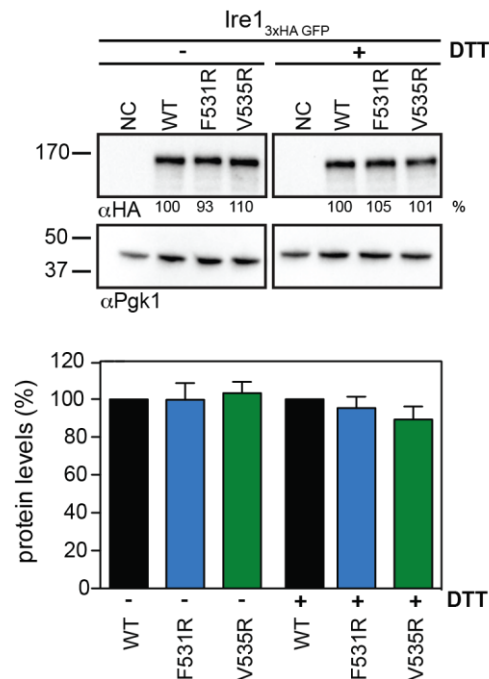


Figure 24 | Mutations in the hydrophobic phase of the AH impair Ire1 functionality.

(A) Sequence of the predicted AH and TMH of Ire1, depicted as described in Fig. 21. (B) Growth assay of *Ire1*^{3xHA-GFP} wild type and AH mutants, including an $\Delta IRE1$ strain (grey). Growth of cells expressing the F531R mutant (blue) or the V535R mutant (green) are depicted. Cells were cultivated in minimal medium (SCD) supplemented with DTT at 30°C for 18 h and the density of the culture was determined using the OD₆₂₀. The errorbars represent the mean \pm SEM of $n = 3$ biological replicates. (C) Lysates from the indicated, exponentially growing cells were immunoblotted using anti-HA antibodies for comparing the level of *Ire1*^{3xHA-GFP} wild type and its mutant variants. The cells were either harvested unstressed or after addition of DTT (1h, 10 mM, YPD media) to induce ER-stress. Lysates from an isogenic wild type strain (NC) served as specificity control, while an immunoblot with anti-Pgk1 antibody served as loading control. Quantification of protein levels were normalized to *Ire1* wild type. The error bars represent the mean \pm SEM of 3 independent experiments.

In order to rule out that these AH-disrupting mutations impair the membrane proper membrane integration of Ire1, subcellular fractionation experiments and extraction assays were performed (Fig. 19 and 25). Both were not extracted from microsomal membranes by urea or Na₂CO₃ treatment, as previously shown for the wild type.

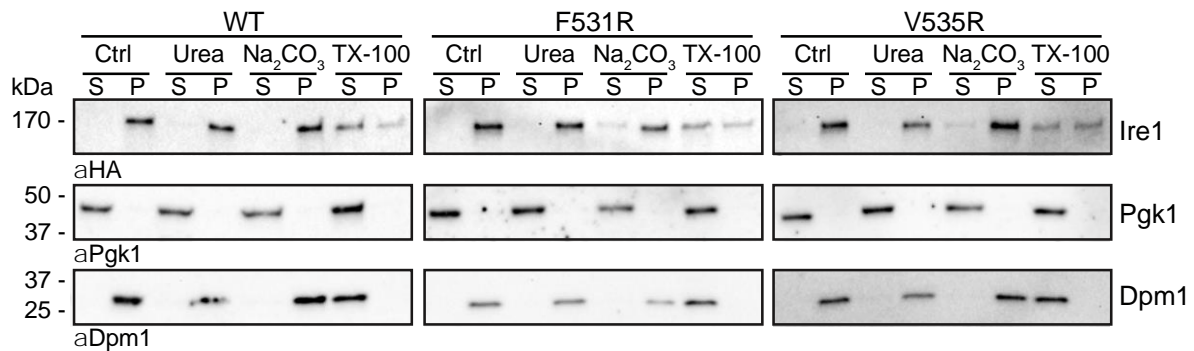


Figure 25 | Fractionation and integration of AH mutants.

80 ODU of exponentially growing cells producing Ire1_{3xHA-GFP} wild type and its mutants were harvested and lysed. Membrane fractionation revealed all variants localized into microsomal membranes (P100) which are pelleted at a centrifugation speed of 100.000x g. Carbonate and urea extraction validates proper membrane integration of all investigated Ire1_{3xHA-GFP} variants, while treatment with Triton X-100 served as a positive control, solubilizing microsomal membranes. Samples were subjected to SDS-PAGE and immunoblotting using an anti-HA antibody for detection of Ire1_{3xHA-GFP}, Pgk1 (cytosolic protein) and Dpm1 (ER membrane protein) antibodies were used to investigate the localization of marker proteins in this assay.

In order to test if an intact juxta-membrane AH is necessary for Ire1 cluster formation during ER stress, confocal fluorescence live cell imaging was performed. Cells were stressed with DTT to induce massive protein misfolding and subjected to confocal fluorescence microscopy to detect GFP-labeled Ire1. Clusters of Ire1 were clearly distinguishable from the background signal caused by auto-fluorescence and were absent in unstressed cells (Fig. 20 B). High intensity clusters were identified and counted by an automated script in Fiji and revealed that their number was significantly reduced in cells expressing the F531R or the V535R mutant compared to the wild type (Fig. 26).

Because DTT induces massive ER stress, a milder form of ER stress was induced that might reflect a more physiological situation. Inositol depletion is a well-established inducer of lipid bilayer stress resulting in the UPR activation without inducing massive protein misfolding (Lajoie et al., 2012; Merksamer et al., 2008; Promlek et al., 2011). Consistently, wild type Ire1 formed smaller clusters of lower intensity under this condition (Fig. 26). Nevertheless, the formation of these clusters was significantly impaired by the F531R and the V535R mutation that disrupt the juxta-membrane AH (Fig. 26). Together, these data suggest that the increased sensitivity of cells expressing *IRE1* with a disrupted juxta-membrane AH is due to a defect in the oligomerization and activation of Ire1 (Halbleib et al., 2017).

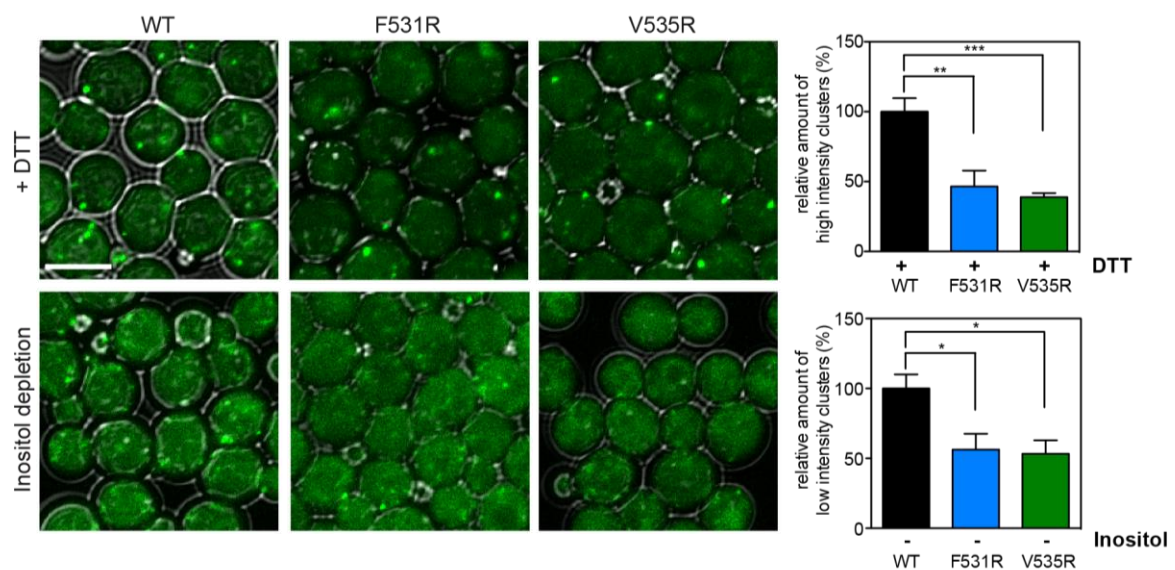


Figure 26 | Mutations in the AH affect the formation of Ire1 clusters in ER-stress.

Live cell confocal microscopy of indicated yeast strains during acute ER stress. Cells were treated with DTT (1.5h, 2 mM, SCD media) or cultured in inositol-depleted medium (3h). Quantification of high and low intensity clusters of Ire1 based on a semi-automated script. A minimum of 40 cells was analyzed for each replicate. The error bars represent the mean \pm SEM. $n = 5$ wild type; $n = 4$ F531R; $n = 10$ V535R for DTT treated cells, $n = 3$ for all strains for inositol depletion experiments. Statistical significance was tested by an unpaired, two-tailed student's t-test. *** $p < 0.001$, ** $p < 0.01$, * $p < 0.05$. Scale bar = 5 μ m.

In order to validate, if a disrupted AH affects the signaling events that mediate the UPR, the mRNA levels of the spliced variant *HAC1* and of selected UPR target genes were determined by qPCR experiments. To investigate levels of spliced *HAC1*, data were normalized to the amount of spliced *HAC1* mRNA in wild type cells for each stress condition that was tested. *HAC1* splicing analysis revealed a significant reduction of the spliced *HAC1* mRNA in cells expressing the V535R mutant compared to wild type Ire1 expressing cells during ER-stress induced either by the presence of DTT or by inositol depletion conditions (Fig. 27 A). This shows that an intact AH is crucial for normal functionality of Ire1.

Further, analysis of mRNA levels of protein disulfide isomerase 1 (*PDI1*), a protein involved in disulfide bridge formation during protein folding (Lamantia et al., 1991; Tachikawa et al., 1991), was performed. The mRNA level of *PDI1* increased in wild type cells >5-fold and >2.5-fold during ER stress induced by DTT and depletion of inositol, respectively (Fig. 27 B). In contrast, mutant cells expressing an AH-disrupted variant of Ire1 barely up-regulated the mRNA of *PDI1* in response to both forms of ER stress (Fig. 27 B).

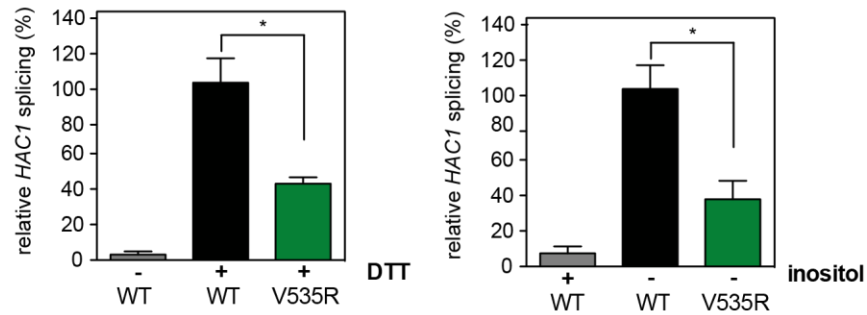
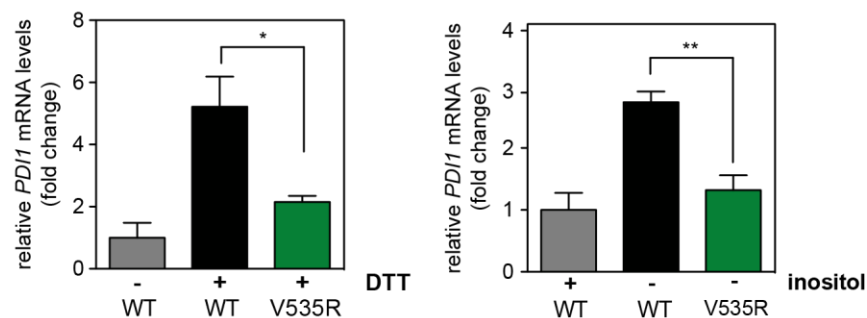
A HAC1 splicing**B PDI1 levels**

Figure 27 | HAC1 splicing and upregulation of PDI1 mRNA levels are reduced in the V535R mutant.

Levels of spliced *HAC1* mRNA (A) and *PDI1* mRNA (B). The indicated cells were stressed by a treatment with DTT (1h, 4 mM, YPD media) or inositol depletion (3h), respectively, and analyzed by qRT-PCR. The data were normalized in (A) to the *HAC1* mRNA level in stressed wild type cells and in (B) to the steady-state level of the *PDI1* mRNA in unstressed cells. All graphs show means \pm SEM for three independent experiments, and statistical significance was tested by an unpaired, two-tailed student's t-test. ** $p < 0.01$, * $p < 0.05$.

Taken together, these data suggest an important role for normal function of the UPR (Halbleib et al., 2017).

5.3.2. A conserved acidic residue at position 540 is important for Ire1 function

Sequence alignments utilizing bioinformatics tools revealed the existence of an acidic residue at the transition of Ire1's juxta-membrane AH and its TMH. The acidic character of the glutamate residue at position 540 in yeast Ire1 is conserved from yeast to man. In Ire1 α from *H. sapiens*, an aspartate residue can be found at the equivalent position, as indicated by sequence alignments of various fungal and mammal Ire1 species (Fig. 28).

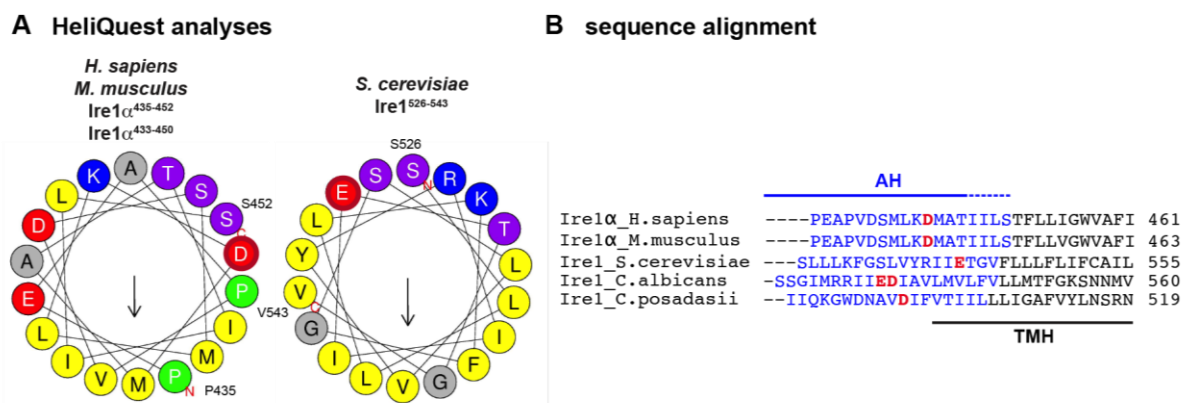


Figure 28 | The negative charge of E540 in Ire1 is conserved among species.

(A) HeliQuest analysis of Ire1 orthologs from mammals and yeast strains highlight the conservation of the negative residue in the hydrophilic phase of the AH. (B) Sequence alignment of Ire1's AH and TMH from indicated species. The sequences of the AH is indicated in blue, while the predicted TMH is shown in black. Negatively charged residues localized at a similar localization as the E540 in *S. cerevisiae* are highlighted in red.

To investigate the role of E540 for Ire1 function, it was substituted by a variety of other amino acids and the sensitivity to ER-stress of cells expressing these mutants was investigated using DTT as stressor (Fig. 29). Cells expressing the E540A mutant was markedly more sensitive to DTT compared to the wild type. Neither the substitution of E540 to glutamine (Q), which structurally rather similar to glutamate (E), nor a mutation to a positively charged lysine (K) rescued this growth phenotype. Substituting E540 by aspartate (D) resulted in a wild type-like growth phenotype, suggesting that the E540D variant of Ire1 is functional. Strikingly, the structurally related asparagine (N) residue at the position of E540 did not rescue the previously described growth defect. Of note, the protein levels of all mutants were comparable to wild type Ire1 levels. These data highlight that a conserved, negatively charged residue at the position E540 is required for normal UPR activation.

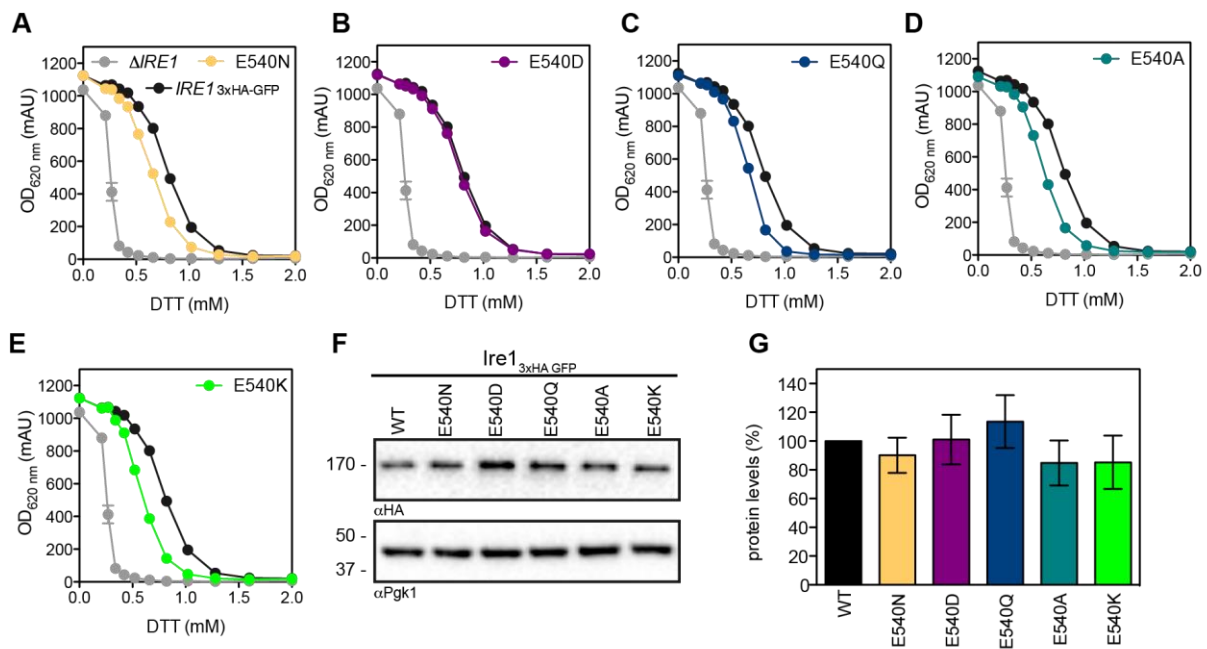


Figure 29 | Substitution of the negative charge at position 540 leads to a functional defect in Ire1.

(A – E) Growth assay of Ire1_{3xHA-GFP}, mutations of the glutamate at position 540 to alanine (A, turquoise), glutamine (Q, blue), aspartate (D, purple), asparagine (N, orange) or lysine (K, green) and an Δ IRE1 strain. Cells were cultivated in minimal medium (SCD) supplemented with DTT at 30°C for 18 h and the density of the culture was determined using the OD₆₂₀. The error bars represent the mean \pm SEM of n = 2 biological replicates. (F) Lysates from the indicated, exponentially growing cells were immunoblotted using anti-HA antibodies for comparing the level of Ire1_{3xHA-GFP} wild type and its mutant variants. An immunoblot with anti-Pgk1 antibody served as loading control. (G) Quantification of protein levels shown in (F) were normalized to Ire1 wild type and Pgk1. The error bars represent the mean \pm SEM of 3 independent experiments.

In order to investigate the impact of the E540A mutation on Ire1 function in the context of different kinds of stress more thoroughly, the potential of this mutant to form high-order oligomers was investigated by confocal fluorescence microscopy on live cells. The formation of Ire1 clusters was induced either by the addition of the ER-stressor DTT to the cultivation medium or by inositol depletion (Fig. 30).

Ire1 clusters were identified and counted using an automated Fiji script and revealed that the occurrence of punctate structures was reduced to \approx 60% for the E540A mutant compared to the wildtype. This defect in cluster formation was comparable to the defect observed for the F531R and V535R mutants that disrupt the amphipathic character of the ER (Fig. 26).

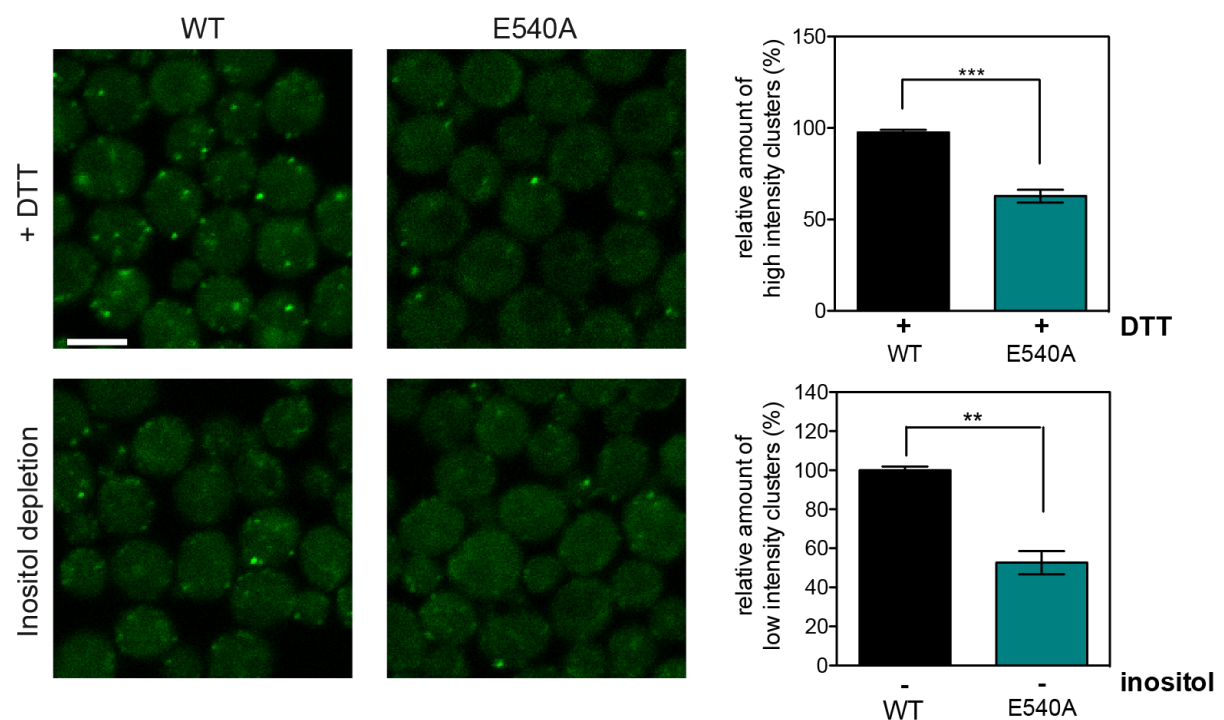


Figure 30 | The E540A mutation affects the formation of Ire1 clusters in ER-stress conditions.

Live cell confocal microscopy of yeast strains expressing Ire1_{3xHA-GFP} wild type or the E540A mutant during acute ER stress. Cells were treated with DTT (1.5h, 2 mM, SCD media) or cultured in inositol-depleted medium (3h). Quantification of high and low intensity clusters of Ire1 based on a semi-automated script. The error bars represent the mean \pm SEM. $n = 3$ for DTT treated cells, $n = 4$ for wild type inositol depletion, $n = 3$ for E540A in inositol depletion experiments. A minimum of 40 cells was analyzed for each replicate. Statistical significance was tested by an unpaired, two-tailed student's t-test. *** $p < 0.001$, ** $p < 0.01$. Scale bar = 5 μ m.

Not surprisingly, unconventional splicing of *HAC1* mRNA in response to both types of ER stress was impaired for the E540A mutant compared to the wildtype (Fig. 31). Consequently, also the induction of the UPR target gene *PDI1* was reduced in this mutant compared to the wild type version. These data, together with indications of a functional defect by increased sensitivity to DTT stress in the growth assay (Fig. 29) and reduced formation of Ire1 clusters (Fig. 30) highlight the functional relevance of the E540 in Ire1.

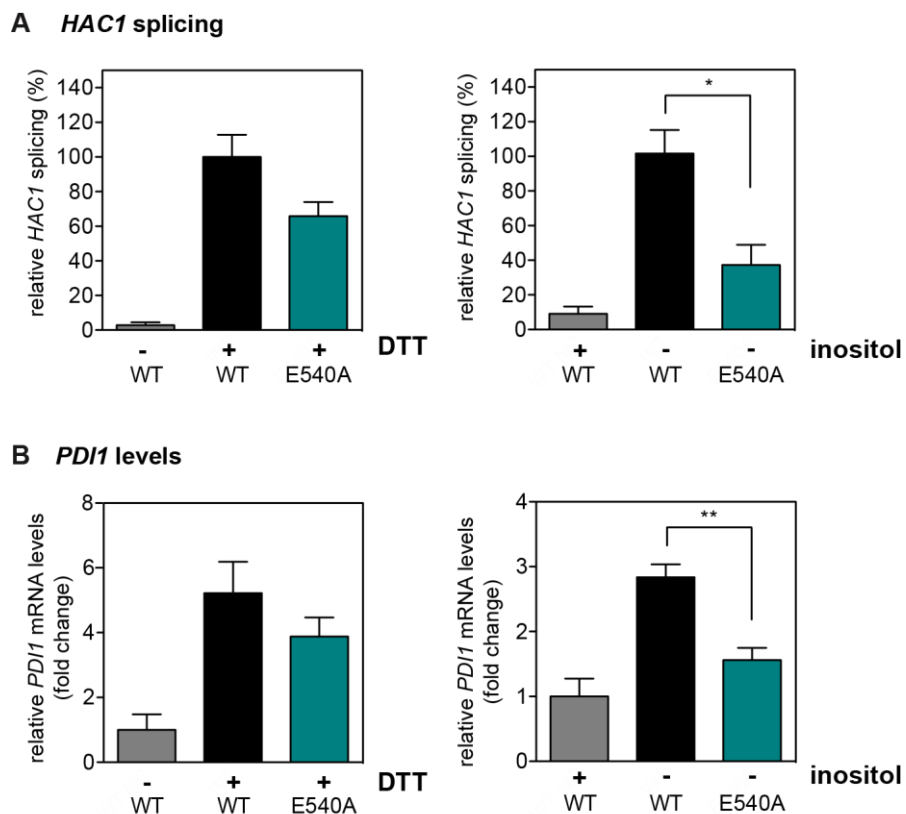


Figure 31 | HAC1 splicing and upregulation of PDI1 mRNA levels is reduced in the E540A mutant.

Levels of spliced *HAC1* mRNA (A) and *PDI1* mRNA (B). The indicated cells were stressed by a treatment with DTT (1h, 4 mM, YPD media) or inositol depletion (3h), respectively, and analyzed by qRT-PCR. The data were normalized in (A) to the *HAC1* mRNA level in stressed wild type cells and in (B) to the steady-state level of the *PDI1* mRNA in unstressed cells. The data were normalized as in Fig. 27. All graphs show means \pm SEM for three independent experiments, and statistical significance was tested by an unpaired, two-tailed student's t-test. ** $p < 0.01$, * $p < 0.05$.

Intriguingly, the glutamate residue at position 540 is located at the interface between Ire1's AH and its TMH. Mutation of the R537 residue, which is located only one helical turn away from the conserved glutamate 540, to alanine (R537A) or glutamate (R537E) did not result in an increased sensitivity of yeast to DTT, indicating the lack of a functional role of this residue in Ire1 (Halbleib et al., 2017).

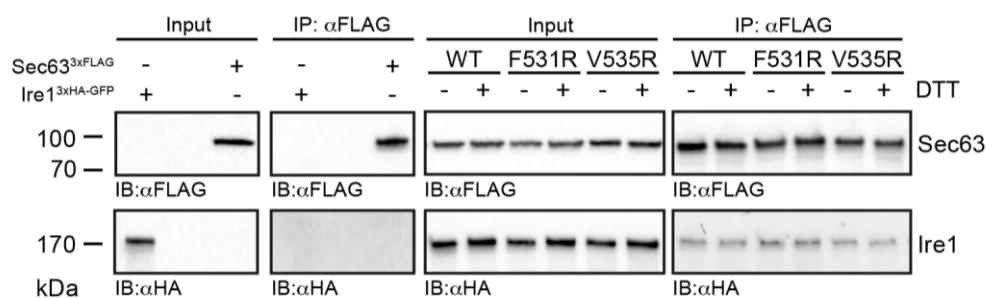
5.4. Functionally impaired AH mutant variants are capable to interact with known interaction partners

The juxta-membrane region of Ire1 is important for the interaction with other proteins. Ire1 has been reported to interact with the ER chaperone Kar2 in subregion V of its luminal domain (residues 455-524) (Kimata et al., 2004). Furthermore, the Ire1 ortholog IRE1 α from *H. sapiens* binds to components of the Sec complex via an interaction with the residues right N-terminally of the TMH of the protein (Plumb et al., 2015). Our bioinformatics analysis suggests that this portion of the protein form a part of an putative AH in IRE1 α (Fig. S1) (Gautier et al.,

2008). Thus, the interaction of Ire1 with the translocon and Kar2 was characterized by co-immunoprecipitation (Co-IP) experiments.

The heterotrimeric Sec61 complex in yeast comprises Sec61, Sbh1 and Sss1 and involve additional components such as its membrane receptor and co-chaperone, the Sec63 protein (Zimmermann et al., 2011). Introduction of a C-terminal tag in Sec61 seems to impair protein translocation as it imposes a cellular defect (this study, data not shown), Therefore, the interaction of Ire1 with Sec63 was tested. Co-IP experiments using Sec63 as a bait revealed an interaction between Sec63 and Ire1 that may be directly or indirectly (Fig. 32 A), as had previously been observed for the human Ire1 ortholog, IRE1 α (Plumb et al., 2015). This interaction was not regulated by ER-stress, as the fraction of co-precipitated Ire1 was identical in stressed and unstressed cells. Importantly, Ire1 mutants with a disrupted AH interacted equally efficient with Sec63 as their wild type counterpart. This indicates that the AH of Ire1 is relevant for the interaction with Sec63 (Fig. 32 A) (Halbleib et al., 2017).

A Sec63 interaction



B Kar2 interaction

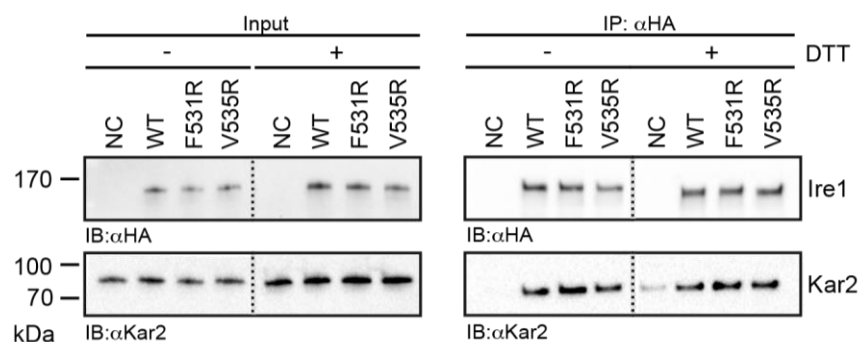


Figure 32 | Ire1 AH mutants retain their ability to interact with known interaction partners.

(A) Cells co-expressing Sec63_{3xFlag} and Ire1_{3xHA-GFP} were lysed prior to an IP using anti-Flag beads. Co-immunoprecipitated Ire1 was detected by immunoblotting using anti-HA antibodies. A strain expressing Sec63_{3xFlag} and the isogenic wild type version of Ire1 was used as a negative control (left). (B) Cells expressing Ire1_{3xHA-GFP} and the endogenous Kar2 were lysed prior to an IP using anti-HA beads. Co-immunoprecipitated Kar2 was detected by immunoblotting using anti-Kar2 antibodies. The isogenic wild type strain BY4741 was used as a negative control (NC). When indicated, cells were treated with DTT (1h, 10 mM, YPD media).

To investigate if the AH of Ire1 is a part of the Kar2 binding site, co-IP experiments with Kar2 were performed in the absence and presence of ER-stress. In line with previously published data, Kar2 could be co-precipitated with wild type Ire1, indicating that there is an interaction of these two proteins irrespectively if the cells are stressed or not (Fig. 32 B) (Halbleib et al., 2017; Kimata et al., 2004). During ER stress induced by DTT the protein level of Kar2 was increased, however the fraction of these molecules interacting with Ire1 was decreased. This effect can be explained by the dissociation of Kar2 during Ire1 activation and goes along with previous observations (Gardner and Walter, 2011; Kimata et al., 2004; Pincus et al., 2010). While Ire1 wild type and mutants bind Kar2 to the same extend in unstressed cells, the interaction of wild type Ire1 and Kar2 appears reduced compared to the interactions of the AH mutants with Kar2 in stressed cells (Fig. 32 B, right panel). The increased interaction of the AH mutants with Kar2 in the presence of ER-stress may be explained by the fact that these mutants exhibit a functional defect, which makes them more likely to interact with the chaperone that keeps Ire1 in a monomeric, inactive state. The fact that the AH mutants still interact with Kar2 indicate that the hydrophobic region of Ire1's AH is not involved in Kar2 binding.

These data provide evidence that AH-disrupting mutants are able to interact with Kar2 and Sec63, highlighting that the functional defects observed for mutant Ire1 do not result from perturbed interactions with these modulatory interaction partners.

5.5. Crosstalk of Ire1's AH with two known luminal interfaces

To investigate whether distinct mutations in the luminal interfaces of Ire1 (Fig. 33A) have an additional effect on the previously characterized AH mutants, yeast ER-stress assays were performed. Cells expressing the V535R or E540A variant, a mutant that impairs the dimerization of Ire1 (IF_{L1}; T226A, F246A), and a mutant that hinders the formation of higher order oligomers (IF_{L2}; W426A) as well as double mutant of either luminal interface with the V535R or E540A mutation were analyzed using a sensitive ER-stress resistance test (Fig. 33 B).

In contrast to studies in minimal medium, the V535R and E540A mutants showed only a slightly increased sensitivity to DTT in rich media (Fig. 33). The IF_{L1} mutation significantly increased the sensitivity of cells to DTT. Most strikingly, the combination of both mutants results in a loss-of-function phenotype. The strong negative epistasis observed for mutations in the IF_{L1} and the AH suggested that both regions contribute to the activation of Ire1 and were observed similarly for mutations between IF_{L2} and the AH (Fig. 33 B).

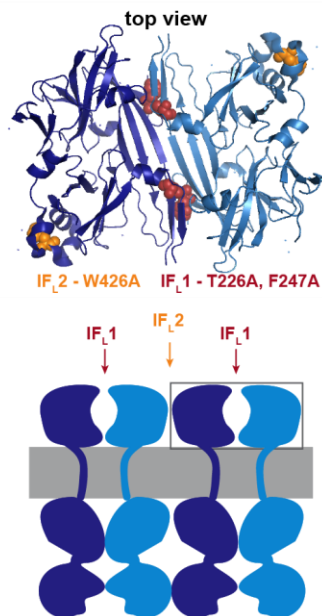
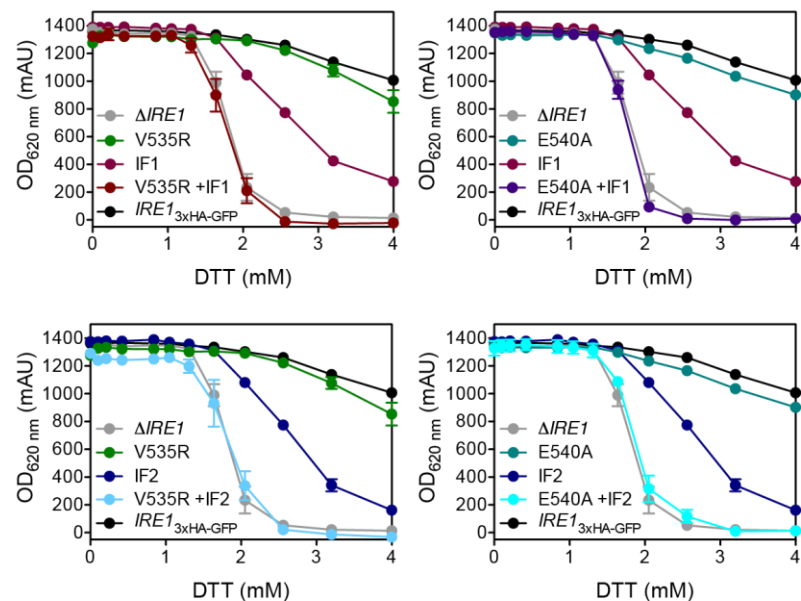
A luminal domain of Ire1**B yeast growth assay**

Figure 33 | A growth assay reveals negative epistasis between mutations in the AH and ER-luminal interfaces.

(A) Model of the dimeric ER-luminal domain (LD) of Ire1 based on the X-ray structure (pdb:2BE1) (Credle et al., 2005) in a top view representation and a schematic illustration of Ire1. Key residues contributing to IF1 (red) and IF2 (yellow) and mutations interfering with Ire1 oligomerization are highlighted. (B) Growth assay of the indicated yeast strains carrying mutations in IF1, IF2, and/or the V535R or E540A mutation of Ire1. Cells were cultivated in rich medium and challenged with DTT for 18 h. Cellular growth was determined using the OD_{620} . The error bars represent the mean \pm SEM of 3 independent experiments.

In order to characterize this strong negative epistasis in greater detail, these mutants were characterized for their ability to splice *HAC1* and to induce UPR target genes in response to two forms of ER stress: DTT in the growth medium or inositol-depletion (Fig. 34). Whenever a disrupted luminal interface was combined with mutations in the AH (V535R or E540A) the activity of the UPR during stress was indistinguishable from the UPR in unstressed cells (Fig. 34) (Halbleib et al., 2017). The strong negative epistasis suggests that these different regions of Ire1 cooperate to induce the oligomerization and hence, the activation of Ire1.

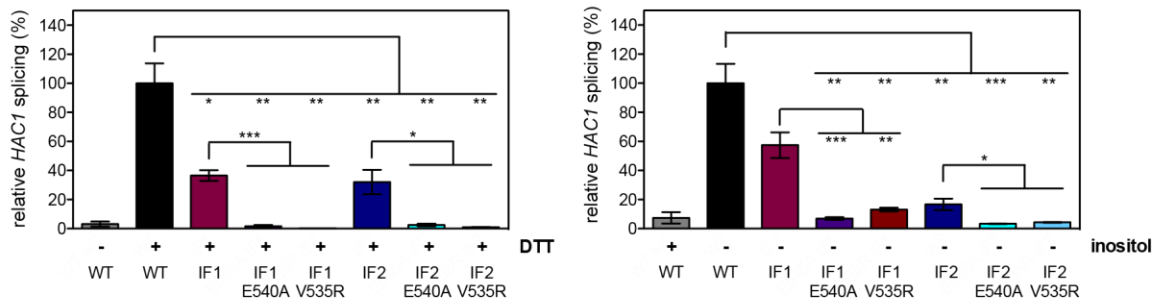
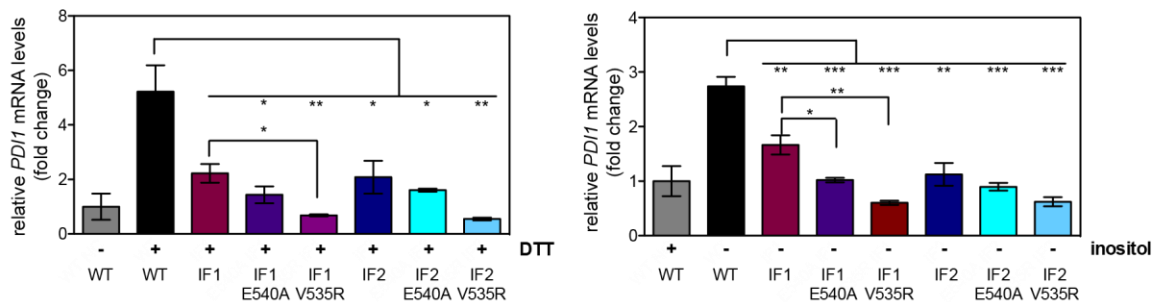
A *HAC1* splicing**B *PDI1* mRNA levels**

Figure 34 | qRT-PCR reveals negative crosstalk between the V535R or E540A mutations and ER-luminal interfaces.

(A) The relative degree of *HAC1* mRNA splicing and (B) the relative level of the *PDI1* mRNA was determined for the indicated stressed and unstressed cells by qRT-PCR. The indicated cells were stressed by a treatment with DTT (1h, 4 mM, YPD media) or inositol depletion (3h), respectively. The data were normalized as in Fig. 27. The error bars represent the average \pm SEM of three independent experiments. Significance was tested by an unpaired, two-tailed student's t-test. *** $p < 0.001$, ** $p < 0.01$, * $p < 0.05$.

5.6. The AH of Ire1 is not required for activation by protein induced ER stress

All cellular stress conditions evoking an active UPR are collectively termed ER stress. Experimentally, ER stress can be pharmacologically induced by different compounds that interfere with protein folding.

To address, if the AH of Ire1 is equally important for the response to distinct types of ER stress, cells were cultivated i) in the presence of tunicamycin (Tm), an inhibitor of N-linked glycosylation, which leads to an accumulation of unfolded proteins, ii) in the presence of DTT, which induces massive ER stress and induces immediate changes of the lipid composition (personal communication Robert Ernst), and iii) in the absence of inositol to deplete an important lipid metabolite, which has been shown induce the UPR by lipid bilayer stress without the accumulation of misfolded proteins (van Anken et al., 2014; Henry et al., 2014; Promlek et al., 2011).

To identify, if the AH disruptive V535R mutant is activated to the same extent as the wild type version, the relative degree of *HAC1* splicing was determined. As previously shown (Fig. 27 A) *HAC1* splicing analysis revealed a significant reduction of mature *HAC1* mRNA in cells expressing the V535R mutant compared to wild type Ire1 expressing cells in the presence of DTT and under inositol depletion conditions. Interestingly, treatment with TM resulted in similar levels of spliced *HAC1* for wild type and mutant Ire1 (Fig. 35 A), indicating that Ire1 can tolerate the V535R mutation in response to TM induced ER stress.

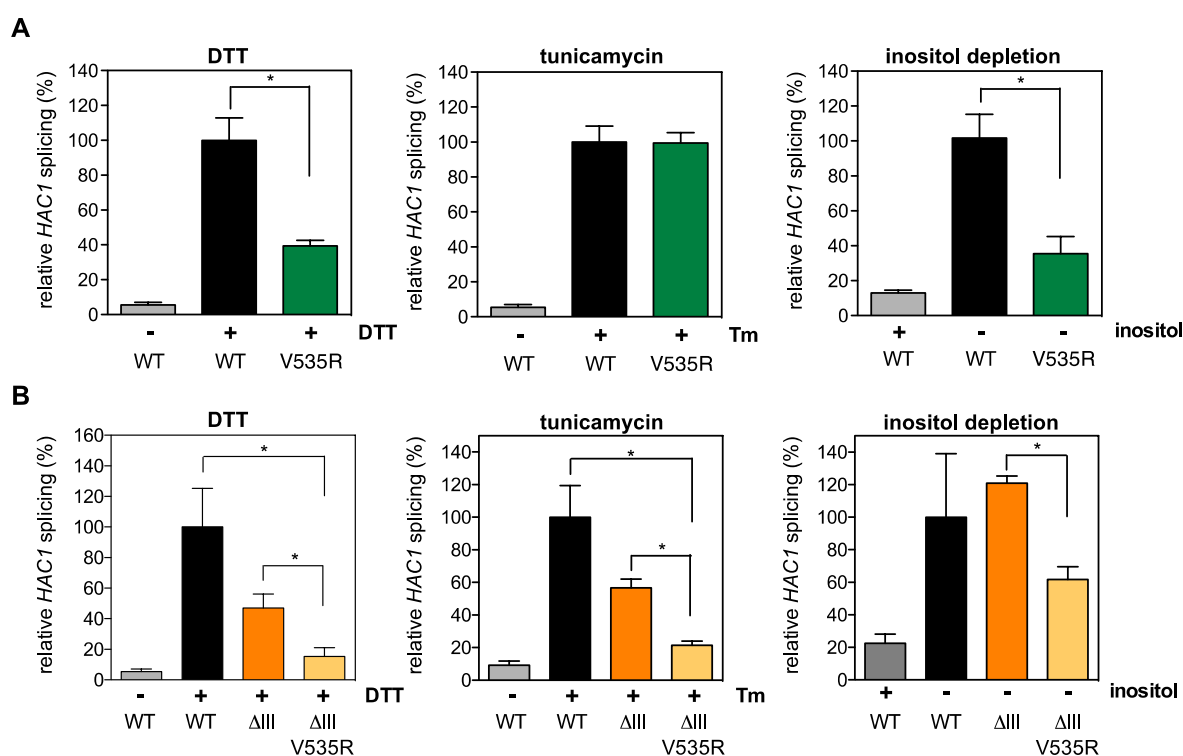


Figure 35 | Activation of the Ire1 by supplementation of different ER stress inducers.

The relative degree of *HAC1* mRNA splicing was determined for the indicated stressed and unstressed cells by qRT-PCR. (A) The indicated cells were stressed by a treatment with DTT (1h, 4 mM, YPD media), TM (1h, 1 μ g/ml, YPD media) or inositol depletion (3h), respectively. The data were normalized to the *HAC1* mRNA level in stressed WT cells. (B) The indicated cells were stressed by a treatment with DTT (30 min, 4 mM, YPD media), TM (30 min, 1 μ g/ml, YPD media) or inositol depletion (3h), respectively. The data were normalized as in (A). The error bars represent the mean \pm SEM. $n = 3$ for all data depicted in (A). $n = 4$ for WT, $n = 3$ for Δ III and Δ III V535R for all experiments depicted in (B). Significance was tested by an unpaired, two-tailed student's t-test. *** $p < 0.001$, ** $p < 0.01$, * $p < 0.05$.

In order to study the relative impact of unfolded proteins binding to Ire1 and of the AH, the Δ III mutant (Δ 253–272) of Ire1 was used, which renders the protein incapable to bind misfolded proteins (Kimata et al., 2007; Promlek et al., 2011). *HAC1* splicing analysis revealed that the levels of spliced *HAC1* were strongly reduced for cells expressing the Δ III mutant during ER-stress induced by Tm or DTT, while there was no clear functional defect of the Δ III mutant

apparent in response to inositol depletion (Fig. 35 B), which is in line with recent literature (Promlek et al., 2011).

Strikingly, the Δ III V535R double mutant was almost entirely unresponsive to the ER stress induced DTT and Tm treatment (Fig. 35 B). Thus, the loss of two independent sensory modules renders the Ire1 entirely unresponsive to ER stress. This observation is consistent with the model that the AH of Ire1 is central to sensing lipid bilayer stress, while unfolded proteins bind to Ire1 via a region that is disrupted in the Δ III mutant. Importantly, the double mutant retained a residual potential to activate the UPR in response to inositol depletion as evidenced by the HAC1 splicing assay (Fig. 35 B, right panel).

The finding that the V535R mutant of Ire1 is defective in *HAC1* splicing in the presence of DTT and inositol depletion induced ER stress but maintains wild type-like *HAC1* splicing levels in the presence of Tm is remarkable. Bearing in mind that different regions in Ire1 act in a cooperative fashion to activate Ire1 (Fig. 34), these data indicate, that Ire1 does not require an intact AH as an oligomerization interface under these stress conditions. It is possible that Tm induces massive protein misfolding in the ER that would overrule the functional defects imposed by the V535R mutation.

5.7. Establishing a minimal sensor domain for *in vitro* studies

This study identified by genetic means that the TM and juxta-membrane region of Ire1, consisting of an ER-luminal AH directly adjacent to and overlapping with the TMH, contribute to the activation of Ire1. However, in order to establish the sensory element and its mechanism, a minimal sensor domain consisting of Ire1's AH and TMH was constructed and studied in defined lipid environments. To this end, a fusion construct was generated, consisting of the maltose-binding protein (MBP) and the AH and TMH of Ire1, including residues 526 – 561 of Ire1. The fusion protein was synthesized in *E. coli* and purified in the presence of Octyl- β -D-glucopyranoside (β -OG) (Fig. 36 A).

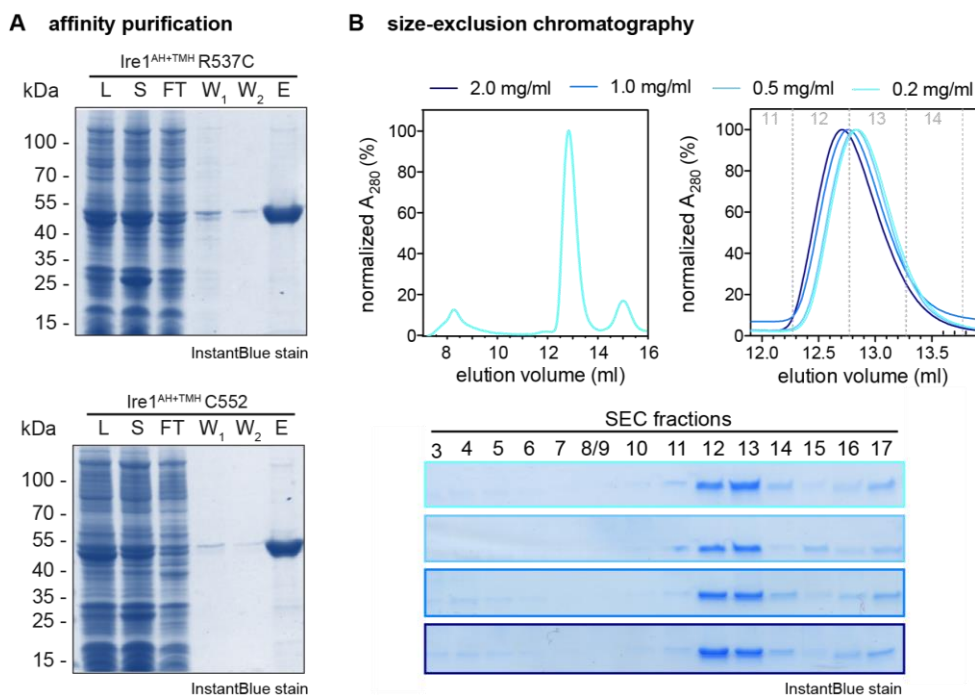


Figure 36 | Purification of spin-labeled MBP-Ire1^{AH+TMH} and analysis of concentration dependent oligomerization.

(A) Affinity purification of the spin-labeled MBP-Ire1^{AH+TMH} wild type and R537C mutant containing residues 526-561 of Ire1. The purification was monitored by subjecting 0.1 OD₆₀₀ equivalents of lysate (L), detergent-solubilized material (S), flow-through (FT), both wash fractions (W₁, W₂) and the elution fraction of the amylose affinity purification to an SDS-PAGE followed by InstantBlue staining. (B) Normalized size-exclusion chromatographs of cysteine-less MBP-Ire1^{AH+TMH} in detergent buffer adjusted to the indicated concentrations and separated on a Superdex 200 10/300 increase column (void volume 8.8 ml). Fractions of the size-exclusion runs were taken and analyzed for their protein content by SDS-PAGE followed by InstantBlue staining.

Of note, for the investigation of the lipid dependent oligomerization of MBP-Ire1^{AH+TMH}, a cysteine-less version of the minimal sensor construct was generated by removing the endogenous cysteine by a C552S mutation. To confirm functionality of the C552S mutant, *in vivo* ER-stress assays were performed revealing an undistinguishable resistance to ER-stress of cells expressing either wild type or the C552S mutant (Fig. 37). Based on this finding, the minimal sensor construct was constructed such that the endogenous cysteine 552 was mutated to serine (C552S) so that a variety of single cysteine mutants could be generated for subsequent spin labeling using MTSSL for cwEPR spectroscopy or crosslinking-experiments.

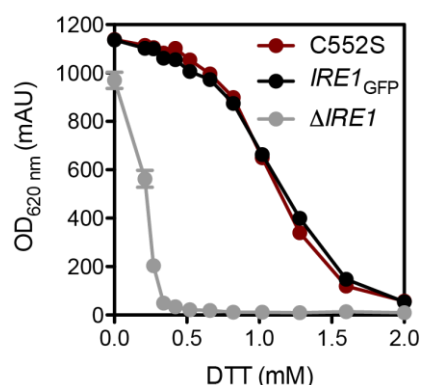


Figure 37 | A ER-stress assay reveals the C552S mutant is fully functional.

Growth of cells expressing the C552S mutant (dark red), a wild type version of *IRE1* (*IRE1_{GFP}*) and the isogenic Δ *IRE1* strain are depicted. Cells were cultivated in minimal medium (SCD) supplemented with DTT at 30°C for 18 h and the density of the culture was determined using the OD_{620} . $n = 2$ for *IRE1_{GFP}* and Δ *IRE1*, $n = 3$ for C552S. The errorbars represent the mean \pm SEM.

Protein purity, here exemplarily shown for the R537C and cysteine-less variant of the MBP-Ire1^{AH+TMH} protein after affinity purification was analyzed by SDS-PAGE followed by InstantBlue staining (Fig. 36 A). The quality of the cysteine-less version of the purified protein was examined by size-exclusion chromatography and SDS-PAGE followed by InstantBlue staining, revealing a peak corresponding to a dimeric equilibrium between monomeric, dimeric and possibly oligomeric species of MBP-Ire1^{AH+TMH} (Fig. 36 B). The elution volume of MBP-Ire1^{AH+TMH} was concentration-dependent: the peak shifted to later elution volumes when the concentration of the protein sample was reduced (Fig. 36 B). This finding suggests a dynamic equilibrium between monomeric and dimeric species of this minimal sensor that cannot be stabilized in a higher oligomeric state as it is lacking the luminal and cytosolic domains of Ire1.

Single cysteine mutants of the minimal sensor domain were reconstituted in defined lipid environments differing in their degree of molecular lipid packing (Fig. 38 A). A series of lipid environments mimicking a broad range from rather loosely to rather tightly packed biological membranes were used. The lipid compositions 1-7 were chosen to form a uniform liquid-disordered membrane phase, whilst covering a wide range of molecular lipid packing densities and maintaining minimal complexity in the lipid headgroup region (Fig. 38 A). These lipid compositions were based entirely on a PC matrix and differed only in their cholesterol content and the proportion of saturated lipid acyl chains. The lipid composition 8 was more complex (Fig. 38 A) and combined several characteristic lipidome changes observed in cells undergoing lipid bilayer stress: an increased degree of lipid saturation, an increased sterol level, and an increased PE:PC ratio (Pineau et al., 2009; Surma et al., 2013; Thibault et al.,

2012). The packing density of these lipid composition can be measured and is reflected by the general polarization (GP) value C-Laurdan, a fluorescence dye which reports on the degree of water penetration in the membrane by a shift of the fluorescence emission spectrum (Kaiser et al., 2011b). C-Laurdan measurements reported that the chosen lipid compositions covered almost the full range of generalized polarization (GP) values reported for organelles along the secretory pathway between the ER and the trans-Golgi network (Fig. 38 B) (Kaiser et al., 2011b; Klemm et al., 2009). The minimal sensor protein was successfully reconstituted in all lipid environments. The resulting proteoliposomes were pelleted by centrifugation (Fig. 38 C) and subjected to quality control (Fig. 39).

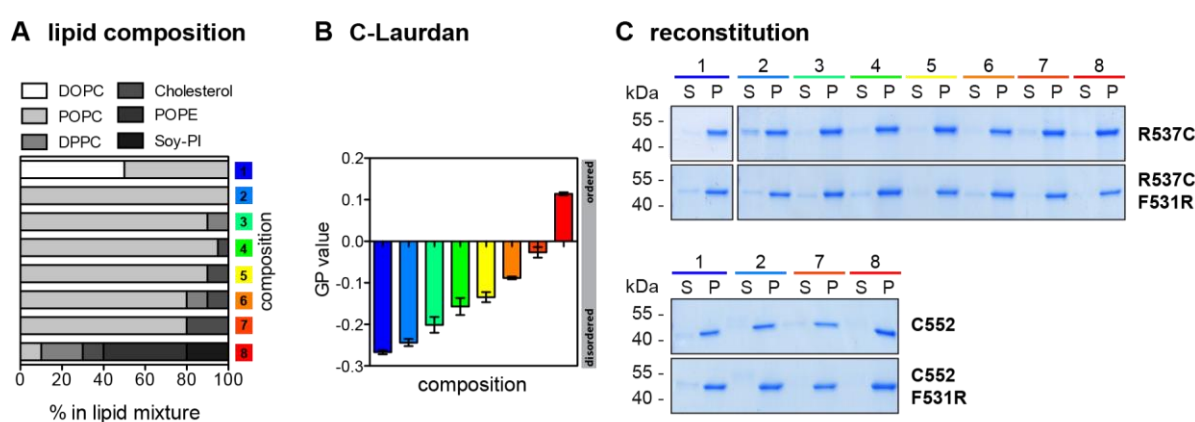


Figure 38 | Reconstitution of spin-labeled MBP-Ire1^{AH+TMH} in different lipid environments.

(A) The indicated spin-labeled mutant versions of the MBP-Ire1^{AH+TMH} fusion protein were reconstituted in liposomes with indicated lipid compositions (1 – 8). The color code for liposome composition is maintained throughout this study. (B) The lipid packing of liposomes with the indicated compositions were determined by fluorescence spectroscopy utilizing C-Laurdan. The degree of lipid packing is represented as a generalized polarization (GP) value, theoretically ranging from -1 for most disordered, to +1 for most ordered membrane lipids. (C) Reconstitution of MBP-Ire1^{AH+TMH} was performed using liposomes of the indicated lipid mixtures. After reconstitution, the resulting proteoliposomes were pelleted (450.000x g, 90 min) and resuspended in reconstitution buffer. To test the reconstitution efficiency, samples of supernatant (S) and pellet (P) after the reconstitution were taken and subjected to an SDS-PAGE followed by InstantBlue staining.

Extensive quality control of the resulting proteoliposomes was performed to validate proper insertion. Membrane extraction experiments using Na₂CO₃ did not extract MBP-Ire1^{AH+TMH} from the membrane, indicating that the protein was not peripherally attached, but efficiently inserted into liposomes. As anticipated for an integral transmembrane protein, only the solubilization of the proteoliposomes by SDS mediated a full extraction of the sensor protein (Fig. 39 A). Sucrose gradients, which were fractionated and analyzed for their protein and lipid contents, revealed that no protein aggregates were present after reconstitution (Fig. 39 B and C).

The orientation of MBP-Ire1^{AH+TMH} insertion in proteoliposomes was investigated by a protease protection assay using Proteinase K (Fig. 39 D). Addition of Proteinase K to proteoliposomes led to a loss of 70 – 80% of the full-length protein, while 20-30% remained protected in the lumen of the proteoliposome. This indicates that a dominant fraction of the fusion protein was integrated with an identical directionality, in which MBP resides outside the proteoliposome and accessible to exogenously added proteases.

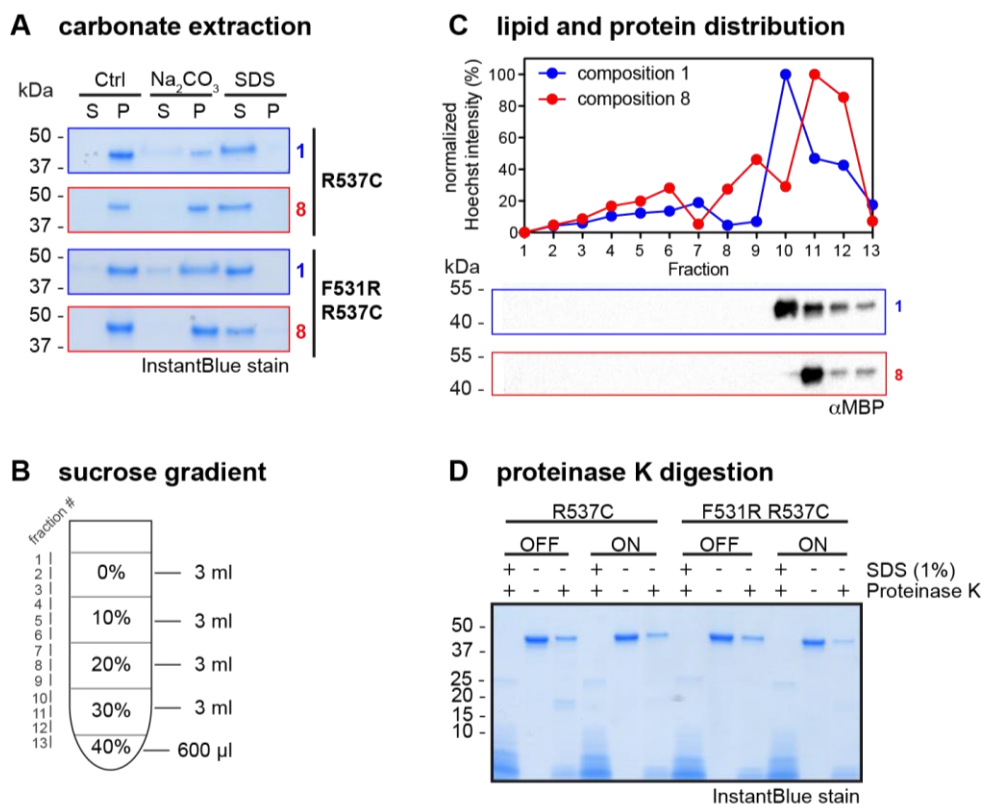


Figure 39 | Quality control of MBP-Ire1^{AH+TMH} containing proteoliposomes.

(A) Proteoliposomes containing the indicated mutants and composed of the indicated lipid mixtures that were reconstituted at a molar protein to lipid ratio of 1:400 were treated with 0.1 M Na₂CO₃ pH 11.0 for extraction of peripherally attached protein from proteoliposomes or 1% SDS as a solubilization control. Samples of supernatant (S) and pellet (P) after the treatment with different additives were taken and subjected to an SDS-PAGE followed by InstantBlue staining (B, C) The quality of the proteoliposomal preparation was further validated by a sucrose step gradient centrifugation (B), followed by an analysis of the lipid and protein distribution in fractions taken after equilibrium centrifugation. Lipid distribution throughout the gradient was monitored by fluorescence spectroscopic measurements utilizing the Hoechst33342 dye. Protein content was monitored by subsection of samples to an SDS-PAGE followed by immunoblotting using anti-MBP antibody. (D) The directionality of protein insertion was monitored by protein digestion using Proteinase K. Samples were treated with Proteinase K, Proteinase K and SDS or neither of the two additives. The amount of full-length protein in each sample was monitored by subsection of samples to an SDS-PAGE followed by Instant Blue staining.

5.8. Membrane-sensitive oligomerization of the minimal sensor

Only *in vitro* experiments provide the opportunity to study the structural dynamics of a sensory protein in a defined lipid environment. Here, MTS labeled single-cysteine mutants of MBP-Ire1^{AH+TMH} were analyzed by cwEPR to explore the membrane-sensitive oligomerization of Ire1 (Fig. 40). The major advantage of cwEPR spectroscopy as opposed to Förster Resonance Energy Transfer (FRET) and microscopy-based approaches is the spatial resolution. Strikingly, cwEPR reports on inter-spin distances between 1.0 and 2.0 nm by spectral broadening (Bordignon and Steinhoff, 2007; Covino et al., 2016). FRET, depending on the coupled fluorophores, occurs in distances between a donor and acceptor dye that is typically in the range of 1 to 10 nm (Hillisch et al., 2001). The low cut-off of detectable distances using cwEPR makes this method much more sensitive and efficient for investigation of TMH oligomerization.

Spin-labeled TMHs must be in a dimeric or higher oligomeric arrangement and have the same membrane topology to evoke broadening of cwEPR spectra. Moreover, cwEPR reports on the mobility of the spin label and on the polarity of its nano-environment. This information can point at conformational changes induced by the properties of the lipid environment.

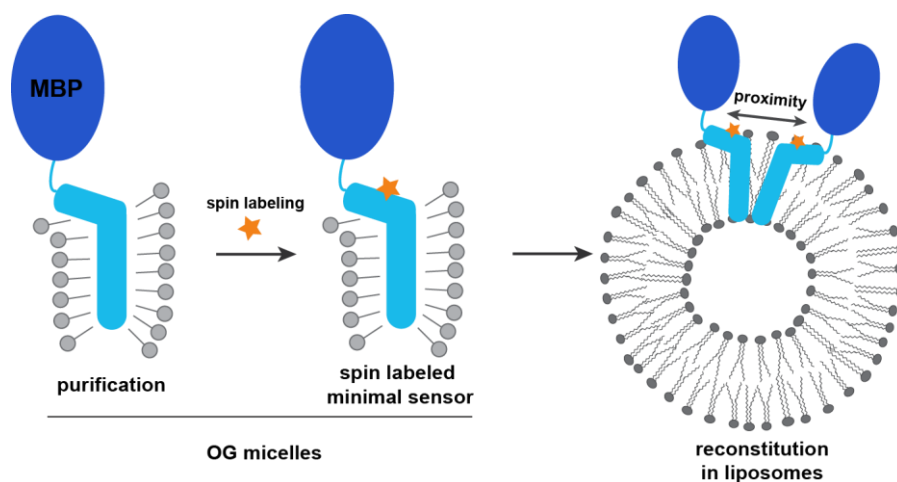


Figure 40 | In vitro strategy to explore lipid modulated oligomerization of MBP-Ire1^{AH+TMH}.

The fusion protein is purified and spin-labeled in the presence of detergent (OG). After reconstitution of the fusion protein into liposomes of different lipid compositions, cwEPR experiments are performed to investigate the average proximity of the spin-labels in the lipid environments indicated in Fig.38 A.

If the predicted, unusual architecture of Ire1's TMH with a juxta-membrane AH is sufficient for the membrane-sensitive oligomerization and activation of Ire1, the minimal sensor should recapitulate this behavior. To investigate the impact of the membrane lipid environment on the oligomeric state of the minimal sensor, the spin-labeled minimal sensor was reconstituted in

defined lipid environments and cwEPR spectra were recorded at 30°C for mobility measurements and at -115°C for distance and polarity measurements (Fig. 38). When the spin probe was installed at position R537 the low temperature (-115°C) spectra were significantly broadened when the minimal sensor was reconstituted in membranes with tightly packed lipids (Fig. 41 A). The more ordered the membrane environment, the more distinct the spectral broadening. Since spectral broadening only occurs if the distal separation of two spin probes does not exceed 2.0 nm (Bordignon and Steinhoff, 2007), this finding indicates that the minimal sensor oligomerizes in more ordered membranes with tight lipid packing.

The semi-quantitative average proximity index L_f/M_f (Covino et al., 2016) was used to illustrate these changes of the interspin proximity (Fig. 41 B and C). There is a tight correlation between the GP lipid order parameter determined with C-Laurdan and the average proximity index (Fig. 38 and 41 C).

Specifically, the average interspin distance when the sensor was reconstituted in the lipid environment with the composition 1 and 2. Increased proportions of acyl chain saturation and/or molar fractions of cholesterol (composition 6 and 7), or an increased PE:PC ratio and acyl chain saturation (composition 8) revealed more intimate inter-spin interactions providing strong evidence for the oligomerization of the minimal sensor in these lipid environments. Strikingly, this membrane-sensitive behavior was dependent on the integrity of the AH. No spectral broadening was obtained when the AH was disrupted by an F531R mutation, while the MTSSL was installed at the position R537 (Fig. 41 A and B). This, together with the extensive genetic data presented in the previous chapters, highlights a crucial role of the AH for the membrane-sensitive oligomerization of Ire1.

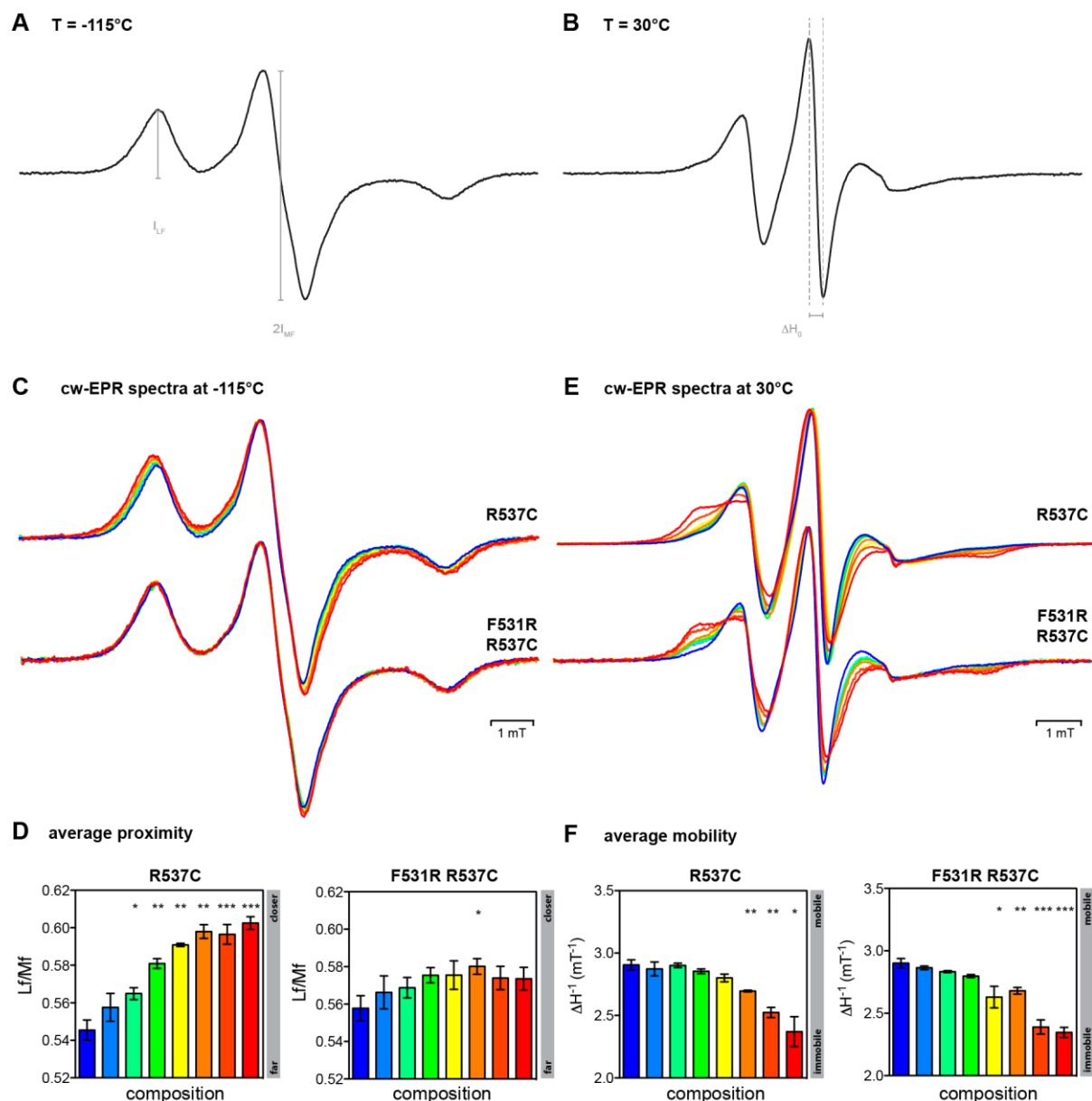


Figure 41 | cwEPR spectroscopy of MBP-Ire1^{AH+TMH} in different lipid environments.

(A) A representative cwEPR spectrum recorded at -115°C is plotted to illustrate how the intensities of the middle ($2 I_{MF}$) and the low field peak (I_{LF}) are derived from the spectra. (B) A representative cwEPR spectrum recorded at 30°C is plotted to illustrate the line width of the middle field peak (ΔH_0) as a reporter for the mobility of the spin probes. (C, E) cwEPR spectra of indicated spin-labeled mutants of MBP-Ire1^{AH+TMH} in different lipid environments recorded at -115°C (C) or 30°C (E) were intensity normalized and plotted against the lipid compositions as in Fig. 36 A used for reconstitution. (D) Semi-quantitative analysis of inter-spin distances. The proximity index Lf/Mf was derived as introduced in (A) from spectra presented in (C) and plotted for the indicated lipid compositions. Higher values indicate lower average interspin distances. (E) Semi-quantitative analysis of spin label mobilities. The mobility parameter ΔH_0 was derived as described in (B) from spectra presented in (E) and plotted for the indicated lipid compositions. Higher values indicate higher mobility of the spin-label. The error bars represent the average \pm SEM for ≥ 3 independent experiments. Significance was tested by an unpaired student's t-test. *** $p < 0.001$, ** $p < 0.01$, * $p < 0.05$.

The mobility of the spin probe in different membrane environments was analyzed from cwEPR spectra recorded at 30°C (Fig. 41 B). Weak interactions of the spin label with its surrounding environment results in a high degree of mobility, which is characterized by a small apparent

hyperfine splitting and line width of the cwEPR spectrum (Bordignon and Steinhoff, 2007). When the motion of the spin probe is restricted by the environment, the apparent hyperfine splitting and line width of the cwEPR spectrum are increased (Bordignon and Steinhoff, 2007). The semi-quantitative parameter ΔH^{-1} for the mobility can be deduced from the line width of the middle field peak and reflects the mobility of the spin label. ΔH^{-1} decreases when the mobility of the spin probe is reduced (Fig. 41 D).

cwEPR measurements (30°C) reveal that the mobility of the spin-probe the position R537 of the minimal sensor domain differs in different lipid environments and irrespectively whether the AH is intact or disrupted by a F531R mutation (Fig. 41 D and F). Expectedly, ΔH^{-1} decreases when the lipid packing of the membrane environment increases. Thus, the reporter is sensitive to changes in environment. As these changes of the mobility are insensitive to the disruption of the AH by the F531R mutation, it is most likely that the mobility reports primarily on interactions of the spin label with the membrane lipids and less so on transient protein-protein interactions that differ between the F531R variant and the wild type variant of the minimal sensor.

As a control, Pulsed Electron-Electron Double Resonance (PELDOR) EPR spectra were recorded with the wild type and the F531R variants of the minimal sensor labeled at position R537 in lipid compositions 1 and 8 (Fig. S2) (performed by Dorith Wunnicke & Inga Hänelt, Institute of Biochemistry, Goethe University Frankfurt). The resulting distance distributions revealed a very short distance, which was observed for the wild type variant of the minimal sensor in lipid composition 8. This distance was neither observed for the respective protein in lipid composition 1, nor for the F531R variant in either lipid composition 2 or 8. Additionally, the modulation depths of these measurements, which reflect the number of interacting spins in the sample, were analyzed. The value for the number of interacting spins in each sample, as calculated from the modulation depths, was comparable and < 2 for all samples (Fig. S2). This indicated the formation of dimers, rather than the formation of oligomers of higher order.

To exclude that the spectral broadening of cwEPR spectra was due to unspecific effects of the lipid environment on the spin probe, spin-diluted control spectra were recorded (Fig. 42 A and B). To this end, the spin labeled minimal was diluted with an unlabeled form at a 5-fold excess, to achieve a so-called no dimer control.

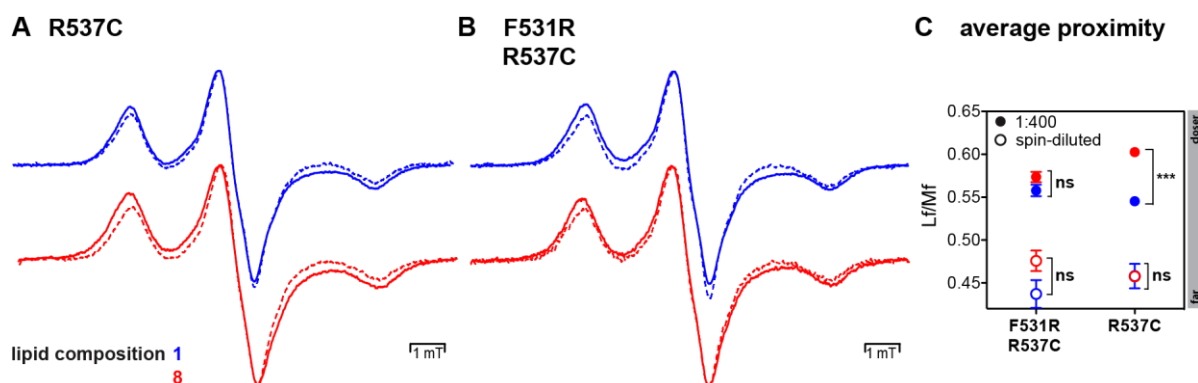


Figure 42 | cwEPR spectra of MBP-Ire1^{AH+TMH} variants and their spin-diluted controls.

(A, B) cwEPR spectra recorded at -115°C and plotted after intensity normalization of the indicated spin-labeled cysteine variants of the minimal sensor reconstituted in liposomes of the indicated lipid compositions 1 and 8 with the previously introduced color code. Spectra of spin-diluted samples, containing a 5-fold excess of non-labeled MBP-Ire1^{AH+TMH} were recorded as a control. (C) The semi-quantitative index Lf/Mf was derived from cwEPR spectra shown in (A) and (B). Higher values indicate low average inter-spin distances. The error bars represent the average \pm SEM for $n = 3$ protein:lipid ratio of 1:400, $n = 2$ for spin-diluted controls. Significance was tested by an unpaired student's t-test. *** $p < 0.001$.

For these no dimer controls, barely any spectral broadening could be observed for both, the wild type and F531R mutant of the minimal sensor. The lack of inter-spin interactions is also reflected by the average proximity values derived from the spectra (Fig. 42 C). These data clearly show that spectral broadening is indeed caused by low inter-spin distances. Thus, the minimal sensor oligomerizes in a membrane-sensitive fashion.

Consequently, the spectral broadening should be dependent on the protein:lipid ratio used for the reconstitution experiments, as this ratio determines the density of the spin-labeled minimal sensor in the membrane. This could be confirmed by reconstitution experiments in which a protein:lipid ratio of 1:1000 was used. Under these condition, the spectral broadening was less pronounced compared to experiments performed with proteoliposomes with a protein:lipid ratio of 1:400 (Fig. 43 A). This is also reflected in the semi quantitative Lf/Mf index (Fig. 43 B) deduced from these spectra.

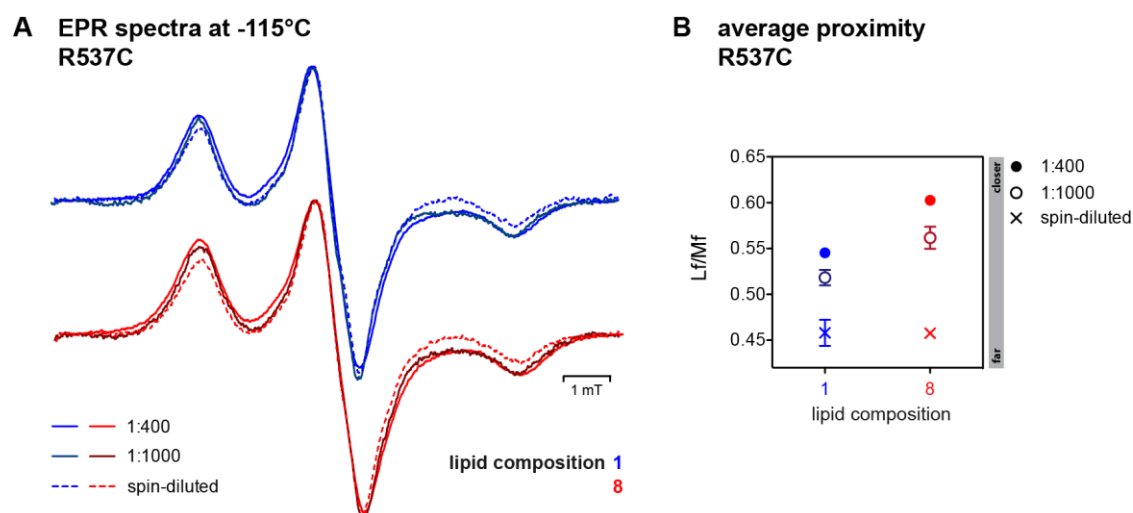


Figure 43 | Concentration dependent spectral broadening of cwEPR spectra from MBP-Ire1^{AH+TMH} variants.

(A) cwEPR spectra recorded at -115°C and plotted after intensity normalization of the indicated spin-labeled cysteine variants of the minimal sensor reconstituted at different protein:lipid ratios in liposomes of the indicated lipid compositions 1 and 8 with the previously introduced color code. Spectra of samples reconstituted at a molar protein:lipid ratio of 1:400 are depicted in light colors, spectra of samples reconstituted at a molar protein:lipid ratio of 1:1000 are depicted in dark colors. Spin-diluted samples, containing a 5-fold excess of non-labeled MBP-Ire1^{AH+TMH} at a molar protein:lipid ratio of 1:400 are depicted in dashed lines. (B) The semi-quantitative index Lf/Mf was derived from cwEPR spectra shown in (A). Higher values indicate low average inter-spin distances. The error bars represent the average \pm SEM for $n = 3$ protein:lipid ratio of 1:400 and 1:1000, $n = 2$ for spin-diluted controls.

In another set of experiments, the endogenous cysteine C552 in the TMH of Ire1 was used as an alternative reporter residue to validate the previously data (Fig. 41 and 44). Two loosely lipid environments with rather loose lipid packing (composition 1 and 2) and two with tighter packed lipids (composition 7 and 8) were used as matrix for the reconstitution. The oligomerization of this alternatively labeled minimal sensor was analyzed with an intact and a disrupted AH (F531R). Expectedly, the spectral broadening was much more pronounced for the variant with an intact AH (Fig. 44 A and B). Thus, an intact AH is crucial for the membrane-sensitive oligomerization of Ire1.

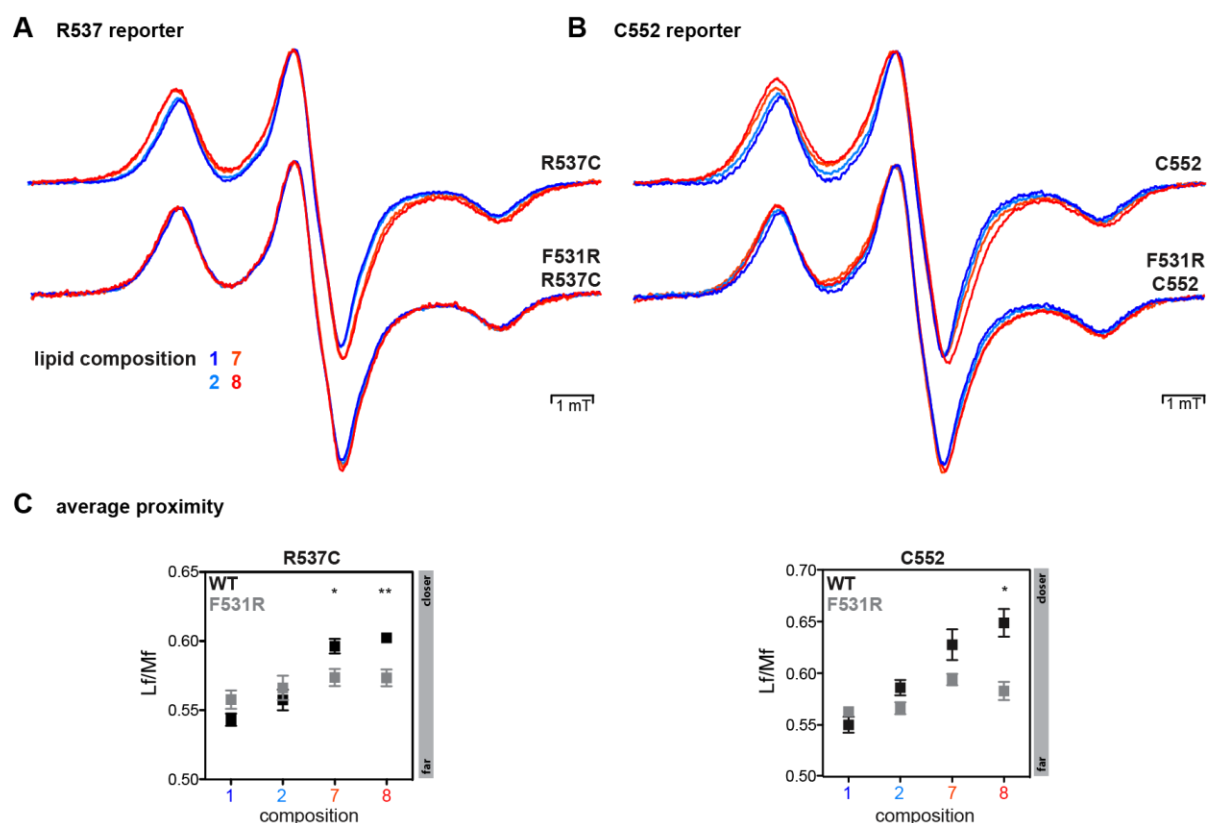


Figure 44 | Alternative C552 residue for cwEPR spectroscopy.

(A, B) cwEPR spectra were recorded at -115°C . The indicated cysteine residues of the minimal sensor were labeled. The spectra were plotted using the color code for the lipid compositions in Fig. 36. (C) Semi-quantitative analysis of interspin distances. The proximity index L_f/M_f was derived from spectra presented in (A, B) and plotted for the indicated mutants and lipid compositions. The error bars represent the average \pm SEM for ≥ 3 independent experiments. Significance was tested by an unpaired student's t-test. *** $p < 0.001$, ** $p < 0.01$, * $p < 0.05$.

The striking dependence of spectral broadening on the molecular lipid packing densities suggests that the oligomerization and activation of Ire1 depends on a collective membrane property and that the AH is crucial for this sensitivity (Halbleib et al., 2017). When lipid packing increases, Ire1 oligomerizes, while a looser lipid packing in the environment would destabilize oligomeric arrangements of Ire1.

5.9. Exploring the structural dynamics of Ire1's AH during activation by lipid bilayer stress

In order to gain insights in to the structural dynamics of the AH (Ire1⁵³⁴⁻⁵³⁹) in different membrane environments, a spin-probe was installed at six consecutive positions in the minimal sensor construct. After reconstituting this construct in two distinct membrane environments corresponding to lipid composition 1 and 8, low temperature cwEPR spectra (-115°C) were recorded to gain information on the average inter-spin proximity and the polarity of the spin probe's environment. cwEPR spectra of the spin labeled mutants Y536C to I539C

were broadened in lipid composition 8 as compared to lipid composition 1 (Fig. 45 A and B), thereby corroborating findings with the minimal sensor labeled at the position of R537 or at the endogenous C552 (Fig. 44). Again, these data suggest that the minimal sensor consisting containing the AH and the TMH of Ire1 shows a membrane-sensitive oligomerization, which is likely to support the oligomerization of Ire1 under conditions of lipid bilayer stress. No spectral broadening, however, was observed when the spin probe was introduced more N-terminally at the positions L534 and V535 (Fig. 45 A and B). This finding suggests an inter-spin distance greater than 2.0 nm at these positions even in oligomers of Ire1.

Analysis of the low temperature cwEPR spectra (-115°C) can also provide information on the polarity of the spin probe's nano-environment based on the hyperfine splitting (A_{zz}). In order to derive values for the hyperfine splitting A_{zz} , the magnetic field difference between the low and high field peaks can be determined, to yield the polarity value $2A_{zz}$ (Bordignon and Steinhoff, 2007). In order to test how individual residues of the AH interact with the lipid matrix and in order to test for major structural changes in the AH region when the minimal sensor is reconstituted in different membrane environments, the $2A_{zz}$ value was extracted for the spin probes installed at the residues Y536 to I539 with the minimal sensor reconstituted in lipid composition 1 and 8. The higher the $2A_{zz}$ value, the more polar the nano-environment of the spin probe (Bordignon and Steinhoff, 2007).

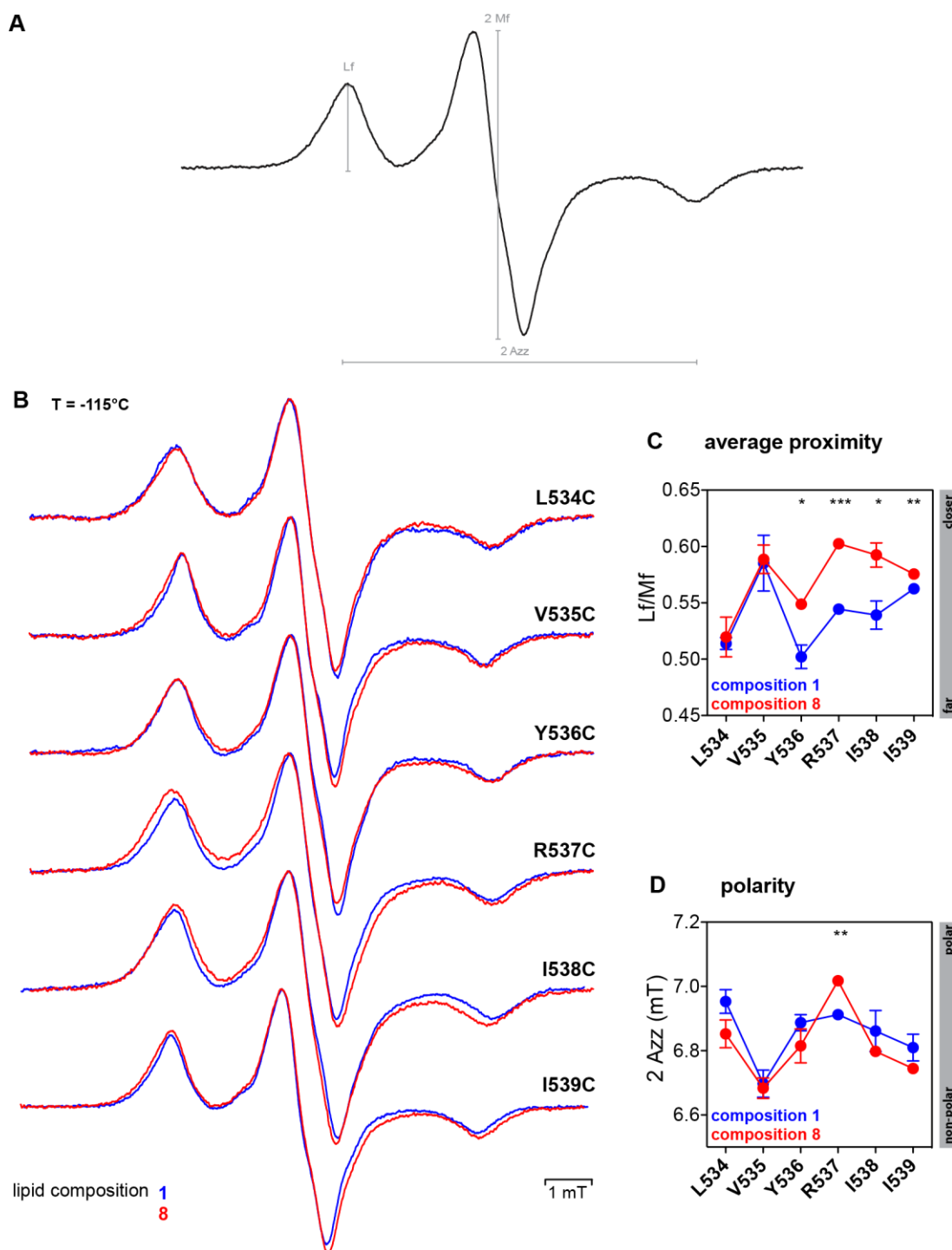


Figure 45 | cwEPR spectra of MBP-Ire1^{AH+TMH} labeled at the indicated residues and reconstituted in distinct membrane environments.

(A) A representative, intensity normalized cwEPR spectrum recorded at -115°C illustrates how the $2A_{zz}$ value is derived from the spectra. (B) The minimal sensor was labeled at the indicated residues and reconstituted in liposomes of different lipid environments illustrated by the previously introduced color code. cwEPR spectra were recorded at -115°C and plotted after intensity normalization. (C) The semi-quantitative index Lf/Mf was derived from cwEPR spectra shown in (B) and plotted against the position of labeling. Higher Lf/Mf values indicate low average inter-spin distances. The error bars represent the average \pm SEM for 3 independent experiments. Significance was tested by an unpaired student's t-test. *** $p < 0.001$, ** $p < 0.01$, * $p < 0.05$. (D) The $2A_{zz}$ tensor is derived from cwEPR spectra and plotted against the position of labeling. The error bars represent the average \pm SEM for 3 independent experiments. Significance was tested by an unpaired student's t-test. ** $p < 0.01$.

When the polarity value $2A_{zz}$ was plotted against the position of labeling, a helical pattern of polarity was observed in both lipid environments (Fig. 45 C). This validates that the predicted AH indeed forms a helix with a more polar and apolar environment. Moreover, this shows that the structure of the AH does not change in rather distinct lipid environments. While the AH is crucial to drive the minimal sensor into oligomers (Fig. 41 - 45), it does not undergo a major change of its secondary structure. The nano-environment of the spin probe was less polar for residues located in the hydrophobic face (V535, I538, I539) than for those pointing towards the hydrophilic face of the AH (L534, R537). The overall polarity of the spin probes did not change remarkably in response to changes in molecular lipid packing. Only for the reporter residue at position R537 the polarity increased in densely packed liposomes (Fig. 45 C). As the average distances of the R537 reporter changed remarkably in different lipid environments, this residue might be at the interface of two Ire1 molecules within the dimer, which naturally would affect the polarity at this position.

Taken together, these data suggest that the AH of Ire1 is stably inserted into the lipid bilayer, irrespective of the lipid packing density. This implicates, that the overall architecture of Ire1's AH overlapping with and adjacent to the TMH is not perturbed by the lipid environment yet sufficient to drive Ire1 in to oligomers during lipid bilayer stress.

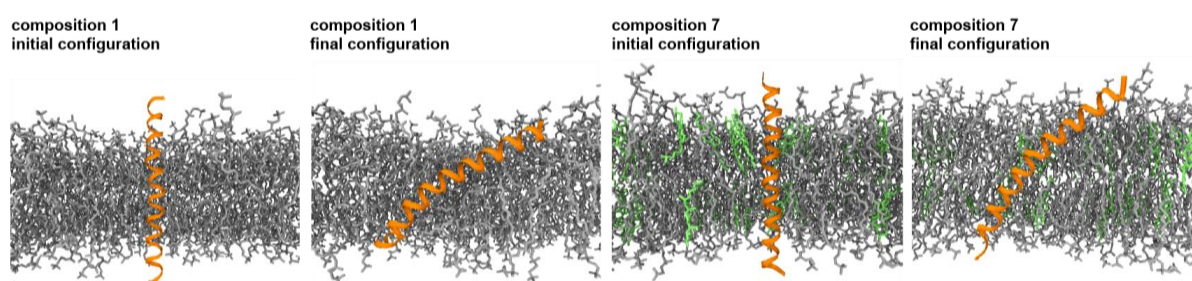


Figure 46 | Representative structures of the initial and final configuration of the Ire1 minimal sensor in MD simulations. Structures from MD simulations of the wild type minimal sensor (Ire1 minimal sensor, orange; POPC and DOPC, grey; cholesterol, green). Representative structures of the wild type minimal sensor modeled as a straight helix into the lipid compositions 1 and 7 from *in vitro* experiments. MD simulations were performed and analyzed by Roberto Covino & Gerhard Hummer, Institute for Theoretical Biophysics, MPI for Biophysics.

Atomistic molecular dynamics (MD) simulations of the minimal sensor of Ire1 (Ire1⁵²⁶⁻⁵⁶¹) were performed in lipid bilayers corresponding to lipid compositions 1 and 7 of the *in vitro* reconstitution experiments (performed by Roberto Covino & Gerhard Hummer, MPI for Biophysics). In these simulations, the hydrophobic portion of the AH entered the lipid bilayer and remained stably inserted throughout the $> 3 \mu\text{s}$ simulation with the hydrophilic portion of the AH facing the aqueous environment (Fig. 46). Intriguingly, the membrane integration of

the AH forced the TMH of Ire1 into a strongly tilted orientation relative to the lipid bilayer and introduced a temporary kink in the minimal sensor.

5.10. AH mutations partially unfold the helix

In vivo experiments (Fig. 24 B, 26 and 27) revealed that the introduction of positive charges into the hydrophobic face of the AH (F531R and V535R) induced a significant functional defect for Ire1. Moreover, *in vitro* experiments using the minimal sensor of Ire1 clearly showed that Ire1 acts as a membrane-packing sensor and uses its AH to sense the properties of the lipid environment, while the introduction of the F531R mutation strongly disabled the minimal sensor to react to changes in the lipid environment (Fig. 41 to 44). Irrespective of the lipid environment, the AH remained inserted and folded, which lead to the hypothesis that the unique combination of a continuous AH and TMH region is required for Ire1 to perform sensing of the lipid environment.

How do the AH mutants (F531R and V535R) interfere with Ire1's functionality? CD spectroscopic characterization of the synthetic AH peptide (Ire1⁵²⁶⁻⁵⁴³) and its mutant variants (F531R and V535R) were performed to elucidate the effect of introducing of a positive charge into the hydrophobic face of the AH (Fig. 47). CD-spectra were recorded in the presence of the non-ionic detergent DDM (1%) and revealed that the F531R and V535R mutant both show strongly reduced α -helical content compared to the wild type peptide (Fig. 47 A).

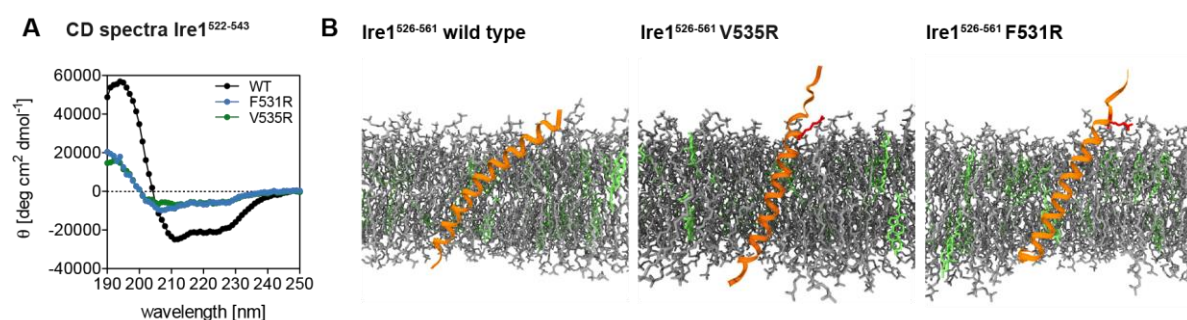


Figure 47 | The AH of Ire1 unfolds when a positive charge is introduced at positions F531 or V535.

(A) CD spectroscopic analysis of the synthetic AH peptide and its mutants in a sodium carbonate buffer (pH 7.0) supplemented with 1% DDM. (B) Representative structure of the Ire1-derived minimal sensor, represented as in Fig. 44, as well as the F531R (red) and V535R (red) mutations in the densely packed lipid environment 7. MD simulations were performed by Roberto Covino & Gerhard Hummer, Institute for Theoretical Biophysics, MPI for Biophysics.

In line with these data, MD simulations validated that both mutations (F31R and V535R) destabilize and unfold, consequently the AH is disrupted (Fig. 47) (performed by Roberto Covino & Gerhard Hummer, MPI for Biophysics).

5.11. The AH of Ire1 induces a local compression in the lipid bilayer

To explore how the membrane environment affects the oligomerization of Ire1, MD simulations of the minimal sensor (Ire1⁵²⁶⁻⁵⁶¹) were performed by Roberto Covino & Gerhard Hummer from the MPI for Biophysics.

The minimal sensor (Ire1⁵²⁶⁻⁵⁶¹) was modelled in two distinct lipid environments that were identical to the lipid environments 1 and 7 used for *in vitro* studies with the minimal sensor domain of Ire1 (Fig. 48). The MD simulations confirmed that composition 7, which contains a high portion of saturated lipid acyl chains and sterols, produces a thicker and more ordered lipid bilayer than composition 1. While the local thickness of the lipid bilayer is fluctuating on the ns time scale, integration of bilayer thickness over time revealed that the minimal sensor induces a significant compression of the lipid bilayer, which was more pronounced in a thicker bilayer with respect to both, relative area and height (Fig. 48 A). Moreover, the local membrane compression induced by the minimal sensor induced substantial disordering of the lipid acyl chains, as defined by a reduction of the acyl chain order parameter S_{CD} , which was also more pronounced in composition 7 (Fig. 48 B).

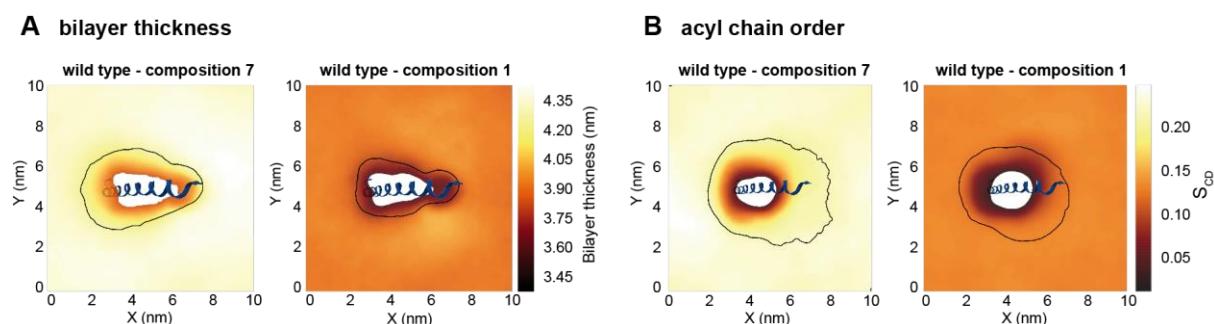


Figure 48 | The minimal sensor peptide induces a lipid bilayer compression and lipid acyl chain disorder.

(A) Membrane thickness around the sensor peptide, defined as the average vertical distance between two phosphate layers, averaged over MD simulations in bilayers of lipid composition 1 and 7 from *in vitro* experiments. The black solid contour line depicts a 3% drop of the bilayer thickness from bulk average. A representative structure of the peptide is shown, with its N-terminus on the right lying on the ER luminal leaflet of the bilayer. (B) The acyl chain order parameter S_{CD} was extracted from MD simulations and reports on the orientational mobility of the C-C bond in the lipid tails. S_{CD} profiles were calculated around the sensor peptide and averaged over MD simulations in the lipid compositions 1 and 7. In average, the TMH region was aligned to a common reference by using rigid body translations and restricted rigid-body rotations around an axis normal to the membrane plane. The solid black contour line indicates a reduction in S_{CD} by 3.5% relative to the average bulk value distant from the peptide. MD simulations were performed and analyzed by Roberto Covino & Gerhard Hummer, Institute for Theoretical Biophysics, MPI for Biophysics.

As membrane thickness and acyl chain order are inherently connected and any lipid bilayer compression comes at an energetic cost, these data indicate that the oligomerization of Ire1 may minimize these energetic costs. The coalescence of two compressed, disordered

nanodomains into a single domain upon dimerization would minimize the total energy of the system. This energy difference increases with the degree of membrane compression such that the driving force for Ire1 dimerization is determined by the membrane lipid composition. The thicker the membrane and the more ordered the lipids within, the higher the driving force of oligomerization. According to this model, Ire1 acts as a membrane-packing sensor, which uses a bilayer compression to sense a bulk property of the lipid bilayer (Halbleib et al., 2017).

5.12. The structural and functional role of Ire1's TMH in ER stress

5.12.1. Structural analysis of the TMH by cysteine cross-linking

To investigate the dimerization interface of Ire1's TMH within the lipid bilayer, a cysteine cross-linking approach was designed. A cysteine scan along the entire TMH was performed to study the crosslinking efficiency of the minimal sensor MBP-Ire1^{AH+TMH} reconstituted in a membrane environment with tightly packed lipids. Thus, single cysteine mutants of the minimal sensor were reconstituted in liposomes consisting of EPL and DPPC (7:3), mimicking a densely packed membrane environment.

The quality of the purified protein was examined as previously described (Fig. 36; 5.7.) and reconstituted into EPL:DPPC liposomes. The protein was successfully integrated and proteoliposomes were harvested by centrifugation (Fig. 49 A). Extensive quality control of proteoliposomes was performed to validate proper insertion (Fig. 49 B to D). Sucrose gradients, which were fractionated and analyzed for their protein and lipid contents, revealed that no protein aggregates were present after reconstitution (Fig. 49 B and C). Membrane extraction experiments using Na₂CO₃ did not extract MBP-Ire1^{AH+TMH} from the membrane, indicating that the protein was efficiently inserted into the ER-membrane (Fig. 49 D).

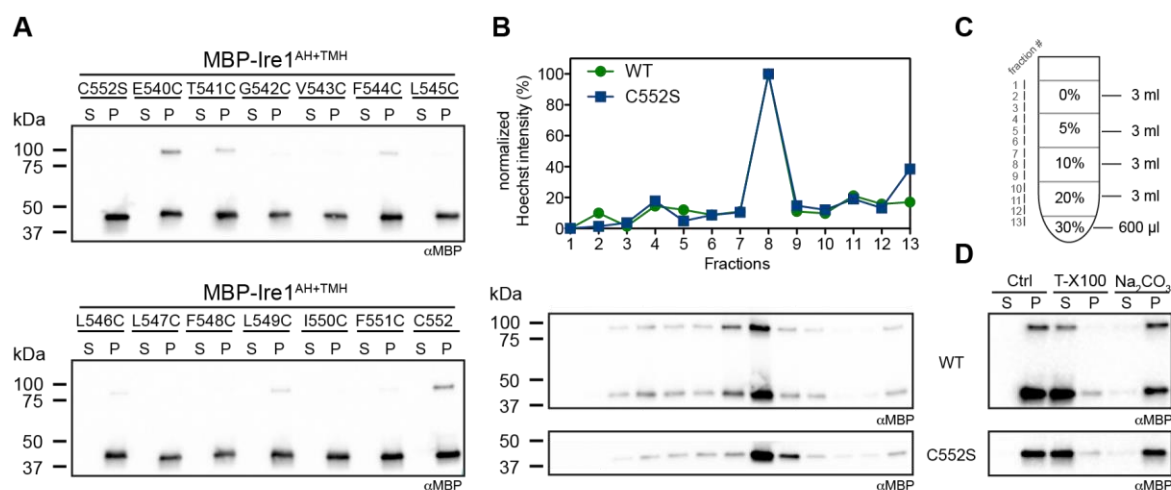


Figure 49 | Reconstitution and quality control of MBP-Ire1^{AH+TMH} containing proteoliposomes.

Proteoliposomes containing the indicated mutants and indicated lipid mixtures at a molar protein to lipid ratio of 1:6000. (A) Reconstitution of MBP-Ire1^{AH+TMH} was performed using EPL:DPPC (7:3) liposomes. After reconstitution, the resulting proteoliposomes were pelleted (450.000x g, 90 min) and resuspended in reconstitution buffer. To test the reconstitution efficiency, samples of supernatant (S) and pellet (P) after the reconstitution were taken and subjected to an SDS-PAGE followed by immunoblotting using anti-MBP antibodies. (B, C) The quality of the proteoliposomal preparation was validated by a sucrose step gradient centrifugation (B), using the depicted sucrose step gradient (C) followed by an analysis of the lipid and protein distribution in fractions taken after equilibrium centrifugation. Lipid distribution throughout the gradient was monitored by fluorescence spectroscopic measurements utilizing the Hoechst33342 dye. Protein content was monitored by subsection of samples to an SDS-PAGE followed by immunoblotting using an α MBP antibody. (D) Proteoliposome containing samples were treated with 0.1 M Na₂CO₃ pH 11.0 for extraction of peripherally attached protein from proteoliposomes or 1% Triton X-100 (T-X100) as a solubilization control. Samples of supernatant (S) and pellet (P) after the treatment with different additives were taken and subjected to an SDS-PAGE followed by immunoblotting using anti-MBP antibodies. (B, C, D) Quality control of the minimal sensor in EPL:DPPC liposomes was established and performed in collaboration with Julian Wagner during his Diploma Thesis under the supervision of Kristina Halbleib.

After reconstitution, crosslinking was performed for 6.5 days by leaving the sample in a normal oxygenated atmosphere and without any added crosslinking reagents. Large differences in cross-linking efficiencies were observed depending on the position of the cysteine ranging from \approx 5 % to 33 % (Fig. 50 A to C). When a cysteine residue was inserted at positions G542, L546, L547, I550 and F551 only 10 % of crosslinking was observed – thus the crosslinking efficiency was low. Cysteine residues at positions E540, V543, L545, F548 and L549 resulted in 15 – 29 % of crosslinking and were classified as residues with intermediate crosslinking efficiency. Finally, cysteine residues at position T541, F544 and C552 resulted in crosslinking is 30% or higher, these residues were classified as residues with high crosslinking efficiency. Moreover, the overall crosslinking efficiency for the N-terminal part of the TMH (E540 – L545) is higher than that of the C-terminal part of the TMH (L546 – C552) (Fig. 50 C). This finding indicates that the AA residues in the N-terminal part of the TMH are in closer proximity to each other than the residues in the C-terminal part of the TMH.

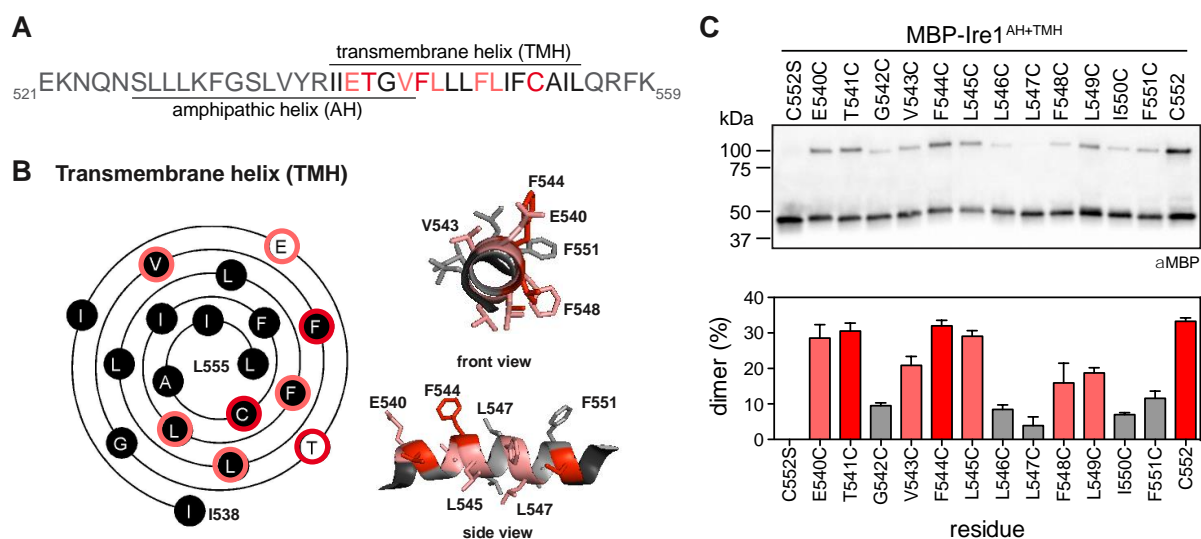


Figure 50 | *In vitro* crosslinking studies of the reconstituted minimal sensor.

The predicted TMH (black) and juxtra-membrane regions (grey) of Ire1. Residues with a crosslinking efficiency below 10% are depicted in black, those over 30% are highlighted in red, intermediate crosslinking residues in salmon (B) Helical wheel analysis (Wenxiang Diagram; (Chou, 2011) of the TMH (Ire1⁵³⁸⁻⁵⁵⁵) of Ire1. Residues are color coded as introduced in (A), the N- and C-terminal residue of respective projections are labeled. (C) Proteoliposome containing samples were incubated in an oxygen containing environment for 6.5 days at 37°C. Dimerization was monitored by subsection of samples to an SDS-PAGE followed by immunoblotting using anti-MBP antibodies. The dimer content was quantified in respective samples. Residues at positions showing crosslinking efficiencies of 30% or higher (red), intermediate crosslinking efficiency 15% < X < 30% (salmon) and <15% (grey) are depicted. Crosslinking experiments were established in collaboration with Julian Wagner during his Diploma Thesis under the supervision of Kristina Halbleib. Data sets of both experimenters were merged. The error bars represent the average \pm SEM for 3 independent experiments.

This crosslinking approach revealed that the TMHs do not just face each other in random orientations. Some residues do not crosslink and therefore do not seem to come in close contact. These data may be interpreted structurally and could be used as constraints for building a model for dimeric TMHs. A particularly tempting model would be the formation of X-shaped dimer, in which the tilted TMHs cross each other in the core of the bilayer around the position of F544C, which showed particularly strong crosslinking. Interestingly, such a conformation has been observed in preliminary MD simulations (Fig. 51) performed by Roberto Covino & Gerhard Hummer from the MPI for Biophysics in Frankfurt.

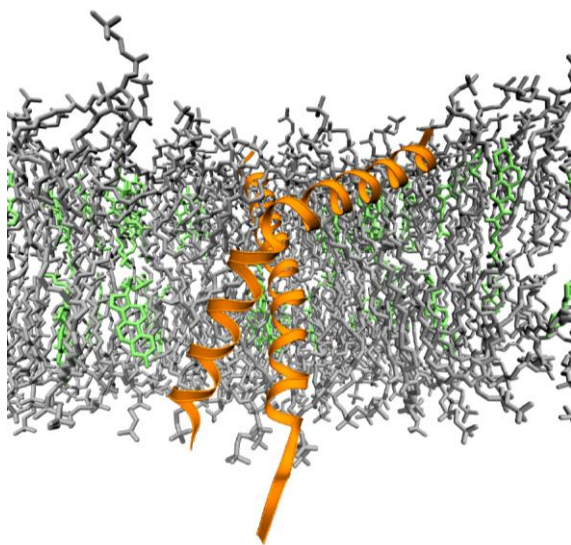


Figure 51 | MD simulations reveal the formation of a X-shaped dimer.

Representative structure of the Ire1-derived minimal sensor, represented as in Fig. 46. in the densely packed lipid environment 7. MD simulations were performed by Roberto Covino & Gerhard Hummer, Institute for Theoretical Biophysics, MPI for Biophysics.

6. Discussion

6.1. Endogenous expression of a fully functional *IRE1* construct

Ire1 is a protein of very low abundance. A single cell carries only approximately 60 (Kulak et al., 2014) to 259 copies of Ire1 (Ghaemmaghani et al., 2003). Because the activity of Ire1 is regulated by its oligomerization, any overexpression of *IRE1* may result in an aberrant activation and signaling outcome. The aim of this thesis was to test the physiological role of the Ire1's transmembrane region for sensing of the physicochemical properties of the ER membrane. Thus, it was crucial to develop tools to study a fully functional variant of Ire1 produced from its endogenous locus under the control of its endogenous promoter. This work establishes for the first time an *IRE1* knock-in construct, which may become a valuable tool for the scientific community.

Previously, the structure-function relationships of Ire1 were studied using *IRE1* expressed from its endogenous promoter on *CEN*-based or 2 μ plasmids (Kimata et al., 2004, 2007; Oikawa et al., 2007; Promlek et al., 2011). These studies provided insights into the mechanisms of activation and signal transduction of Ire1 for orchestrating the UPR, in response to ER-stress. In some cases, Ire1 has been studied using C-terminal 3xHA, 3xFLAG or other epitope tags to monitor Ire1 protein levels and the Ire1 localization (Kimata et al., 2004, 2007; Oikawa et al., 2007; Promlek et al., 2011; Rubio et al., 2011). However, the introduction of sizeable epitope tags irrespectively whether they are installed at the N- or the C-terminus of Ire1 impair its function.

Thus, establishing an fully functional, internally-tagged variant of *IRE1* with a yeast optimized version of GFP inserted at a flexible loop at position H875 was an important advance (van Anken et al., 2014). This thesis describes a new generation of this construct: The incorporation of a 3xHA epitope tag directly N-terminally to the GFP allows for sensitive immunoblot detection (Fig. 18 A). The resulting construct remained functional in sensitive ER stress resistance tests (Fig. 18 B) and has been used throughout this study to investigate structure-function relationships of Ire1 by genetic means *in vivo*.

Noteworthy, the knock-in construct is the first fully functional version of *IRE1* expressed at such low levels. When *IRE1* is expressed from its own promoter on a *CEN*-based plasmid, it is 2.7-fold higher expressed compared to the newly established knock-in construct (Fig. 20 A) and shows rather large cell-to-cell variations of expression, which are not observed for the knock-in construct (Fig. 20 B). Moreover, this is the first construct that allowed for a robust

detection of Ire1 in cell lysates by immunoblotting. Thus, the established knock-in construct of *IRE1* may provide an important tool for studying the UPR and structure-function relationships of Ire1 *in vivo* when produced at the near-endogenous level.

6.2. An array of functional *in vivo* assays in combination with *in vitro* studies is required to analyze Ire1 mutants

In order to test the impact of mutations on the functionality of *IRE1*, an array of biochemical and cell biological assays had to be established. The combination of these assays allows for in depth analysis of *IRE1* and its mutant variants in stressed and unstressed cells at different stages of UPR activation and signaling. ER-stress resistance tests relying on the growth of stressed cells serve as a quick prescreening method to identify mutants with functional defects. One caveat of this assay is that it cannot detect an increased basal activity of the UPR. Another limitation of this assay is that it does not distinguish between an increased rate of cell death and reduced cellular growth rates. In order to track the function of Ire1 and its mutant variants more directly, other assays were employed: i) confocal fluorescence live cell imaging was performed to investigate Ire1 clustering, ii) the degree of *HAC1* splicing and iii) the mRNA level of the UPR target gene *PDI1* were analyzed by RT-qPCR. The combination of these functional tests helped to explore both loss-of-function and gain-of-function mutants of *IRE1*.

When using reporters for the UPR activity, it is important to consider the sensitivity and the temporal resolution of a particular assay. GFP reporters fused to four repeats of the UPR element integrated into the genome are highly sensitive tools to monitor the UPR activity over a relatively long period of time (Jonikas et al., 2009; Pollard et al., 1998; Surma et al., 2013). The same is true for UPR-lacZ reporters (Promlek et al., 2011). As in previous studies (Kimata et al., 2003, 2004, 2007; Oikawa et al., 2007; Promlek et al., 2011; Sidrauski and Walter, 1997; Sidrauski et al., 1996) the activity of the UPR was scored in this thesis by determining the degree of *HAC1* splicing. This sensitive reporter for UPR activity allows for an accurate estimation of UPR activity at a given time. The temporal resolution of protein-based reporters relies on the life-time of GFP or lacZ and thus integrate the UPR-activity over a relatively long time. The spliced mRNA of *HAC1*, however, is rather short-lived (half-time of approx. 20 min) and thus reflects more directly the current state of Ire1 activation (Sidrauski et al., 1996).

A number of observations suggested that yeast Ire1 and mammalian UPR transducers can react to lipid bilayer stress (Han et al., 2006; Lajoie et al., 2012; Pineau et al., 2009; Promlek

et al., 2011; Surma et al., 2013; Thibault et al., 2012; Volmer et al., 2013). The underlying mechanism, however, had not been elucidated. A recent study by Volmer *et al.* focused on the activation of the UPR sensors IRE1 α and PERK by lipid bilayer stress (Volmer et al., 2013). The authors used variants of IRE1 α and PERK lacking their luminal domains (Δ LD), and soluble constructs, consisting only of the cytosolic domains of IRE1 α or PERK fused C-terminally to immunodetection tags for a functional analysis *in vivo*. Furthermore, they overproduced and isolated these PERK constructs for reconstitution experiments to investigate the mechanism by which an increased acyl-chain saturation might activate PERK in defined lipid environments composed of DOPC (PC with two monosaturated acyl chains) and DSPC (PC with two saturated acyl chains) (Volmer et al., 2013). Proteoliposomes containing various PERK variants were subjected to an auto-phosphorylation assay and showed that PERK activity increases in response to an increased in acyl-chain saturation when tethered to the membrane (Volmer et al., 2013). This study was an important advance and showed, that the LD of both UPR sensors might be dispensable for the activation in response to lipid bilayer stress, while a membrane tether is indispensable for activation. However, the experimental system had particular limitations and a defined structural feature that would be necessary for sensing lipid bilayer stress was not reported.

The limitations of the assays with respect to sensitivity have been revisited and carefully evaluated by the authors (Volmer and Ron, 2015). When studying the regulation of signaling-active proteins in defined lipid environments, it is important to take into account the possibility of lipid phase segregation. The use of DSPC containing lipid in reconstitution experiments with PERK might result into the formation of DSPC containing gel phases and concomitantly the accumulation of PERK in a coexisting fluid lipid phase. The accumulation of PERK in the fluid lipid phase would result in an increased auto-phosphorylation that depends on the DSPC content. It is questionable, whether this mode of PERK activation is physiologically relevant. Despite these limitations, the findings by Volmer *et al.* provided important insights into the role of lipids in the activation of UPR transducers.

One of the key findings of this thesis is the identification an ER-luminal AH in Ire1 as a key structural element for sensing lipid bilayer stress (Halbleib et al., 2017). The functional relevance of this structural element was established by genetic means using extensive functional profiling of the UPR activity *in vivo*. MD simulations and *in vitro* experiments with an isolated minimal sensor provided evidence for a membrane-based mechanism of UPR activation.

Although this work provided a new perspective on the mechanisms of UPR activation, several key questions remain. What is the dominant factor that drives Ire1 activation *in vivo* and under physiological conditions – unfolded proteins or the ER lipid composition? Do all conditions of lipid bilayer stress have common features? How does the lipid composition affect the sensitivity of the UPR to unfolded proteins and *vice versa*? Only by studying the complex events underlying the UPR activation with purified components will ultimately solve these important questions in cell biology.

6.3. A membrane-based mechanism for Ire1 activation by lipid bilayer stress

All the conditions that activate the UPR by lipid bilayer stress share one striking commonality: they are predicted to increase the packing density and thickness of the ER membrane (Han et al., 2010; Lajoie et al., 2012; Pineau et al., 2009; Promlek et al., 2011; Surma et al., 2013; Thibault et al., 2012). The data presented in this thesis show that Ire1 senses aberrant lipid compositions by sensing physicochemical properties of the ER membrane, rather than stably binding or recognizing individual lipid molecules.

Systematic analysis of the TMH region of Ire1 in *S. cerevisiae* revealed the existence of an AH directly adjacent to and overlapping with the ER-luminal end of the TMH of Ire1 (Fig. 23). MD simulations show that the AH of Ire1 induces a local membrane compression and acyl chain disordering (Fig 48), achieved by the unusual architecture of Ire1's TMH region. As membrane thickness and acyl chain order are inherently connected and any lipid bilayer compression comes with an energetic cost (Mouritsen and Bloom, 1984; Nezil and Bloom, 1992), the proposed mechanism of Ire1 activation by lipid bilayer stress is a direct consequence of the reduction of this energetic cost (Fig. 52). The membrane compression induced by two individual Ire1 monomers is larger than that induced by one Ire1 dimer. In this way, Ire1 oligomerization is energetically more favorable, than maintaining Ire1 monomers. Further, breaking up oligomeric configurations of Ire1 becomes energetically increasingly unfavorable, with an increasing membrane thickness and acyl chain order. In this way, bulk physical properties of the membrane lipid environment can determine the typical lifetime of these presumably rather short-lived dimers. The prolonged physical proximity of the TMH regions of two Ire1 molecules during lipid bilayer stress hence increases the likelihood for them to establish a stable dimerization interface via the known interaction interface IF_L1 in the lumen of the ER previously characterized by X-ray crystallography (Aragón et al., 2009; Credle et al., 2005). When an AH mutation (F531R or V535R; Fig. 52, depicted in red) is introduced,

the AH of Ire1 fails to insert into the lipid bilayer and unfolds, as shown by cwEPR and CD spectroscopic measurements and MD simulations (in collaboration with Roberto Covino & Gerhard Hummer, MPI for Biophysics) and renders Ire1 incapable to react to changes in its lipid environment. Thus, this thesis provides compelling evidence that bulk membrane properties contribute to the oligomerization of Ire1 and identifies the AH as key structural element for Ire1's response.

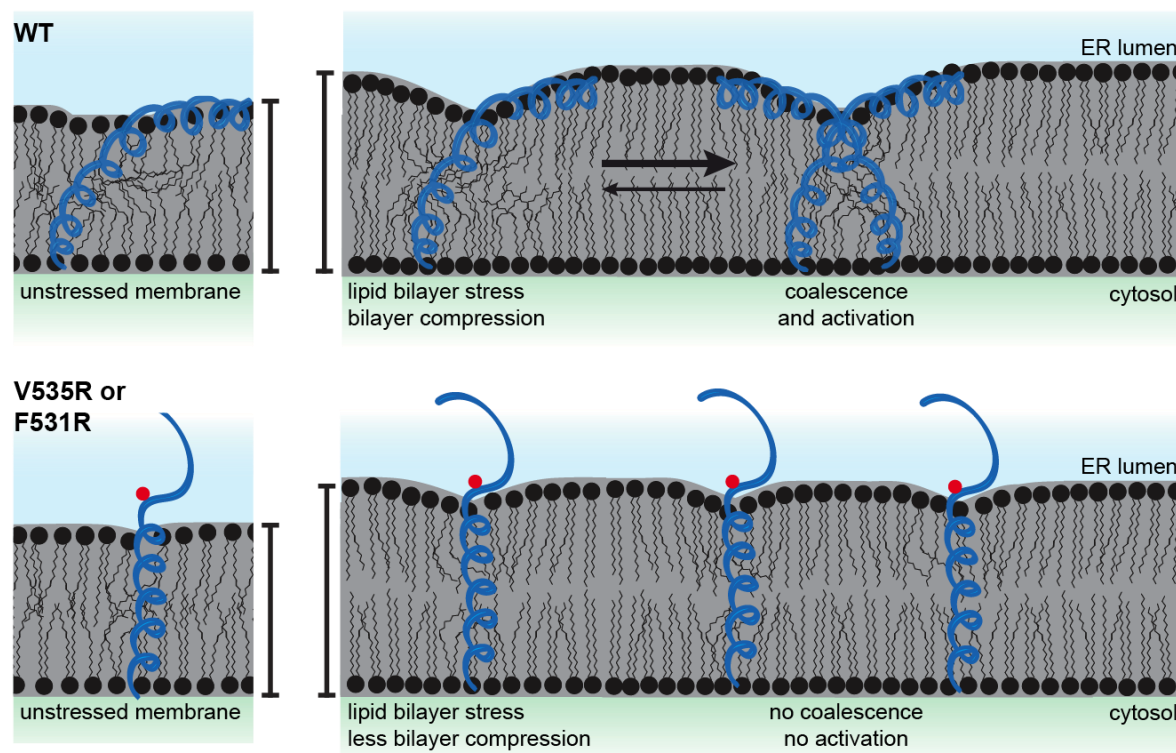


Figure 52 | Schematic model of the membrane-based mechanism of Ire1 activation by lipid bilayer stress.

The juxta-membrane AH on the ER-luminal side of Ire1 wild type (top) causes a local membrane compression. The total area of membrane compression is minimized upon dimerization of Ire1. If the amphipathic character of the AH is disrupted by mutation (red), the corresponding residues fail to insert into the lipid bilayer and thus cause substantially less membrane compression.

Further, a conserved negative amino acid residue may play a crucial role in this membrane-based mechanism. The E540 in Ire1 from *S. cerevisiae* is located near the phospholipid head groups at the water-lipid interface and might electrostatically interact with the membrane lipids. MD simulations suggest that the E540 plays a crucial part in the compression of the lipid bilayer as it is positioned at the position of maximal membrane compression (Fig. 53). As a negatively charged amino acid at this position is absolutely required for full functionality of Ire1 (Fig. 29 to 31), this finding suggests that an electrostatic interaction of E540 with the lipid head groups might support the local bilayer compression. Future reconstitution

experiments of Ire1 and its mutants at position E540 in defined, yet complex lipid mixtures shall establish the role of E540 in greater details.

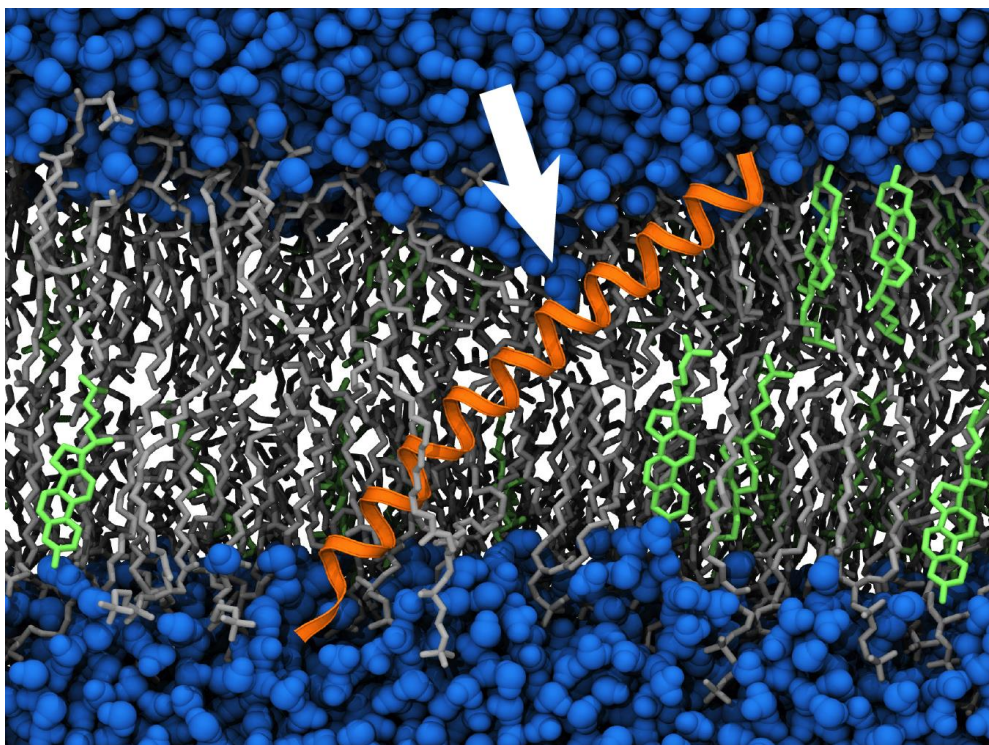


Figure 53 | MD simulations of the minimal sensor domain.

Structure from MD simulations of the WT minimal sensor (Ire1 minimal sensor, orange; POPC and DOPC, grey, cholesterol, green; water molecules, blue). The position of the E540 residue is highlighted (white arrow). The WT minimal sensor was modeled into the lipid composition 7 from *in vitro* experiments. MD simulations were performed and analyzed by Roberto Covino and Gerhard Hummer, Institute for Theoretical Biophysics, MPI for Biophysics.

6.3.1. Ire1 is not the only protein activated by a membrane-based mechanism

The membrane lipid composition can affect the oligomeric state, conformation or activity of membrane proteins as exemplified by soluble N-ethylmaleimide-sensitive-factor attachment receptor (SNARE) proteins (Milovanovic and Jahn, 2015; Milovanovic et al., 2015), mechano-sensitive channels (Lundbaek et al., 2010) and G-protein coupled receptors (Botelho et al., 2006; Periole et al., 2007).

The regulation of membrane protein activity by membrane lipids occurs through mechanisms ranging from specific chemical interactions between proteins and individual lipid molecules, to non-specific interactions between proteins and the bilayer behaving as a collective with physical properties such as thickness, intrinsic monolayer curvature or elastic moduli

(Andersen and Koeppe, 2007; Lee, 2005; Lundbaek, 2008; Marsh, 2008). While specific regulation may be caused by the interaction of proteins with lipid head groups (Hilgemann et al., 2001; Lee, 2003; McLaughlin and Murray, 2005; Suh and Hille, 2008), many membrane proteins are affected by collective lipid bilayer properties arising from the hydrophobic coupling between the protein and the bilayer (Lundbaek et al., 2010). Membrane proteins perturb the surrounding lipids and this perturbation will incur an energetic cost. Especially those membrane proteins that undergo large conformational changes must locally deform the lipid bilayer. The energetic costs of these deformations are determined to a large extent by the lipid composition of the bilayer and can potentially affect the energetics and dynamics of membrane proteins (Nielsen et al., 1998).

There is a general trend that membrane proteins that are targeted to different organelles of the secretory pathway differ in their hydrophobic length (Sharpe et al., 2010). It has been hypothesized that protein sorting is governed by a mechanism based on hydrophobic mismatch (Mouritsen and Bloom, 1984). When the thickness of the membrane does not match TMH length, the hydrophobic mismatch will induce an elastic bilayer deformation, in which the lipid acyl chains in the vicinity of the TMH are extended or compressed and potentially splayed relative to each other (Mouritsen and Bloom, 1984). Elastic bilayer deformations come at an energetic cost that is described as the bilayer deformation energy required for bilayer compression. This deformation energy is dependent on the area and bending angle of compression, which varies with membrane curvature (Lundbaek and Andersen, 1999). These principles are used by cellular systems for example to mediate the sorting of proteins, to allow their packaging into vesicles for lateral protein sorting throughout the secretory pathway (Kaiser et al., 2011a). Protein sorting will be determined by both, the thickness and material properties of the bilayer. As cholesterol alters these physical bilayer properties, it dramatically potentiates the effects of the changes in bilayer thickness alone (Kaiser et al., 2011a; Lundbaek et al., 2003).

How can the formation of a compressed lipid nanodomain lead to protein clustering? Protein clustering can be driven by hydrophobic mismatch. It is energetically more favorable to cluster TMHs of similar length in the same region rather than to accommodate them separately (Kaiser et al., 2011a; Mouritsen and Bloom, 1984; de Planque et al., 1998; Sparr et al., 2005). The oligomeric state of rhodopsin, for instance, has been shown to depend on the acyl-chain length of lipids that were used for reconstitution (Kusumi and Hyde, 1982). Recent studies on SNARE proteins revealed that syntaxin 1 and 4 cluster by a combination of hydrophobic

mismatch, which occurs by cholesterol-induced membrane thickening, and electrostatic interactions with ions and PI(4,5)P₂ (Milovanovic et al., 2015).

Studies on several membrane channels and transporters revealed it is not unusual that conformational changes underlying membrane protein function involve local deformations of the lipid bilayer. The cation-selective gA channel, a gramicidin channel, forms by the trans-bilayer dimerization of two subunits (Fig. 54). This formation of the gA channel is associated with a local bilayer deformation, when the bilayer hydrophobic thickness exceeds the hydrophobic length of the channel, to match the hydrophobic exterior of the channel (Andersen and Koeppe, 2007; Lundbaek, 2008; Lundbaek and Andersen, 1999; Lundbaek et al., 2010). The energetic cost of this deformation varies with the physical properties of the bilayer and has a defined impact on the lifetime of the channel lifetime, its rate of appearance, and its dimerization constant (Andersen and Koeppe, 2007; Lundbaek, 2006).

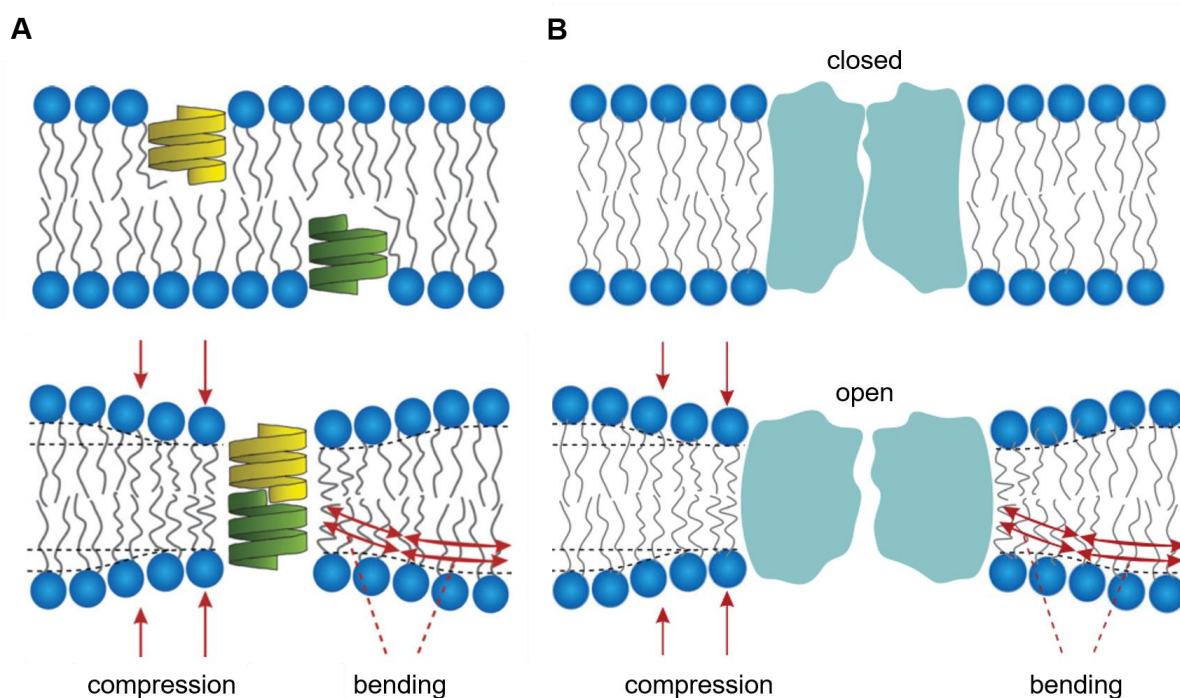


Figure 54 | Channel formation and regulation is associated with local bilayer deformation.

(A) Gramicidin channel formation by trans-bilayer dimerization of two subunits (yellow, green) results in a local bilayer deformation. Modified from Lundbaek *et al.* (Lundbaek et al., 2010) (B) Hydrophobic coupling of an ion channel (bilayer-spanning membrane protein) (light blue) and its surrounding lipid bilayer. A local bilayer deformation is caused by a protein conformational change. Modified from Lundbaek *et al.* (Lundbaek et al., 2010)

These examples illustrate that many proteins are affected by collective properties of the lipid bilayer and highlight the importance of maintaining these physicochemical membrane properties.

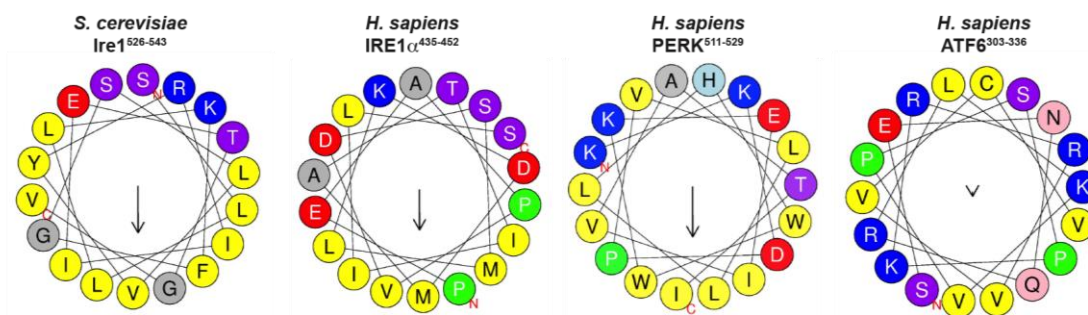
6.4. Conservation of the membrane-based activation mechanism of Ire1 by lipid bilayer stress

The UPR is conserved throughout the eukaryotic kingdom, but the number of UPR stress transducers has increased throughout evolution (Mori, 2009). *S. cerevisiae* employs Ire1 as its sole UPR sensor. In *Drosophila melanogaster* (*D. melanogaster*) and *Caenorhabditis elegans* (*C. elegans*), the genes of all three UPR sensors also found in mammals are expressed (Hollien and Weissman, 2006; Shen et al., 2001). The Ire1 branch is responsible for the induction of most UPR target genes, including ERAD components and ER chaperones (Hollien and Weissman, 2006; Shen et al., 2005). Intriguingly, ERAD components and ER chaperones are fully induced in *atf-6* knockdown worms, indicating that the ATF6 branch is not functional in *D. melanogaster* and *C. elegans* (Shen et al., 2005). Mammals use all three branches: Ire1, PERK and ATF6. Why did the complexity of UPR sensors increase during evolution? What are the specific functions of these three branches?

Extensive genome-wide searches utilizing mini-arrays revealed, that the mammalian XBP1 downstream of Ire1 has similar functions as Hac1 from *S. cerevisiae* (Acosta-Alvear et al., 2007; Shaffer et al., 2004; Sriburi et al., 2007; Travers et al., 2000). This indicates that the general role of IRE1 branch for cellular homeostasis is conserved throughout evolution.

It remains elusive, however, whether the mechanisms of Ire1 activation by aberrant membrane lipid environments is conserved. Is it possible that this function of yeast Ire1 has been passed over to other UPR branches? HeliQuest analyses (Gautier et al., 2008) revealed the existence of a putative juxta-membrane AH in two mammalian UPR sensors: IRE1 α and PERK (Fig. 55).

A HeliQuest analysis of AHs



B Sequence alignment

		AH	
<i>S. cerevisiae</i>	Ire1	--SLLLKFGSLVYRIIETGVFLLLFIFCAIL	555
<i>H. sapiens</i>	IRE1 α	---PEAPVDSMLKDMATIILSTFLLIGWVAFI	461
<i>H. sapiens</i>	PERK	-KKDPVLLLHWKEIVATILFCIIATTFIVRR	542
<i>H. sapiens</i>	ATF6	--SENQRLKVPSPKRRVVCVMIVLAFIILNYG	332
		TMH	

Figure 55 | Bioinformatics analyses suggests the existence of putative AH motifs in mammalian UPR sensors.

(A) HeliQuest analyses (Gautier et al., 2008) of Ire1 from *S. cerevisiae*, as well as mammalian orthologs IRE1 α , PERK and ATF6. The hydrophobic moment of each predicted region is depicted as arrows in the center of respective helical wheel representation. (B) Sequence alignment of UPR sensors shown in (A). Sequence alignment of Ire1's AH and TMH from indicated species. The sequences of the AH are indicated in blue, while the predicted TMH is shown in black.

This finding suggests that the activity of two mammalian UPR sensors, IRE1 α and PERK, may be modulated in response to changing membrane lipid environments to counteract lipid bilayer stress. This would be consistent with recent observations by the David Ron laboratory (Ariyama et al., 2010; Kono et al., 2017; Volmer and Ron, 2015; Volmer et al., 2013). It remains to be experimentally proven, whether IRE1 α and PERK indeed use a similar mechanism as Ire1 from *S. cerevisiae* to sense and respond to lipid bilayer stress. Only a thorough and parallel characterization of all three branches of the UPR in different cell types can reveal unique features and cell-specific adaptation of the UPR network.

It been established, that the UPR can be activated by aberrant membrane lipid environments, and not exclusively by misfolded proteins. Now, it is time to revisit the function of Ire1, PERK and ATF6 in diseases, along with the role of the ER membrane lipid composition in this context. The UPR has been implicated in a variety of pathological conditions, including neurodegenerative diseases, type II diabetes and cancer (Fu et al., 2011; Özcan et al., 2004; Walter and Ron, 2011). The newly established molecular basis of UPR activation by lipid bilayer stress in this study, provides a membrane-based perspective to the role of lipids in neurodegenerative diseases and for the integrity of professional secretory cells in chronic ER-stress (Halbleib et al., 2017).

6.5. Crosstalk of protein folding and lipid bilayer stress

The interdependence of protein and lipid homeostasis has been characterized by genetic means in this thesis (1.4). Ire1 is a perfect illustration of this phenomenon, combining sense and control elements for the homeostasis of protein folding and lipid metabolism. Nevertheless, important questions remain: How does Ire1 integrate the information of two types of stress to yield a single outcome: the ER stress response? What is the relative contribution of protein folding stress and lipid bilayer stress for Ire1 activation? Does one stress modulate Ire1's sensitivity to the other stress? As a first step to investigate these important questions, a mutant variant of Ire1 that is incapable to bind unfolded proteins (Δ III mutant) was used in this study (Kimata et al., 2004, 2007; Promlek et al., 2011).

With the Δ III variant of Ire1, and a Δ III AH double mutant, the different modes of UPR activation can be partially disentangled (Fig. 56). The response of these Ire1 variants to three different ER stress inducing conditions differs strongly and suggests that different ER stressors activate Ire1 in different modes: lipid bilayer stress and the induction of protein misfolding. While the UPR activation by DTT is impaired by the Δ III mutant, there is still a significant residual UPR activity (Figure 35 B). Thus, DTT activates Ire1 by both modes: lipid bilayer stress and by inducing protein misfolding. The same can be observed for Tm-induced ER stress (Figure 35 B). In contrast, if the AH is disrupted by a V535R mutant, there is only a defect in response to DTT but not to Tm. This suggests, that DTT and Tm are different types of stress and it can be speculated that Tm induces a type of ER-stress that is more dominantly based on protein misfolding, while lipid bilayer stress seems to contribute more significantly to the ER-stress induced by DTT. Inositol-depletion seems to be a rather lipid bilayer centered stress. When Ire1 cannot bind unfolded proteins (Δ III) there is no defect in the response to inositol depletion. However, when the membrane-sensitive AH is disrupted by the V535R mutation alone or in combination with the Δ III mutant, a significant functional impairment in the response to inositol-depletion can be observed.

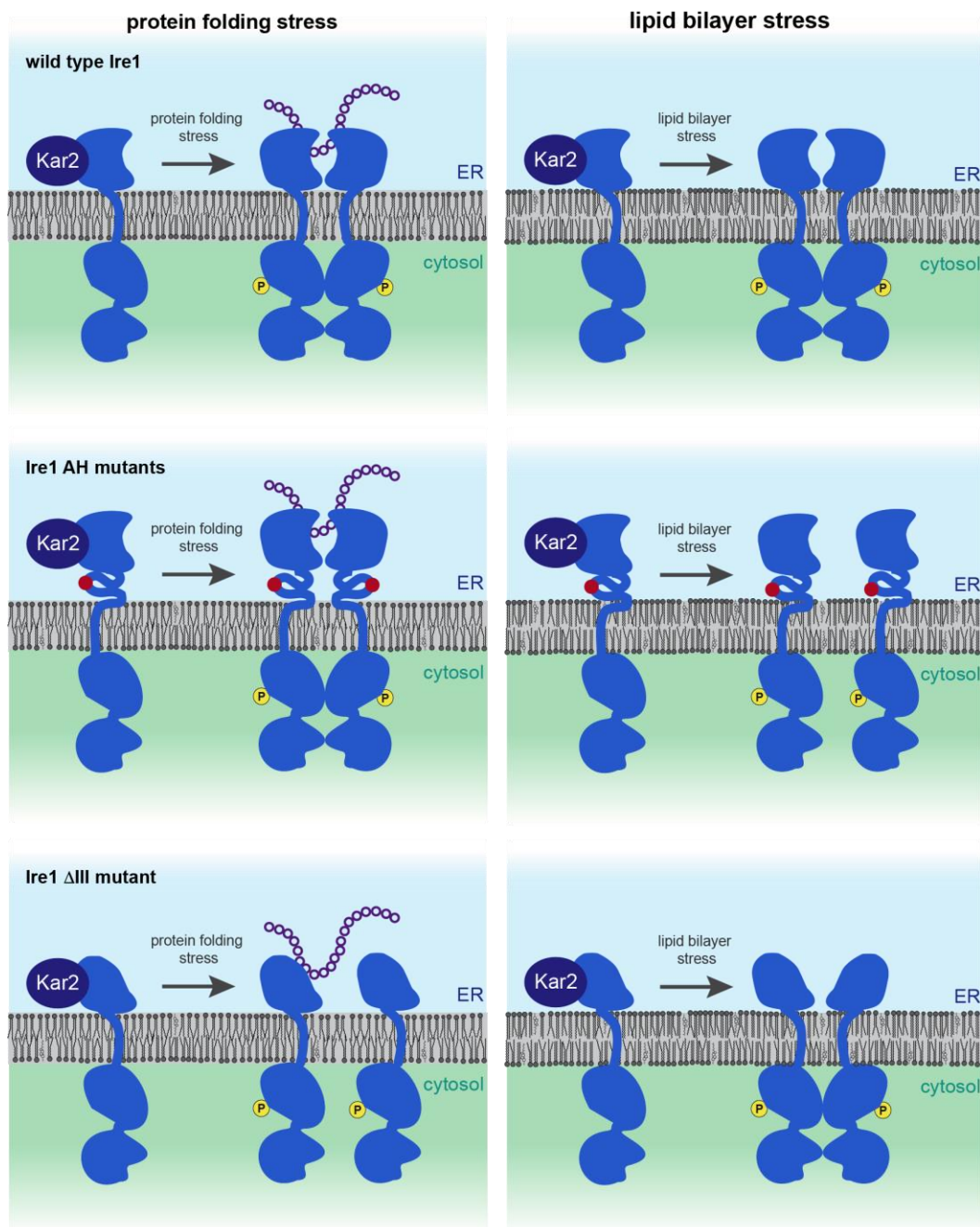


Figure 56 | Functionality of Ire1 and its mutants in the presence of different ER-stress inducers.

Activation of Ire1 and its mutants by protein folding stress (left) and lipid bilayer stress (right). Wild type Ire1 is depicted as introduced in Fig. 8. The AH mutations V535R and F531R are depicted in red, the Δ III variant of Ire1 is shown as a truncated version of the lumenal domain.

It remains to be elucidated what the relative contribution of either type of stress is for Ire1 activation or how one stress modulates Ire1's sensitivity to the other stress. Nevertheless, this study first identifies the existence of an AH as a second sensory module in Ire1, which is required for Ire1 activation by lipid bilayer stress and works cooperatively with other regions of the protein to activate Ire1 in protein folding and lipid bilayer stress conditions.

References

- Acosta-Alvear, D., Zhou, Y., Blais, A., Tsikitis, M., Lents, N.H., Arias, C., Lennon, C.J., Kluger, Y., and Dynlacht, B.D. (2007). XBP1 controls diverse cell type- and condition-specific transcriptional regulatory networks. *Mol. Cell* 27, 53–66.
- Aguilar, P.S., Hernandez-Arriaga, A.M., Cybulski, L.E., Erazo, A.C., and de Mendoza, D. (2001). Molecular basis of thermosensing: a two-component signal transduction thermometer in *Bacillus subtilis*. *EMBO J.* 20, 1681–1691.
- Altabe, S.G., Aguilar, P., Caballero, G.M., and de Mendoza, D. (2003). The *Bacillus subtilis* Acyl Lipid Desaturase Is a $\Delta 5$ Desaturase. *J. Bacteriol.* 185, 3228–3231.
- Alvarez-Vasquez, F., Sims, K.J., Cowart, L.A., Okamoto, Y., Voit, E.O., and Hannun, Y.A. (2005). Simulation and validation of modelled sphingolipid metabolism in *Saccharomyces cerevisiae*. *Nature* 433, 425–430.
- Andersen, O.S., and Koeppe, R.E. (2007). Bilayer thickness and membrane protein function: an energetic perspective. *Annu. Rev. Biophys. Biomol. Struct.* 36, 107–130.
- Anelli, T., and Sitia, R. (2008). Protein quality control in the early secretory pathway. *EMBO J.* 27, 315–327.
- van Anken, E., Pincus, D., Coyle, S., Aragón, T., Osman, C., Lari, F., Gómez Puerta, S., Korennykh, A. V, and Walter, P. (2014). Specificity in endoplasmic reticulum-stress signaling in yeast entails a step-wise engagement of HAC1 mRNA to clusters of the stress sensor Ire1. *Elife* 3, 1–17.
- Antonny, B. (2011). Mechanisms of membrane curvature sensing. *Annu. Rev. Biochem.* 80, 101–123.
- Aragón, T., van Anken, E., Pincus, D., Serafimova, I.M., Korennykh, A. V, Rubio, C.A., and Walter, P. (2009). Messenger RNA targeting to endoplasmic reticulum stress signalling sites. *Nature* 457, 736–740.
- Ariyama, H., Kono, N., Matsuda, S., Inoue, T., and Arai, H. (2010). Decrease in membrane phospholipid unsaturation induces unfolded protein response. *J. Biol. Chem.* 285, 22027–22035.
- Bagnat, M., and Simons, K. (2002). Lipid rafts in protein sorting and cell polarity in budding yeast *Saccharomyces cerevisiae*. *Biol. Chem.* 383, 1475–1480.
- Bagnat, M., Keränen, S., Shevchenko, A., and Simons, K. (2000). Lipid rafts function in biosynthetic delivery of proteins to the cell surface in yeast. *Proc. Natl. Acad. Sci. U.S.A* 97, 3254–3259.
- Bell, R.M., Ballas, L.M., and Coleman, R.A. (1981). Lipid topogenesis. *J. Lipid Res.* 22, 391–403.

- Bertolotti, A., Zhang, Y., Hendershot, L.M., Harding, H.P., and Ron, D. (2000). Dynamic interaction of BiP and ER stress transducers in the unfolded-protein response. *Nat. Cell Biol.* *2*, 326–332.
- Bigay, J., and Antonny, B. (2012). Curvature, lipid packing, and electrostatics of membrane organelles: defining cellular territories in determining specificity. *Dev. Cell* *23*, 886–895.
- Bigay, J., Casella, J.-F., Drin, G., Mesmin, B., and Antonny, B. (2005). ArfGAP1 responds to membrane curvature through the folding of a lipid packing sensor motif. *EMBO J.* *24*, 2244–2253.
- Bjorkman, P.J., Saper, M.A., Samraoui, B., Bennett, W.S., Strominger, J.L., and Wiley, D.C. (1987). Structure of the human class I histocompatibility antigen, HLA-A2. *Nature* *329*, 506–512.
- Bogdanov, M., Heacock, P.N., and Dowhan, W. (2002). A polytopic membrane protein displays a reversible topology dependent on membrane lipid composition. *EMBO J.* *21*, 2107–2116.
- Bordignon, E., and Steinhoff, H.-J. (2007). Membrane protein structure and dynamics studies by site-directed spin labeling ESR. In *ESR Spectroscopy in Membrane Biophysics*, M.A. Hemminga, and L.J. Berliner, eds. (New York: Springer Science and Business Media), pp. 129–164.
- Botelho, A.V., Huber, T., Sakmar, T.P., and Brown, M.F. (2006). Curvature and hydrophobic forces drive oligomerization and modulate activity of rhodopsin in membranes. *Biophys. J.* *91*, 4464–4477.
- Botstein, D., and Fink, G.R. (1985). *Yeast: An experimental organism for modern biology.* *1*.
- Botstein, D., and Fink, G.R. (2011). *Yeast: An experimental organism for 21st century biology.*
- Boumann, H.A., Gubbens, J., Koorengel, M.C., Oh, C., Martin, C.E., Heck, A.J.R., Patton-Vogt, J., Henry, S.A., de Kruijff, B., and de Kroon, A.I.P.M. (2006). Depletion of phosphatidylcholine in yeast induces shortening and increased saturation of the lipid acyl chains: evidence for regulation of intrinsic membrane curvature in a eukaryote. *Mol. Biol. Cell* *17*, 1006–1017.
- Bretscher, M.S., and Munro, S. (1993). Cholesterol and the Golgi apparatus. *Science* *261*, 1280–1281.
- Brooks, A.J., Dai, W., O'Mara, M.L., Abankwa, D., Chhabra, Y., Pelekanos, R. a, Gardon, O., Tunny, K. a, Blucher, K.M., Morton, C.J., et al. (2014). Mechanism of activation of protein kinase JAK2 by the growth hormone receptor. *Science* *344*, 1249783.
- Calfon, M., Zeng, H., Urano, F., Till, J.H., Hubbard, S.R., Harding, H.P., Clark, S.G., and Ron, D. (2002). IRE1 couples endoplasmic reticulum load to secretory capacity by processing the XBP-1 mRNA. *Nature* *415*, 92–96.
- Carman, G.M., and Han, G.-S. (2009). Regulation of phospholipid synthesis in yeast. *J. Lipid Res.* *50*, 69–73.

- Carman, G.M., and Henry, S.A. (1999). Phospholipid biosynthesis in the yeast *Saccharomyces cerevisiae* and interrelationship with other metabolic processes. *Prog. Lipid Res.* *38*, 361–399.
- Chandra, S., Chen, X., Rizo, J., Jahn, R., and Südhof, T.C. (2003). A broken α -helix in folded α -synuclein. *J. Biol. Chem.* *278*, 15313–15318.
- Chang, H.J., Jones, E.W., and Henry, S.A. (2002). Role of the unfolded protein response pathway in regulation of INO1 and in the sec14 bypass mechanism in *Saccharomyces cerevisiae*. *14*, 29–43.
- Chapman, R.E., Walter, P., Eustice, D., Sherman, F., Nakashima, N., Kanaoka, Y., and Ono, Y. (1997). Translational attenuation mediated by an mRNA intron. *Curr. Biol.* *7*, 850–859.
- Chawla, A., Chakrabarti, S., Ghosh, G., and Niwa, M. (2011). Attenuation of yeast UPR is essential for survival and is mediated by IRE1 kinase. *J. Cell Biol.* *193*, 41–50.
- Chou, K.-C. (2011). Wenxiang: a web-server for drawing wenxiang diagrams. *Nat. Sci.* *3*, 862–865.
- Cohen, N., Breker, M., Bakunts, A., Pesek, K., Chas, A., Argemí, J., Orsi, A., Gal, L., Chuartzman, S., Wigelman, Y., et al. (2017). Iron affects Ire1 clustering propensity and the amplitude of endoplasmic reticulum stress signaling. *J. Cell Sci.* *130*, 3222–3233.
- Contreras, F.-X., Ernst, A.M., Haberkant, P., Björkholm, P., Lindahl, E., Gönen, B., Tischer, C., Elofsson, A., von Heijne, G., Thiele, C., et al. (2012). Molecular recognition of a single sphingolipid species by a protein's transmembrane domain. *Nature* *481*, 525–529.
- Coskun, U., and Simons, K. (2011). Cell membranes: the lipid perspective. *Structure* *19*, 1543–1548.
- Coskun, Ü., Grzybek, M., Drechsel, D., and Simons, K. (2011). Regulation of human EGF receptor by lipids. *Proc. Natl. Acad. Sci. U. S. A.* *108*, 9044–9048.
- Covino, R., Ballweg, S., Stordeur, C., Michaelis, J.B., Puth, K., Wernig, F., Bahrami, A., Ernst, A.M., Hummer, G., and Ernst, R. (2016). A eukaryotic sensor for membrane lipid saturation. *Mol. Cell* *63*, 49–59.
- Cox, J.S., and Walter, P. (1996). A novel mechanism for regulating activity of a transcription factor that controls the unfolded protein response. *Cell* *87*, 391–404.
- Cox, J.S., Shamu, C.E., and Walter, P. (1993). Transcriptional induction of genes encoding endoplasmic reticulum resident proteins requires a transmembrane protein kinase. *Cell* *73*, 1197–1206.
- Cox, J.S., Chapman, R.E., and Walter, P. (1997). The unfolded protein response coordinates the production of endoplasmic reticulum protein and endoplasmic reticulum membrane. *Mol. Biol. Cell* *8*, 1805–1814.
- Credle, J.J., Finer-Moore, J.S., Papa, F.R., Stroud, R.M., and Walter, P. (2005). On the mechanism of sensing unfolded protein in the endoplasmic reticulum. *Proc. Natl. Acad. Sci. U. S. A.* *102*, 18773–18784.

- Cui, W., Li, J., Ron, D., and Sha, B. (2011). The structure of the PERK kinase domain suggests the mechanism for its activation. *Acta Crystallogr.* *67*, 423–428.
- Cybulski, L.E., del Solar, G., Craig, P.O., Espinosa, M., and de Mendoza, D. (2004). *Bacillus subtilis* DesR functions as a phosphorylation-activated switch to control membrane lipid fluidity. *J. Biol. Chem.* *279*, 39340–39347.
- Cybulski, L.E., Martín, M., Mansilla, M.C., Fernández, A., and de Mendoza, D. (2010). Membrane thickness cue for cold sensing in a bacterium. *Curr. Biol.* *20*, 1539–1544.
- Danne, L., Aktas, M., Gleichenhagen, J., Grund, N., Wagner, D., Schwalbe, H., Hoffknecht, B., Metzler-Nolte, N., and Narberhaus, F. (2015). Membrane-binding mechanism of a bacterial phospholipid N-methyltransferase. *Mol. Microbiol.* *95*, 313–331.
- Daum, G., Lees, N.D., Bard, M., and Dickson, R. (1998). Biochemistry, cell biology and molecular biology of lipids of *Saccharomyces cerevisiae*. *Yeast* *14*, 1471–1510.
- Degreif, D., de Rond, T., Bertl, A., Keasling, J.D., and Budin, I. (2017). Lipid engineering reveals regulatory roles for membrane fluidity in yeast flocculation and oxygen-limited growth. *Metab. Eng.* *41*, 46–56.
- Deguil, J., Pineau, L., Rowland Snyder, E.C., Dupont, S., Beney, L., Gil, A., Frapper, G., and Ferreira, T. (2011). Modulation of lipid-induced ER stress by fatty acid shape. *Traffic* *12*, 349–362.
- Devaux, P.F. (1991). Static and dynamic lipid asymmetry in cell membranes. *Biochemistry* *30*, 1163–1173.
- Dickson, R.C. (1998). Sphingolipid functions in *Saccharomyces cerevisiae*: Comparison to mammals. *Annu. Rev. Biochem.* *67*, 27–48.
- Dowhan, W., and Bogdanov, M. (2009). Lipid-dependent membrane protein topogenesis. *Annu. Rev. Biochem.* *78*, 515–540.
- Drbal, K., Moertelmaier, M., Holzhauser, C., Muhammad, A., Fuertbauer, E., Howorka, S., Hinterberger, M., Stockinger, H., and Schütz, G.J. (2007). Single-molecule microscopy reveals heterogeneous dynamics of lipid raft components upon TCR engagement. *Int. Immunol.* *19*, 675–684.
- Drin, G., and Antony, B. (2010). Amphipathic helices and membrane curvature. *FEBS Lett.* *584*, 1840–1847.
- Drin, G., Casella, J.-F., Gautier, R., Boehmer, T., Schwartz, T.U., and Antony, B. (2007). A general amphipathic alpha-helical motif for sensing membrane curvature. *Nat. Struct. Mol. Biol.* *14*, 138–146.
- Ejsing, C.S., Sampaio, J.L., Surendranath, V., Duchoslav, E., Ekroos, K., Klemm, R.W., Simons, K., and Shevchenko, A. (2009). Global analysis of the yeast lipidome by quantitative shotgun mass spectrometry. *Proc. Natl. Acad. Sci. U. S. A.* *106*, 2136–2141.
- Elbaz, Y., and Schuldiner, M. (2011). Staying in touch: the molecular era of organelle contact sites. *Trends Biochem. Sci.* *36*, 616–623.

- Ellgaard, L., and Helenius, A. (2003). Quality control in the endoplasmic reticulum. *Nat. Rev. Mol. Cell Biol.* *4*, 181–191.
- Ernst, R., Ejsing, C.S., and Antonny, B. (2016). Homeoviscous adaptation and the regulation of membrane lipids. *J. Mol. Biol.* *428*, 4776–4791.
- Fairn, G.D., Schieber, N.L., Ariotti, N., Murphy, S., Kuerschner, L., Webb, R.I., Grinstein, S., and Parton, R.G. (2011). High-resolution mapping reveals topologically distinct cellular pools of phosphatidylserine. *J. Cell Biol.* *194*, 257–275.
- Fonseca, S.G., Gromada, J., and Urano, F. (2011). Endoplasmic reticulum stress and pancreatic β -cell death. *Trends Endocrinol. Metab.* *22*, 266–274.
- Fu, S., Yang, L., Li, P., Hofmann, O., Dicker, L., Hide, W., Lin, X., Watkins, S.M., Ivanov, A.R., and Hotamisligil, G.S. (2011). Aberrant lipid metabolism disrupts calcium homeostasis causing liver endoplasmic reticulum stress in obesity. *Nature* *473*, 528–531.
- Funakoshi, M., and Hochstrasser, M. (2009). Small epitope-linker modules for PCR-based C-terminal tagging in *Saccharomyces cerevisiae*. *Yeast* *26*, 185–192.
- Gardner, B.M., and Walter, P. (2011). Unfolded proteins are Ire1-activating ligands that directly induce the unfolded protein response. *Science* *333*, 1891–1894.
- Gasteiger, E., Hoogland, C., Gattiker, A., Duvaud, S., Wilkins, M.R., Appel, R.D., and Bairoch, A. (2005). Protein Analysis Tools on the ExPASy Server. In *The Proteomics Protocols Handbook*, pp. 571–608.
- Gautier, R., Douguet, D., Antonny, B., and Drin, G. (2008). HELIQUEST: a web server to screen sequences with specific alpha-helical properties. *Bioinformatics* *24*, 2101–2102.
- Ghaemmaghami, S., Huh, W.-K., Bower, K., Howson, R.W., Belle, A., Dephoure, N., O'Shea, E.K., and Weissman, J.S. (2003). Global analysis of protein expression in yeast. *Nature* *425*, 737–741.
- Goldstein, J.L., DeBose-Boyd, R. a, and Brown, M.S. (2006). Protein sensors for membrane sterols. *Cell* *124*, 35–46.
- Goyal, U., and Blackstone, C. (2013). Untangling the web: Mechanisms underlying ER network formation. *Biochim. Biophys. Acta - Mol. Cell Res.* *1833*, 2492–2498.
- Graham, T.R. (2004). Flippases and vesicle-mediated protein transport. *Trends Cell Biol.* *14*, 670–677.
- Gueldener, U., Heinisch, J., Koehler, G.J., Voss, D., and Hegemann, J.H. (2002). A second set of loxP marker cassettes for Cre-mediated multiple gene knockouts in budding yeast. *Nucleic Acids Res.* *30*, e23.
- Halbleib, K., Pesek, K., Covino, R., Hofbauer, H.F., Wunnicke, D., Hänel, I., Hummer, G., and Ernst, R. (2017). Activation of the unfolded protein response by lipid bilayer stress. *Mol. Cell* *67*, 673–684.

- Hammond, G.R. V., Fischer, M.J., Anderson, K.E., Holdich, J., Koteci, A., Balla, T., and Irvine, R.F. (2012). PI4P and PI(4,5)P2 are essential but independent lipid determinants of membrane identity. *Science* 337, 727–730.
- Han, G.-S., Wu, W.-I., and Carman, G.M. (2006). The *Saccharomyces cerevisiae* Lipin homolog is a Mg²⁺-dependent phosphatidate phosphatase enzyme. *J. Biol. Chem.* 281, 9210–9218.
- Han, S., Lone, M.A., Schneiter, R., and Chang, A. (2010). Orm1 and Orm2 are conserved endoplasmic reticulum membrane proteins regulating lipid homeostasis and protein quality control. *Proc. Natl. Acad. Sci. U. S. A.* 107, 5851–5856.
- Hancock, J.F. (2006). Lipid rafts: contentious only from simplistic standpoints. *Nat. Rev. Mol. Cell Biol.* 7, 456–462.
- Harding, H.P., Zhang, Y., and Ron, D. (1999). Protein translation and folding are coupled by an endoplasmic-reticulum-resident kinase. *Nature* 397, 271–274.
- Haze, K., Yoshida, H., Yanagi, H., Yura, T., and Mori, K. (1999). Mammalian transcription factor ATF6 is synthesized as a transmembrane protein and activated by proteolysis in response to endoplasmic reticulum stress. *Mol. Biol. Cell* 10, 3787–3799.
- Haze, K., Okada, T., Yoshida, H., Yanagi, H., Yura, T., Negishi, M., and Mori, K. (2001). Identification of the G13 (cAMP-response-element-binding protein-related protein) gene product related to activating transcription factor 6 as a transcriptional activator of the mammalian unfolded protein response. *Biochem. J.* 355, 19–28.
- Hebert, D.N., and Molinari, M. (2007). In and out of the ER: protein folding, quality control, degradation, and related human diseases. *Physiol. Rev.* 87, 1377–1408.
- Hegde, R.S., and Ploegh, H.L. (2010). Quality and quantity control at the endoplasmic reticulum. *Curr. Opin. Cell Biol.* 22, 437–446.
- Henry, S.A., Kohlwein, S.D., and Carman, G.M. (2012). Metabolism and regulation of glycerolipids in the yeast *Saccharomyces cerevisiae*. *Genetics* 190, 317–349.
- Henry, S.A., Gaspar, M.L., and Jesch, S.A. (2014). The response to inositol: regulation of glycerolipid metabolism and stress response signaling in yeast. *Chem. Phys. Lipids* 180, 23–43.
- Hilgemann, D.W., Feng, S., and Nasuhoglu, C. (2001). The complex and intriguing lives of PIP2 with ion channels and transporters. *Sci. STKE* 2001, re19.
- Hillisch, A., Lorenz, M., and Diekmann, S. (2001). Recent advances in FRET: distance determination in protein-DNA complexes. *Curr. Opin. Struct. Biol.* 11, 201–207.
- Hofbauer, H.F., Schopf, F.H., Schleifer, H., Knittelfelder, O.L., Pieber, B., Rechberger, G.N., Wolinski, H., Gaspar, M.L., Kappe, C.O., Stadlmann, J., et al. (2014). Regulation of gene expression through a transcriptional repressor that senses acyl-chain length in membrane phospholipids. *Dev. Cell* 29, 729–739.

- Hollien, J., and Weissman, J.S. (2006). Decay of endoplasmic reticulum-localized mRNAs during the unfolded protein response. *Science* *313*, 104–107.
- Holthuis, J.C.M., and Levine, T.P. (2005). Lipid traffic: floppy drives and a superhighway. *Nat. Rev. Mol. Cell Biol.* *6*, 209–220.
- Holthuis, J.C.M., and Menon, A.K. (2014). Lipid landscapes and pipelines in membrane homeostasis. *Nature* *510*, 48–57.
- Hoppe, T., Matuschewski, K., Rape, M., Schlenker, S., Ulrich, H.D., and Jentsch, S. (2000). Activation of a membrane-bound transcription factor by regulated ubiquitin/proteasome-dependent processing. *Cell* *102*, 577–586.
- Inda, M.E., Vandenbranden, M., Fernández, A., de Mendoza, D., Ruyschaert, J.-M., and Cybulski, L.E. (2014). A lipid-mediated conformational switch modulates the thermosensing activity of DesK. *Proc. Natl. Acad. Sci. U. S. A.* *111*, 3579–3584.
- Inoue, H., Nojima, H., and Okayama, H. (1990). High efficiency transformation of *Escherichia coli* with plasmids. *Gene* *96*, 23–28.
- Ito, H., Fukuda, Y., and Murata, K. (1983). Transformation of intact yeast cells treated with alkali Transformation of Intact Yeast Cells Treated with Alkali Cations. *J. Bacteriol.* *153*, 166–168.
- Jesch, S.A., Liu, P., Zhao, X., Wells, M.T., and Henry, S.A. (2006). Multiple endoplasmic reticulum-to-nucleus signaling pathways coordinate phospholipid metabolism with gene expression by distinct mechanisms. *J. Biol. Chem.* *281*, 24070–24083.
- Jesch, S.A., Gaspar, M.L., Stefan, C.J., Aregullin, M.A., and Henry, S.A. (2010). Interruption of inositol sphingolipid synthesis triggers Stt4p-dependent protein kinase C signaling. *J. Biol. Chem.* *285*, 41947–41960.
- Jonikas, M.C., Collins, S.R., Denic, V., Oh, E., Quan, E.M., Schmid, V., Weibezahn, J., Schwappach, B., Walter, P., Weissman, J.S., et al. (2009). Comprehensive characterization of genes required for protein folding in the endoplasmic reticulum. *Science* *323*, 1693–1697.
- Jumpertz, T., Tschapek, B., Infed, N., Smits, S.H.J., Ernst, R., and Schmitt, L. (2011). High-throughput evaluation of the critical micelle concentration of detergents. *Anal. Biochem.* *408*, 64–70.
- Kaiser, H.-J., Lingwood, D., Levental, I., Sampaio, J.L., Kalvodova, L., Rajendran, L., and Simons, K. (2009). Order of lipid phases in model and plasma membranes. *Proc. Natl. Acad. Sci. U. S. A.* *106*, 16645–16650.
- Kaiser, H.-J., Or, A., Róg, T., Nyholm, T.K.M., Chai, W., and Feizi, T. (2011a). Lateral sorting in model membranes by cholesterol-mediated hydrophobic matching. *Proc. Natl. Acad. Sci. U. S. A.* *108*, 16628–16633.
- Kaiser, H.-J., Surma, M. a, Mayer, F., Levental, I., Grzybek, M., Klemm, R.W., Da Cruz, S., Meisinger, C., Müller, V., Simons, K., et al. (2011b). Molecular convergence of bacterial and eukaryotic surface order. *J. Biol. Chem.* *286*, 40631–40637.

- Kawahara, T., Yanagi, H., Yura, T., and Mori, K. (1997). Endoplasmic reticulum stress-induced mRNA splicing permits synthesis of transcription factor Hac1p/Ern4p that activates the unfolded protein response. *Mol. Biol. Cell* 8, 1845–1862.
- Kim, H.M., Choo, H.-J., Jung, S.-Y., Ko, Y.-G., Park, W.-H., Jeon, S.-J., Kim, C.H., Joo, T., and Cho, B.R. (2007). A two-photon fluorescent probe for lipid raft imaging: C-Laurdan. *ChemBioChem* 8, 553–559.
- Kimata, Y., and Kohno, K. (2011). Endoplasmic reticulum stress-sensing mechanisms in yeast and mammalian cells. *Curr. Opin. Cell Biol.* 23, 135–142.
- Kimata, Y., Kimata, Y.I., Shimizu, Y., Abe, H., Farcasanu, I.C., Takeuchi, M., Rose, M.D., and Kohno, K. (2003). Genetic evidence for a role of BiP / Kar2 that regulates Ire1 in response to accumulation of unfolded proteins. *14*, 2559–2569.
- Kimata, Y., Oikawa, D., Shimizu, Y., Ishiwata-Kimata, Y., and Kohno, K. (2004). A role for BiP as an adjustor for the endoplasmic reticulum stress-sensing protein Ire1. *J. Cell Biol.* 167, 445–456.
- Kimata, Y., Ishiwata-Kimata, Y., Ito, T., Hirata, A., Suzuki, T., Oikawa, D., Takeuchi, M., and Kohno, K. (2007). Two regulatory steps of ER-stress sensor Ire1 involving its cluster formation and interaction with unfolded proteins. *J. Cell Biol.* 179, 75–86.
- Klemm, R.W., Ejsing, C.S., Surma, M.A., Kaiser, H.-J., Gerl, M.J., Sampaio, J.L., de Robillard, Q., Ferguson, C., Proszynski, T.J., Shevchenko, A., et al. (2009). Segregation of sphingolipids and sterols during formation of secretory vesicles at the trans-Golgi network. *J. Cell Biol.* 185, 601–612.
- Klose, C., Surma, M.A., and Simons, K. (2013). Organellar lipidomics—background and perspectives. *Curr. Opin. Cell Biol.* 25, 406–413.
- Kodaki, T., and Yamashita, S. (1987). Yeast phosphatidylethanolamine methylation pathway. Cloning and characterization of two distinct methyltransferase genes. *J. Biol. Chem.* 262, 15428–15435.
- Kodaki, T., and Yamashita, S. (1989). Characterization of the methyltransferases in the yeast phosphatidylethanolamine methylation pathway by selective gene disruption. *Eur. J. Biochem.* 185, 243–251.
- Kohno, K. (2010). Stress-sensing mechanisms in the unfolded protein response: similarities and differences between yeast and mammals. *J. Biochem.* 147, 27–33.
- Koning, A.J., Lum, P.Y., Williams, J.M., and Wright, R. (1993). DiOC6 staining reveals organelle structure and dynamics in living yeast cells. *Cell Motil. Cytoskeleton* 25, 111–128.
- Kono, N., Amin-Wetzel, N., and Ron, D. (2017). Generic membrane-spanning features endow IRE1 α with responsiveness to membrane aberrancy. *Mol. Biol. Cell* 28, 2318–2332.
- Korennykh, A., and Walter, P. (2012). Structural basis of the unfolded protein response. *Annu. Rev. Cell Dev. Biol.* 28, 251–277.

- Korennykh, A. V., Egea, P.F., Korostelev, A.A., Finer-Moore, J., Zhang, C., Shokat, K.M., Stroud, R.M., and Walter, P. (2009). The unfolded protein response signals through high-order assembly of Ire1. *Nature* *457*, 687–693.
- Koumenis, C. (2006). ER stress, hypoxia tolerance and tumor progression. *Curr. Mol. Med.* *6*, 55–69.
- Krahmer, N., Guo, Y., Wilfling, F., Hilger, M., Lingrell, S., Heger, K., Newman, H.W., Schmidt-Supprian, M., Vance, D.E., Mann, M., et al. (2011). Phosphatidylcholine synthesis for lipid droplet expansion is mediated by localized activation of CTP:Phosphocholine cytidylyltransferase. *Cell Metab.* *14*, 504–515.
- Krogh, A., Larsson, B., von Heijne, G., and Sonnhammer, E.L.. (2001). Predicting transmembrane protein topology with a hidden markov model: application to complete genomes. *J. Mol. Biol.* *305*, 567–580.
- Kulak, N.A., Pichler, G., Paron, I., Nagaraj, N., and Mann, M. (2014). Minimal, encapsulated proteomic-sample processing applied to copy-number estimation in eukaryotic cells. *Nat. Methods* *11*, 319–324.
- Kusumi, A., and Hyde, J.S. (1982). Spin-label saturation-transfer electron spin resonance detection of transient association of rhodopsin in reconstituted membranes. *Biochemistry* *21*, 5978–5983.
- Lajoie, P., Moir, R.D., Willis, I.M., and Snapp, E.L. (2012). Kar2p availability defines distinct forms of endoplasmic reticulum stress in living cells. *Mol. Biol. Cell* *23*, 955–964.
- Lamantia, M., Miurat, T., Tachikawat, H., Kaplan, H.A., Lennarz, W.J., and Mizunagat, T. (1991). Glycosylation site binding protein and protein disulfide isomerase are identical and essential for cell viability in yeast (protein folding/*Saccharomyces cerevisiae*/photoaffinity labeling). *Biochemistry* *88*, 4453–4457.
- Lee, A.. (2003). Lipid–protein interactions in biological membranes: a structural perspective. *Biochim. Biophys. Acta - Biomembr.* *1612*, 1–40.
- Lee, A.G. (2005). How lipids and proteins interact in a membrane: a molecular approach. *Mol. Biosyst.* *1*, 203–212.
- Lee, K.P.K., Dey, M., Neculai, D., Cao, C., Dever, T.E., and Sicheri, F. (2008). Structure of the dual enzyme Ire1 reveals the basis for catalysis and regulation in nonconventional RNA splicing. *Cell* *132*, 89–100.
- Levental, I., Lingwood, D., Grzybek, M., Coskun, U., and Simons, K. (2010). Palmitoylation regulates raft affinity for the majority of integral raft proteins. *Proc. Natl. Acad. Sci. U. S. A.* *107*, 22050–22054.
- Lin, J.H., Walter, P., and Yen, T.S.B. (2008). Endoplasmic reticulum stress in disease pathogenesis. *Annu. Rev. Pathol.* *3*, 399–425.
- Lin, J.H., Li, H., Zhang, Y., Ron, D., and Walter, P. (2009). Divergent effects of PERK and IRE1 signaling on cell viability. *Cell* *4*, 1–6.

- Lingwood, D., and Simons, K. (2010). Lipid rafts as a membrane-organizing principle. *Science* 327, 46–50.
- Longtine, M.S., Iii, A.M.K., Demarini, D.J., and Shah, N.G. (1998). Additional modules for versatile and economical PCR-based gene deletion and modification in *Saccharomyces cerevisiae*. 961, 953–961.
- Lundbaek, J.A. (2006). Regulation of membrane protein function by lipid bilayer elasticity—a single molecule technology to measure the bilayer properties experienced by an embedded protein. *J. Phys. Condens. Matter* 18, S1305–44.
- Lundbaek, J.A. (2008). Lipid bilayer-mediated regulation of ion channel function by amphiphilic drugs. *J. Gen. Physiol.* 131, 421–429.
- Lundbaek, J.A., and Andersen, O.S. (1999). Spring constants for channel-induced lipid bilayer deformations estimates using gramicidin channels. *Biophys. J.* 76, 889–895.
- Lundbaek, J.A., Andersen, O.S., Werge, T., and Nielsen, C. (2003). Cholesterol-induced protein sorting: An analysis of energetic feasibility. *Biophys. J.* 84, 2080–2089.
- Lundbaek, J.A., Collingwood, S.A., Ingólfsson, H.I., Kapoor, R., and Andersen, O.S. (2010). Lipid bilayer regulation of membrane protein function: gramicidin channels as molecular force probes. *J. R. Soc. Interface* 7, 373–395.
- Lykidis, A. (2007). Comparative genomics and evolution of eukaryotic phospholipid biosynthesis. *Prog. Lipid Res.* 46, 171–199.
- Marsh, D. (2008). Protein modulation of lipids, and vice-versa, in membranes. *Biochim. Biophys. Acta* 1778, 1545–1575.
- Martin, C.E., Oh, C.-S., and Jiang, Y. (2007). Regulation of long chain unsaturated fatty acid synthesis in yeast. *Biochim. Biophys. Acta* 1771, 271–285.
- Mayor, S., and Pagano, R.E. (2007). Pathways of clathrin-independent endocytosis. *Nat. Rev. Mol. Cell Biol.* 8, 603–612.
- McGraw, P., and Henry, S.A. (1989). Mutations in the *Saccharomyces cerevisiae* *opi3* gene: effects on phospholipid methylation, growth and cross-pathway regulation of inositol synthesis. *Genetics* 122.
- McLaughlin, S., and Murray, D. (2005). Plasma membrane phosphoinositide organization by protein electrostatics. *Nature* 438, 605–611.
- van Meer, G., and Vaz, W.L.C. (2005). Membrane curvature sorts lipids. Stabilized lipid rafts in membrane transport. *EMBO Rep.* 6, 418–419.
- van Meer, G., Voelker, D.R., and Feigenson, G.W. (2008). Membrane lipids: where they are and how they behave. *Nat. Rev. Mol. Cell Biol.* 9, 112–124.
- Merksamer, P.I., Trusina, A., and Papa, F.R. (2008). Real-time redox measurements during endoplasmic reticulum stress reveal interlinked protein folding functions. *Cell* 135, 933–947.

- Mesmin, B., and Maxfield, F.R. (2009). Intracellular sterol dynamics. *Biochim. Biophys. Acta - Mol. Cell Biol. Lipids* 1791, 636–645.
- Milovanovic, D., and Jahn, R. (2015). Organization and dynamics of SNARE proteins in the presynaptic membrane. *Front. Physiol.* 6, 89.
- Milovanovic, D., Honigmann, A., Koike, S., Göttfert, F., Pähler, G., Junius, M., Müller, S., Diederichsen, U., Janshoff, A., Grubmüller, H., et al. (2015). Hydrophobic mismatch sorts SNARE proteins into distinct membrane domains. *Nat. Commun.* 6, 5984.
- Mitra, K., Ubarretxena-Belandia, I., Taguchi, T., Warren, G., and Engelman, D.M. (2004). Modulation of the bilayer thickness of exocytic pathway membranes by membrane proteins rather than cholesterol. *Proc. Natl. Acad. Sci. U. S. A.* 101, 4083–4088.
- Mori, K. (2009). Signalling pathways in the unfolded protein response: development from yeast to mammals. *J. Biochem.* 146, 743–750.
- Mori, K., Ma, W., Gething, M.J., and Sambrook, J. (1993). A transmembrane protein with a cdc2+/CDC28-related kinase activity is required for signaling from the ER to the nucleus. *Cell* 74, 743–756.
- Mori, K., Kawahara, T., Yoshida, H., Yanagi, H., and Yura, T. (1996). Signalling from endoplasmic reticulum to nucleus: transcription factor with a basic-leucine zipper motif is required for the unfolded protein-response pathway. *Genes to Cells* 1, 803–817.
- Mouritsen, O.G., and Bloom, M. (1984). Mattress model of lipid-protein interactions in membranes. *Biophys. J.* 46, 141–153.
- Nakamura, M.T., and Nara, T.Y. (2003). Essential fatty acid synthesis and its regulation in mammals. *Prostaglandins. Leukot. Essent. Fatty Acids* 68, 145–150.
- Nakamura, M.T., and Nara, T.Y. (2004). Structure, function, and dietary regulation of $\Delta 6$, $\Delta 5$, and $\Delta 9$ desaturases. *Annu. Rev. Nutr.* 24, 345–376.
- Nielsen, C., Goulian, M., and Andersen, O.S. (1998). Energetics of inclusion-induced bilayer deformations. *Biophys. J.* 74, 1966–1983.
- Nikawa, J.-I., and Yamashita, S. (1992). IRE1 encodes a putative protein kinase containing a membrane-spanning domain and is required for inositol phototrophy in *Saccharomyces cerevisiae*. *Mol. Microbiol.* 6, 1441–1446.
- Nixon-Abell, J., Obara, C.J., Weigel, A. V, Li, D., Legant, W.R., Xu, C.S., Pasolli, H.A., Harvey, K., Hess, H.F., Betzig, E., et al. (2016). Increased spatiotemporal resolution reveals highly dynamic dense tubular matrices in the peripheral ER. *Science* 354, aaf3928.
- Oikawa, D., Kimata, Y., and Kohno, K. (2007). Self-association and BiP dissociation are not sufficient for activation of the ER stress sensor Ire1. *J. Cell Sci.* 120, 1681–1688.
- Okada, T., Haze, K., Nadanaka, S., Yoshida, H., Seidah, N.G., Hirano, Y., Sato, R., Negishi, M., and Mori, K. (2003). A serine protease inhibitor prevents endoplasmic reticulum stress-induced cleavage but not transport of the membrane-bound transcription factor ATF6. *J. Biol. Chem.* 278, 31024–31032.

- Özcan, U., Cao, Q., Yilmaz, E., Lee, A.-H., Iwakoshi, N.N., Ozdelen, E., Tuncman, G., Görgün, C., Glimcher, L.H., and Hotamisligil, G.S. (2004). Endoplasmic reticulum stress links obesity, insulin action, and type 2 diabetes. *Science* *306*, 457–461.
- Parasassi, T., De Stasio, G., d'Ubaldo, A., and Gratton, E. (1990). Phase fluctuation in phospholipid membranes revealed by Laurdan fluorescence. *Biophys. J.* *57*, 1179–1186.
- Park, E., and Rapoport, T.A. (2012). Mechanisms of Sec61/SecY-mediated protein translocation across membranes. *Annu. Rev. Biophys.* *41*, 21–40.
- Park, S.H., and Blackstone, C. (2010). Further assembly required: construction and dynamics of the endoplasmic reticulum network. *EMBO Rep.* *11*, 515–521.
- Periole, X., Huber, T., Marrink, S.-J., and Sakmar, T.P. (2007). G Protein-coupled receptors self-assemble in dynamics simulations of model bilayers. *J. Am. Chem. Soc.* *129*, 10126–10132.
- Pietzsch, J. (2004). Mind the membrane. *Horizon Symposia: A Living Frontier*. 1–4.
- Pincus, D., Chevalier, M.W., El-samad, H., and Walter, P. (2010). BiP binding to the ER-stress sensor Ire1 tunes the homeostatic behavior of the unfolded protein response. *PLoS Biol.* *8*, e1000415.
- Pineau, L., Colas, J., Dupont, S., Beney, L., Fleurat-Lessard, P., Berjeaud, J.-M., Bergès, T., and Ferreira, T. (2009). Lipid-induced ER stress: synergistic effects of sterols and saturated fatty acids. *Traffic* *10*, 673–690.
- de Planque, M.R.R., Greathouse, D. V., Koeppe, R.E., Schäfer, H., Marsh, D., and Killian, J.A. (1998). Influence of lipid/peptide hydrophobic mismatch on the thickness of diacylphosphatidylcholine bilayers. A ^2H NMR and ESR study using designed transmembrane α -helical peptides and gramicidin A. *Biochemistry* *37*, 9333–9345.
- Plumb, R., Zhang, Z.-R., Appathurai, S., and Mariappan, M. (2015). A functional link between the co-translational protein translocation pathway and the UPR. *Elife* *4*, 53–66.
- Pollard, M.G., Travers, K.J., and Weissman, J.S. (1998). Ero1p: a novel and ubiquitous protein with an essential role in oxidative protein folding in the endoplasmic reticulum. *Mol. Cell* *1*, 171–182.
- Pranke, I.M., Morello, V., Bigay, J., Gibson, K., Verbavatz, J.-M., Antony, B., and Jackson, C.L. (2011). α -Synuclein and ALPS motifs are membrane curvature sensors whose contrasting chemistry mediates selective vesicle binding. *J. Cell Biol.* *194*, 89–103.
- Printsev, I., Curiel, D., and Carraway, K.L. (2016). Membrane protein quantity control at the endoplasmic reticulum. *J. Membr. Biol.* 1–14.
- Prinz, W.A., Grzyb, L., Veenhuis, M., Kahana, J.A., Silver, P.A., and Rapoport, T.A. (2000). Mutants affecting the structure of the cortical endoplasmic reticulum in *Saccharomyces cerevisiae*. *J. Cell Biol.* *150*, 461–474.

- Promlek, T., Ishiwata-Kimata, Y., Shido, M., Sakuramoto, M., Kohno, K., and Kimata, Y. (2011). Membrane aberrancy and unfolded proteins activate the endoplasmic reticulum stress sensor Ire1 in different ways. *Mol. Biol. Cell* 22, 3520–3532.
- Puhka, M., Vihinen, H., Joensuu, M., and Jokitalo, E. (2007). Endoplasmic reticulum remains continuous and undergoes sheet-to-tubule transformation during cell division in mammalian cells. *J. Cell Biol.* 179, 895–909.
- Puhka, M., Joensuu, M., Vihinen, H., Belevich, I., and Jokitalo, E. (2012). Progressive sheet-to-tubule transformation is a general mechanism for endoplasmic reticulum partitioning in dividing mammalian cells. *Mol. Biol. Cell* 23, 2424–2432.
- Puth, K., Hofbauer, H.F., Sáenz, J.P., and Ernst, R. (2015). Homeostatic control of biological membranes by dedicated lipid and membrane packing sensors. *Biol. Chem.* 396, 1043–1058.
- Quiroga, R., Trenchi, A., González Montoro, A., Valdez Taubas, J., and Maccioni, H.J.F. (2013). Short transmembrane domains with high-volume exoplasmic halves determine retention of Type II membrane proteins in the Golgi complex. *J. Cell Sci.* 126, 5344–5349.
- Radhakrishnan, A., Goldstein, J.L., McDonald, J.G., and Brown, M.S. (2008). Switch-like control of SREBP-2 transport triggered by small changes in ER cholesterol: a delicate balance. *Cell Metab.* 8, 512–521.
- Rape, M., Hoppe, T., Gorr, I., Kalocay, M., Richly, H., and Jentsch, S. (2001). Mobilization of processed, membrane-tethered SPT23 transcription factor by CDC48(UFD1/NPL4), a ubiquitin-selective chaperone. *Cell* 107, 667–677.
- Ron, D., and Walter, P. (2007). Signal integration in the endoplasmic reticulum unfolded protein response. *Nat. Rev. Mol. Cell Biol.* 8, 519–529.
- Rubio, C., Pincus, D., Korennykh, A., Schuck, S., El-samad, H., and Walter, P. (2011). Homeostatic adaptation to endoplasmic reticulum stress depends on Ire1 kinase activity. *193*, 171–184.
- Ruipérez, V., Darios, F., and Davletov, B. (2010). Alpha-synuclein, lipids and Parkinson's disease. *Prog. Lipid Res.* 49, 420–428.
- Sal-Man, N., Gerber, D., Bloch, I., and Shai, Y. (2007). Specificity in transmembrane helix-helix interactions mediated by aromatic residues. *J. Biol. Chem.* 282, 19753–19761.
- Schindelin, J., Arganda-Carreras, I., Frise, E., Kaynig, V., Longair, M., Pietzsch, T., Preibisch, S., Rueden, C., Saalfeld, S., Schmid, B., et al. (2012). Fiji: an open-source platform for biological-image analysis. *Nat. Methods* 9, 676–682.
- Schneider, R., Brügger, B., Sandhoff, R., Zellnig, G., Leber, A., Lampl, M., Athenstaedt, K., Hrastrnik, C., Eder, S., Daum, G., et al. (1999). Analysis of the lipid molecular species composition of yeast subcellular membranes reveals acyl chain-based sorting / remodeling of distinct molecular species en route to the plasma membrane. *Cell* 146, 741–754.
- Schuck, S., Prinz, W.A., Thorn, K.S., Voss, C., and Walter, P. (2009). Membrane expansion alleviates endoplasmic reticulum stress independently of the unfolded protein response. *J. Cell Biol.* 187, 525–536.

- Schuldiner, M., and Weissman, J.S. (2013). The contribution of systematic approaches to characterizing the proteins and functions of the endoplasmic reticulum. *Cold Spring Harb. Perspect. Biol.* *5*, a013284.
- Schuldiner, M., Collins, S.R., Thompson, N.J., Denic, V., Bhamidipati, A., Punna, T., Ihmels, J., Andrews, B., Boone, C., Greenblatt, J.F., et al. (2005). Exploration of the function and organization of the yeast early secretory pathway through an epistatic miniarray profile. *Cell* *123*, 507–519.
- Segrest, J.P., De Loof, H., Dohlman, J.G., Brouillette, C.G., and Anantharamaiah, G.M. (1990). Amphipathic helix motif: Classes and properties. *Proteins Struct. Funct. Genet.* *8*, 103–117.
- Shaffer, A.L., Shapiro-Shelef, M., Iwakoshi, N.N., Lee, A.-H., Qian, S.-B., Zhao, H., Yu, X., Yang, L., Tan, B.K., Rosenwald, A., et al. (2004). XBP1, downstream of Blimp-1, expands the secretory apparatus and other organelles, and increases protein synthesis in plasma cell differentiation. *Immunity* *21*, 81–93.
- Sharpe, H.J., Stevens, T.J., and Munro, S. (2010). A Comprehensive Comparison of transmembrane domains reveals organelle-specific properties. *Cell* *142*, 158–169.
- Shen, X., Ellis, R.E., Lee, K., Liu, C.-Y., Yang, K., Solomon, A., Yoshida, H., Morimoto, R., Kurnit, D.M., Mori, K., et al. (2001). Complementary signaling pathways regulate the unfolded protein response and are required for *C. elegans* development. *Cell* *107*, 893–903.
- Shen, X., Ellis, R.E., Sakaki, K., and Kaufman, R.J. (2005). Genetic interactions due to constitutive and inducible gene regulation mediated by the unfolded protein response in *C. elegans*. *PLoS Genet.* *1*, e37.
- Shibata, Y., Voeltz, G.K., and Rapoport, T.A. (2006). Rough sheets and smooth tubules. *Cell* *126*, 435–439.
- Sidrauski, C., and Walter, P. (1997). The transmembrane kinase Ire1p is a site-specific endonuclease that initiates mRNA splicing in the unfolded protein response. *Cell* *90*, 1031–1039.
- Sidrauski, C., Cox, J.S., and Walter, P. (1996). tRNA Ligase is required for regulated mRNA splicing in the unfolded protein response. *Cell* *87*, 405–413.
- Sikorski, R.S., and Hieter, P. (1989). A system of shuttle vectors and yeast host strains designed for efficient manipulation of DNA in *Saccharomyces cerevisiae*. *Genetics* *122*, 19–27.
- Simons, K., and Gerl, M.J. (2010). Revitalizing membrane rafts: new tools and insights. *Nat. Rev. Mol. Cell Biol.* *11*, 688–699.
- Simons, K., and Toomre, D. (2000). Lipid rafts and signal transduction. *Nat. Rev. Mol. Cell Biol.* *1*, 31–39.
- Simons, K., and Vaz, W.L.C. (2004). Model systems, lipid rafts, and cell membranes. *Annu. Rev. Biophys. Biomol. Struct.* *33*, 269–295.

- Singer, S.J., and Nicolson, G.L. (1972). The fluid mosaic model of the structure of cell membranes. *Science* *175*, 720–731.
- Sohn, H.W., Tolar, P., and Pierce, S.K. (2008). Membrane heterogeneities in the formation of B cell receptor-Lyn kinase microclusters and the immune synapse. *J. Cell Biol.* *182*, 367–379.
- Sparr, E., Ganchev, D.N., Snel, M.M.E., Ridder, A.N.J.A., Kroon-Batenburg, L.M.J., Chupin, V., Rijkers, D.T.S., Killian, J.A., and de Kruijff, B. (2005). Molecular organization in striated domains induced by transmembrane α -helical peptides in dipalmitoyl phosphatidylcholine bilayers. *Biochemistry* *44*, 2–10.
- Sriburi, R., Bommasamy, H., Buldak, G.L., Robbins, G.R., Frank, M., Jackowski, S., and Brewer, J.W. (2007). Coordinate regulation of phospholipid biosynthesis and secretory pathway gene expression in XBP-1(S)-induced endoplasmic reticulum biogenesis. *J. Biol. Chem.* *282*, 7024–7034.
- Stordeur, C., Puth, K., Sáenz, J.P., and Ernst, R. (2014). Crosstalk of lipid and protein homeostasis to maintain membrane function. *Biol. Chem.* *395*, 313–326.
- Strahl, T., and Thorner, J. (2007). Synthesis and function of membrane phosphoinositides in budding yeast, *Saccharomyces cerevisiae*. *Biochim. Biophys. Acta - Mol. Cell Biol. Lipids* *1771*, 353–404.
- Stukey, J.E., McDonough, V.M., and Martin, C.E. (1990). The OLE1 gene of *Saccharomyces cerevisiae* encodes the $\Delta 9$ fatty acid desaturase and can be functionally replaced by the rat stearoyl CoA desaturase gene. *J. Biol. Chem.* *265*, 20144–20149.
- Sud, M., Fahy, E., Cotter, D., Brown, A., Dennis, E.A., Glass, C.K., Merrill, A.H., Murphy, R.C., Raetz, C.R.H., Russell, D.W., et al. (2007). LMSD: Lipid maps structure database. *Nucleic Acids Res.* *35*, 527–532.
- Suh, B.-C., and Hille, B. (2008). PIP2 is a necessary cofactor for ion channel function: how and why? *Annu. Rev. Biophys.* *37*, 175–195.
- Surma, M.A., Klose, C., Klemm, R.W., Ejsing, C.S., and Simons, K. (2011). Generic sorting of raft lipids into secretory vesicles in yeast. *Traffic* *12*, 1139–1147.
- Surma, M.A., Klose, C., Peng, D., Shales, M., Mrejen, C., Stefanko, A., Braberg, H., Gordon, D.E., Vorkel, D., Ejsing, C.S., et al. (2013). A lipid E-MAP identifies Ubx2 as a critical regulator of lipid saturation and lipid bilayer stress. *Mol. Cell* *51*, 519–530.
- Tabas, I., and Ron, D. (2011). Integrating the mechanisms of apoptosis induced by endoplasmic reticulum stress. *Nat. Cell Biol.* *13*, 184–190.
- Tachikawa, H., Miura, T., Katakura, Y., and Mizunaga, T. (1991). Molecular structure of a yeast gene, PDI1, encoding protein disulfide isomerase that is essential for cell growth. *J. Biochem* *110*, 306–313.
- Thibault, G., Shui, G., Kim, W., Mcalister, G.C., Ismail, N., Gygi, S.P., Wenk, M.R., and Ng, D.T.W. (2012). The membrane stress response buffers lethal effects of lipid disequilibrium by reprogramming the protein homeostasis network. *Mol. Cell* *48*, 16–27.

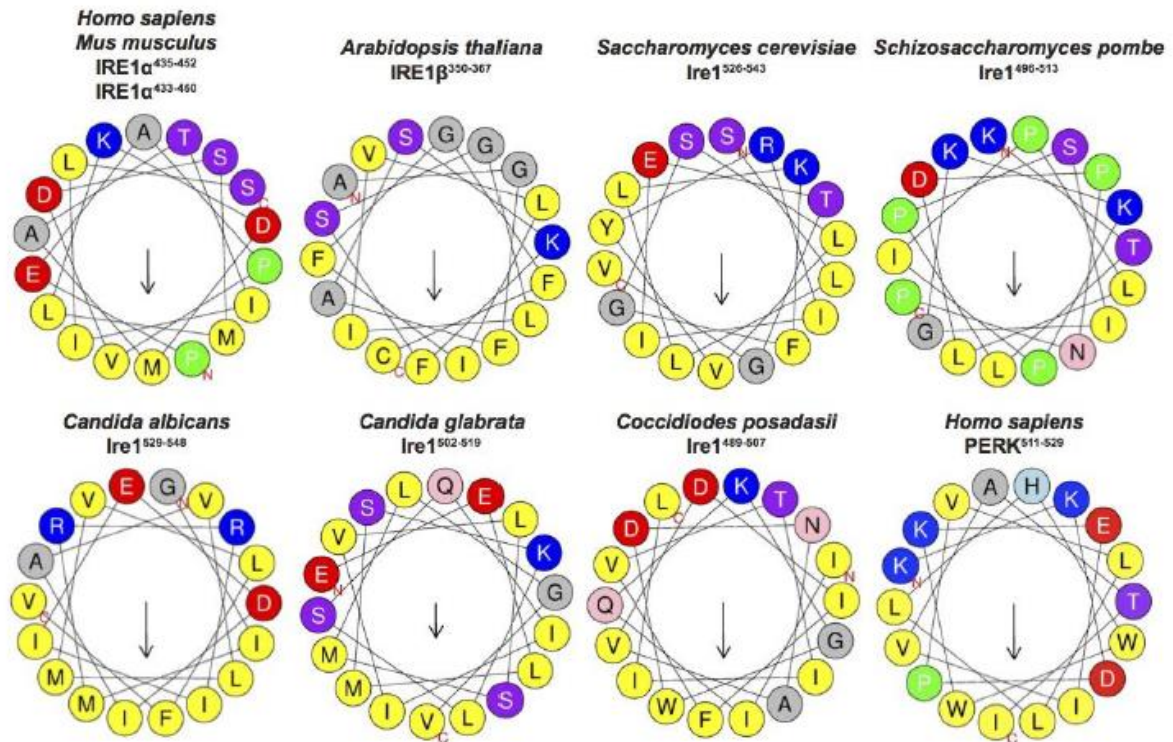
- Tirasophon, W., Welihinda, A.A., and Kaufman, R.J. (1998). A stress response pathway from the endoplasmic reticulum to the nucleus requires a novel bifunctional protein kinase/endoribonuclease (Ire1p) in mammalian cells. *Genes Dev.* *12*, 1812–1824.
- Tiwari, R., Köffel, R., and Schneider, R. (2007). An acetylation/deacetylation cycle controls the export of sterols and steroids from *S. cerevisiae*. *EMBO J.* *26*, 5109–5119.
- Travers, K.J., Patil, C.K., Wodicka, L., Lockhart, D.J., Weissman, J.S., and Walter, P. (2000). Functional and genomic analyses reveal an essential coordination between the unfolded protein response and ER-associated degradation. *Cell* *101*, 249–258.
- Vishwakarma, R.A., Vehring, S., Mehta, A., Sinha, A., Pomorski, T., Herrmann, A., and Menon, A.K. (2005). New fluorescent probes reveal that flippase-mediated flip-flop of phosphatidylinositol across the endoplasmic reticulum membrane does not depend on the stereochemistry of the lipid. *Org. Biomol. Chem.* *3*, 1275–1283.
- Voeltz, G.K., Rolls, M.M., and Rapoport, T.A. (2002). Structural organization of the endoplasmic reticulum. *EMBO Rep.* *3*, 944–950.
- Volmer, R., and Ron, D. (2015). Lipid-dependent regulation of the unfolded protein response. *Curr. Opin. Cell Biol.* *33*, 67–73.
- Volmer, R., van der Ploeg, K., and Ron, D. (2013). Membrane lipid saturation activates endoplasmic reticulum unfolded protein response transducers through their transmembrane domains. *Proc. Natl. Acad. Sci. U. S. A.* *110*, 4628–4633.
- Walter, P., and Ron, D. (2011). The unfolded protein response: from stress pathway to homeostatic regulation. *Science* *334*, 1081–1086.
- Wang, X., Bogdanov, M., and Dowhan, W. (2002). Topology of polytopic membrane protein subdomains is dictated by membrane phospholipid composition. *EMBO J.* *21*, 5673–5681.
- White, S.H., and von Heijne, G. (2005). Do protein-lipid interactions determine the recognition of transmembrane helices at the ER translocon? *Biochem. Soc. Trans.* *33*, 1012–1015.
- Yadav, R.S., and Tiwari, N.K. (2014). Lipid Integration in Neurodegeneration: An Overview of Alzheimer's Disease. *Mol. Neurobiol.* 1–9.
- Yamakawa, T., and Iida, T. (1953). Immunochemical study on the red blood cells. I. Globoside, as the agglutinin of the ABO system on erythrocytes. *Jpn. J. Exp. Med.* *23*, 327–331.
- Yamamoto, K., Sato, T., Matsui, T., Sato, M., Okada, T., Yoshida, H., Harada, A., and Mori, K. (2007). Transcriptional induction of mammalian ER quality control proteins is mediated by single or combined action of ATF6 α and XBP1. *Dev. Cell* *13*, 365–376.
- Ye, J., Rawson, R.B., Komuro, R., Chen, X., Davé, U.P., Prywes, R., Brown, M.S., and Goldstein, J.L. (2000). ER stress induces cleavage of membrane-bound ATF6 by the same proteases that process SREBPs. *Mol. Cell* *6*, 1355–1364.
- Yoshida, H., Haze, K., Yanagi, H., Yura, T., and Mori, K. (1998). Identification of the cis-acting endoplasmic reticulum stress response element responsible for transcriptional induction of mammalian glucose-regulated proteins. *J. Biol. Chem.* *273*, 33741–33749.

- Yoshida, H., Okada, T., Haze, K., Yanagi, H., Yura, T., Negishi, M., and Mori, K. (2001). Endoplasmic reticulum stress-induced formation of transcription factor complex ERSF Including NF-Y (CBF) and activating transcription factors 6alpha and 6beta that activates the mammalian unfolded protein response. *Mol. Cell. Biol.* *21*, 1239–1248.
- Yoshida, H., Oku, M., Suzuki, M., and Mori, K. (2006). pXBP1(U) encoded in XBP1 pre-mRNA negatively regulates unfolded protein response activator pXBP1(S) in mammalian ER stress response. *J. Cell Biol.* *172*.
- Yoshida, H., Uemura, A., and Mori, K. (2009). pXBP1(U), a negative regulator of the unfolded protein response activator pXBP1(S), targets ATF6 but not ATF4 in proteasome-mediated degradation. *Cell Struct. Funct.* *34*, 1–10.
- Zech, T., Ejsing, C.S., Gaus, K., de Wet, B., Shevchenko, A., Simons, K., Harder, T., Aivazian, D., Stern, L., Altman, A., et al. (2009). Accumulation of raft lipids in T-cell plasma membrane domains engaged in TCR signalling. *EMBO J.* *28*, 466–476.
- Zhang, W., Bogdanov, M., Pi, J., Pittard, A.J., and Dowhan, W. (2003). Reversible topological organization within a polytopic membrane protein is governed by a change in membrane phospholipid composition. *J. Biol. Chem.* *278*, 50128–50135.
- Zimmermann, R., Eyrisch, S., Ahmad, M., and Helms, V. (2011). Protein translocation across the ER membrane. *Biochim. Biophys. Acta - Biomembr.* *1808*, 912–924.
- Zinser, E., Sperka-Gottlieb, C.D., Fasch, E. V, Kohlwein, S.D., Paltauf, F., and Daum, G. (1991). Phospholipid synthesis and lipid composition of subcellular membranes in the unicellular eukaryote *Saccharomyces cerevisiae*. *J. Bacteriol.* *173*, 2026–2034.

Supplementary Information

Conservation of the AH in *IRE1* among species

A HeliQuest analysis of AHs



B Sequence alignment

		AH	
<i>Homo sapiens</i>	IRE1 α	----PEAPVDSMLKDMATIILSTFLLIGWVAFI	461
<i>Mus musculus</i>	IRE1 α	----PEAPVDSMLKDMATIILSTFLLVGWVAFI	463
<i>Arabidopsis thaliana</i>	IRE1 β	----AGFASKF'SGLIVLIPGFVCTMLSVCGLFF	378
<i>Saccharomyces cerevisiae</i>	Ire1	---SLLLKFGSLVYRIIETGVFLLFLIFCAIL	555
<i>Schizosaccharomyces pombe</i>	Ire1	KTLPSIGKKPIPLLDPNPISSTPISITFWVIMF	528
<i>Candida albicans</i>	Ire1	--SSGIMRRIIEDIAVLMVLFVLLMTFGKSNNMV	560
<i>Candida glabrata</i>	Ire1	--EELMSKLSQIIVLSMLGVFALSTFFIFIYSRVT	533
<i>Coccidioides posadasii</i>	Ire1	--IIQKGDNAVDIFVTIILLLLIGAFVYLNERN	519
<i>Homo sapiens</i>	PERK	--KKDPVLLLHWKKEIVATILFCIIATTFIVRR	542
		-----TMH	

Fig. S1 | A juxta-membrane AH is conserved in *IRE1*.

(A) HeliQuest analysis of Ire1 orthologs from mammals, plants and yeast strains highlights the conservation of a juxta-membrane AH in UPR transducers. (B) Sequence alignment of Ire1's AH and TMH from indicated species. The sequences of the AH is indicated in blue, while the predicted TMH is shown in black. This illustration is taken from Halbleib *et al.* (Halbleib *et al.*, 2017).

PELDOR Experiments of the reconstituted minimal sensor domain of Ire1

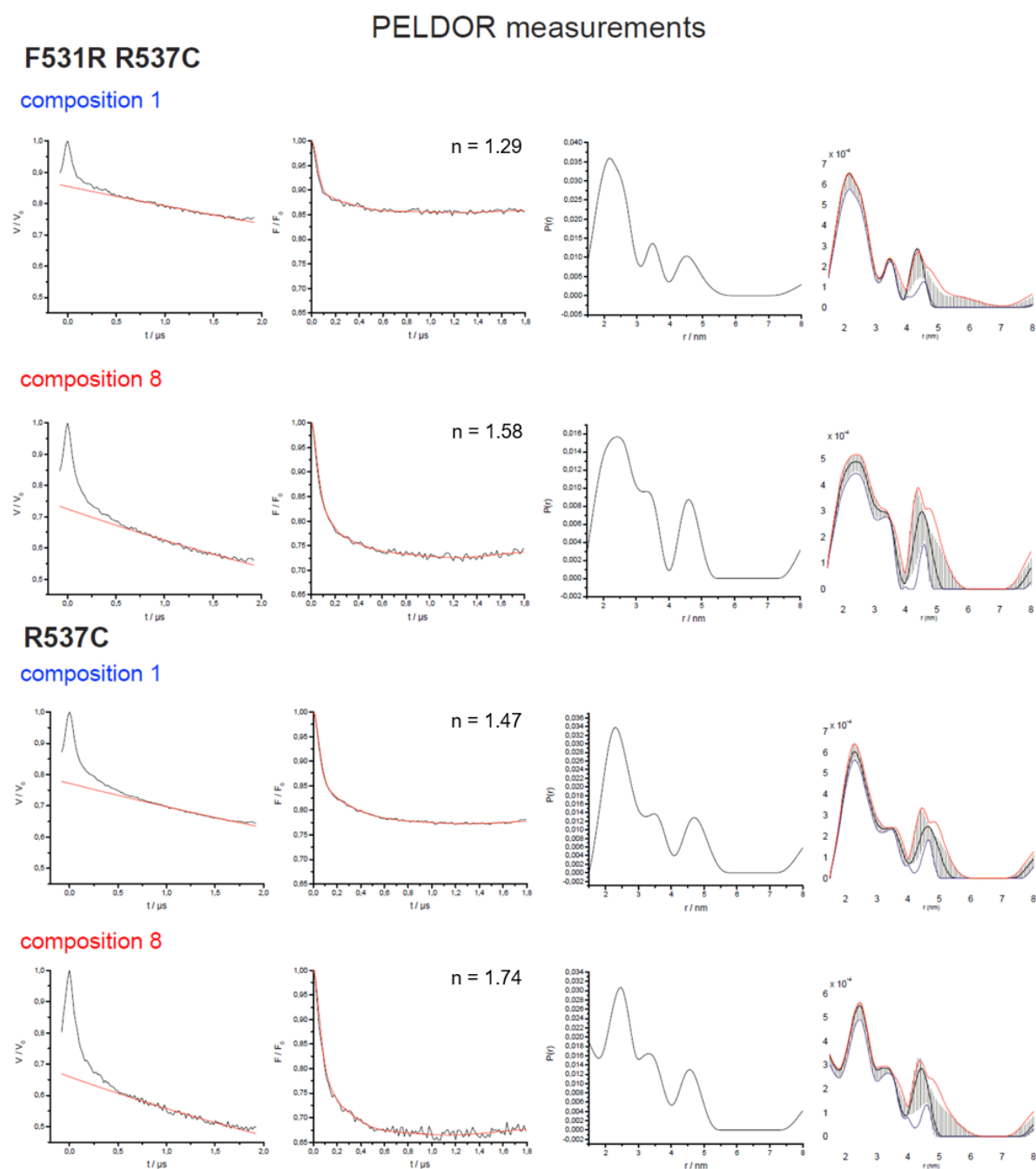


Fig. S2 | PELDOR measurements of the minimal sensor domain of Ire1 in different lipid environments.

PELDOR data of MBP-Ire1^{AH+TMH} R537C and F531R R537C, labeled with MTSSL at position R537 in lipid composition 1 (blue) and 8 (red). Normalized Q-band PELDOR traces (first column) were corrected for intermolecular background function applying a mono-exponential fit, resulting in the form factor (second column). The indicated number of spins (n) was calculated from the modulation depth of the data presented (second column). The third column shows the distance distributions calculated by the DEERAnalysis software using Tikhonov regularization. The fourth column gives the mean \pm SEM for the calculated distance distributions.

Danksagung

Ich möchte mich bei allen bedanken, die zum Gelingen dieser Arbeit beigetragen haben und im Folgenden einige Personen nennen, bei denen ich mich besonders herzlich bedanken will.

Meinem Doktorvater, Prof. Dr. Robert Ernst, danke ich für die Möglichkeit diese Arbeit in seiner Arbeitsgruppe anzufertigen. Herzlichen Dank für das spannende Projekt, die Möglichkeit meine eigenen Ideen einzubringen, Dein stetiges Interesse, die andauernde Ermunterung neue Methoden zu erlernen und mich fachlich, sowie persönlich weiterzuentwickeln, sowie Deine permanente Bereitschaft zu kritischen Diskussionen. Vielen Dank, Robert!

Ich möchte auch Prof. Dr. Martin Grininger für die Übernahme des Zweitgutachtens danken.

Weiterhin möchte ich mich bei meinen Kollaborationspartnern bedanken, ohne die diese Arbeit in diesem Umfang nicht möglich gewesen wäre:

Jun Prof. Dr. Inga Hänel & Dr. Dorith Wunnicke (Institut für Biochemie, Goethe Universität Frankfurt), danke ich für die Einführung in die Welt der cwEPR Spektroskopie, sowie die stetige Bereitschaft meine Daten zu diskutieren. Weiterhin möchte ich mich besonders bei Dr. Dorith Wunnicke für die Durchführung von PELDOR Messungen bedanken. Ihr wart mir eine große Hilfe, vielen Dank!

I would also like to kindly thank Prof. Dr. Gerhard Hummer & Dr. Roberto Covino (Institut für theoretische Physik, MPI für Biophysik) for the performance of MD simulations on the minimal sensor peptide of Ire1. Thank you!

Danken möchte ich ebenfalls Jun Prof. Dr. Michaela Müller-McNicoll (Institut für Zellbiologie & Neurowissenschaft, Goethe Universität Frankfurt) für die Möglichkeit, qPCR Experimente in ihrem Labor durchzuführen. Danke auch an Oliver Schwich für die Unterstützung bei technischen Problemen.

Ich möchte mich zudem bei Prof. Dr. Robert Tampé, PD Dr. Rupert Abele und Dr. Martin Vabulas für die Möglichkeit bedanken, Arbeitsgeräte aus Ihren Laboren zu verwenden.

Ganz besonderer Dank gilt den derzeitigen und ehemaligen Mitgliedern des Arbeitskreis Ernst, im Besonderen Dr. Claudius Stordeur, Dr. Elena Widerhold, Dr. Harald Hofbauer, Jonas Michaelis, Julian Wagner, Maja Rennig, Kristina Pesek, und Stephanie Ballweg. Vielen Dank für die intensiven Diskussionen im Seminar und den Input während der Kaffeepause. Ganz

besonders möchte ich Kristina und Steffi danken, dafür dass ihr meine Launen ausgehalten, mich in schwierigen Momenten aufgemuntert, und immer ein offenes Ohr für mich zur Verfügung hattet. Danke für Eure Unterstützung und das von Freundschaft geprägte Arbeitsklima.

Allen Praktikanten, Bachelor- und Diplomstudenten, die mich über die Dauer meiner Doktorarbeit auf meinem Weg begleitet haben – Kristina Pesek, Heidi Zetschke, Jonas Michaelis, Laura Henke und Julian Wagner – möchte ich ebenfalls danken.

Meine Kollegen in den Arbeitskreisen Abele, Hänelt und Tampé danke ich für die besonders freundliche Atmosphäre und die konstruktive Kritik im Freitagseminar. Hierbei möchte ich diejenigen hervorheben, die mir über die Zeit besonders ans Herz gewachsen sind und mich zum Teil seit meinem ersten Praktikum auf meinem Weg begleitet haben: Dr. Kristin Kiosze-Becker, Gerda Fleischmann, Dr. Franz Tumulka, Christoph Bock, Dr. Tina Zollmann, Charlott Stock und Dr. Anne Nöll.

Ich danke Kristina Pesek, Harald Hofbauer und Stephanie Ballweg für das gewissenhafte Korrekturlesen meiner Veröffentlichungen, sowie dieser Dissertation.

Ganz besonders möchte ich mich bei meinen Freunden und meiner Familie bedanken, der ich diese Arbeit widme. Besonders bei meiner Mutter und meinen Geschwistern kann ich mich nicht genug für die Unterstützung über die Zeit meiner Doktorarbeit bedanken. Danke für all die lieben Worte, das Verständnis und die Liebe, die Ihr mir entgegengebracht habt. Gleiches gilt für meinen Mann Thilo. Ich bin Dir unendlich dankbar für Deine Unterstützung, den Glauben an mich, Deine Geduld und Deine Aufmunterung in jeglicher Situation. Du bist mein Fels in der Brandung.

Curriculum vitae

Kristina Halbleib (geb. Puth)

Dipl. Biochem.

Rathausgasse 4A
60389 Frankfurt

Date of birth: 22.02.1988

Mobile: +49 (0) 176-32146567
Email: Kristinahalbleib@gmail.com



Professional experience

-
- | | |
|-------------------|---|
| 04/2017 – present | <p>Life Science Consultant
KVALITO Deutschland GmbH, Dresden
Service delivery to clients in the pharmaceutical and biotech industry</p> <ul style="list-style-type: none"> • Weleda AG (Schwäbisch Gmünd, Germany) • Tillotts Pharma, Zeria Group (Basel, Switzerland) <p>Projects and roles:</p> <ul style="list-style-type: none"> • Validation Expert, Quality Assurance • Project Management |
| 12/2012 – 03/2017 | <p>Scientific employee
at the Institute of Biochemistry & BMLS, Goethe University Frankfurt,
Group of Prof. Dr. Robert Ernst</p> <ul style="list-style-type: none"> • Independent planning, performance and analysis of scientific projects • Successful publication of three first author publications • Supervision and guidance of master-, diploma- and bachelor students • Preparation and delivery of scientific presentations |

Education

-
- | | |
|-------------------|---|
| 12/2012 – 03/2017 | <p>PhD Student in Biochemistry
at the Institute of Biochemistry & BMLS, Goethe University Frankfurt,
Prof. Dr. Robert Ernst</p> <ul style="list-style-type: none"> • Title of PhD thesis: “Activation of the unfolded protein response sensor <i>Ire1</i> by lipid bilayer stress” • Member of the integrated research training group TRAM, of the collaborative research center SFB807 “Transport and communication across biological membranes” |
| 01/2012 – 09/2012 | <p>Diploma Thesis
at the Institute of Biochemistry, Goethe University Frankfurt,
Prof. Dr. Robert Tampé</p> <ul style="list-style-type: none"> • Title of Diploma Thesis: “Characterization of the ribosome recycling factor <i>ABCE1</i> from <i>Chaetomium thermophilum</i>” |

- 10/2007 – 09/2012 **Study of Biochemistry**
Goethe University Frankfurt
- Degree: diploma in biochemistry
- 04/2011 – 07/2011 **Studies Abroad**
at the California Institute of Technology, Pasadena, California (USA),
Prof. Dr. Paul H. Patterson
- **Research interest:** Immunotherapy in neurodegenerative diseases
“Effect of intrabodies on huntingtin phosphorylation“
- 1998 – 2007 **Helmholtzschule, Frankfurt**
- Higher education entrance qualification (Abitur)
- 07/2004 – 12/2004 **Studies Abroad**
Marjory Stoneman Douglas High School, Parkland, Florida (USA)
- Student exchange program

Publications and Awards

- 2017 **Halbleib, K.**, Pesek, K., Covino, R., Hofbauer, H.F., Wunnicke, D., Hänel, I., Hummer, G., Ernst, R.
Activation of the unfolded protein response by lipid bilayer stress.
Mol. Cell. (2017), Vol. 67, 673-684
- 10/2016 EMBO Conference, Girona, Spain
Structure and Function of the Endoplasmic Reticulum
Poster Award (first place out of 123 poster submissions)
- 2016 Covino, R.* , Ballweg, S.* , Stordeur, C.* , Michaelis, J.B., **Puth, K.**,
Wernig, F., Bahrami, A., Ernst, A.M., Hummer, G., Ernst, R.
A eukaryotic sensor for membrane lipid saturation.
Mol. Cell. (2016), Vol. 63, 49-59.
- 2015 **Puth, K.***, Hofbauer, H.F.* , Saenz, J., Ernst, R.
Homeostatic control of biological membranes by dedicated lipid and
membrane packing sensors.
Biol. Chem. (2015), Vol. 396 (9-10), 1043-1058.
- 2014 Stordeur, C.* , **Puth, K.***, Saenz, J., Ernst, R.
Crosstalk of lipid and protein homeostasis to maintain membrane
function.
Biol. Chem. (2014), Vol. 395(3), 313-326.

* First author

Extended vocational training

- 09/2017 **Professional Scrum Master & Product Owner Certification**
Agile Project Management
- 04/2017 **ITIL Foundation Certification**
IT Service Management, APMG International

- 05/2015 **Workshop: „*Team Work and Leadership Competencies*“**
Sanja Stevic, Golin Science Management
- 12/2014 **Workshop: “*Biotech Quality Manager/ Regulatory Affairs*
Manager“**
Dr. C. Grote-Westrick
- 11/2014 **Workshop: “*Project Management in Biotech Industries*“**
Dr. C. Grote-Westrick

Eidesstattliche Erklärung

Ich erkläre hiermit an Eides Statt, dass ich die vorgelegte Dissertation

„Activation of the unfolded protein response sensor Ire1 by lipid bilayer stress“

selbstständig angefertigt und mich anderer Hilfsmittel als der angegebenen nicht bedient habe, insbesondere, dass aus Schriften Entlehnungen, soweit sie in der Dissertation nicht ausdrücklich als solche mit Angabe der betreffenden Schrift bezeichnet sind, nicht stattgefunden haben.

Frankfurt am Main, den _____

(Unterschrift)